Ubiquitin and ubiquitin-like host modifications in *Listeria monocytogenes* infection

Von der Fakultät für Lebenswissenschaften

der Technischen Universität Carolo-Wilhelmina zu Braunschweig

zur Erlangung des Grades einer

Doktorin der Naturwissenschaften

(Dr. rer. nat.)

genehmigte

D i s s e r t a t i o n

von Anne Kummer

aus Suhl

1. Referent: Prof. Dr. Lothar Jänsch

2. Referentin: Prof. Dr. Susanne Engelmann

eingereicht am: 15.06.2016

mündliche Prüfung (Disputation) am: 02.12.2016

Druckjahr 2017

Vorveröffentlichungen der Dissertation

Teilergebnisse aus dieser Arbeit wurden mit Genehmigung der Fakultät für Lebenswissenschaften, vertreten durch den Mentor der Arbeit, in folgenden Beiträgen vorab veröffentlicht:

Publikationen:

Kummer A, Nishanth G, Kochel J, Klawonn F, Schlüter D & Jänsch L.: Listeriosis down-regulates hepatic cytochrome P450 enzymes in sub-lethal murine infection. Proteomics Clin Appl (2016, 10(9-10), 1025-1035).
doi: 10.1002/prca.201600030

Iphöfer A, Kummer A, Nimtz M, Ritter A, Arnold T, Frank R, van den Heuvel J, Kessler BM, Jänsch L & Franke R.: Profiling ubiquitin linkage specificities of deubiquitinating enzymes with branched ubiquitin isopeptide probes. Chembiochem (2012, 13(10), 1416-20).
doi: 10.1002/cbic.201200261

Tagungsbeiträge:

Kummer A, Kärst U, Jänsch L.: Ubiquitin and Ubiquitin-like modifications in Listeria infection - closing gaps about the role of Deubiquitinating enzymes in Listeria invasion (Talk). Annual LISTRESS-Meeting 2012; Paris (2012)

Kummer A, Kärst U, Jänsch L.: Ubiquitin and Ubiquitin-like modifications in Listeria infection: The role of Deubiquitinating enzymes (Talk). Annual LISTRESS-Meeting 2013. Madrid (2013)

Posterbeiträge:

Kummer A, Kärst U, Jänsch L.: Ubiquitin and Ubiquitin-like host modifications in *Listeria* infection (Poster); ERA-NET PathoGenoMics, Joint Annual Seminar. Teneriffa (2012)

Kummer A, Iphöfer A, Nimtz M, Franke R & Jänsch L.: Targeting Deubiquitinating Enzymes In Human Diseases (Poster). Proteomic Forum. Berlin (2013)

Kummer A, Franke R, Nishanth G, Schlüter D & Jänsch L.: Targeting Deubiquitinating Enzymes In Human Diseases (Poster). 18th Joint Meeting of the Signal Transduction Society (STS). Weimar (2014)

Contents

1 Introduction

1.1 Ubiquitin- and Ubiquitin-like Modifiers

Ubiquitin-like modifiers (UBLs) are a group of post-translational modifications which are structurally characterized by their so called β-grasp fold spanning approximately 70 amino acids (aa) and often reversibly conjugated to other proteins *via* their C-terminal glycine [1]. To date, the group of UBLs comprises 12 confirmed members and families presented and summarized in Table 1 as well as additional putative UBLs [2]. Furthermore, prokaryotic proteins with a similar protein fold, which are regarded as precursor for the ubiquitin system were identified in recent years [3]. All UBLs contribute to the regulation of cellular functions in their unique ways, together spanning all relevant processes in the cell from protein degradation and DNA repair to immune control and autophagy [2, 4, 5]. The most relevant and best studied UBLs are presented in detail below.

1.1.1 Ubiquitin

The founding member of the UBLs is the 76-aa containing polypeptide ubiquitin (Ub) that received its name due to the ubiquitous presence and high conservation throughout all eukaryotes [4]. It is translated as a linear precursor-protein of multiple head-to-tail fused Ub-moieties or fused to other proteins and is processed rapidly by deubiquitinating enzymes (DUBs) to create free Ub [1]. Individual Ub-moieties show the characteristic β-fold grasp consisting of 5 β-sheets and an opposed α-helix (Fig 1), generating a high structural stability against pH-shifts and high temperatures [1,6]. Ub is liked to substrate proteins *via* its C-terminal glycine which is attached to an amino group of the target protein, predominantly lysine (Lys), forming an ε-isopeptide bond [7]. Apart from its importance as the first polypeptide modifier, Ub is the best characterized PTM of this group and in addition also the most complex member, due to the ability

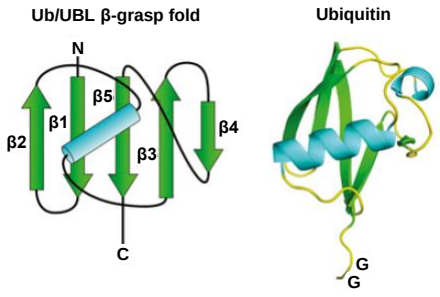

Figure 1. Ub/UBL beta-grasp fold and ubiquitin structure. β-sheets are represented in green, α-helices in blue. Modified from Vierstra [1].

to not only become conjugated to target proteins but also to other Ub-moieties to form different and highly complex chain types [8]. Ub itself contains seven lysine (K) residues, K6, K11, K27, K29, K33, K48 and K63 and all of them as well as the N-terminal methionine are potential starting points for poly-Ub chain-building. Interestingly, distinct types of ubiquitination are implied in different cellular functions (Fig 2). The "simplest" Ub-modification, monoubiquitination, and if multiply attached multi-monoubiquitination, is a frequent modification of histones, where it provides a base for protein interactions with methyltransferases and other proteins [9]. Apart from this function, monoubiquitination was described to play a role in protein localization and modulation of activity [8].

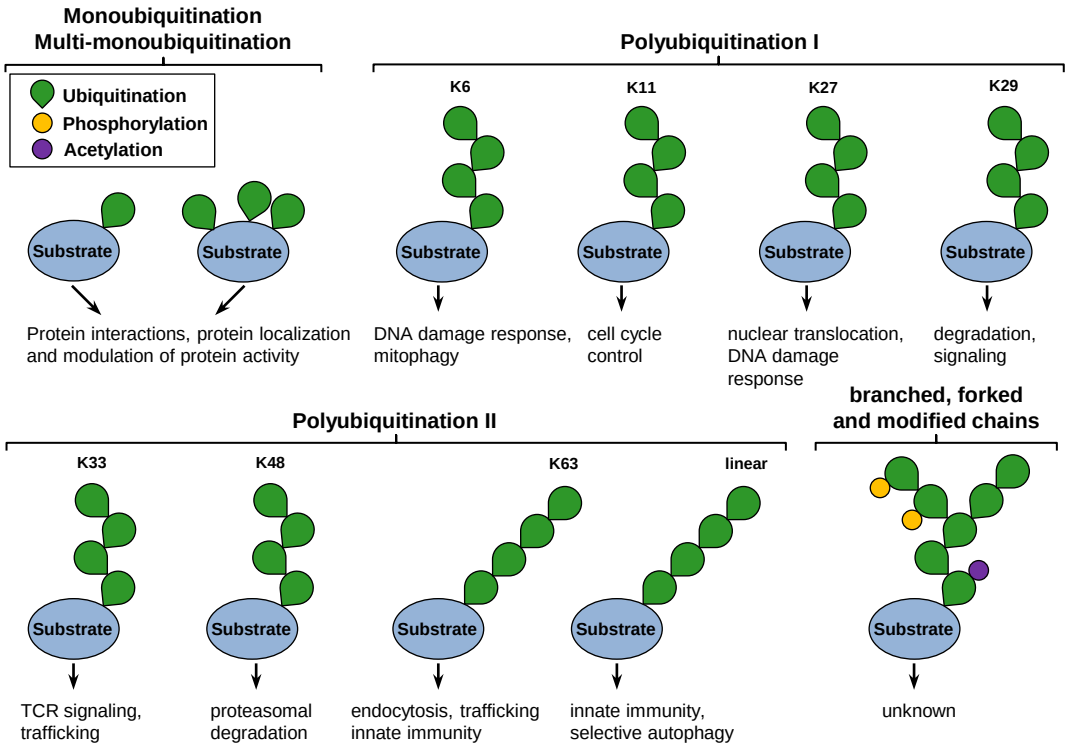

Figure 2. Overview of the types of mono- and polyubiquitination and associated cellular functions. Substrate proteins are represented in blue and ubiquitin-moieties in green. K refers to the lysine utilized for chain assembly. Phosphorylation is illustrated in yellow, acetylation in purple. Modified from Ye & Rape and expanded with recently described functions from Akutsu et al. [8, 10].

In contrast, polyubiquitination adopts a variety of manifestations (Fig 2). The canonical poly-Ub chain comprises of at least 4 Ub-moieties linked by K48 and targets modified proteins for proteasomal degradation [4]. Additionally, K48 poly-Ub chains are also implicated in non-proteolytic functions, e.g. activation and inactivation of certain proteins [11]. In recent years, not only K48 but also other chain types were described to

facilitate distinct functions. K6 and K27 polyubiquitination, for example, are implicated in DNA damage response, while K11 poly-Ub chains control cell-cycle progression and K29 and K33 play a role in different signaling cascades (Fig 2) [8, 10].

Most notably, chains that are methionine-linked and therefore often referred to as M1 chains as well as K63 chains adopt a more linear and open conformation than all the other chains [12], leading to a distinct functional repertoire especially in regulation of protein complex-building in innate immunity [13]. Additionally, K63 and M1 poly-Ub chains are involved in autophagic processes, e.g. selective autophagy and endocytosis [10, 14]. Although the functions of different chain types were extensively researched in the last years and become more well described, novel chain-varieties emerge perpetually. The most recent additions to the complexity of the ubiquitin-code entail branched, forked and mixed-linkage Ub-chains [10] as well as post-translational modifications of ubiquitin by kinases and acetylases. For those Ub-varieties, functional descriptions are limited to a few cases [15]. Furthermore, hybrid-UBL chains were recently described, combining ubiquitin and the UBLs SUMO and NEDD8 in distinct mixed chains [16, 17].

In general, it is assumed that all Ub-chain types target proteins to a variety of degradation pathways [14, 18] and all possible chain-types and -variations are being utilized *in vivo* [10]. Although ubiquitination is implicated in a wide variety of functions, other UBLs are important players in the regulation of cellular processes as well, and are even involved in functions overlapping with those mentioned for ubiquitin.

1.1.2 SUMO

Small Ubiquitin-related Modifier (SUMO) is one of the most extensively studied UBLs and present in 3 to 4 paralogs in vertebrates [19]. Although sequence identity of SUMO to Ub is not high (18 %), it contains the typical β-grasp fold and is additionally able to form poly-SUMO-chains [20] as well as hybrid Ub-SUMO chains [17]. Two of the 4 human paralogs, SUMO-2 and SUMO-3, often referred to as SUMO-2/3, share 95 % of sequence identity and are readily conjugated to proteins, as is SUMO-4, which is 87 % identical to SUMO2 [19, 21]. The last paralog, SUMO-1 has only 50 % similarity to SUMO2 and additionally lacks the consensus motif needed to build poly-SUMO chains [22]. However, only one SUMO-conjugating enzyme, Ubc9, is known so far and is facilitating conjugation of all SUMOs [23]. Ubc9 is predominantly localized in the nucleus and associated to filaments. Additionally, SUMOs themselves are spatially restricted to nuclear compartments with exception of SUMO-3, which is also found in the cytoplasm [24]. Nevertheless, SUMOylation is implicated in DNA repair, nuclear transport and cell cycle progression as well as adaptation to stress stimuli, and over 600 putatively SUMOylated proteins are described so far [23]. Furthermore, SUMOylation regulates innate immune components during viral infection and recently it was also shown that *Listeria monocytogenes* impairs SUMOylation for efficient infection [25, 26].

1.1.3 NEDD8

Neuronal-precursor-cell expressed developmentally down-regulated 8 (NEDD8) has a sequence identity of about 55 % as compared to ubiquitin and thus is the most similar UBL [2,22]. NEDD8, like Ub and SUMO, is also able to form poly-NEDD8 chains through different lysine residues as well as mixed chains with ubiquitin, then functioning as a chain terminator [16, 27]. The predominant function of NEDD8 is the activation of the cullin sub-units of RING Ub-ligases enhancing their ligase activities [2]. Notably, NEDDylation was recently found to be involved in a number of functions in transcriptional regulation and signaling not linked to cullin activation [16,28]. In signaling processes, NEDD8 can be attached to receptor tyrosine kinases, as described for EGFR and TGFß*R*II, by the E3-Ub ligase c-Cbl which also ubiquitinates the receptors. Astonishingly, NEDDylation of EGFR boosts subsequent ubiquitination and degradation while NEDDylation of TGFß*R*II leads to prolonged signaling and stabilization [29, 30].

1.1.4 ISG15

Interferon-stimulated gene 15 (ISG15) was the first UBL to be discovered and owes its name to the fact that it is inducible by type-1 interferons (IFN) [19]. ISG15, in contrast to ubiquitin, consists of 2 β-grasp folds with a sequence identity of 32 and 37 %, respectively (Table 1), and is far less conserved among eukaryotes than ubiquitin, hinting towards a specialized role in higher eukaryotes [31]. Indeed, ISG15 is not only conjugated to lysine residues of target proteins but also secreted upon IFN-stimulation from different cell types [32]. However, both forms show immunomodulatory functions especially in immune responses to viruses but also to bacteria [5, 32–34]. To activate these specialized functions, the ISG15 conjugation system is also induced by IFNs [31], restricting the ISGylation of proteins to precise time frames and situations. Interestingly, patients with an ISG15 deficiency do not develop severe viral infections, although ISG15 counteracts viral infection and several viruses possess countermeasures against ISG15 [31,35]. Instead, patients suffered from Mendelian susceptibility to mycobacterial disease (MSMD), which is a rare disorder ultimately leading to susceptibility to *Salmonella* and *Mycobacterium tuberculosis* as well as weakly virulent mycobacterial strains, indicating a primary role of ISG15 in immunity against certain bacteria. Notably, ISG15 knock-out mice are also susceptible to *Listeria monocytogenes* infections [34].

1.1.5 UFM1

Ubiquitin-fold modifier (UFM1) is a more recently discovered UBL with minimal sequence identity (Table 1). Nevertheless, conjugation machinery and removing enzymes are described, rendering the system functional [24, 36]. However, only few UFMylation-targets are identified and the proposed physiological functions in erythroid development and ER-stress response need to be strengthened by further results [19, 37].

Table 1. Known ubiquitin-like modifiers and regulatory enzymes. The information were acquired from UniProt KB and assembled from literature [2,22,24]. Modified and extended from Hochstrasser et al. [2]

UBL	seq. identity [%]	Functions	activating enzyme(s)	conjugating enzyme(s)	removing enzyme(s)
ubiquitin	100	degradation, immune system regulation, endocytosis, chromatin remodeling	UBA6	many	many
NEDD8 (Rub1)	55	Activation of Cullin E3-ligases	UBE1C-APPBP	UBE2M UBE2F [38]	UCHL3 [39], SENP8 [40]
ISG15	32, 37	anti-viral immune response [5]	UBE1L	UB2E1, UB2E2, UB2L6	USP18 [41]
SUMO (2-4)	18	DNA repair, nuclear transport, cell cycle progression [42]	SAE1, SAE2, Uba2-Aos1	UBC9	SENP1-7 [43]
UFM1	14		UBA5	UFC1	UfsP1, UfsP2 [36]
Atg8	10	autophagy	Atg7	Atg3	
Atg12	17	autophagy	Atg7	Atg10	
FUBI	38				
FAT10	32, 40	proteasomal degradation [44]	UBA6		
Urm1	12		Uba4	Ahp2	

1.1.6 Conjugation and Deconjugation of Ubiquitin

Ubiquitin and most of the UBLs are conjugated by a cascade of enzymes including three major steps. Accordingly, the enzymes are named E1 for the activating enzymes, E2 for the conjugating enzymes and E3 for the UBL ligases [4], while deconjugation is carried out in a one-step reaction by deconjugating enzymes. For simplification purposes, Figure 3 illustrates this machinery only for ubiquitin, which is the best described modifier. For most UBLs, the enzymatic reactions for both processes are assumed to be similar and known activating, conjugation and deconjugating enzymes are listed in Table 1 [2, 22].

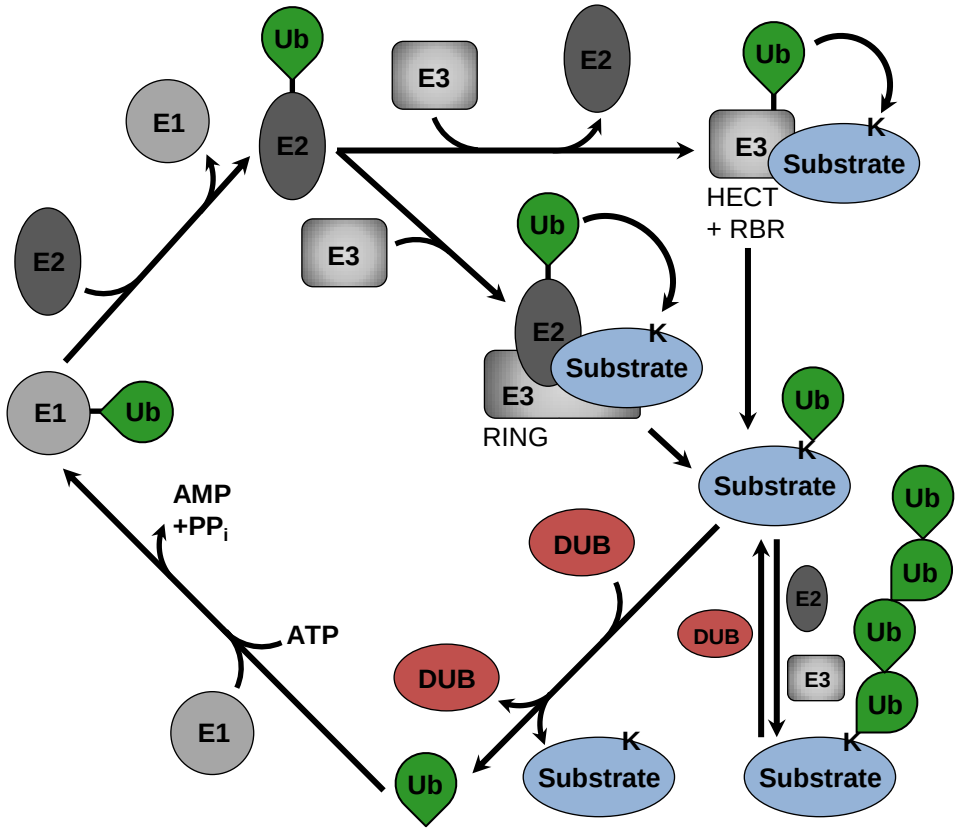

Figure 3. Conjugation and deconjugation of UBLs using the example of ubiquitin. Ubiquitin is represented in green. The E1, E2 and E3 enzymes are parts of the conjugation machinery (gray) where E1 = activating enzyme, E2 = conjugating enzyme and E3 = ligase. Deubiquitinating enzymes (DUBs) are presented in red and constitute the deconjugating enzymes.

In the first step of conjugation, ubiquitin is linked to the active center cysteine (Cys) residue of the E1 forming a thioester bond utilizing ATP. The now charged E1 then associates with an E2 conjugation enzyme leading to the transfer of Ub to the E2

enzyme via trans-thioesterification. Subsequently, the E2 enzymes interact with E3 ligases which recognize the substrate proteins and therefore are crucial for the specificity of ubiquitination reactions.

For ubiquitin, two mechanisms of ligation are described (Fig 3). RING (Really interesting new gene) domain-containing E3 ligases work as a bridge between the E2 enzyme and the substrate and the Ub-moiety is directly transferred from E2 onto the substrate protein. In contrast to that, HECT (Homologous to E6-AP Carboxyl Terminus) and RBR (RING Between RING) domain-containing E3 ligase-dependent ligation occurs by transfer of the Ub onto the ligase and the following transfer to the Lys of the substrate protein in two distinct steps [45, 46]. Finally, conjugation of Ub-moieties is repeated to create distinct poly-Ub chains. In some cases, alternate E2 enzymes specialized in chain-elongation are recruited to the E3 enzyme [46]. The conjugating reactions are compensated by deconjugating enzymes, for Ub termed deubiquitinating enzymes (DUBs), which remove ubiquitin from substrates using different modes of action (Section 1.2) and restore the pool of free cellular ubiquitin.

In general, the conjugation machinery of Ub and UBLs is organized in a hierarchical manner. While only two E1 enzymes are known in human, about 40 E2 and over 600 E3 ubiquitin ligases contribute to ubiquitination and formation of poly-Ub chains. At least for SUMO and NEDD8, a similar complexity is assumed. However, for SUMO only one E2 enzyme, UBC9, is known so far, while 2 conjugating enzymes are described for NEDD8 (Table 1). In contrast to the conjugation cascade, deconjugation of Ub is facilitated by about 90 DUBs in human [47]. For some of the other UBLs, deconjugation enzymes are described, albeit not in high abundance (Table 1).

Nevertheless, deconjugating enzymes play an important role in regulation of ubiquitin and UBL-mediated processes by shaping the modification of distinct proteins and add an additional layer of control and specificity.

1.2 Deubiquitinating Enzymes

Deubiquitinating enzymes (DUBs) remove ubiquitin, and some additionally UBLs, from substrate proteins. Although specific deconjugation enzymes for UBLs are described (Table 1), DUBs are the most abundant group and are therefore further described. In general, DUBs are isopeptidases, belonging either to the papain-like cysteine(Cys)-proteases or zinc-dependent metalloproteases [48]. On the basis of sequence similarity and core domains, DUBs are classified into five DUB-families (Table 2). Additionally, there is one protein, monocyte chemotactic protein–induced protein 1 (MCPIP), that also has deubiquitinating activity, but does not fit into one of the DUB-families defined so far [49]. Notably, although all known DUBs are assigned to their families, for some of them functional activity is unlikely, due to missing catalytic residues [50].

Table 2. DUB-families, member numbers and reaction mechanisms. Member numbers were taken from Coyne et al. [51] taking also putatively inactive and hypothetical DUBs into account.

DUB-family	Abbrev.	reaction mechanism	# of members
Ubiquitin-Specific Proteases	USP	Cys protease	56
Ubiquitin C-terminal hHydrolases	UCH	Cys protease	4
Ovarian TUmor domain-containing	OTU	Cys protease	16
Macado-Josephin Disease domain-containing	MJD	Cys protease	4
JAB1/MPN/Mov34 metalloenzyme domain-containing	JAMM	metalloprotease	11

Apart from family-associated core domains, most DUBs contain a repertoire of other domains, facilitating, e.g. protein- and ubiquitin-binding [52]. Those domains are crucial for the regulation of DUB-activity and -specificity as they provide a distinct protein environment by interaction with other proteins and thus promote formation of multi-enzyme complexes [53]. Structural elucidation of DUBs, especially in complex with ubiquitin moieties or activity-based probes, shows that DUBs undergo activating rearrangements of the active-site upon substrate-binding. The deubiquitinase OTULIN is even supported by a histidine (His) residue of ubiquitin, which completes the catalytic triad of the DUB [12, 53].

Furthermore, DUBs are regulated by a multitude of post-translational modifications, e.g. acetylation, phosphorylation and ubiquitination [54], adding an additional layer of activity-regulation.

Taken together, all these features generate DUB-specificity for different substrate groups, which can be summarized as presented in Figure 4 and will be described hereafter.

Ubiquitin-chains can be removed by different mechanisms which are not restricted to distinct DUB-families. First, recognition of distinct parts of poly-Ub chains leads to two types of peptidase activities independent from substrate proteins (Fig 4A). Chains can either be cleaved from the distal end of the chain by DUBs exerting exopeptidase activity or cleaved amid the chain by endopeptidases. In contrast to that, chain amputation directly at the substrate requires recognition of the respective protein and results in a deubiquitinated protein and a free ubiquitin-chain (Fig 4B). The third mechanism of

Ub-cleavage is the removal of single ubiquitin moieties from substrate proteins. DUBs performing this task are either promiscuous or substrate-specific and are needed if DUBs leave a Ub-stub behind after cleavage [46, 55]. Apart from different cleaving mechanisms, DUBs exert specificity by substrate or chain-binding (Fig 4D-F). As mentioned before, chain-specific DUBs are able to recognize different chain types and specifically cleave them. For example, Cylindromatosis (CYLD), a USP, shows a preference for K63-linked chains, but is only able to exert exopeptidase activity, leaving the proximal Ub attached [52, 56]. In contrast, most OTU family members show linkage preferences. OTUD3, for example, is able to cleave a chain at any Ub in a chain [57]. Another group of DUBs gains specificity by recognizing the substrate of ubiquitination (Fig 4E) and remove ubiquitin either directly at the target-protein by *en bloc*-cleavage or at the following Ub, also leaving a stub behind. Notably, most of the USP family DUBs are believed to be substrate-specific but promiscuous regarding chain types [45]. Last but not least, some DUBs are specific for recycling activities, cleaving either unanchored Ub-chains or peptides linked to ubiquitin (Fig 4F) by recognition of the glycine-glycine motif of ubiquitin or the Lys-anchored peptide.

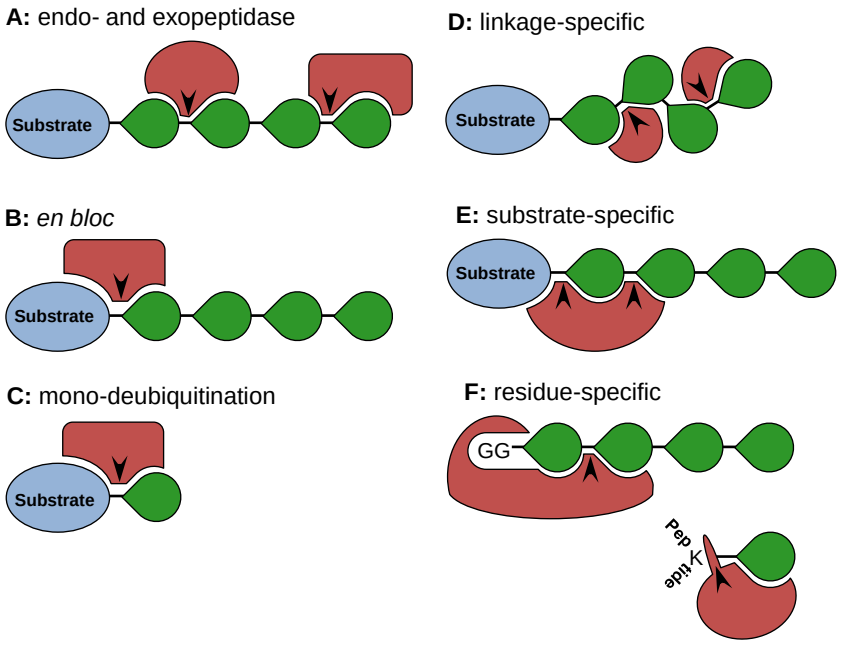

Figure 4. Modes of action leading to DUB specificity at different levels. (A-C) Distinct mechanisms of Ub-cleavage. (D-F) Mechanisms facilitating specificity by substrate recognition. Adapted from Komander et al. and Heride et al. [46, 55].

Although these different mechanisms contribute to distinct specificities of DUBs throughout the cells, categories of DUB functions are readily definable. Recycling, as mentioned before, is one of them and important for restoring of the free ubiquitin pool and rescuing Ub from degradation. However, the most prominent role of DUBs is to remove single ubiquitin moieties and ubiquitin chains from substrates. While removal of a degrading signal rescues substrate-proteins from proteasomal or lysosomal degradation, removal of a non-degrading Ub-chain can lead to protein activation or inactivation [55]. Apart from chain cleavage, DUBs process the linear precursor proteins of ubiquitin to obtain free, active mono-ubiquitin. The most sophisticated function executed by DUBs is chain editing, whereby one Ub-chain type is substituted by another. This function requires DUBs to either form complexes with E3 ligases or combine both ligating and deconjugating activities [45, 55]. The most prominent example exerting this function is the DUB A20 which has the ability to remove K63 poly-Ub chains from proteins and subsequently to attach K48-linked chains to target the substrates for proteasomal degradation [58].

1.2.1 Reaction Mechanisms

Two distinct biochemical reaction mechanisms underlie all cleavages realized by DUBs. While most of the enzymes belong to the class of papain-like cysteine proteases (USP, UCH, OTU, MJD), JAMM family DUBs utilize a cytidine deaminase-like metalloprotease mechanism. Both reactions are illustrated below.

1.2.1.1 Papain-like Cysteine Proteases

Papain-like cysteine protease DUBs contain two catalytically active and highly conserved residues, Cys and His, forming a catalytic dyad. Additionally, a third residue, usually glutamine (Gln), glutamate (Glu) or asparagine (Asn), supports the reaction, but is less important and not found in all Cys protease DUBs [55]. Following the binding to a ubiquitinated substrate or poly-Ub chain, a nucleophilic attack of the Cys towards the carbonyl carbon of the peptide bond occurs (Fig 5A). This attack then results in a negatively charged transition state and the formation of an oxyanion which is stabilized by nearby residues building an oxyanion-hole (Fig 5B). Subsequently, an acyl-intermediate forms as the His imidazole ring donates a proton and the proximal ubiquitin is released, while the distal Ub stays covalently liked to the active-site Cys. In a second reaction step, a water molecule enters the reactive center (Fig 5C) and through hydrolysis again evokes a negatively charged transition state with a tetrahedral intermediate (Fig 5D). Finally, the distal Ub is released (Fig 5E) and the catalytic triad reverts to its original state for further reactions [52, 55, 59].

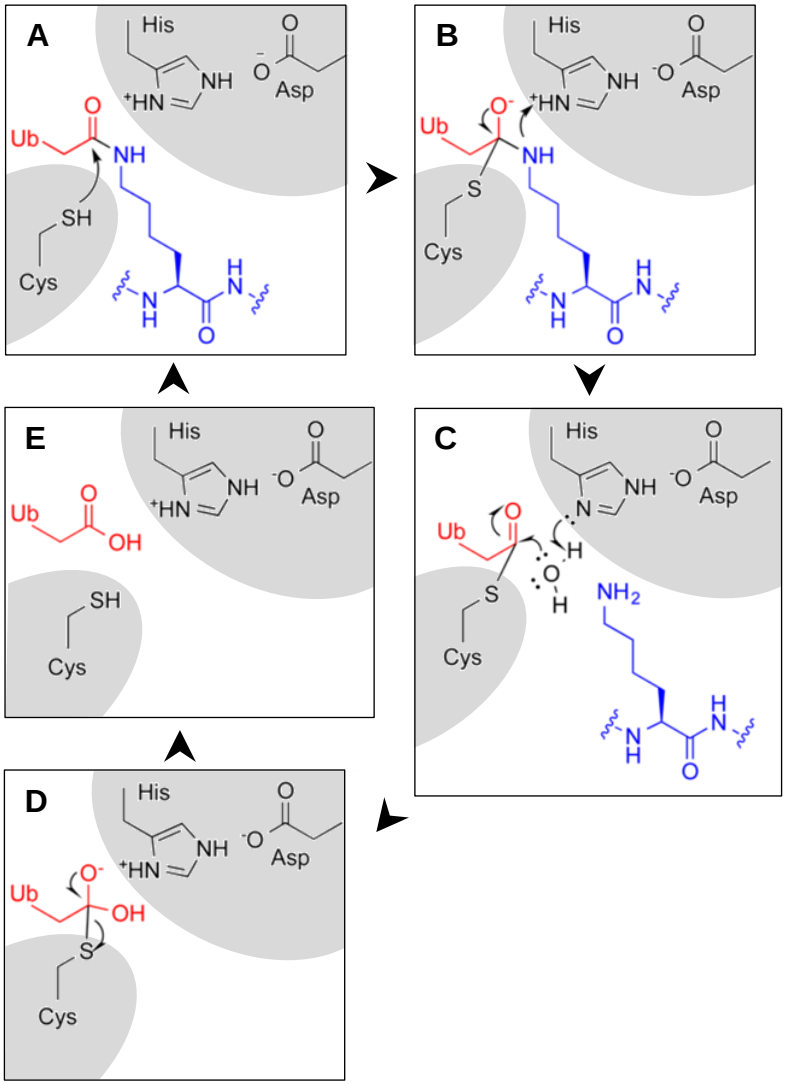

Figure 5. Molecular reaction mechanism of papain-like cysteine protease DUBs. The distal ubiquitin (C-terminus) is illustrated in red, the proximal ubiquitin (lysine side chain) in blue. The residues of the catalytic triad are presented in black, highlighted in light gray. Modified from Ndubaku & Tsui [59].

1.2.1.2 Metalloproteases

In contrast to the cysteine protease class DUBs, no covalent interactions between Ub-chain and enzymes occurs in JAMM metalloprotease DUBs although the general reaction mechanism is similar. As the term metalloprotease suggests, a Zinc ion (Zn^{2+}) is coordinated by aspartate (Asp) and two His residues and is serving as the active ion. Additionally, the substrate and a water molecule are coordinated by a serine (Ser) and Glu. At the beginning of the reaction (Fig 6A), the substrate is coordinated by Glu, Asp and Ser residues while a water molecule, activated by the Zn^{2+} ion, carries out a nucleophilic attack against the carbonyl carbon of the peptide bond. This attack results in a negatively charged tetrahedral intermediate state with Glu serving as a proton acceptor (Fig 6B). The collapse of the intermediate then leads to cleavage of the substrate chain and subsequently, both coordinated Ub-moieties are released (Fig 6C) [52, 55].

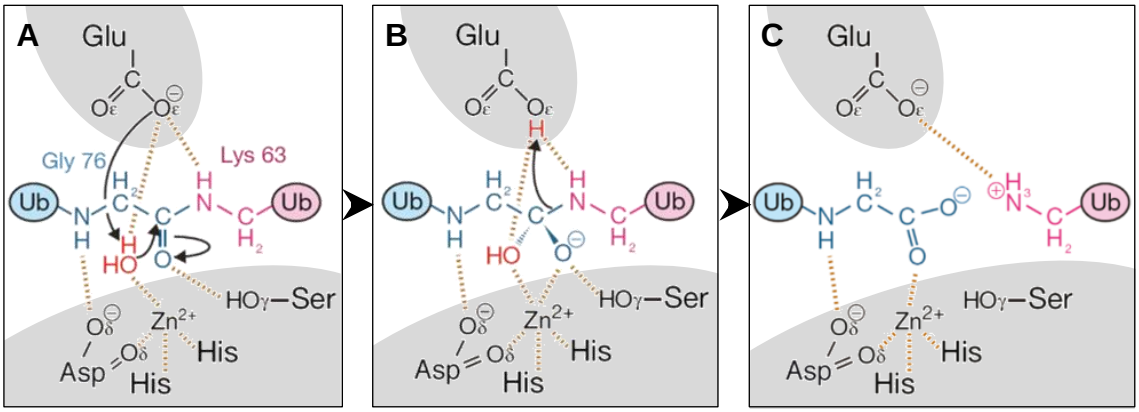

Figure 6. Reaction mechanism of JAMM metalloprotease DUBs. The proximal Ub is illustrated in pink, the distal ubiquitin in blue, the water molecule in red. The catalytically active residues are presented in black and highlighted in light gray. Orange dashed lines represent ionic interactions. Modified from Komander et al. [55].

1.2.2 DUBs in Immunity and Bacterial Infection

Apart from the roles of DUBs in physiological processes like DNA repair, control of receptors and channels and maintaining of the cellular ubiquitin balance [52], some DUBs were shown to be crucial mediators of deubiquitination in innate and adaptive immune responses [60].

For example, the USP-family deubiquitinase CYLD deubiquitinates TNF-receptor associated factors (TRAFs) and thereby downregulates nuclear factor kappa B (NF-κB) activation [61, 62]. Additionally, CYLD forms a complex with a Ub-ligase and, by chain editing from K63 to K48 chains, contributes to decreased inflammatory signaling [63, 64]. In combination, those findings suggest a potential value in inhibition of CYLD for control

of inflammation and infection [60, 65, 66].

Another example is the OTU-family DUB A20, which is NF-κB responsive and has dual deconjugating and ligating activities already mentioned above [58]. A20 is involved in a negative feedback-loop regulating NF-κB at various levels, e.g by chain-editing on RIP1 [58]. Furthermore, A20 competitively binds E2-conjugation enzymes and ubiquitinates them, thereby provoking shut-down of E3-ligases involved in NF-κB activation [58, 67] but also trims Ub-chains at other distinct protein complexes [68]. In contrast to CYLD, abolishment of A20 does not simply attenuate NF-κB-dependent processes, but shifts the cell or tissue homeostasis towards auto-reactivity and autoimmunity [68]. For example, an A20-knockout in dendritic cells (DCs) leads to a hyper-sensitivity of mice towards low doses of lipopolysaccharide (LPS) and subsequently to death [69].

Apart from these two prominent examples of deubiquitinating enzymes, several de-SUMOylases and the deISGylase USP18 are involved in processes related to immune responses [60]. Upon ISG15 induction, USP18 is also expressed during bacterial and viral infections. Furthermore, USP18 regulates interferon (IFN)-β stimulated proteins at the genome-level [60, 70] and knock-out mice show an increased susceptibility towards bacterial infections [52, 60].

1.2.2.1 DUBs in Bacterial Infection

Interestingly, DUBs do not only play a crucial role in immunity, but are also influenced by or influence themselves the course of infection with a whole series of pathogens [60].

CYLD, for example, is described as a negative regulator of *E.coli* pneumonia and *Haemophilus influenzae*-induced inflammation and potentiates *Streptococcus pneumonia* induced lethality [71–73]. In *Listeria monocytogenes (Lm)* infection, CYLD activity also impairs the antibacterial immune response by inhibition of receptor-interacting serine/threonine kinase 2 (RIPK2) and the interleukin (IL)-6/STAT3-mediated fibrin production [66, 74]. In contrast, the truncated form of CYLD, sCYLD, augments inflammatory responses in Lm infection [75] as does a deubiquitination-deficient truncation of CYLD [65]. Other USP-family DUBs were also found to be involved in bacterial infection:

- USP7 is decreased in *Helicobacter pylori* infection [76].
- USP10 is indirectly inhibited by the Cif toxin of *Pseudomonas aeruginosa* which stabilizes the USP10-G3BP1 complex [77].
- USP22 is required for *Francisella tularensis* replication [78].

Apart from the USP-family, also DUBs from other families were described to be involved in bacterial infection. OTUB1 attenuates bacterial internalization of *Yersinia enterocolitica* and *Y. pseudotuberculosis* [79], while UCHL1 promotes internalization of *Salmonella enterica* and *Listeria monocytogenes* [80].

1.2.2.2 Bacterial DUBs

In addition to the influence on host-DUBs that pathogens exhibit, some viral and bacterial pathogens did acquire or evolve enzymes with deubiquitinase activities, which allow the pathogens to directly interfere with the host ubiquitin-system. Most of the bacterial DUBs described so far are implicated in suppression of NF-κB activation or pathogen survival e.g. chlamydial ChlaDUB1, *Yersinia* YopJ or *Salmonella enterica* SseL and AvrA [60]. Notably, all of the bacterial DUBs identified to date are exclusively expressed by Gram-negative bacteria.

In general, it is becoming obvious that DUBs regulate a multitude of immune response-related processes and are of high importance for bacterial infections. Although functions in Lm infection were described recently, especially for CYLD, information on the activity of DUBs in the different stages of Lm pathophysiology is limited. To overcome this limits, so called activity-based probes are a valuable tool to characterize DUB abundance and activity.

1.3 Activity-based Probes for the Analysis of Deubiquitinating Enzymes

Activity-based probes (ABPs) are small constructs for labeling and enrichment of enzyme classes developed in the field of chemical proteomics for a multitude of enzyme classes. In contrast to classical proteomics approaches, enzymes are enriched or detected on the basis of their activity or affinity rather than sheer protein abundance [81]. As a consequence, by using these probes for activity-based protein profiling (ABPP), it becomes possible to assess the activity status of whole enzyme families [82]. Probes for the detection of DUB activities are targeted towards the nucleophile of the active cysteine, thereby allowing covalent labeling of cysteine-protease DUBs [83]. In general, DUB-probes comprise of three modules (Fig 7A), a recognition or retrieval element, a specificity element and a warhead also called reactive group. While warheads and recognition-groups are most variable, for the specificity element, Ub-, SUMO-, NEDD8-, ISG15- and UFM1-containing probes were utilized for the identification of active deconjugating enzymes until now [36, 84, 85]. Equipped with a combination of the mentioned modules, ABPs are utilized to label the DUB or deconjugating enzyme family of interest in gel- or blot-based applications, e.g. immunoblotting. Detection of the labeled enzymes *via* specific detection of a recognition element like an epitope-tag or fluorochrome enables the comparison of the DUB activities of different sample states (Fig 7 B). Furthermore, ABPs also allow for the enrichment of DUBs *via* a retrieval element like an epitope-tag or biotin and subsequent characterization of the enriched enzymes by mass-spectrometry [86]. In recent years, a battery of C-terminal electrophilic probes to label and enrich DUBs was designed, some of which are described below.

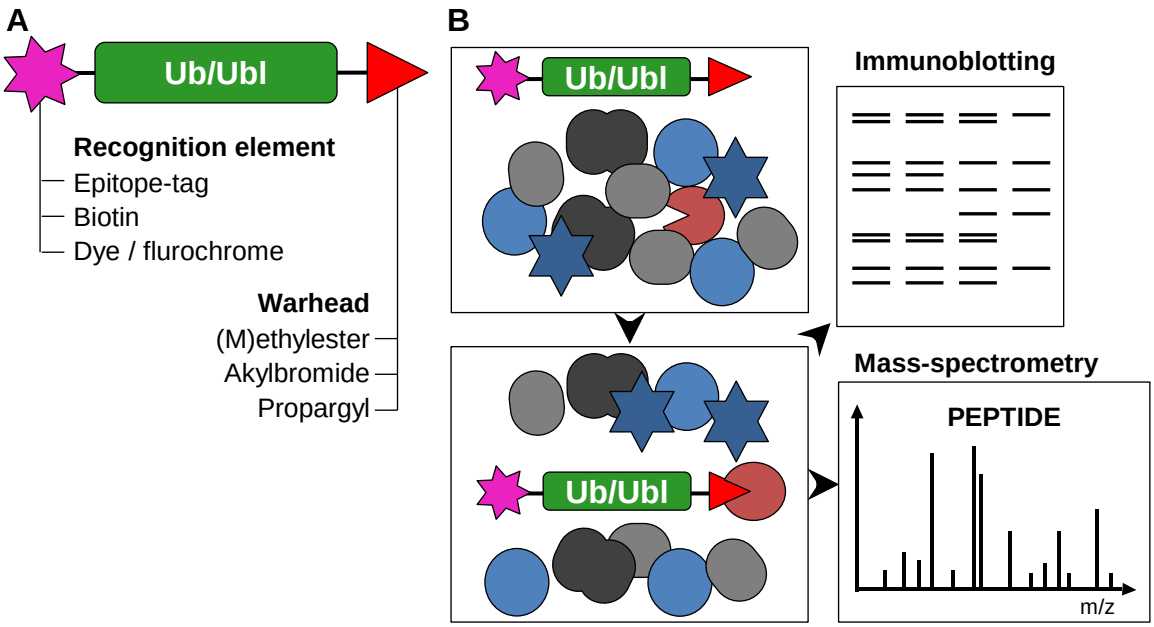

Figure 7. Key features of activity-based probes targeting Ub/UBLs and examples of application. (A) Classical activity-based probes for DUBs comprise of a recognition element (pink star), a specificity element, which is either a Ub-moiety or a UBL (green), and a reactive group also termed warhead (red). (B) Prototypic applications of DUB activity-based probes. Modified from Ekkebus et al. [83].

1.3.1 C-terminal Electrophilic Probes for DUB Profiling

The first C-terminal electrophilic probes for DUBs were designed in the Ploegh lab in the early 2000s [87,88]. Among them, two Michael acceptor warheads, vinyl methyl ester (VME) and vinyl methyl sulfone (VS) coupled to an HA-Ub construct showed broad reactivity towards DUBs, while bromoethylamine (Br_2) did bind to a smaller number of known DUBs but for the first time detected an OTU-family DUB [88]. Because of the labeling of fewer DUBs and the poor catalytic yield of HAUb-VS [89], HAUb-VME developed into a widely used gold-standard for activity-based DUB profilings. The second generation of HAUb-probes entailed 3 novel warheads with an unchanged HAUb construct. While these probes did not outperform HAUb-VME in its DUB-binding, two of the probes (HAUb-OEtVS and TF_3BOK) enriched enzymes of the Ub conjugation machinery [90].

The most recent additions to the DUB-reactive warheads in classical ABPs are C-terminal alkynes, e.g. propargylate and derivatives. Those probes allow an enrichment of DUBs which is at least comparable to HAUb-VME if not superior [91,92].

Additionally, not only warheads but also recognition elements were permuted to generate different probe types. McGouran and colleagues developed fluorescent probes

carrying the fluorescent group C-terminal of the VME-like warhead, reasoning that this position leaves the Ub-fold intact and requires minimal protein manufacturing [93]. Another change to the recognition element was introduced by Claessen and colleagues by adding biotin for enrichment and incorporating an additional, cleavable linker to minimize the background caused by unspecific binding of proteins to the Streptavidin beads [94].

However, those probes have limited substrate specificities: While DUBs often recognize either two or more Ub-moieties, or attached Ub and substrate protein simultaneously, all of the ABPs mentioned above fail to reproduce this distinct environment.

1.3.2 Probes Introducing Context-specificity

Recently, probe development led to the incorporation of context specificity especially for the surroundings of Ub-chains. DUBs often have 2 or even 3 binding pockets to recognize Ub-chain topologies and cleave their substrates from the proximal site (Fig 8A(1)). Thus, classical C-terminal probes, which solely bind to the S1 site, are not able to make use of the binding specificities of DUBs facilitated by UB-binding at the S1' or S2 sites (Fig 8A(2)) [83]. In order to overcome this limitations, a range of probes was developed which introduces further specificity elements to the probe design. Most of the concepts add a second Ub-moiety resulting in an internal Di-Ub probe, which then binds to the S1' and S1 binding sites of the captured DUB (Fig 8A(3)). Those Di-Ub probes aim to recreate the native Di-Ub peptide bond (Fig 8B1) as effectively as possible (Fig 8B(2-5)).

Ubiquitin-Isopeptide Probes (UIPPs): The first published Di-Ub probes were the so called Ubiquitin-Isopeptide Probes (UIPPs) refined and published during this study, which harbor a peptide as an additional specificity element (Fig 8B(2)) [95, 96]. Furthermore, a glycine vinyl formic acid (VA) warhead was included to covalently capture DUBs, thereby elongating the isopeptide bond by two atoms. Nevertheless, UIPPs mimicking K48 and K63 Ub linkages were produced and successfully utilized for labeling of recombinant deubiquitinases and DUBs in cell lysates thereby uncovering different binding specificities [95].

In contrast to the other concepts, which will be described below (Fig 8B(3-5)), UIPPs do not carry a full proximal ubiquitin moiety. This might cause decrease in facilitating Ub-linkage specificity, but is a considerable advantage for the profiling of substrate specificity (Fig 8A(4)). In this concept, merely the sequence of the peptide has to be interchanged for a substrate protein sequence to enable substrate specificity profiling [95, 96]. Additionally, substrates are mostly larger than a single Ub-moiety and it is thus more likely that the direct sequence surroundings of the Ub-binding site are involved in mediating specificity.

For the other Di-Ub concepts described so far, adaptation to substrate Ub-linkages would be possible in principle, but require new synthesis protocols to be designed for the

production of substrate-mimicking units.

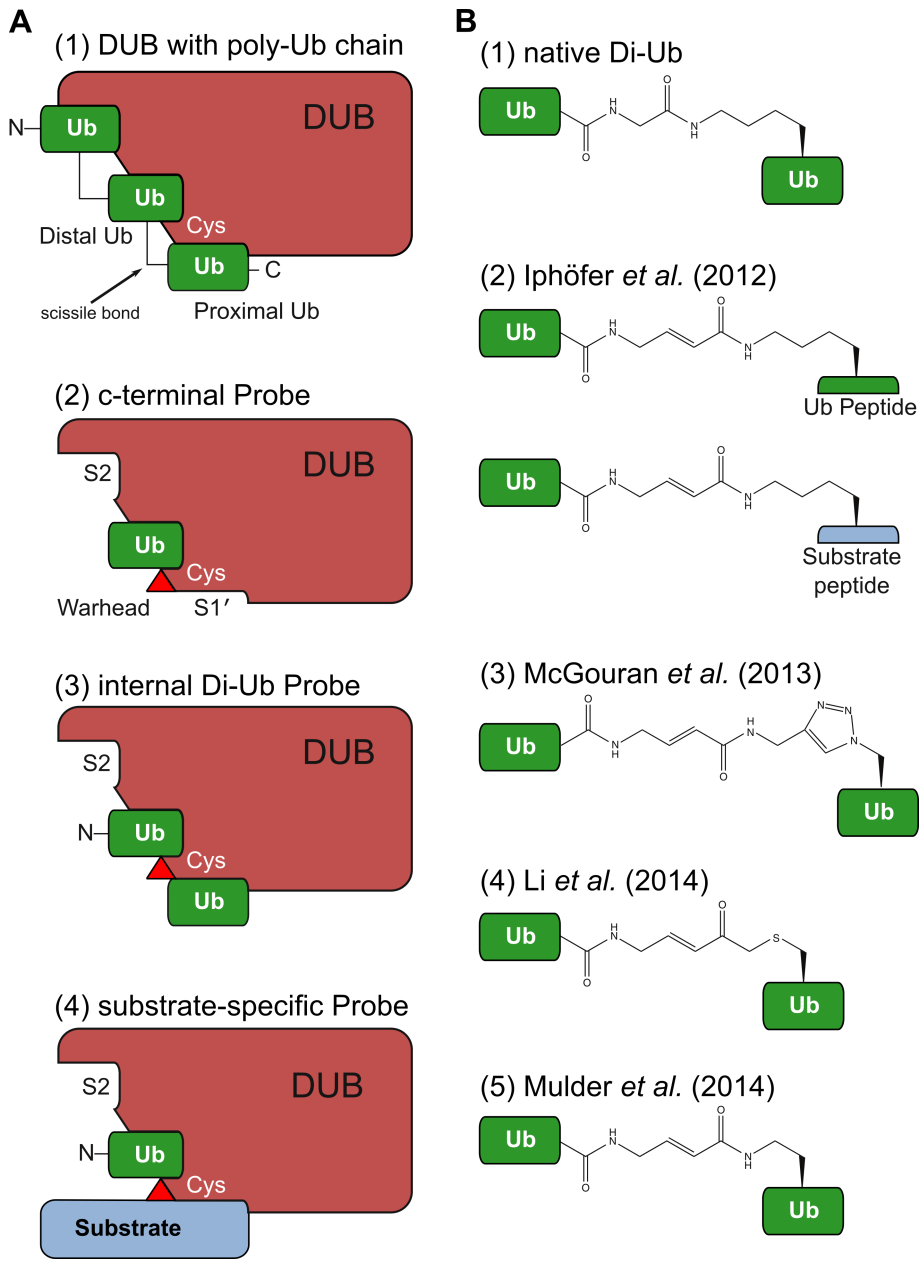

Figure 8. Schematic representation of DUB probe-binding and different probes resembling diubiquitin. (A) Ubiquitin and probe-binding modes of DUBs. (B) Overview of probes mimicking diubiquitin to uncover chain specificities of DUBs in comparison to native diubiquitin. The red triangle illustrates the position of the reactive warhead next to the active-site cysteine. Modified from Ekkebus et al. [83]

Other Di-Ub Probes: Apart from the UIPPs, further concepts for Di-Ub probes were implemented in recent years. McGouran and colleagues used click chemistry to produce full Di-Ub probes, which mimic all 8 Ub-linkages. Due to the similar warhead used and the added click chemistry handle, these probes also have an elongated linker (Fig 8B(3)). Especially for the M1 linkage, the authors speculate that this extended linkage influences DUB-binding and specificity [97]. While Li and colleagues also used a vinyl amide warhead in their Di-Ub probe (Fig 8B(4)), the linker between the 2 Ub-moieties closely resembles the native bond. To realize this shorter linker, lysines at the proximal Ub where mutated to cysteines [83, 98]. Another approach utilized chemical ligation to produce Di-Ub probes for K48, K63 and linear chains with a dehydroalanine warhead [99]. An interesting concept was presented by Mulder and colleagues, introducing a ligation handle, which is used to construct Di-Ub probes with a linker closely resembling the isopeptide bond of native Di-Ub (Fig 8B(5)). This approach resulted in a set of 7 Di-Ub probes which bound specifically to recombinant DUBs. Additionally, the introduction of the electrophilic warhead in the last step of the ligation allows for a broader spectrum of reagents as well as the synthesis of more complex structures [100]. In contrast to the described probes and concepts, Flierman and colleagues designed the first Di-Ub probes which bind to the S2 and S1 site of DUBs. Those probes revealed that DUBs indeed utilize those sites for the discrimination of Ub-chains [83] and are readily probable [101].

While a whole battery of different ABPs for the capture of DUBs was designed and produced in the last years, most studies focus on the initial characterization of probes either using recombinant enzymes or utilizing few cell lines, e.g. EL-4, to evaluate the binding properties of novel probes. In contrast, only few studies utilized probes to characterize samples of biological interest [102, 103], for inhibitor studies [104, 105] or to detect pathogenic DUB-activities [94, 106], leaving the potential of this concept largely unexploited.

1.4 *Listeria monocytogenes*

Listeria monocytogenes (Lm) is a Gram-positive, rod-shaped, pathogen with an intracellular life style, which is found ubiquitously in different environments e.g. soil, water, animals, humans and also various food products. By ingestion of contaminated food such as vegetables, meat or unpasteurized milk and cheese, the bacterium causes listeriosis, a foodborne disease [107, 108]. While healthy patients either present febrile diarrhea or are asymptomatic, in immunocompromised patients, the elderly and pregnant women as well as newborns, life-threatening symptoms like meningitis, miscarriage or stillbirth, sepsis and bacteremia may occur. Although the incidence of listeriosis in general is as low as 0.1-0.9 cases per100,000 inhabitants (EU, 2011) the mortality is very high, ranging from 20 to 30 % [108] and the incidence is rising constantly in the last years [109]. In

Germany, listeriosis is counted among the diseases with the highest mortality regarding those subjected to registration [110], and is therefore a great public health concern as a re-emerging disease.

1.4.1 Cell Invasion

Lm as an intracellular bacterium is able to invade different cell types, including enterocytes, hepatocytes, fibroblasts, as well as epithelial and endothelial cells [107]. While the entry into phagocytic macrophages, which are a major target of Lm, is passive, entry-processes into non-phagocytic cells are triggered by bacterial proteins [107].

Entry: To enter those cells, Lm binds to the cell surface utilizing its invasins Internalin A (InlA) and Internalin B (InlB) in combination or separately (Figure 9). The cellular receptor of InlA is the adhesion molecule E-cadherin, which is involved in adherens junction formation [111]. InlA-mediated invasion is species specific, as InlA interacts with human, guinea pig, and rabbit E-cadherin but not with the mouse and rat homologs. Thus, oral infection of the latter organisms is ruled out, since Lm cannot cross the intestinal barrier in these species, as the process is InlA-dependent [112].

The second internalin implicated in cell entry, InlB, interacts with the hepatocyte growth factor receptor (HGFR/c-Met) functionally mimicking its natural ligand HGF, as well as glycosaminoglycans and the receptor of the globular part of the complement component C1q (gC1q-R) [111]. Furthermore, involvement of the transmembrane glycoprotein CD44v6as a co-receptor of c-Met is suggested [113]. However, the role of the latter three interactions is not clearly defined [114–116]. The InlB/c-Met invasion-axis is also species-specific, allowing invasion in human, gerbil, mouse and rat but not in rabbit and guinea pig [112]. Both invasins trigger rearrangement of the actin cytoskeleton and endocytosis to facilitate cell invasion [111]. In addition, another virulence factor, Vip, interacts with host Gp96 and crucially supports Lm infection *in vivo* [108, 117].

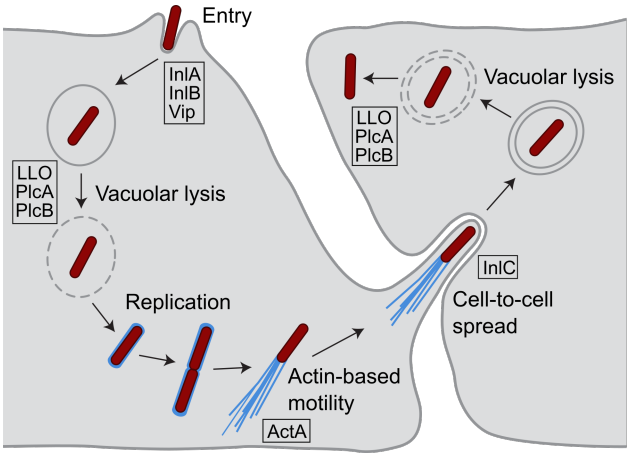

Figure 9. Invasion, replication and cell-spread of Lm in epithelial cells. *Listeria* enters epithelial cells, disrupts vacuoles and, following replication, spreads to neighboring cells, thereby allowing dissemination through tissue-barriers as well as formation of reservoirs. Different stages of cell invasion are driven by listerial proteins which are presented in small boxes. InlA: Internalin A, InlB: Internalin B, InlC: Internalin C, LLO: Listeriolysin O, Plc: Phospholipase, ActA: actin assembly-inducing protein. Modified from Pizarro-Cerda et al. [111].

Vacuolar Lysis and Cell-to-cell Spread: Following entry, Lm accomplishes rupture of the bacteria-containing phagosomes to escape to the cytoplasm by utilizing its pore-forming toxin listeriolysin O (LLO) as well as phospholipases A and B [108]. Once in the cytoplasm, Lm is able to replicate and subsequently establish motility by polymerization of host actin [112]. With the help of ActA, the actin assembly-inducing protein of Lm, the bacterium recruits host components, e.g. the Arp2/3 complex, Enabled/vasodilator-stimulated phosphoprotein (Ena/VASP) and profilin to finally bind actin and form comet-tails driving motility and cell-to-cell spread [118]. Interestingly, ΔActA mutants of Lm are rapidly ubiquitinated and targeted to autophagy [119], revealing ActA-coating as a potent interfering mechanism to subvert Ub-mediated host-processes.

Contact of the motile Lm with the cell membrane leads to formation of bacteria-containing protrusions, allowing invasion of neighboring cells by utilizing another listerial internalin, InlC [112]. Lysis of the secondary vacuole is dependent on LLO and phospholipases B and C, and releases Lm into the cytoplasm of the newly infected cells [120].

1.4.1.1 Activation of c-Met by InlB

As briefly mentioned earlier, InlB binds to c-Met and activates the receptor-tyrosine kinase by mimicking HGF despite of the structural and sequence differences between the two ligands [121]. HGF consists of an α- and β -domain and interacts with the propeller-like Sema-domain of c-Met (Fig 10A) [122]. In contrast, InlB mainly interacts with the IgG-domains of c-Met, while only a small patch of the InlB inter-repeat shows binding to the Sema-domain [123]. Most interestingly, although both ligands bind to c-Met utilizing different surface patches of c-Met, both, HGF and InlB, evoke auto-phosphorylation and activation of c-Met and down-stream signaling components [121, 124].

Signaling: A prominent example of downstream signaling cascades is the Ras-MAPK axis. Recruitment of adapter molecules like GRB2 leads to the activation of small GTPases, e.g. Ras, the mitogen-activated protein kinase (MAPK) cascade. As a consequence, terminal kinases like Erk1/2, JNK or p38 kinases are activated (Fig 10B) by HGF and InlB alike, albeit with slightly different dynamics [124–126]. Finally those kinases translocate to the nucleus, inducing different gene expression programs leading to proliferation, transformation, differentiation and apoptosis [126]. Another commonly activated transcription factor is the Signal transducer and activator of transcription 3 (STAT3), which upon phosphorylation, homodimerizes and also controls cell proliferation and transformation [127, 128]. Furthermore, HGF-mediated activation of c-Met leads to activation of the Phosphoinositide 3-kinase (PI3K)-Akt axis, either directly, or indirectly via Ras. This axis ultimately activates further components, thereby augmenting protein translation, cell growth and proliferation, and furthermore protects cells from apoptosis [126]. Notably, PI3K-activation is critical for Lm to breach host barriers [129].

Additionally, NF-κB is activated downstream of PI3K-Akt or Src-kinase signaling both by HGF and InlB [126]. While in HGF-mediated signaling the induced proliferation and survival benefits the cell, the immune-regulatory functions of NF-κB pose a problem for *Listeria*.

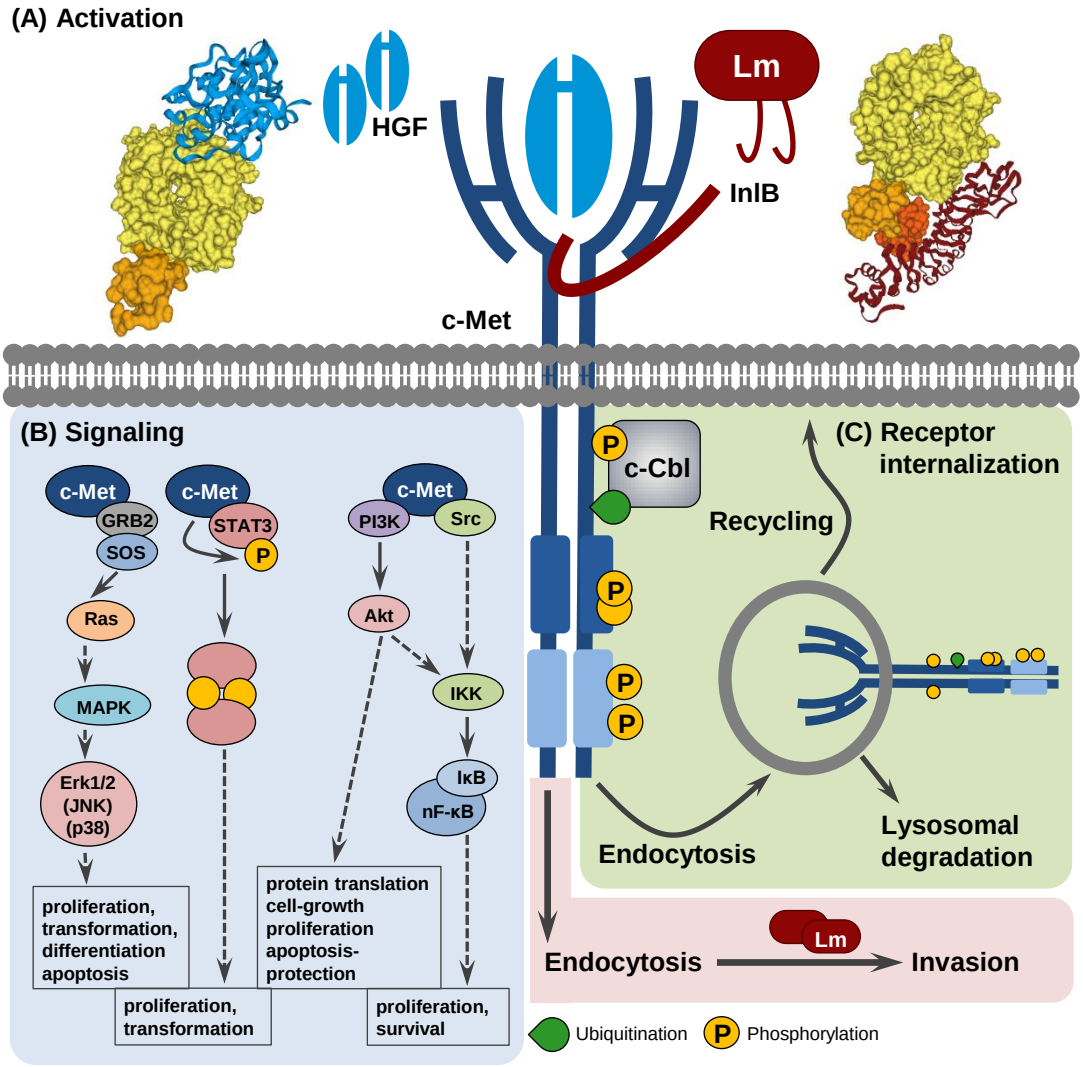

Figure 10. Overview of c-Met activation, signaling and receptor recycling following binding of HGF or InlB (*Listeria*). (A) Activation of c-Met by HGF or InlB interaction. Blue structure: ß-chain of HGF, yellow: c-Met Sema-domain, orange: c-Met PSI and IgG-domain, red: InlB. Structures modified from Stamos and Niemann et al. [122, 123] (B) Downstream-signaling following activation. SOS: son of sevenless, GRB2: growth factor receptor-bound protein 2, MAPK: mitogen-activated protein kinase, STAT3: Signal transducer and activator of transcription 3. Modified from Trusolino et al. [126]. (C) Receptor fate after activation.

Interestingly, InlC, which was described in the context of cell-to-cell spread, on a molecular level interferes with this signaling cascade by targeting IκB and thereby dampening NF-κB activation [130].

Receptor Internalization: Apart from the shared signaling cascades, both HGF and InlB induce internalization of c-Met with similar dynamics *via* a clathrin-mediated endocytosis mechanism [111, 124, 126]. More recently, also clathrin independent mechanisms were debated [131, 132]. However, the initial event leading to endocytosis is the post-translational modification of c-Met (Fig 10C). Following auto-phosphorylation of c-Met at the tyrosines (Y) 1234 and 1235 as well as Y1003, the ubiquitin-ligase c-Cbl is recruited and ubiquitinates c-Met presumably in form of a multi-monoubiquitination or K48 poly-Ub chains [133–136]. Although 13 ubiquitinated lysines are described for c-Met (Table S1), the precise sites which are ubiquitinated following activation by HGF or InlB are not known so far and knowledge of the role of ubiquitination and involvement of DUBs is inconclusive until now [132, 134, 135, 137].
After endocytosis, c-Met is sorted to multivesicular bodies via recruitment of the endosome-localized hepatocyte growth factor-regulated tyrosine kinase substrate (Hrs). Subsequently, the receptor is targeted to lysosomal degradation [132]. In recent years, receptor recycling of c-Met was described in different settings after HGF-stimulation or constitutive activation [138–140]. While for the related receptor tyrosine kinase EGFR (epidermal growth-factor receptor) the processes themselves and the contribution of ubiquitination are well described, knowledge for c-Met is limited [132, 136].

Although qualitative differences between HGF and InlB-induced endocytosis and signaling were described previously [124, 141, 142], addition of HGF is sufficient to evoke invasion of InlB-deficient Lm mutants, suggesting major analogy between HGF and InlB [143].

1.4.2 *Listeria monocytogenes* Infection

To cause the fatal symptoms of listeriosis mentioned earlier, Lm has to evade the host immune system and disseminate from the gastrointestinal tract. After ingestion of contaminated food, Lm is able breach of the intestinal barrier by rapid transcytosis in an InlA-dependent manner (Figure 11) [144]. The significance of InlA is further emphasized by the occurrence of functional InlA in 96 % of clinical as compared to 65 % in food isolates [145]. After crossing of this first barrier, Lm is able to reach the bloodstream *via* intestinal lymph nodes and then to cause a systemic infection. Interestingly, shortly after dissemination into the bloodstream, *Listeriae* are already engulfed by dendritic cells (DC) in the spleen where bacterial killing is initiated [146, 147]. In total, only 5 to 10 % of the bacteria are taken up by the spleen, while 90 % of the inoculum in intravenous infection ends up in the liver and leads to mounting of a systemic immune response

towards Lm. However, surviving Lm replicate within macrophages in the spleen and liver, reaching a peak at about 2- 3 days after infection [148]. Besides the reservoirs in liver and spleen, Lm is able to break through the blood-brain and placental barriers alike. Notably, crossing of either of those barriers was reported to require InlA and InlB activities interdependently [149, 150].

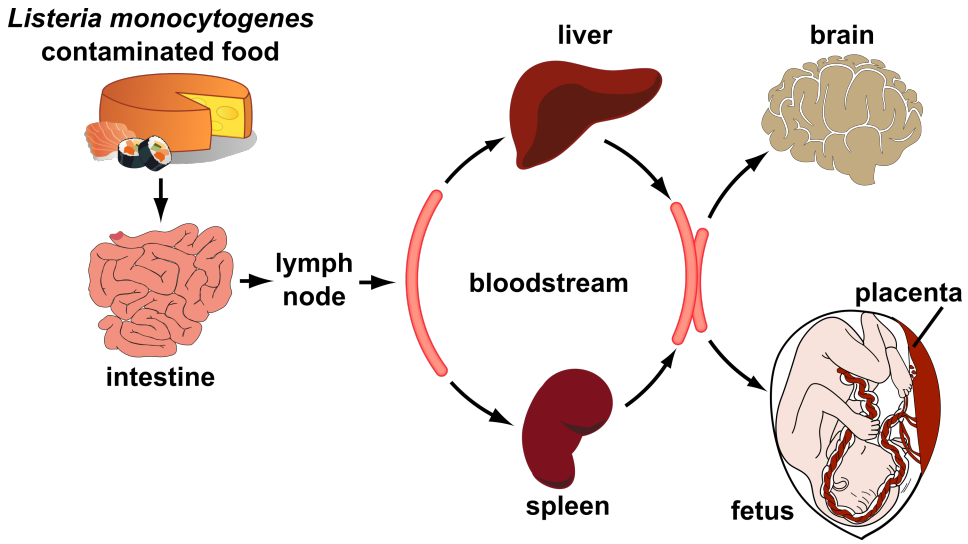

Figure 11. Steps of Lm infection *in vivo* causing Listeriosis. After ingestion, Lm crosses the intestinal barrier and disseminates systematically. Modified from Cossart and Toledo-Arana [151].

1.4.2.1 Cellular Hepatic Immune Response to *Listeria monocytogenes* Infection

Kupffer Cells, Neutrophils and NK Cells: Upon systemic infection of the host, high numbers of Lm enter the liver, where they are trapped by Kupffer cells (KCs) which are the liver resident macrophage population (Fig 12). Additionally, KCs can promote an inflammatory response by producing a number of cytokines including interleukin (IL) 1β and 6 as well as tumor necrosis factor alpha (TNFα) [152]. However, the major signal orchestrating the bactericidal inflammation in liver is the rapid Lm-induced necroptosis of KCs. Those cells, which are then heavily infected with Lm, die as early as 4 h after infection [153].

However, KCs as well as hepatocytes are capable of receptor-mediated activation of IL-23 recruited neutrophils [154], which also contribute to Lm clearance, especially in high-dose infections. Although different mechanisms for that protective effect, e.g. direct killing of bacteria or stimulation of hepatocyte apoptosis, are discussed, recent results suggest elimination of dead KCs and TNFα -secretion as probable functions [152, 153, 155].

In turn, TNFα in synergy with secreted IL-12 drive NK cell activation and subsequent

IFNγ secretion. Interestingly, excessive IFNγ production by a specific NK cell subset is advantageous to Lm as it impairs migration of phagocytic cells. Indeed, the listerial protein p60 evokes the activation of host NK cells [156, 157]. Nevertheless, IFNγ also confers resistance against Lm to hepatocytes, which are the major pool of intracellular and associated *Listeriae* during liver infection [152].

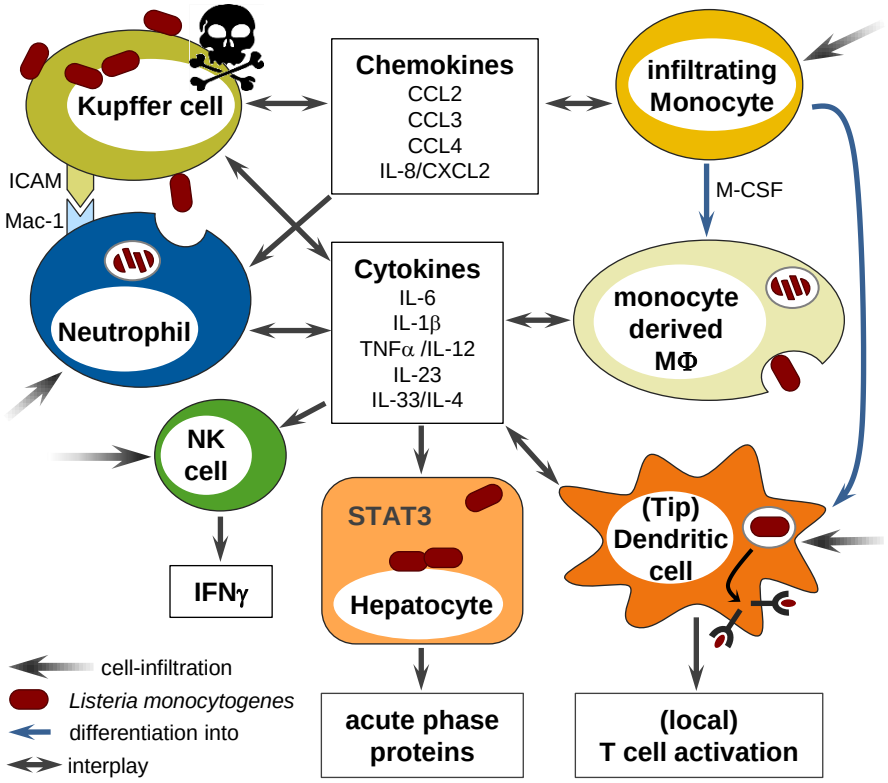

Figure 12. Immune responses to hepatic Lm infection. Schematic representation of different cell types, cytokines and chemokines involved in the hepatic immune response to Lm. ICAM: intercellular adhesion molecule, Mac-1: macrophage-1 antigen, CCL: chemokine (C-C motif) ligand, CXCL: chemokine (C-X-C motif) ligand, IL: interleukin, TNF: tumor necrosis factor, IFN: interferon, STAT: Signal Transducers and Activators of Transcription, M-CSF: macrophage colony-stimulating factor, NK cell: natural killer cell, MΦ: macrophage, Tip: tumor necrosis factor/inducible nitric oxide synthase-producing. Adapted from Cousens and Wing [152].

Hepatocytes: Although hepatocytes are not professional immune cells, they contribute to the immune response against Lm in different ways e.g. by killing of Lm, apoptosis, interaction with other immune cells and secretion of cyto- and chemokines [152]. Most importantly, hepatocytes also mount the systemic so-called acute-phase response (APR) by secreting a whole arsenal of proteins aiming at the neutralization of invading pathogens

as well as the limitation of tissue damage and promotion of repair processes [152, 158]. Major regulators of the APR in hepatocytes are STAT3 and its crosstalk with NF-κB-dependent signaling pathways [158]. Interestingly, STAT3, which is induced by IL-6, is tightly regulated by deubiquitination facilitated by CYLD, and while a short form of this deubiquitinase augments innate immunity, full-length CYLD restricts the immune response towards Lm [66, 74, 75].

Infiltrating Monocytes, Macrophages and TipDCs: During the first days of infection, inflammatory monocytes massively infiltrate the liver guided by a chemokine (C-C motif) ligand 2 (CCL2) gradient created by the liver itself [159]. Once at their destination, they rapidly differentiate into monocyte-derived macrophages (MoMs) or tumor necrosis factor/inducible nitric oxide synthase-producing dendritic cells (TipDCs) [153, 160] (Fig 12). TipDCs can serve as antigen presenting cells (APCs) during early infection, locally activating $CD8^+$ T cells following contact to Lm [161] and releasing TNFα and nitric oxide (NO). In contrast, conventional DCs serve as APCs by migration to neighboring lymph nodes and activate $CD8^+$ T cells at a systemic level [148]. Once differentiated, MoMs heavily proliferate as a response to hepatocytes-secreted IL-33 and exhibit a highly bactericidal phenotype by producing reactive oxygen species (ROS) and nitric oxide synthases (NOS) [148]. Notably, at day 3 p.i., once bacterial loads are successfully controlled by the innate immune response, monocytes shift to an anti-inflammatory, KC-like phenotype. This shift is initiated by increasing IL-4 levels in the liver. Thus, acute inflammation is dampened and the liver is protected from excessive tissue damage allowing the return to homeostasis [153].

Adaptive Immune Response: By way of DCs, both $CD4^+$ and $CD8^+$ T cells are activated following Lm infection, and cytotoxic CD8 cells were found to be crucial for complete Lm clearance [148]. To realize their anti-listerial role, CD8 T cells secrete IFNγ to activate macrophages and additionally lyse infected cells by targeted excretion of perforin and granzymes [162]. This primary T cell response reaches its peak at day 7 to 9 p.i and then decreases between days 9 and 14 [163]. In contrast, B cells only play a minor role during Lm infection as antibodies are of limited use against intracellular pathogens. However, B cells are involved in stimulation and maintenance of the T cell response [148, 162].
In general, the hepatic immune response to Lm is a sophisticated system composed of interacting cell types and secreted messengers. Although some aspects were extensively researched, protein regulation leading to the described phenotype often remains elusive.

1.5 Sepsis - a Life-threatening Manifestation of Listeriosis

As mentioned previously, listeriosis may be accompanied by life-threatening symptoms, especially in the elderly and immunocompromised patients [164]. In Germany, 609 cases of listeriosis were reported to the Robert Koch Institute in 2014 of which 34 were pregnancy-related and 29 newborn-listeriosis cases. The evaluation of the data revealed a generally increasing incidence in recent years with a saltatory increase of about 30 % in 2014 as compared to the previous year [110]. Furthermore, Preussel and colleagues report an outstanding role of reduced immunocompetence for listeriosis acquisition and identify cold cooked sausages as well as pre-sliced and packed cheese irrespective of variety as main sources for infection in Germany [164]. In conjunction with a reported mortality of listeriosis ranging between 15 and 30 % despite of adequate treatment [109], listeriosis poses a major health care problem as a re-emerging disease.

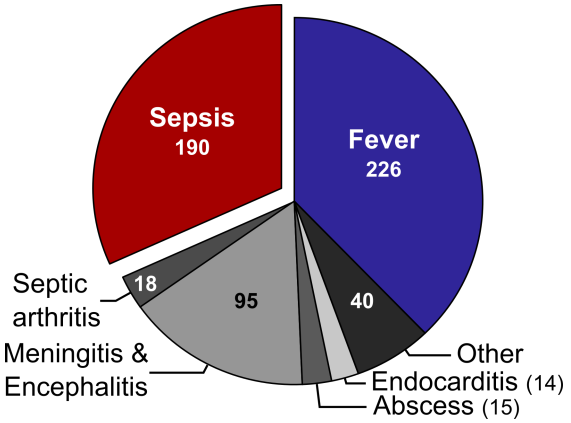

Figure 13. Manifestations reported for listeriosis cases in Germany in 2014. Data were taken from the annual of notifiable diseases 2014 (Infektionsepidemiologisches Jahrbuch meldepflichtiger Krankheiten für 2014) published by the Robert Koch Institute [110]. The slice representing sepsis cases is colored in red, while mild listeriosis cases with fever as only symptom are represented in blue. In total, 546 cases of non-pregnancy associated listeriosis were reported in 2014, whereby reporting of multiple symptoms was allowed.

Of the cases of non-pregnancy associated listeriosis reported in 2014, 41 % showed fever as only symptom representing disease progression without complications (Fig 13). Notably, of the severe manifestations reported, sepsis was the most common with 35 % and thus nearly as frequent as uncomplicated cases [110]. In contrast, meningitis and encephalitis, which show comparable mortalities were reported in 17 % of all cases, while abscesses, endocarditis, septic arthritis and infections of other organs were less frequently reported (Fig 13).

Sepsis, often found in listeriosis, is indeed a major problem in medicine and a leading cause of death with word-wide increasing case numbers. The rapid progression often leads to multi organ dysfunction and thus, to a high mortality even in intensive care units (ICUs) [165, 166].

1.5.1 Course of Sepsis Progression

Sepsis, which is a life-threatening syndrome and not a disease *per se*, is classically defined based on clinical criteria [167]. The foundation for diagnostics is the definition provided

by Levy and colleagues, which is widely used in critical care and is based on the concept of "systemic inflammatory response syndrome" (SIRS) introduced in 1992 [168, 169].

SIRS: SIRS is likely to be caused by a number of infectious and non-infectious conditions and occurs in patients without infection after trauma, thermal injury and inflammatory processes as a part of the systemic immune response [169]. Clinically, SIRS is defined by the following four criteria (Fig 14):

- abnormal body temperature, defined as either fever with a core temperature above 38 °C or hypothermia with a temperature less than 36 °C,
- an increased heart rate with more than 90 beats per minute (bpm), or 2 standard deviations (SD) above the normal value for the patient age,
- an increased respiratory rate of 20 breaths per minute (Tachypnea) or a partial pressure of Carbon Dioxide in arterial blood ($PaCO_2$) smaller than 32 mmHg,
- abnormal white blood cell (WBC) counts with less than 4,000 or more than 12,000 cells per µl, or more than 10 % immature forms [168, 170].

The extended definition added additional criteria, e.g. altered mental status, hyperglycemia, hyperlactatemia and altered levels of C-reactive protein as well as procalcitonin in plasma. Furthermore, a whole list of hemodynamic parameters was proposed [169]. However, clinical studies often use the simplified four-point definition of SIRS only [165,171,172], as the extended one was primarily established to enable safe diagnostics in ICUs.

Sepsis: Sepsis is defined by the occurrence of at least 2 out of 4 SIRS criteria or "some" of the extended criteria and a strongly suspected or documented infection (Fig 14) [168, 169]. For the diagnosis, early signs of the immune response to infection are sufficient, even if the infection itself is not verifiable [169]. The diagnosis of sepsis is not limited to bacterial infections but includes fungi, parasites and viruses as infectious agents [170]. Notably, not all patients developing a sepsis show two or more SIRS criteria. In a recent study, 1.5 % of the screened patients developed dysfunction of organs and had an infection while displaying less than 2 criteria [165]. Additionally, not all patients that meet the SIRS criteria and display an infection are categorized as septic by clinicians due to the distinct characteristics of some infections, e.g. mild viral respiratory tract infections. Thus, the latest perception of sepsis is "that [it] arises when the body's response to an infection injures its own tissues and organs" [173, 174].

Nevertheless, the mortality rate of patients diagnosed with sepsis is estimated at 10 to 20 % and the estimated incidence is 75 to 120 cases per 100,000 population and is rising [165, 170].

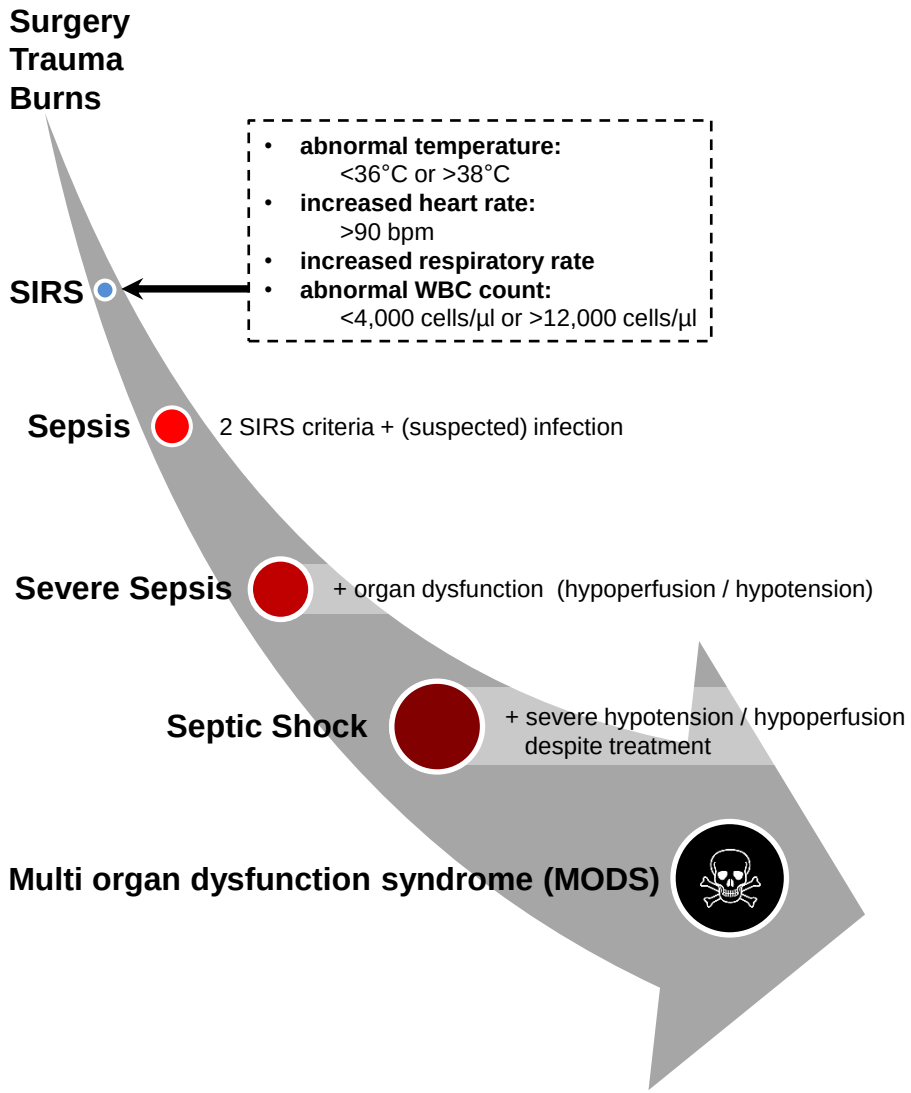

Figure 14. Emergence and progression of sepsis. Clinical criteria for the different states of sepsis are given, starting from the classical 4-criteria definition of systemic inflammatory response syndrome (SIRS). bpm: beats per minute, WBC: white blood cells. Definitions were assembled according to the consensus definitions of sepsis published by the ACCP/SCCM in 1992 [168]. For extended definitions, see full text.

Severe sepsis: In case of hypotension, tissue hypoperfusion, which can not be explained by other causes than sepsis, or sepsis-induced organ dysfunction, the syndrome fulfills the definition of severe sepsis (Fig 14) [168, 169]. Hypoperfusion and hypotension may lead to blood overacidification (lactic acidosis) and urine hypoproduction (oliguria) as visibly symptoms used for diagnosis [175]. Along with the occurrence of organ dysfunction, the

estimated fatality rate increases to 20 to 50 %, a recent study from Engel and colleagues even reported a mortality of 55 % for severe sepsis in German ICUs [165, 170].

Septic shock, multi organ dysfunctions and persistent critical illness: If organ dysfunction, hypoperfusion or hypotension persist despite of fluid resuscitation, patients are classified as presenting a septic shock (Fig 14) [168] which once again raises the estimated fatality rates to then 40 to 80 % [170].

After first organ dysfunctions occur, the syndrome often and quickly progresses towards a multi organ dysfunction syndrome (MODS), which is diagnosed when homeostasis cannot be maintained without intervention [169]. Due to exogenous organ support, patients that would have died few years ago often survive but can develop persistent critical illness (PCI). PCI has an estimated mortality of 20 to 40 % and patients are frequently disabled [176].
While mortality of sepsis, severe sepsis and septic shock decreases due to improving ICU management [170, 177], the incidence increases world-wide, making sepsis a major cause of death in hospitalized patients and a burden for the health care system [165, 176].

1.5.2 Assessment of Sepsis and Prognosis of Progression - Current Methods and Limitations

As sepsis is a syndrome and not a disease, diagnostics rely on physical examination, radiographic and laboratory testing and often the clinician's assessment that a patient "looks septic" [169, 178]. To assess a patient's status, several methods are applied dependent on the purpose of the assessment. Among physicians, different scoring systems are in use especially in ICUs, while academic scientists are in search for one or more reliable diagnostic biomarkers [179]. The ultimate goal of this search is not only to define sepsis by molecular markers, but to also enable distinction between SIRS and sepsis as well as the different sepsis stages, and finally to predict the individual course of the syndrome [179, 180].

Scores: In critical care medicine, scoring systems are utilized to describe a patient's status and in part to predict the course of sepsis progression. Three prominent examples are

- the sepsis-related/sequential organ failure assessment (SOFA),
- the acute physiology and chronic health evaluation II (APACHE II)
- and the simplified acute physiology score (SAPS II).

Additionally, a whole battery of other scoring systems exists [181–184]. To indicate the capacity of these systems to discriminate between patients that die and patients that

survive, the area under the curve of the receiver operating characteristic (AUCROC) is utilized. A perfect test would yield a value of 1, while a result of 0.5 is no better than chance alone. For predictive scoring systems, values above 0.8 are considered good, above 0.9 excellent. While SOFA is a solely descriptive score, assessing the patient's status each day, SAPS II and APACHE II allow an outcome-prediction with an AUCROC of 0.86 for both [184].

However, despite the remarkable predictive power of scoring systems, they do neither contribute to the development of drugs against sepsis nor to the biochemical characterization of underlying processes.

1.5.2.1 Biomarkers in Sepsis

In recent years, several molecular markers were suggested, that are either of diagnostic value, allowing discrimination between SIRS and sepsis, or of prognostic value, predicting progression or outcome of the syndrome, or ideally both [179].

A first class of potential biomarkers includes molecules present in body fluids, especially blood (Fig 15A). The main advantage of those molecules is the relatively simple access through blood sampling and serum extraction.

C-reactive Protein: C-reactive protein (CRP) is synthesized in the liver during acute-phase response and serves as a pattern recognition receptor (PRR) to activate the complement system [185]. Following secretion, CRP is found in blood plasma. In sepsis diagnostics, CRP is utilized to distinguish between non-infectious SIRS and bacterial infection especially in pediatrics [179, 186]. While the AUCROC for this application is relatively good (0.77-0.92), due to its low specificity, CRP can not distinguish between sepsis and other infection-related syndromes caused by bacterial infections [187, 188].

Procalcitonin: Another acute-phase protein, procalcitonin (PCT), the precursor of the hormone calcitonin, is also considered a biomarker for sepsis. Its serum concentration rapidly increases following bacterial, fungal, or parasitic infection [180]. Furthermore, the levels again decrease upon recovery after peaking at 24 to 48 h of infection, linking long-lasting elevated levels with poor prognosis [180, 187]. However, although recent studies indicate a role as indicator for sepsis, the results are not conclusive, hinting towards a non-sufficiency as a stand-alone marker [180, 188, 189]. Although PCT showed a good sensitivity and specificity for discrimination between sepsis and non-infectious SIRS [190], in practice, PCT levels are only moderately more predictive than CRP or the infection probability score (IPS), which is a combination of 6 parameters [180]. Furthermore, PCT is not detectable in some sepsis cases, increasing the risk of false negative results [189].

Angiopoietins: Two angiopoietins (Ang-1 and Ang-2) are antagonistic factors, which compete for the tyrosine kinase receptor Tie2 on endothelial cells [179]. While in healthy people Ang-1 levels are higher than Ang-2 levels, Ang-2 levels increase in inflammation, as Ang-2 is released by endothelial cells (Fig 15A). This shifts the Ang-1 / Ang-2 equilibrium and causes leakage in microvasculature leading to endothelial activation or even dysfunction [180]. In sepsis, both Ang-1 and Ang-2 levels are considered as prognostic biomarkers. While low Ang-1 levels at submission to the ICU are associated with a poor prognosis, Ang-2 levels correlate with scores of APACHE and SOFA, which assess the severity of sepsis [191, 192]. However, before angiopoietin levels are usable in a clinical environment, analytical methods, thresholds and sample collection protocols need to be defined clearly [180, 192].

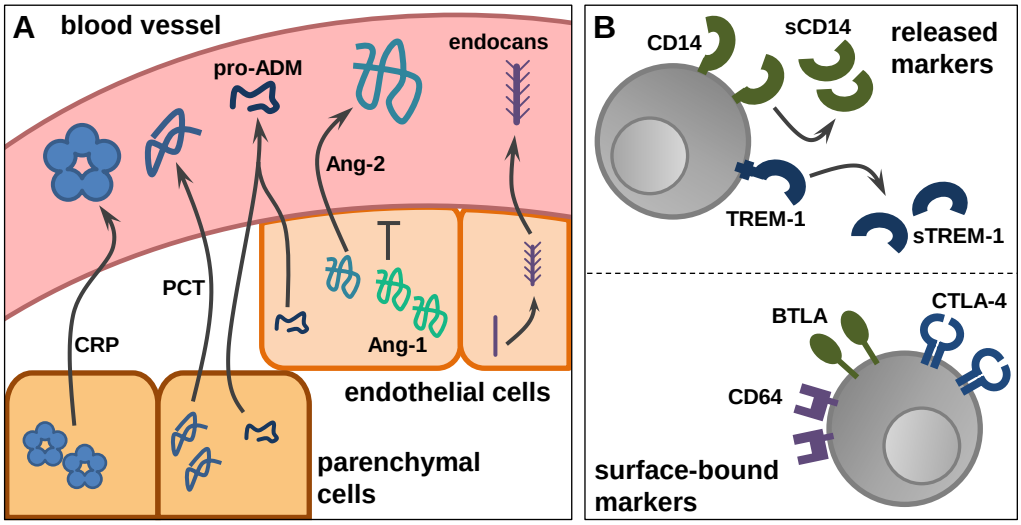

Figure 15. Biomarkers in sepsis. (A) Biomarkers detectable in serum. (B) Surface molecules of immune cells proposed as biomarkers either in a released or surface-bound state. Abbreviations: C-RP: c-reactive protein, PCT: procalcitonin, pro-ADM: proadrenomedullin ,Ang-1: Angipoeitin-1, Ang-2: Angiopoeitin-2, uPAR: Urokinase plasminogen activator surface receptor, CD14: cluster of differentiation 14, TREM-1: Triggering receptor expressed on myeloid cells 1, sTREM-1: soluble TREM-1, CD64: Fc-gamma receptor 1 (FcγRI), CTLA-4: cytotoxic T-lymphocyte-associated protein 4, BTLA: B- and T-lymphocyte attenuator.

Proadrenomedullin: Proadrenomedullin (pro-ADM), secreted by a multitude of tissues, is the stable pro-hormone of ADM, which has vasodilatory and immune modulating functions and is implied in organ blood supply [187]. Pro-ADM is suggested as a prognostic biomarker correlating with increasing severity and death but with no diagnostic value for sepsis [187, 193].

Endocan: Endocan is a proteoglycan produced in endothelial cells and released as a response to inflammatory stimuli [179]. Recent studies proposed a correlation between endocan release into blood and severity of sepsis, occurrence of organ dysfunction and mortality [179]. However, elevated endocan synthesis and release are not specific for sepsis but also discussed as a marker for tumor progression and acute lung disorders [194].

In contrast to the molecular markers present in blood and body fluids and produced by a wide variety of non-immune cells, some biomarker candidates are cell-surface proteins expressed on different types of professional immune cells. While some of these markers are of interest in their bound state, others are proteolytically cleaved and present in blood and other body fluids after release (Fig 15B).

Released Surface Receptor Markers: A soluble form of CD14, named sCD14 or presepsin is generated during inflammation and serum levels increase in response to bacterial pathogens [187]. In recent studies, presepsin was suggested as both, diagnostic and prognostic marker, but the most promising results concern the differentiation between SIRS and sepsis and bacterial and non-bacterial infection, respectively [188, 195, 196].

Another molecule expressed on innate immune cells and subsequently released into body fluids is the triggering receptor expressed on myeloid cells-1 (TREM-1). Different studies revealed potential suitability of soluble TREM-1 (sTREM-1) in diagnosis and prognosis. However, due to small study sizes and contradicting results, the utility of sTREM-1 as a sepsis biomarker remains ambiguous [179, 187, 188].

Surface-bound Receptors: In contrast to sCD14 and sTREM-1, CD64, an Fc-gamma receptor on neutrophils and other leukocytes, is not released into body fluids. Several studies therefore investigated CD64 expression on neutrophils, revealing high expression in septic patients and lower expression in patients without infection [179]. Furthermore, CD64 levels seem not affected by auto-immune diseases, making this receptor a promising biomarker for the presence of infection [188].

Similar to CD64, B- and T-lymphocyte attenuator (BTLA) is expressed on a variety of immune cells. An increased $BTLA^+$/ $CD4^+$ lymphocyte frequency was associated with infections as compared to non-septic, but critically ill patients. Furthermore, patients with a high amount of $BTLA^+$ cells were more susceptible for nosocomial infections [197].

Another negative regulator of T-cell responses, cytotoxic T-lymphocyte antigen-4 (CTLA-4), is also found with increased frequency in sepsis and an antibody against CTLA-4 improved survival in a murine model [198].

However, for both, BTLA and CTLA-4, further clinical studies are needed to validate the potential of those molecules as biomarkers [179]. Apart from the single molecules, cytokine and chemokine signaling as well as different cell types, e.g. DCs and regulatory

T cells, are analyzed for their diagnostic and prognostic values.

In summary, only two of the presented molecules, CRP and PCT, are utilized in clinical routines, and even those two are outperformed by the prognostic power of scoring systems if used stand-alone. One feasible way to overcome this problem might be to combine several biomarkers to enhance sensitivity and specificity of the prediction [179, 180, 187].

Another approach is the systematic analysis of patient samples, e.g. body fluids or cells, by means of the Omics technologies to uncover groups of molecules that are utilizable as combined biomarker sets either for diagnostic or prognostic purposes.

1.5.2.2 Omics Technologies in Sepsis-related Biomarker Discovery

DNA and RNA Level Omics: Omics methods allow the analysis of cellular components at different levels, starting from genetic information (Figure 16(1)). On this first level of genetic information, especially epigenetics and the genome-wide analysis of single-nucleotide polymorphisms (SNPs) offer clinical usefulness [178]. SNPs reveal patient-individual susceptibility and risk of death, and thus are a promising tool for risk stratification [178, 199].

In contrast, epigenetic analyses could yield biomarkers for the early diagnosis and progression of sepsis alike, provided that DNA modifications are afflicted [178]. However, until now, only few studies utilizing epigenetics for sepsis diagnosis were performed, including an analysis of histone modifications and the investigation of methylation patterns in septic newborns [200, 201].

The second target of sepsis-related biomarker-research is the ribonucleic acid (RNA) level (Fig 16(2)). Of particular interest at this level are messenger RNA (mRNA) and microRNA (miRNA) expression profilings. While mRNAs represent the entirety of all expressed protein-coding genes and thus proteins and protein isoforms, miRNAs are post-transcriptional regulators of gene expression. For both, mRNA and miRNA, first studies are promising in identifying of sets of markers and single entities with diagnostic and prognostic value. However, further evaluation in larger studies is needed to validate the clinical suitability [178, 199].

Proteomics: In contrast to the previously described Omics approaches, proteomics maps the functional repertoire of cells at a certain time point in form of actually expressed proteins (Fig 16(3)).

Recent studies targeted either distinct cell types or body fluids in clinical settings or used animal or cell-line models (reviewed in [202]). Many of the studies were able to confirm regulation of known and proposed biomarkers and added novel candidates to the lists. For example, Kalenka and colleagues reported differences in serum-protein composition between patients with sepsis and septic shock for the first time and utilized

those proteins for survival prediction successfully. Thereby, they proved the idea of prognostic markers found by proteomics [203]. A similar pilot study by Su and colleagues also confirmed the suitability of urine for the detection of prognostic markers [171]. Most recently, platelets from septic patient sera were characterized proteomically in comparison to platelets from healthy persons [172]. This study by Liu and colleagues also identified five differentially expressed proteins.

In addition to protein content and regulation, proteomic techniques allow monitoring of post-translational modifications, which are crucial regulators of protein activity. For example, Cuello and colleagues identified the redox status of long pentraxin 3, leading to differential oligomerization, as a reliable predictor for disease outcome in a murine sepsis model [204].

However, the diagnostic and prognostic values of identified potential markers need to be verified in large-scale studies and furthermore, the challenge of identification of low expression proteins needs to be tackled for future research [178, 199, 202].

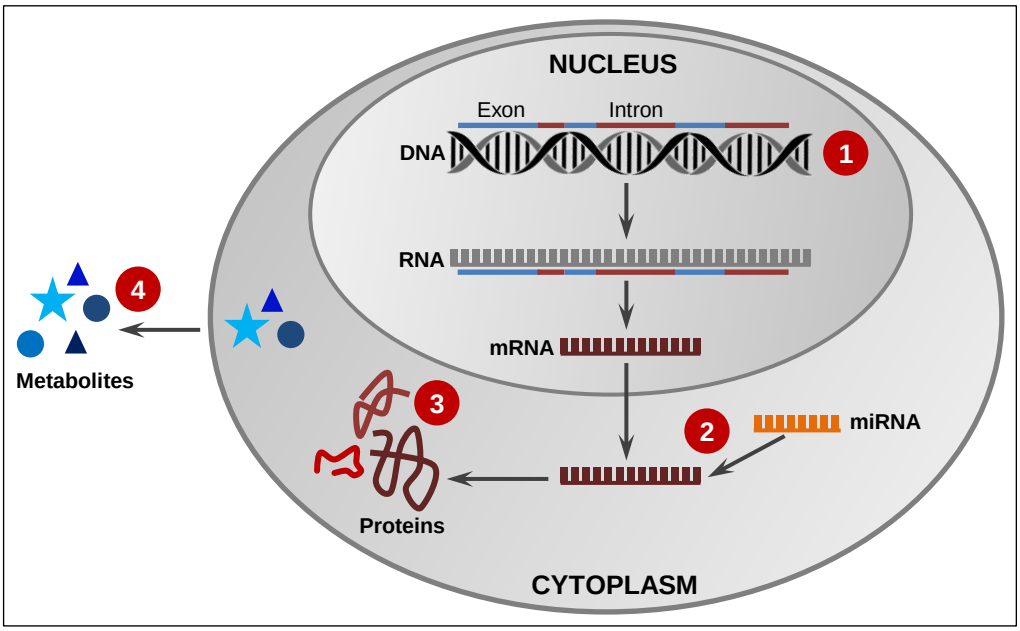

Figure 16. Omics approaches to detect novel biomarkers for sepsis at different cellular levels. 1: Epigenetics & SNPs, 2: Transcriptomics, 3: Proteomics, 4: Metabolomics. Adapted from Skibsted et al. [178]. DNA: deoxyribonucleic acid, RNA: ribonucleic acid, mRNA: messenger RNA, miRNA: microRNA.

Metabolomics: Metabolite analysis is the Omics approach furthest downstream from genomics and simultaneously the most recent addition to Omics technologies in sepsis-related research [178]. Until now, only one study utilizing patient samples supports

the idea of changing metabolites in plasma samples as diagnostic or prognostic biomarkers [205]. However, model studies using rats could build a foundation for outcome predictions with high specificity and sensitivity [199].

Even though Omics technologies uncovered several new candidates for diagnostic or prognostic biomarkers in sepsis, validation studies and proposals for clinical use are largely missing. Because of that, the practical utility as well as sensitivity and specificity of the candidate panels are still uncertain. Additionally, it must be assumed that in the process of validation some of markers will be proven false, leaving behind the need for further biomarker studies.

2 Aims of the Study

Ubiquitin and Ubiquitin-like modifiers (UBLs) are small proteins that serve as post-translational modifications in many cellular processes including immunity. The high complexity created by manifold chain formation of UBLs is under tight control of about 100 deconjugating enzymes, which shape and remove UBL-modifications.

Deubiquitinating Enzymes (DUBs), which remove ubiquitin, are the largest and best described group of deconjugating enzymes. Some DUBs are crucial regulators of innate and adaptive immune responses and are implicated in diseases and infections. Viral as well as bacterial pathogens influence DUB activities and furthermore acquired or evolved enzymes with deubiquitinating activity themselves.

Listeria monocytogenes (Lm) is one widely used model-organism for bacterial infection and intracellular lifestyle of pathogens. Moreover, listeriosis is also a major health concern and a re-emerging disease which can cause life-threatening symptoms in risk patients.

The most frequent severe symptom occurring is sepsis, which is characterized by a rapid progression and high mortality even in intensive care units. The major challenge in sepsis-related research at the moment is the identification of molecular markers to allow correct diagnosis of sepsis as well as an early prognosis of progression.
Listeria invades cells by utilizing the receptor-tyrosine kinase c-Met as well as the adhesin E-cadherin, which are activated by the listerial factors Internalin B and Internalin A, respectively. While the invasion route *via* E-cadherin and InlA is dependent on receptor-ubiquitination by the Ub-ligase Hakai, the role of c-Cbl-mediated ubiquitination of c-Met is contentiously discussed. At the moment, it is not clear which DUBs and Ub-sites are involved in activation by InlB and whether Lm interferes with (de)ubiquitination of the receptor. Even though some DUBs, e.g. CYLD, are described to be involved in systemic *Listeria* infection, an overview of the entirety of DUB-activities is also missing. Chemical proteomics can provide small, covalently binding, activity-based probes (ABPs) based on ubiquitin and UBLs to tackle this gap. These tools enable systematic detection and even enrichment of active DUBs as compared to the other ubiquitin-processing enzyme families.

This study aims at the detection and description of active DUBs as an enzyme class involved in *Listeria monocytogenes* infection and subsequently emerging disease symptoms. Furthermore, this study attempts to tackle technical limitations of DUB detection by improvement of currently available DUB activity-based probe concepts. For this purpose, the following main research questions are to be answered.

Firstly, are ubiquitination and DUB-activities involved in InlB/c-Met mediated cell invasion of *Listeria*? To answer this question on a cellular level, the role of c-Met ubiquitination in receptor internalization after activation with the listerial virulence-factor InlB should be examined utilizing "ubiquitination-resistant" c-Met mutants. Moreover, DUB candidates, that are able to directly deubiquitinate c-Met are to be defined and characterized regarding their localization. To achieve this, novel sequence-specific tools are to be designed, which are able to covalently bind DUBs capable of c-Met deubiquitination.

Secondly, does Lm infection deregulate Ub-mediated processes and DUB-activities *in vivo*? To elucidate this question, the global protein regulation during Lm infection as well as DUB-activities should be analyzed in a sub-lethal Lm infection model. Special attention should be payed to Ub and UBL-system regulating components and their role in the pathophysiology of Lm infection and bacterial clearance. A workflow for the systematic detection of physiological DUB-activities should be established utilizing suitable activity-based probes. As it is not clear whether the available ABPs assess the actual activity of DUBs, a promising ABP-candidate is to be evaluated regarding its selectivity.

Thirdly, can DUB-activities serve as molecular biomarkers for the diagnosis or prognosis of sepsis? To examine this question, blood lymphocytes from ICU patients are to be collected from patients with sepsis as well as controls and DUB-activity patterns are to be obtained. To utilize DUB-activity patterns for such an application, a workflow for the analysis as well as a statistical approach for the comparison of patterns are to be conceptualized.

3 Materials and Methods

3.1 Antibodies and Recombinant Proteins

3.1.1 Antibodies

All antibodies, primary and secondary, used in this thesis are summarized in Tables 3 and 4. For primary antibodies, the antigen, host and clone, if monoclonal, are given as well as the manufacturer and the dilution the antibody was used in. The abbreviations in brackets state the use of the antibody, WB = western blot and IF = immunofluorescence. For secondary antibodies, name, manufacturer, antigen species, host species, dilution and the conjugate are given. Conjugates are either horseradish peroxide (HRP), cyanines (Cy) or Alexa Fluor fluorochromes (AF).

Table 3. Secondary antibodies utilized for western blot analytics and immunofluorescence. JIR = Jackson ImmunoResearch, MP = Molecular Probes, AF = Alexa Fluor, Cy = cyanine.

name	manufacturer	antigen species	host	conjugate	dilution
A4a	JIR	mouse	goat	HRP	1:3000 (WB)
B4c	JIR	rabbit	goat	HRP	1:3000 (WB)
G4c	JIR	goat	donkey	HRP	1:3000 (WB)
A7c	JIR	mouse	goat	Cy3	1:250 (IF)
B7c	JIR	rabbit	goat	Cy3	1:250 (IF)
X7c	JIR	rabbit	donkey	Cy3	1:250 (IF)
G9c	JIR	goat	donkey	Cy2	1:250 (IF)
A12c	MP	mouse	goat	AF 488	1:250 (IF)
B12c	MP	rabbit	goat	AF 488	1:250 (IF)
B13c	MP	rabbit	goat	AF 594	1:250 (IF)

Table 4. Primary antibodies utilized for western blot analytics and immunofluorescence. WB = Western Blot, IF = immunofluorescence, CST = Cell Signaling Technologies, SySy = Synaptic Systems

antigen	manufacturer	clone	host	dilution
actin	Sigma	polyclonal	rabbit	1:10,000 (WB)
β-actin	Sigma	AC-15	mouse	1:10,000 (WB)
phospho-Akt	CST	587F11	mouse	1:500 (WB)
phospho-Erk 1/2	CST	D13.14.4E	rabbit	1:8000 (WB)
GFP	SySy	polyclonal	rabbit	1:1000 (WB)
c-Met	CST	D1C2	rabbit	1:3000 (IF) 1:2000 (WB)
c-Met	CST	L6E7	mouse	1:200 (IF)
phospho c-Met	CST	D26	rabbit	1:2000 (WB)
CYLD	CST		rabbit	1:200 (IF)
GAPDH	CST	14C10	rabbit	1:10,000 (WB)
GAPDH	ABD SeroTec	4G5	mouse	1:10,000 (WB)
HA-peptide	Roche	12CA5	mouse	1:1000 (WB)
HIS-Tag	Novagen		mouse	1:1000 (WB)
HSP90	R&D Systems	polyclonal	goat	1:500 (WB)
UCHL3	CST	polyclonal	rabbit	1:1000 (WB)
USP2	Santa Cruz	C-20	mouse	1:200 (IF)
USP21	Sigma	polyclonal	rabbit	1:200 (IF)
USP8	Santa Cruz	F-3	rabbit	1:100 (IF)
VCPIP1	OriGene	polyclonal	rabbit	1:2000 (IF)

3.1.2 Hepatocyte Growth Factor (HGF)

Full-length HGF was provided by Dr. Joop van den Heuvel and prepared by Nadine Konisch & Daniela Gebauer (all PREX/SFPR, Helmholtz Center for Infection Research, Braunschweig).

CHO lec3.2.8.1 EGT 92/A50.373 cells were cultivated in a 5 L-Batch-reactor in ProCHO5 medium supplemented with 7.5 mM glutamine (both Sartorius). As the protein was secreted during cell cultivation, the supernatant was harvested by centrifugation with a Sorvall™ RC 12BP Plus Large Capacity Centrifuge (Thermo Scientific) at 7332×g for 30 min while cooling to 4°C. Then, 0.1 % (v/v) sodium azide was added and the supernatant was concentrated using two Pellicon 2 ultra-filtration cassettes (Merck Millipore) until a final volume of 1 L was reached. After sterilization by filtration using Sartobran 300 capsules with 0.45µm and 0.2µm pore size (Sartorius), the protein was applied onto a 5 mL HiTrap Heparin column (GE Healthcare), eluted utilizing a salt-gradient from 0 to 100 % HiTrap buffer B (50 mM Tris/HCl, 2 M NaCl, pH 8.0.) and collected in 2 mL fractions were. After inspection via SDS-PAGE, fractions were pooled and activated utilizing HGF-A leading to incomplete conversion of single-chain HGF (scHGF) to two-chain HGF (tcHGF). Subsequently, the protein was dialyzed against 50 mM Tris/HCl, 250 mM NaCl, pH 8,0 and the chromatography was repeated another three times. Each time, the fractions were inspected by SDS-PAGE and the desired fractions were then dialyzed against 50 mM HEPES, 250 mM NaCl, pH 7,4 until no scHGF could be detected. For the final clean up, a 1 mL MonoS GL column (GE Healthcare) coupled to an Äkta Purifier System was utilized. A gradient from 250 mM to 1 M NaCl utilizing MonoQ buffers A and B (50 mM HEPES and 1 M NaCl (B), pH 7.4, degassed) yielded the final fractions of pure tcHGF, which were, after pooling, dialyzed against 50 mM HEPES, 600 mM NaCl, pH 7,4. The protein content of the fractions was measured by Nanodrop 2000 (Peglab, Germany) in the 1 Abs = 1 mg/mL mode and then corrected using the extinction coefficient of 1.8. Finally, tcHFG was aliquoted and stored at -80 °C. For each experiment series, tcHGF was checked for activity by cell-scattering and activation of c-Met signaling cascade (p-Erk1/2 & p-Akt). The control buffer used for stimulation experiments was obtained from the final dialysis step.

3.1.3 Internalin B (InlB)

The recombinant InlB full-length protein used in this study was kindly provided by Dr. Jörn Krause and produced by Claudia Hanko (both SFPR, Helmholtz Center for Infection Research, Braunschweig).

Escherichia coli (*E.coli*, Rosetta/Rosetta 2) cells from glycerol stocks were cultivated at 37°C over night (o/N), with shaking in Lysogeni broth (LB; 15 g/L yeast extract, 10 g/L tryptone, 7 g/L sodium chloride, autoclaved) using chloramphenicol and ampicilin as selective antibiotics (1µg/mL each). The next day, starter culture was diluted 1:100

into fresh flasks and the inoculated cultures were grown to an optical density (OD) of 0.5-0.8 at 37°C and 110 rpm. Subsequently, expression of InlB was induced by reduction of temperature to 20°C, addition of isopropyl-β-D-1-thiogalactopyranoside (IPTG) and incubation o/N. Cells were harvested by centrifugation and lysed by addition of ice-cold *E.coli* Lysis-buffer (1x PBS, 1 / 25 mL Complete Protease Inhibitor (Roche), 1.6 µg/mL DNAse, 0.8 M $MgCl_2$) and cell disruption using a French Press or sonicator. After centrifugation to remove insoluble protein and cell debris at 16.000 rpm for 1 h at 4°C (Sorvall Centrifuge, Rotor: SS-34), the lysate was incubated with pre-conditioned glutathione sepharose (GSH) in a 50 mL glass column with glass filter for 1 h at 4°C and gentle shaking, to allow the binding of the InlB glutathione S-transferase (GST)-tag to the beads. Subsequently, unbound protein was discarded and GSH was washed with ice-cold PBS twice and re-equilibrated in ice-cold PreS-Cleavage Buffer (50 mM MES, pH 6.0). Thereafter, the beads were incubated with PreScission Protease (#27-0843-01, GE Healthcare) in PreS-cleavage buffer o/N while shaking at room temperature (RT). The next day, the cleaved InlB was collected, remaining GSH particles were sedimented by centrifugation and InlB was dialyzed against SourceQ-buffer A (50 mM MES, 300 mM NaCl, pH 6.0 (NaOH), degassed). Thereafter, InlB was purified utilizing an Äkta purifier system (GE Healthcare) equipped with a MonoQ column (SourceQ 15, GE Healthcare). A gradient from 0 % to 100 % SourceQ Buffer B (50 mM MES and 1 M NaCl, pH 6.0 (NaOH), degassed) was used to separate InlB from contaminants via ion exchange chromatography. The resulting 1 mL fractions were then analyzed via SDS-PAGE and according to the apparent purity, the fractions were selected for use in stimulation experiments. The protein content of the fractions was measured by Nanodrop 2000 (Peglab, Germany) in the 1 Abs = 1 mg/mL mode and then corrected using the extinction coefficient of 0.69. The resulting molecular weight of InlB was 67606 kDa. InlB full-length was stored at -80°C until use and for each experiment series checked for activity by cell-scattering and activation of c-Met signaling cascade (p-Erk1/2 & p-Akt). The control buffer used contained an estimated sodium chloride concentration (500 mM) and 50 mM MES corresponding to the salt-gradient of the MonoQ column.

3.1.4 Recombinant Deubiquitinating Enzymes

All recombinant deubiquitinating enzymes used are listed in Table 5. Except for BRCC3, which carries a GST-Tag, all enzymes posses a poly-histidin tag (HIS_6-Tag) utilized for western blot detection. For non-full length DUBs, the name is tagged with XXX_{CD} marking the enzyme as short form with only the active center recombinantly produced. The enzymes were purchased either from Enzo Life Sciences (Lörrach, Germany), Life Sensors (Malvern, UK), Boston Biochem (Cambridge, UK) or Abnova (Taipei City, Taiwan), as stated in Table 5.

Table 5. Recombinant deubiquitinating enzymes used in this study. XXX_{CD} denotes DUBs of which only the active domain was recombinantly produced.

Name	product code	manufacturer	conc. [mg/mL]	assay [µg]	MW [kDa]
$USP2_{CD}$	E-506	Boston Bio	1.58	0.5	42
USP5	DB516	Life Sensors	0.6862	1	94
USP7	E-518	Boston Bio	2.1	1	42
USP8	E-520	Boston Bio	0.953	0.5	131
USP9x	E-552	Boston Bio	0.4	1	292
USP10	DB514	Life Sensors	0.0495	0.5	99
USP14	DB505	Life Sensors	1.36	0.5	68
USP15	UW9845	Enzo	1	1	109.2
USP20	DB520	Life Sensors	1.05	0.5	105
USP21	DB509	Life Sensors	0.189	0.5	73
USP25	E-546	Boston Bio	1.25	0.5	123
USP28	DB525	Life Sensors	0.7	0.5	123
USP47	DB510	Life Sensors	1.57	1	157
CYLD	E-556	Boston Bio	1.18	1	108
UCHL1	DB104	Life Sensors	1.25	1	25
UCHL3	UW9745	Enzo	1	0.3	29
UCHL5	DB102	Life Sensors	0.98	0.25	49
BAP1	E-345	Boston Bio	0.405	2	81
OTUB1	E-522	Boston Bio	1.66	0.5	33.2
OTUB2	E-554	Boston Bio	1.4	0.5	28
$A20_{CD}$	E-344	Boston Bio	2.26	0.5	46
ATXN3	E-341	Boston Bio	1.05	0.5	42
ATXN3L	DB402	Life Sensors	4.1	0.5	41
JosD1	DB403	Life Sensors	1.1	0.5	22
Yod1	DB202	Life Sensors	0.6232	0.5	38
AMSH	DB301	Life Sensors	0.49	0.5	49
BRCC3-GST	H00079184-P01	Abnova	0.2	0.5	62.5

3.2 Cell-biological Methods

3.2.1 Media and Supplements

All media and supplements were purchased from Life Technologies (Gibco / Invitrogen, Paisley, UK) unless otherwise stated. Fetal bovine serum (FCS) was purchased either from PAA Laboratories (Fetal Bovine Serum GOLD) or Sigma Aldrich, St. Louis, USA. All media and PBS were sterilized by filtration utilizing Steritop Filter Units (Merck Millipore, Billerica, USA). All media used are shown in Table 6.

3.2.2 Cell Lines and Cells

Utilized cell lines are listed and described in Table 7. Peripheral blood mononuclear cells (PBMCs) were isolated either from Buffy coats of healthy donors or sterile blood samples of sepsis patients. Buffy coats were kindly provided by the Deutsches Rotes Kreuz (NSTOB Springe), blood samples of sepsis patients were collected in the surgical ICU (OVGU Magdeburg, Dr. Lodes) and prepared by the work group medical microbiology (OVGU Magdeburg, Prof. Dr. Schlüter).

3.2.3 Cell Culture and Harvesting

All cell lines referred to in Table 7 were cultured in treated culture dishes or 24, 12-well plates (all Nunc^{TM}, Thermo Scientific) utilizing Innova incubators (New Brunswick Scientific). Culture conditions were 37°C and 7.5 % carbon dioxide (CO_2). The culture media and supplements used for particular cell lines are listed in Table 6.

At 80-90 % confluence or twice a week, cells were passaged. Therefore, the adherent cells were washed with PBS once and trypsinized (0.05 % Trypsin with 5 mM EDTA) for 5 min at 37°C. Afterwards, full medium or FACS-buffer (1xPBS, 2 % FBS, 1 mM EDTA) was added to stop the proteolytic cleavage and cells were spun down at 170×g for 5 - 10 minutes at RT utilizing a Multifuge 1 S-R (Heraeus). Subsequently, the supernatant was discarded and cells were resuspended in fresh medium for further cultivation or FACS-buffer for measurement at the Accuri flow cytometer (Accuri Cytometers Inc.).

Table 6. Cell media used for maintenance of cell lines and cultivation of cells.

Medium	Base	Supplements	Cell line / Cell type
$DMEM_{full}$	Dulbecco's modified Eagle's Medium (DMEM) 1 g/l glucose	10 % FBS 2 mM glutamine 50 mg/l streptomycin 50,000 units/mL penicillin	HeLa S3 EL-4
$DMEM_{-pen/strep}$	Dulbecco's modified Eagle's Medium (DMEM) 1 g/l glucose	10 % FBS 2 mM glutamine	HeLa S3 (microscopy and transfection)
$DMEM_{MM}$	Dulbecco's modified Eagle's Medium (DMEM) 1 g/l glucose	none	HeLa S3 (starvation)
$RPMI\text{-}1640_{full}$	Roswell Park Memorial Institute Medium (RPMI-1640)	10 % FBS 2 mM glutamine 50 mg/l streptomycin 50,000 units/mL penicillin	peripheral blood mononuclear cells (PBMCs)

Table 7. Properties of used cell lines.

Cell line	Description (organism, tissue/cell type, disease, ref. name)	Morphology & growth properties	Medium
EL-4	mouse, T lymphocyte, lymphoma, ATCC® TIB-39™	lymphoblast, suspension cells, adherent (treated culture dishes)	$DMEM_{full}$
HeLa S3	human, cervix, adenocarcinoma, ATCC® CCL-2.2™	epithelial, adherent	$DMEM_{full}$ $DMEM_{-pen/strep}$ $DMEM_{MM}$

3.2.4 Transient Transfection of HeLa S3 Cells

HeLa S3 cells were seeded either in 24-well plates, for microscopy and transfection controls, or 12-well plates for western blot analysis at a cell density of 1.3×10^4/cm in $DMEM_{-pen/strep}$ to avoid interference of antibiotics with the transfection and microscopy. Additionally, wells for microscopy contained sterile glass cover slips with 12 mm in diameter (Hecht Assistent, Germany) and were grounded with a damp tissue to ensure even distribution of cells.

After seeding, cells were incubated for 24 h at 37°C and medium was substituted by fresh medium shortly before transfection. In parallel, the transfection mix was prepared in a 96-well plate with v-bottom. For 24-well plates, 50 µL of $DMEM_{MM}$ mixed with 0.7 µg of DNA per well and Fugene transfection reagent (Promega, Fitchburg, USA) in a ratio of 1:3 and then incubated for 15 minutes at RT (see 3.5.2 for a list of used constructs). For 12-well plates all volumes were scaled up by a factor of 1.84 to account for the increased area of the wells. After incubation, the transfection mix was added drop-wise to the wells and cells were cultivated for another 24 h.

The next day, cells for control of transfection efficiency (3.2.5) were trypsinized as described in 3.2.3 and for all other cells destined for stimulation experiments, medium was changed to $DMEM_{MM}$ except for control samples which are labeled as non-starved. In that case, medium was exchanged against fresh $DMEM_{-pen/strep}$ to remove excessive transfection complex.

3.2.5 Flow-cytometric Analysis of Transfection Efficiency of HeLa S3 Cells

Initial transfection stability as well as transfection efficiency for the stimulation experiments was checked by flow cytometry as all used constructs contained an eGFP-tag allowing to test for green fluorescence as a transfection marker. Therefore, cells were trypsinized after 24 and 48 h and following centrifugation (5 min, 410×g) resuspended in 300 µL of FACS-buffer. To examine the cell viability after transfection and ensure that eGFP-positive cells were alive, propidium iodide (PI, Sigma-Aldrich) was added to all samples up to a final concentration of 0.75 µg/mL. As negative controls, cells which were also grown in 24-well plates without further treatment were used. For the positive control, cells were incubated in 0.25 % Triton X-100 in PBS on ice for 5 min to permeabilize the cells and stained with PI in parallel.

All samples were then transferred to 5 mL FACS-tubes and measured immediately at the **B**D Accuri C6 Flow Cytometer operated via BD Accuri C6 Analysis Software (1.0.264.21, BD Biosciences, USA). EGFP and PI both were excited with the 488 mm laser and analyzed in channel 1 (533 nm, 30 nm window) and channel 3 (630 nm; long pass filter), respectively. The evaluation strategy is shown in Figure 17. The samples were first gated for cells in general, then for live/dead utilizing PI staining and unstained control cells and finally for eGFP-fluorescence in living cells. Furthermore, all cells were

monitored for the proportions of living and dead cells among the non-transfected and transfected cells.

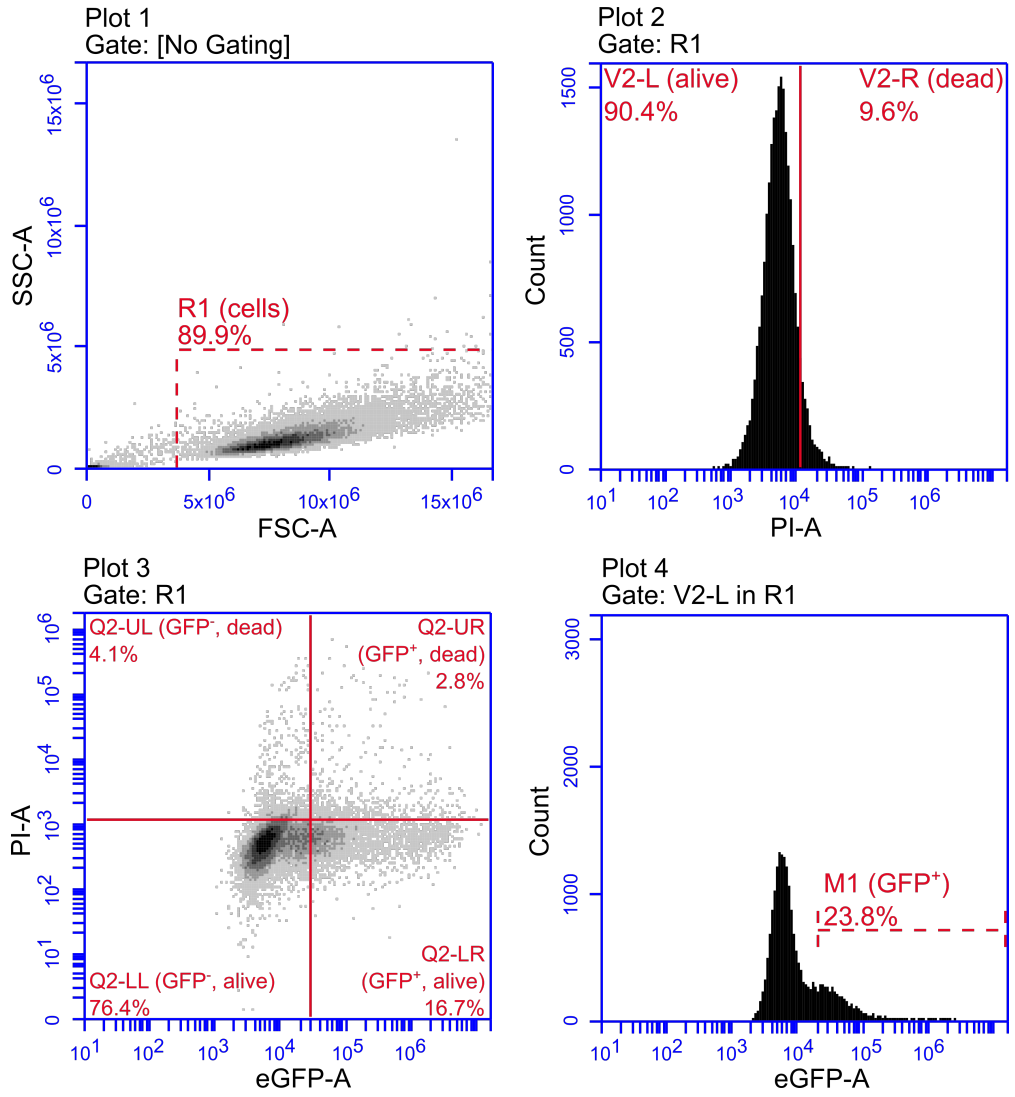

Figure 17. Evaluation strategy of transfection efficiency by flow cytometry. In Plot 1 a rectangular gate (R1) was set to select all cells. The rectangular shape is due to the need of the PI positive control to fall at least partly into the gate. Then, in Plot 2 the samples are divided into a PI_{neg} (alive) and a PI_{pos} (dead) population. To determine the amount of $eGFP^+$ cells, two parallel approaches were pursued. On the one hand, as shown in Plot 3, all cells were divided into 4 populations, PI_{pos} and $eGFP^-$ (UL), PI_{pos} and $eGFP^+$ (UR), PI_{neg} and $eGFP^-$ (LL) and PI_{neg} and $eGFP^-$ (LR). The second approach is shown in Plot 4, which determines the $eGFP^+$ cells among the living cells and utilizes the live/dead-gate from Plot 2.

3.2.6 Stimulation of Cells with HGF and InlB

Both HGF and InlB were produced in-house as described in 3.1.2 and 3.1.3 and stored as a high concentration stock at -80°C.

Before stimulation experiments were carried out, HGF and InlB were tested for protein integrity and ability towards HeLa S3 cells to activate the c-Met signaling cascade, namely p-Erk 1/2 and p-Akt (5 min) and to induce cell scattering (24 h). Therefore, different concentrations of both proteins, ranging from 0.02 nM to 20 nM, were applied to the cells and subsequently signaling activity was verified by western blotting using antibodies against phosphorylated Erk1/2 and phosphorylated Akt (see Table 4). Scattering was examined via life-cell microscopy.

Prior to stimulation, cells were starved with $DMEM_{MM}$ for 24 h including three changes of medium at 0 h, 2 h and 20-22 h starvation time to remove the excess supplements. For stimulation, the cell medium was aspirated and fresh minimal medium with a final concentration of 10 nM HGF or InlB was added. Cells were then incubated for a given time with the proteins and afterwards the stimulation was stopped either by PFA-fixation or addition sample buffer. For microscopy images, cover slips with cells on it were washed 2 min before end of stimulation and then fixed with 4 % PFA. For western blot analysis, cells were also washed with PBS and the stimulation was stopped by addition and rapid dispersion of reducing 4-time concentrated sample buffer and 1 % (v/v) Benzonase (EMPROVE® bio: Merck Millipore, Billerica, USA) using cell scrapers.

The control buffers used contained an 500 mM NaCl and 50 mM MES for InlB and 50 mM HEPES, 600 mM NaCl, pH 7.4, for HGF. For the transfection experiments both control buffers were added to the stimulation solution of the other protein and to the control solution to eliminate differences in buffer composition.

3.2.7 Immunofluorescence Analysis of HeLa S3 Cells

All used antibodies and respective dilutions used can be found in Tables 4 and 3 in chapter 3.1.1.

For immunofluorescence analysis cells were cultured in 24-well plates with 12 mm glass cover slips (Hecht Assistent, Germany) on the bottom of the cavity which were grounded with a damp tissue to ensure even distribution of cells. Depending on the experiments, cells were transfected and stimulated as described in 3.2.4 and 3.2.6.

At first, cells were fixed with fixation solution (1x PBS, 4 % paraformaldehyde (PFA)) for 20 min at RT, washed with PBS and permeabilized with cold IF permeabilization solution (1x PBS, 0.15 % Triton-X100) for 5 min. Subsequently, cells were blocked with blocking solution (1x PBS, 1 % bovine serum albumin (BSA), 0.1 % Tween-20), for 30 min at RT and incubated with the desired primary antibodies diluted in blocking solution in a humid dark chamber at 4°C o/N. On the next day, the cover slips were rinsed with washing solution (1x PBS, 0.1 % Tween-20) thrice and the incubated with secondary

antibodies and the DNA counter-stain DAPI (Sigma-Aldrich, St.Louis, USA) at a final concentration of 1 ng/mL staining mix. Thereafter, cover slips were again washed with washing solution (2x), PBS (1x), dehydrated in 70 and 96 % ethanol for 1 min each and dried on filter paper for a short time. Finally, cover slips were embedded in pre-warmed Mowiol® 4-88 Embedding solution (Sigma-Aldrich) onto Superfrost Microscope slides (Thermo Scientific) and dried at RT in the dark o/N.

Microscopic analysis was carried out at an inverted microscope (Ti-Eclipse, Nikon) using a Plan-Apochromat 100x/1.45 immersion oil objective and epifluorescence illumination from IntensiLight (Nikon) light source. The microscope and camera were operated with the NIS-Elements AR software (7.30.02, Nikon) and images were acquired utilizing a cooled, charge-coupled device camera with back-illumination (CoolSnap MYO, Roper Scientific).

For image evaluation and processing NIS-Elements and Fiji (ImageJ) image processing package were utilized [206, 207].

3.2.8 Isolation of Cell Populations from Blood of Healthy Donors

Buffy coats of healthy human donors for cell isolation were provided by Deutsches Rotes Kreuz (NSTOB, Springe) and tested negatively for the presence of HI-, HB- and HC-virus particles. The protocol used was adapted from Böyum A. (1968) as follows [208]. The content of each Buffy coat was equally distributed to two 50 mL reaction tubes pre-filled with 7.5 mL buffy buffer (PBS supplemented with 4 % FBS) and gently mixed. Subsequently, the mixture was slowly pipetted onto an cushion of 14 mL Ficoll-Paque (1.0077±0.001 g/mL at 20°C, GE Healthcare, Chalfont St Giles, UK) and the gradient centrifugation was carried out at 840×g for 25 min with disabled breaks. Subsequently, PBMCs were extracted from the interphase of the gradient and washed twice with 50 mL of buffy buffer by centrifugation at 410×g for 10 min to remove the Ficoll. To isolate granulocytes and erythrocytes after PBMCs were extracted, the gradient was carefully aspirated and the white layer directly above the erythrocytes (granulocytes) and a portion of the erythrocytes were extracted and also twice washed with buffy buffer. After resuspension, PBMCs and granulocytes, if collected, were filtered through a 40 µm pore-size cell strainer (Falcon), diluted to a total volume of 50 mL and counted using trypan blue and a hemocytometer. In case of clearly visible erythrocyte contamination, i.e. a red pellet, erythrocytes were destroyed by lysis using ACK-buffer (0.15 M NH_4Cl, 10 mM $KHCO_3$, 0.1 mM Na_2EDTA, pH 7.2-7.4 (HCl), sterile filtered). Therefore, cells were resuspended in 10 mL of ACK-buffer by inversion of tube, incubated, filled to 50 mL with buffy buffer and centrifuged at 410×g for 10 min .Finally, the cells were portioned to 1x10^8 cells, pelleted again at 410×g for 10 minutes for PBMCs and granulocytes and at 1100×g for erythrocytes and stored free of supernatant at -80°C until use.

3.2.9 Isolation of PBMCs from Blood of Sepsis Patients

All blood samples were collected in the surgical intensive care unit (ICU) of the university hospital of the OVGU Magdeburg (Dr. Lodes) and prepared by the work group medical microbiology (OVGU Magdeburg, Prof. Dr. Schlüter).

To acquire PBMCs from sepsis patients, 7 mL of RPMI were sterilely pipetted into a 15 mL reaction tube in advance and approximately 7 mL of patient blood was then added to the tube. After collection, the samples were send to medical microbiology work group and PBMCs were isolated there.

Therefore, 15 mL of Ficoll were pipetted into a 50 mL reaction tube and the blood-medium mixture was pipetted slowly on top of the ficoll to prevent mixing of the phases. Then, the tube was centrifuged at 2340 rpm for 20 min w/o break in a Rotanta 460 R centrifuge (Hettich, Tuttlingen, Germany). After removing of the upper layer (plasma), PBMCs were taken from the gradient, transferred into a new 50 mL tube and washed with 3-times the transferred volume of PBS. If the cell pellet was reddish after centrifugation, an erythrocyte lysis was carried out using AKR-buffer (0.15 M NH_4Cl, 10 mM $KHCO_3$, 0.1 mM Na_2EDTA). Cells were incubated for 5 min in 10 mL of AKR-buffer, washed with PBS and centrifuged again. After cell counting, cells were transferred into a 1.5 mL reaction tube and the pellet was stored at -80°C until it was transported to Braunschweig on dry ice.

After thawing on ice, cells were subjected to glass-bead lysis (see subsection 3.4.1).

3.2.10 Flow-cytometric Analysis of Mouse Liver Leukocytes

For L.m. infected mice (subsection 3.6.1), the leukocytes contained in the liver were analyzed at day 1, 3, and 9 p.i. as well as in uninfected controls. Therefore, animals were anesthetized with isoflurane. Thereafter, mice were intracardially perfused with 0.9% PBS to remove contaminating intravascular leukocytes. The livers were dissected, the tissue was minced through a 100 µm cell strainer and leukocytes were separated by Percoll gradient centrifugation (GE Healthcare) as described before [209]. The leukocytes were re-suspended in cell culture medium and the cell numbers were determined. The isolated leukocytes were then analyzed by flow cytometry on a FACS Canto with FACS Diva software (both from BD Biosciences). Cells were stained with anti-CD45 in combination with anti-CD4 and CD3 for CD4 T cells, anti-CD8 and CD3 for CD8 T cells, anti-NK1.1 and CD3 for natural killer (NK) cells, F4/80 and CD11b for macrophages, CD11c and CD11b for dendritic cells (DCs), CD11b, Ly6G and Ly6C for inflammatory monocytes, and neutrophils (see Table 8). All antibodies were obtained from BD Biosciences.

Table 8. Marker combinations used to determine populations of liver leukocytes in L.m. infected mice. To determine the leukocyte population, cells were stained for CD45. If cells were $CD45^+$, they were regarded as leukocytes and gated according to the markers listed. CD = cluster of differentiation

marker combination	cell type
$CD3^+$, $CD4^+$	$CD4^+$ T cells
$CD3^+$, $CD8^+$	$CD8^+$ T cells
$CD19^+$, $CD45RB200^+$	B cells
$CD3^-$, $NK1.1^+$	natural killer (NK) cells
$CDIIc^+$	dendritic cells (DCs)
$CD11b^+$, $F4/80^+$	macrophages (MΦ)
$CD11b^+$, Ly-$6C^{high}$, Ly-$6G^-$	inflammatory monocytes
$CD11b^+$, Ly-$6C^{medium}$, Ly-$6G^+$	neutrophils

3.3 Synthesis and Ligation of Activity-based Probes

The basic protocol for the synthesis and ligation of activity-based C-terminal probes was adapted from literature [88] and used as described earlier [96, 210]. For Ubiquitin Isopeptide Probes (UIPPs), the protocol was adapted from Iphöfer et al.(2012) [95]. All reactive groups and warhead-constructs were produced and provided by Antje Ritter, Tatjana Arnold and Dr. Raimo Franke (all CBIO, Helmholtz Center for Infection Research, Braunschweig). Two types of warheads were utilized in this study, classical C-terminal electrophiles (3.3.1.1) and isopeptide warheads (3.3.1.2), and the synthesis of both is described briefly below.

3.3.1 Warhead Synthesis

All solvents used were low moisture and HPLC-grade, all chemicals (reagent grade) were used as supplied. Analytical thin-layer chromatography was performed on E. Merck silica gel 60 F254 plates (0.25 mm). Isotopic composition of the compounds was confirmed using ultra-high resolution and high accuracy mass spectrometry (Thermo Scientific LTQ Orbitrap Velos).

3.3.1.1 C-terminal Electrophiles

The electrophiles VA and VME were synthesized as described earlier [95]. Starting from 50 mg of dried N-tert-butyloxycarbonyl-(E)-4-amino-2-butenoic acid (VA), which was

dissolved in absolute DMF, and activated with DIPEA (0.745 mM). Subsequently, EDC (0.375 mM), HOBt and 2- fluoroethylamine hydrochloride (0.375 mM) were added and the solution was stirred o/N at RT. The next day, the reaction was stopped by adding phosphate buffer (pH 7) and after addition of saturated NH_4Cl extracted with ethyl acetate. The combined ethyl acetate layer were washed with saturated NaCl solution and subsequently dried (anhydrous $MgSO_4$), filtered and concentrated. The produced N-tert-butyloxycarbonyl-(E)-4-amino-2-butenoic acid fluoroethylester (VFEA) was then purified using silica gel chromatography and eluted with 50 % ethyl acetate in dichloromethane to yield the purified compound. All C-terminal electrophiles used in this study are shown in Table 9.

Table 9. C-terminal electrophilic warheads prepared for and used in this study.

short name	full name	MW of warhead [Da]	source / literature
VME	vinylmethylester	115.06	in-house [88]
VA	vinylformicacid	202.11	in-house [95]
VFEA	vinylmonofluoroethylamide	145.08	in-house

3.3.1.2 Isopeptide Warheads

In short, peptides were synthesized as C-terminal amides on polyoxyethxlene-grafted polystyrene residues utilizing an automated multiple peptide synthesizer (Syro I, MultisynTech, Witten, Germany) at a 25 µM scale. For each amino acid coupling cycle, 5 equivalents of Fluorenylmethyloxycarbonyl-protected amino acids, DIC and HOBt in DMF were coupled for two times 1 h plus additional time for capping with acetic anhydride/pyridine in DMF. Lysine, the amino acid used in ligation to attach the warhead, was incorporated carrying an Mtt-protecting group on the ε-amino group. Finally, the N-terminus was acetylated for 30 min using acetic anhydride/pyridine in DMF. Subsequently, the Mtt-group was cleaved of and N-tertbutyloxycarbonyl-(E)-4-amino-2-buteinoic acid was added in a relative ratio (125 µM, 25.2 mg) to the resin after pre-activation with DIC and HOBt in DMF. After 5 days of shaking, peptides were cleaved from the resin as C-terminal amides using TFA, DCM, water and triisopropylsilane in a ratio of 70:20:5:5 for 4 h, precipitated (ter-butylmethyl ether/cyclohexane), extracted with water and lyophilized. For more details see Iphöfer et al. (2012) [95]. An overview of all produced isopeptide warheads is given in Table 10.

Table 10. Isopeptide warheads produced for and utilized in this study. All marked lysines (K) were modified with the VA reactive group as described in 3.3.1.2. Adjacent lysines were replaced by alanine (A) and are marked in italics in the respective peptide sequences.

name	peptide sequence	MW of warhead [Da]
$Ub_{20\text{-}28}$-K27(VA)	SDTIENV**K**A	976.0
$Ub_{28\text{-}36,K33A}$-K29(VA)	AD**K**IQD*A*EG	954.5
$Ub_{30\text{-}39}$-K33(VA)	IQD**K**EGIPPD	1111.2
$Ub_{42\text{-}54}$-K48(VA)	RLIFAG**K**QLEDGR	1502.7
$Ub_{54\text{-}73}$-K63(VA)	RTLSDYNIQ**K**ESTLHLVLR	2286.6
c-$Met_{958\text{-}70,K959A}$-K962(VA)	R*A*QI**K**DLGSELVR	1607.97
c-$Met_{1098\text{-}109,K1104A}$-K1103(VA)	LDNDG**K***A*IHCAV	1377.38
c-$Met_{1098\text{-}109,K1103A}$-K1104(VA)	LDNDG*A***K**IHCAV	1377.38
c-$Met_{1156\text{-}66}$-K1161(VA)	VLPYM**K**HGDLR	1451.49
c-$Met_{1254\text{-}64,K1263A}$-K1259(VA)	SLQTQ**K**FTT*A*S	1334.75

3.3.2 Production of HA-Ub_{75}

The first step for probe synthesis was to produce hemagglutinin (HA) tagged ubiquitin (Ub). Therefore, 400 mL of TB (12 g/l tryptone, 24 g/l yeast extract, 4 % (v/v) glycerol, 100 mL/l TB-salt stock (0.17 M KH_2HPO_4, 0.72 M K_2HPO_4) autoclaved) supplemented with 0.1 % (v/v) ampicilin and kanamycin were inoculated with *E.coli* $BL21^+$cells containing a pTYB2-vector (NEB) comprised of HA-Ub fused to a chitin binding domain (CBD) and an intein domain as well as antibiotic resistance to ampicilin. After over night incubation at 37°C and 130 rpm in a Multitron incubator (Infors HT, Einsbach, Germany), the pre-culture was used to inoculate an Labfors 5 L fermenter (Infors) for protein production. Production was induced by 0.5M IPTG and carried out at 20°C o/N. The next morning, cells were harvested by centrifugation at 3000×g for 30 min, resuspended in PBS and aliquoted into 50 mL Falcons containing pellets of 10-15 mL volume and stored at -80°C until further use. The fermenter was run by Daniela Gebauer (RPEX, Helmholtz Center for Infection Research, Braunschweig).

For protein extraction, cell pellets were resuspended in HA-Ub lysis buffer (50 mM HEPES, 100 mM NaOAc, 1/50 mL Complete Protease Inhibitor (Roche) w/o EDTA, 1 µL/10 mL DNAse, pH 6.5 (acetic acid)) at 4°C with stirring and subsequently homogenized in two cycles in a homogenizer at 16,000 - 20,000 psi. After centrifugation at 36,000×g for 30 min at 4°C (Sorvall^{TM} RC6 centrifuge, Thermo Scientific, USA)

and filtration through a 0.45 µm nylon (NY) membrane, the lysate was applied onto a pre-conditioned glass column containing a 10 mL chitin-bead bed (Ref: S6651L, New England Biolabs, Ipswich, USA). Subsequently, the column was filled with lysis buffer to prevent adsorption of the beads to the column wall and incubated for 5 h at 4°C with gentle shaking to allow binding of the CBD to the beads. Following incubation, unbound proteins were washed off by filling the column twice and the column was transferred to RT. To prepare for HA-Ub cleavage, the bead-bed was rinsed with 50 mM MesNa (Fluka (now Sigma-Aldrich)) in lysis buffer, re-filled again to 1 mL above the bed, sealed and incubated o/N at 37°C.

The next day, cleaved HA-Ub was collected and the column was rinsed with an additional bed-height of lysis-buffer. After filtering through a 0.32 µm NY syringe filter and buffer exchange to ABP-buffer A (50 mM NaOAc, pH 4.5 (acetic acid), degassed) using a VivaSpin membrane concentrator (Hybond membrane, cutoff: 5000 Da, Sartorius Stedim, Germany) centrifuging at 3000×g, HA-Ub was applied to cation exchange chromatography (CIEX). Therefore, a gradient of 0 to 100% ABP-buffer B (50 mM NaOAc, 1 M NaCl (B), pH 4.5 (acetic acid), degassed) on a MonoS column (10/100 (400mg), GE Healthcare) coupled to an Äkta purifier system 900 coupled to Fraction Collector Frac-950 (GE Healthcare) was utilized to separate reactive HA-Ub_{75} from the co-occurring non-reactive form. The resulting fractions were analyzed by MALDI-TOF/TOF (3.3.4) and HA-Ub-containing fractions were pooled and the buffer was again changed to ABP-buffer A. Finally, the HA-Ub solution was concentrated until the volume was below 500 µL and stored at 4°C until the reactive group was ready for ligation. Protein concentration was determined by NanoDrop 2000 (Peglab) measurement in triplicates.

3.3.3 Ligation and Clean-up of ABPs

The respective warheads (see Tables 9 and 10) were dissolved in ligation buffer (100 mM HEPES, pH 7.5, sterile filtered through syringe filter (0.2 µm)) and was adjusted to pH 8 using 0.1 M ammonium bicarbonate. Then, 50 µL of 2 M N-hydroxysulfosuccinimide (S-NHS) and the reactive HA-Ub were added. After adjusting to pH 8 again if necessary, the ligation solution was incubated o/N at 37°C. On the next day, the solution containing the ligated ABP was again filtered through an NY syringe filter (0.22 µm) and subjected to a buffer exchange to ABP-buffer A. To further purify the ABP, the solution was again fractionated by cation exchange chromatography as described before and fractions were analyzed by MALDI-TOF. If the desired fractions containing the ABP were not clearly separable from the residual HA-Ub, a second round of CIEX using CIM® SO3 (0.34 mL) disk or tube (1 mL) monolithic column (Bia Separations, Villach, Austria) was conducted. Finally, the ABP-containing fractions were combined and the buffer was exchanged against probe-buffer (50 mM HEPES, pH 7.4). After validation via ESI-MS, the probe was aliquoted and stored at -80°C.

3.3.4 MALDI-TOF and ESI-MS Analysis of HA-Ub and ABP-ligation Products

To determine and select ABP- and HA-Ub-containing fractions during ligation steps, MALDI-TOF/TOF was used. Therefore, 1 µL of fractions distributed throughout the chromatography peak was mixed with 1µL of 0.1 M sinapinic acid dissolved in 60 % acetonitrile (AcN), 0.1% trifluoroacetic acid (TFA) as matrix on an MTP 384 ground steel target (Bruker Daltonics) and dried for a few minutes. Subsequently, the Ultraflex-TOF/TOF was utilized using matrix-assisted laser desorption/ionization to determine the components of the applied fractions. As calibration solution, the protein calibration standard I (Bruker Daltonics, Billerica, USA) was used allowing measurements in a mass range between 3000 and 25,000 Da. The maximal allowed error for measurements were 100 ppm. All samples were then monitored for the distinct masses of possible HA-Ub populations and for the respective probe masses, which were derived from the masses of HA-Ub and the respective warheads (see Tables11 as well as 9 and 10) subtracting the mass of a water molecule eliminated in the ligation step. Only fractions mainly containing the desired masses were further processed, other fractions were discarded.

Additionally, final ABP-product was measured by electrospray ionization needle injection to confirm the product and to assess the purity of the product used. Therefore, a small portion of the final ABP-solution (3-4 ng/µL, 10 µL) was acidified using 20 % (v/v) formic acid and cleaned by pipetting through C4 ZipTip® pipette tips, binding all protein components, and subsequent elution in 65 % MeOH in 0.1 % FA. After drying in a speedvac centrifuge (RC10101, Sorvall), the sample was resuspended in 10 µL of 0.1 % FA and subjected directly to the needle measurement.

Table 11. Main HA-Ub populations monitored by MALD-TOF/TOF for determination of purity in probe ligation. For ligation, only HA-Ub_{MesNa} and HA-Ub_{Mes} (*) were of interest. The other masses were treated as contaminants.

product	description	MW [Da]
HA-Ub	non-reactive HA-Ub	10159.6
HA-Ub_{MesNa}*	reactive form	10323.8
HA-Ub_{Mes}*	reactive form w/o sodium	10282.9
HA-$Ub_{MesNa}\Delta$M1	reactive form, methionine 1 cleaved	10192.7
HA-$Ub_{Mes}\Delta$M1	reactive form, methionine 1 cleaved	10151.8

3.4 Biochemical Methods

3.4.1 Glass-bead Cell Lysis

Cells and tissues either subjected to western blotting (section 3.4.6) or prepared for proteomics (section 3.7) were lysed by glass-bead lysis. Therefore, glass beads were added to cell pellets or tissue powders in a 1:1 ratio. Then, the same amount of ice-cold glass-bead lysis buffer (50 mM HEPES, 250 mM sucrose, 5 mM $MgCl_2$, 1 % (v/v) IGEPAL (Sigma-Aldrich, St.Louis, USA), 1 µL/10 mL Benzonase (freshly added)) was added and samples were vigorously vortexed for 30-45 min at 4°C, using a shaker (IKA Vibrax) at 2200 rpm and subsequently sonicated for additional 10-15 min in an ice-cold ultra-sonic bath (Sonorex TK52, Bandelin). Afterwards, crude lysates were transferred into new reaction tubes and centrifuged for 20 min at 4°C and 14,000×g to remove cell debris. If necessary, centrifugation was repeated up to three times. Samples were then stored on ice until further use.

3.4.2 Labeling of Cell Lysates with ABPs

After glass-bead lysis, protein concentration was determined using BradfordRed assay. The assay was measured at 660 nm in an Infinite M200 Elisa plate reader (Tecan) using BSA dilutions from 0.1 - 1 mg/mL as standard curve. Subsequently, the lysates were diluted in 50 mM HEPES, pH 8.0 (NaOH) to distinct concentrations (e.g. 20 µg for 10-well gels, 10 µg for 17-well gels) for western blot applications and with NET-buffer (50 mM Tris, 150 mM NaCl, 5 mM EDTA, 0.5 % (v/v) IGEPAL, pH 7.5 (NaOH)) for proteomic work flows. Then, the pH was checked again and if necessary, adjusted to 8.0 with $NaHCO_3$ and defined amounts of ABPs were added and the samples incubated for 1 h at 37°C. Control samples were treated the same way, but HEPES was added instead of an ABP. To arrest the reaction for western blot samples, reducing 4×sample buffer was added. For proteomic samples, reaction was stopped by addition of 10 % SDS-solution to a final concentration of 0.3 % and incubation at RT for 15 min.

3.4.3 Shift-Assay

To evaluate the binding capability of DUBs and ABPs, so called shift-assays were carried out. This method is based on the covalent binding between ABP and deubiquitinase, resulting in a 10 kDa shift of protein mass, clearly visible on SDS-PAGE.

Given amounts of recombinant HIS_6-tagged DUBs (see Table 5) were pre-incubated in ABP-reaction buffer (50 mM TRIS, 50 mM NaCl, 1 mM DTT and 1 mM ATP freshly added, pH 8.0) at RT for 15 min. Afterwards, 0.1 - 0.3 µg of the respective ABPs were added and the samples incubated for 1-2 h at 37°C. To stop the reaction, 4x reducing probe buffer was added to the samples. Finally, samples were either subjected

to SDS-PAGE or stored at -20°C. To evaluate the shift-assays, an α-HIS antibody was used in western blotting (Table 4) at a dilution of 1:1000, yielding specific signals for the reactive DUB population.

3.4.4 Deubiquitination Assay

Recombinant DUBs (2 µg) were pre-incubated in 50 mM NaCl, 50 mM TRIS, 1 mM ATP, 10 mM DTT, pH 8, for 15 min at RT. Subsequently, 3 µg of K63-linked (Ub4) tetra-ubiquitin chains were added and the samples were taken directly after mixing and after 10, 30 and 60 min of incubation to assess the ability of the tested DUBs to cleave K63-linked Ub-tetramers. The respective aliquots were pipetted into 4x probe buffer to stop the reaction. After incubation, samples were applied to SDS-PAGE, washed with water, fixed with 10 % EtOH (tech.) and 10 % acetic acid and stained with colloidal coomassie according to Kang (0.02 % CBB-G250, 5 % aluminum-sulfate(14,18)hydrate, 10 % EtOH, 2 % orthophosphoric acid) [211]. Therefore, gels were washed with MQ for 15 min, incubated in coomassie solution over night and then destained using 10 % EtOH (tech.) and 2 % phosphoric acid.

3.4.5 Gel Electrophoresis

SDS-polyacrylamide gel electrophoresis (SDS-PAGE) was carried out based on a protocol adapted from Laemmli [212].

To separate proteins for subsequent western blotting, precast NuPAGE® Bis-Tris gradient (4-12%) gels were run with diluted MOPS SDS buffer utilizing an XCell SureLock® Mini-Cell (all Thermo Fisher Scientific, Waltham, USA). Before loading, samples were diluted in Roti-Load 1 reducing sample buffer (Carl Roth, Karlsruhe, Germany), heated for 3 min at 95°C and centrifuged for 2 min at RT. Subsequently, gels were run for 50 - 55 min at 180 V. For protein size estimation Page Ruler Plus or Page Ruler prestained protein ladder were used (Thermo Fisher Scientific).

3.4.6 Western Blotting

After gel electrophoresis, gels were equilibrated in blotting buffer (25 mM Tris Base, 0.192 M glycine, 0.02% SDS, 20 % MeOH (p.a.)) and then transferred onto a polyvinylidene fluoride (PVDF) membrane for western blot analysis [213]. Therefore, the PVDF membrane was activated in MeOH (p.a.) for 20 sec and also equilibrated in blotting buffer. For wet-blotting an XCell II™ Blot Module (Thermo Fisher Scientific) was used with the enclosed sponge pads soaked in blotting buffer. The blotting sandwich contained 4 sponge pads, 2 Whatman paper sheets, the PVDF-membrane and the gel. In the case of parallel blotting, two membranes and gels were arranged in the blotting cell. The blotting chamber was then filled with buffer, the outer chamber with MQ. Blot settings differed

between the applications. For α-HA blots, transfer was carried out at 100 mA, 25 V for 2 h 10 min, for all other blots, transfer was conducted at 30 V with non-restricted mA for 50 min to 1 h 15 min. After transfer, the membrane was incubated for 1 h in the appropriate blocking solution (5 % (w/v) skimmed milk in PBS (137 mM NaCl, 2.7 mM KCl, 10 mM Na_2HPO_4, 2 mM KH_2HPO_4, pH 7.4 (HCl)) forα-HA blots, 5 % (w/v) BSA in TBS-T for phospho-Ab blots, 5 % (w/v) skimmed milk in TBS-T for standard blots) and then incubated with primary antibody o/N at 4°C in blocking solution. A list of all used antibodies and their respective dilutions is presented in chapter 3.1.1. The next day, the PVDF-membrane was washed three times for 10 min using distinct washing solutions (PBS-T (1x PBS, 0.1 % (v/v) Tween 20), and PBS, TBS-T (1x TBS, 0.1 % (v/v) Tween 20) and TBS) and incubated with matching secondary antibodies (Table 3) for 1 h 15 min at RT using 0.5 % BSA/skimmed milk in washing solution. Subsequently, the blot was washed again as described before. Finally, the PVDF-membrane was developed utilizing ECL™ Prime Western Blotting Detection Reagent (GE Healthcare, Chalfont St Giles, UK). Therefore, an 1:1 mix of the luminol and the peroxide solution was pipetted directly onto the PVDF-membrane and chemiluminescence was detected by a LAS-3000 CCD-camera (Fujifilm).

For incubation with multiple antibodies, blots were stripped by washing with strip-buffer A (0.2 M glycine, 0.5 M NaCl, pH 2.0 (HCl)) and B (0.5 M Tris, pH 11.0 (NaOH)) for 10 min and intermediate rinsing with washing solution. Afterwards, the membrane was treated as described above with addition of 0.1 % (v/v) NaN_3 to the primary antibody solution. All acquired images were evaluated using AIDA Image Analyzer, 4.15, Raytest, Straubenhardt, Germany.

3.5 Methods of Molecular Biology

3.5.1 Transfection, Amplification and Isolation of pcDNA 3.1 c-Met eGFP

The pcDNA 3.1 c-Met-eGFP vector was designed by Małgorzata Szczodrak (PhD thesis, 2009) and kindly made available by Prof. Klemens Rottner (Molecular Cell Biology, TU Braunschweig, Braunschweig). The vector contains full-length, human c-Met with a C-terminal peptide linker (PGIHRPVAT) and eGFP as well as ampicilin and neomycin resistance cassettes and has a size of 11,362 base pairs.

The vector was transfected into *E.coli* DH5α cells by heat shock transformation. Therefore, 500 ng of DNA was pipetted to the cells one ice and incubated for 25 min. Afterwards, the cells were heated to 42°C for 45 sec, cooled on ice for 2 min, plated on LB-agar plates containing ampicilin and finally incubated o/N at 37°C.

The next day, single colonies were picked for cryo-stocks (5 mL LB culture) and DNA preparation. For DNA preparation, a 75 mL culture of the picked clone in LB medium containing 0.1 µg/mL ampicilin was incubated o/N at 37°C. The following day, the cells

were harvested by centrifugation and DNA was prepared by following the instructions for Maxi-Preps of the NucleoBond® PC 100 kit (Macherey-Nagel, Düren, Germany) protocol for high copy-number plasmids. After drying, DNA was resuspended in MQ water. For the cryo-culture, 1 mL of the o/N culture was mixed with 200 µL of 87 % glycerol and frozen at -80°C for long-time storage.

Table 12. Primers used to validate pcDNA 3.1 c-Met eGFP sequence utilizing MWG biotech sequencing service.

Read	Primer name	direction	Primer sequence
1	c-Met seq1	reverse	CAAAGGCATGGACATAC
2	c-Met seq2	forward	CAGATCATCCATTGCA
3	c-Met seq3	forward	GTCAATTCAGCGAAGTC
4	c-Met seq4	forward	GCATTTCAATATGCCA
5	c-Met seq5	forward	AGTTATGATCTCAATG
6	c-Met seq6	forward	TAGCCTGATTGTGCA
7	EGFP – N1 rev	reverse	MWG standard primer

Sequencing of all construct was performed by MWG-Biotech / Eurofins genomics. Therefore, 10 pmol/µL of each primer (Table 12) was pre-mixed with with 50-100 ng/µL DNA in 15 µL total volume and sent to MWG. Evaluation of sequencing data was carried out using VectorNTI Suite 8.

3.5.2 Site-directed Mutagenesis of c-Met

To produce ubiquitination-deficient variants of c-Met, a site-directed mutagenesis approach was conducted. Therefore, the QuikChange II XL Site-Directed Mutagenesis Kit (Agilent Technologies, Santa Clara, USA) was used following the instructions of the manufacturer. In short, 125 ng of mutagenesis primers (Table S3) and 10 ng of the template DNA were mixed with 10x reaction buffer, dNTPs, Quick Solution and ddH_2O and 1 µL of PfuUltra HF DNA polymerase was added. Subsequently, a PCR was carried out, using the following program:

- heating to 95°C for 1 min
- 18 cycles of 95°C for 50 s, 60°C for 50 s, 68°C for 12 min
- 68°C for 7 min
- 4°C on hold.

After PCR, the samples were digested with DpnI for 1 h at 37°C to get rid of the parental plasmid and then transfected into *E.coli* XL-10 cells. Therefore, cells were thawed, mixed with β-mercaptoethanol, incubated (10 min), mixed with the PCR-products and incubated for 30 min, all on ice. Following heat shock for 30 sec at 42°C, cells were cooled 2 min on ice and then mixed with pre-warmed LB-medium and incubated for 1 h. Finally, the LB-suspension was plated onto LB-Agar plates.

For each mutant, 5 clones were picked and DNA was analyzed after preparation using the respective sequencing primers listed in Table 12 to validate the mutation. One of the clones with the correct mutation was then sequenced fully.

3.5.3 RT-PCR of Mouse Liver Cytokines

RT-PCR was carried out in cooperation with the working group Medical Microbiology of Prof. Dirk Schlüter (University hospital (OVGU), Medical Microbiology, Magdeburg).

As a control for infection experiments (3.6.1), cytokine profiles were determined. Therefore, mRNA form livers of non-infected and L.m.-infected mice was isolated using an RNAeasy kit (Qiagen). Subsequently, the SuperScript reverse transcriptase kit with oligo(dT) primers (Invitrogen) was used to transcribe mRNA into cDNA and the RT-PCR for HPRT, TNF, IL-6, IL-1ß, IL-12 and IL-18 was conducted utilizing a Taqman gene expression assay (Applied Biosystems) on a Lightcycler 480 system (Roche). The quantification was carried out following the $\Delta\Delta$CT threshold cycle (CT) method using HPRT as the reference gene [214]. Finally, data was then visualized using GraphPad Prism (GraphPad software, USA).

3.6 Microbiological Methods

3.6.1 Infection of Mice with *Listeria monocytogenes*

All infection experiments were conducted in cooperation with the working group Medical Microbiology of Prof. Dirk Schlüter and carried out by Dr. Nishanth Gopala Krishna (both University hospital (OVGU), Medical Microbiology, Magdeburg).

For proteomic and DUB analyses, female C57BL/6 wild type (wt) mice were infected with a sub-lethal dose of *Listeria monocytogenes*(Lm) for 1, 3 and 9 days and compared to non-infected mice. EGD strain L.m. was grown in Brain Heart Infusion (BHI) broth (Sigma) and aliquots of log-phase cultures were stored at –80°C. For intravenous infection, fresh log-phase cultures were prepared from frozen stocks and 1 x 10^4 L.m. were diluted in 200 µL PBS (sterile, pyrogen-free, pH 7.4) and then injected into the caudal vein. After indicated time-points the mice were directly sacrificed or anesthetized and then sacrificed and livers were dissected and prepared as stated in the individual subsections (3.6.2, 3.5.3 and 3.2.10). For the proteome work flow (3.7.1), liver pieces were snap-frozen in 2-methyl-butane and stored at -80°C.

3.6.2 Determination of Colony Forming Units

CFU-determination was carried out by Dr. Nishanth Gopala Krishna (University hospital (OVGU), Medical Microbiology, Magdeburg).

Livers for flow-cytometric analysis were partly used to determine the colony forming units (CFU). Therefore, homogenized (tissue grinder) liver pieces were diluted 10-fold and homogenates were plated on BHI agar plates. After incubation at 37°C for 24 h, bacterial colonies were counted microscopically.

3.7 Proteomic Methods

3.7.1 Preparation of Mouse Liver Samples

After infection with L.m. (see section 3.6.1), mice were sacrificed on day 1, 3 and 9 post inoculation (p.i.) and the livers were snap-frozen in 2-methyl-butane and stored at -80°C. Upon completion of sampling, the liver pieces were ground using liquid-nitrogen cooled mortar and pestle, transferred to 2 mL reaction tubes and stored on ice. Subsequently, the liver powder was subjected to glass-bead lysis as described in subsection 3.4.1.

3.7.2 Peptide Generation for Liver Proteome Studies

After glass-bead lysis (3.4.1) protein lysate accounting for 70 µg protein was diluted using MQ and precipitated by addition of 100 % EtOH (p.a.) and 88 mM NaOAc, pH 5.0, and incubation o/N at RT. The next day, samples were centrifuged at 14,000×g for 1 h and air-dried after removing the EtOH/NaOAc mixture. Subsequently, the pellet was dissolved in iTRAQ® dissolution buffer (0.5 M triethyammonium bicarbonate (TEAB) and, after addition of reducing agent (1/10 of dissolution buffer volume, 50 mM tris-(2-carboxyethyl)phosphine (TCEP)), incubated for 1 h at 60°C. Next, cysteine blocking reagent (200 mM methyl methanethiosulfonate (MMTS) in isopropanol) was added and the sample was incubated for 15 min at RT. After reduction and alkylation, samples were subjected to tryptic digestion o/N. Therefore, activated (50 mM acetic acid) sequencing modified trypsin (Promega, Madison, USA) was added to the sample at a ratio of 1:100 (trypsin:protein) and the sample was incubated at 37°C o/N. The next day, a small aliquot of the sample was subjected to digestion control via LC-MS/MS and RawMeat. If digestion control was successful, peptides were subjected to iTRAQ® labeling (subsection 3.7.3).

3.7.3 ITRAQ-labeling of Peptides

For relative quantification of peptides and proteins, isobaric tags for relative and absolute quantification (iTRAQ)® were used (SCIEX, Framingham, USA). The labeling allows mixing of sample and evaluation of the distinct reporters (114, 115, 116 and 117) in the

LC-MS/MS analyses. All labels are reactive to primary amines and add an isobaric mass tag of 145 Da to peptides, that will fragment in LC-MS/MS measurements to reveal the individual reporter groups [215].

To label samples for DUB-enrichment or proteome sample-sets, samples were spun down for 20 min at 14,000×g and iTRAQ reagents were added to peptides generated either on-bead and subsequently cleaned (subsections 3.7.7 and 3.7.4) or directly following digestion (3.7.2), respectively. Samples had to be prepared in dissolution buffer. Subsequently, ethanol (p.a.) was added to reach a solvent concentration of about 70 %, taking into account that the reagents are solved in AcN and samples were incubated 3 h at slightly elevated temperature (25°C) with shaking. After labeling, samples were dried in a speedvac and in parallel, labeling-efficiency was evaluated via LC-MS/MS analysis. If the efficiency was greater then 95 % based on the area of the labeled peptides' MS peaks, sample preparation was resumed and all samples were subjected to solid-phase extraction to remove the TEAB-buffer (3.7.4).

3.7.4 Desalting and Clean-up of Peptides

Desalting and clean-up of peptides was carried out using reverse phase (RP) solid-phase extraction (SPE) cartridges from Waters choosing either 1cc HLB or 3cc HLB columns (Waters, Milford, USA) guided by the peptide-amount of the samples. Columns were equilibrated using 100 % MeOH (p.a.), 100 % AcN (p.a.), SPE-buffer B and SPE-buffer A (0.2 % FA, 0.5 % AcN (A), 60 % AcN (B) in MQ), consecutively. After preparation, samples were applied onto the column and the flow-through was collected in reaction tubes. Subsequently, the bound peptides were washed twice with SPE-buffer A and eluted with SPE-buffer B, utilizing an appropriate pipette to remove all liquid from the column by pressure. To increase the yield, the flow-through and first wash fraction of the previous run were applied onto the re-equilibrated column and treated as before. Both elutions were pooled and dried using a speedvac.

3.7.5 De-complexation of Peptide Samples by SCX

To reduce the sample complexity, peptides were fractionated utilizing strong cation exchange chromatography (SCX). After peptide clean up (3.7.4 or 3.7.8) previously dried samples were dissolved in SCX buffer A (25 % AcN, 0.065 % FA) and centrifuged for 20 min 109,000xg to remove impurities. Fractionation was then carried out using a MonoS-PC1.6/5 column coupled to an Ettan microLC system (Amersham Biosciences (GE Healthcare)) with a SunCollect micro-fraction collector (MALDI spotter, Sunchrom). The system was operated at a constant flow-rate of 150 µL/min running a 15 min gradient from 0 % to 35 % SCX buffer B (25 % AcN, 0.065 % FA, 500 mM potassium chloride) followed by a gradient to 100 % buffer B in 7 min and collecting fractions continuously minute-wise. For samples with an estimated peptide amount above

80 µg, two consecutive runs were conducted. Finally, fractions were pooled according to the approximate peptide concentration to yield 15 final fractions for LC-MS/MS analyses. After SCX, all fractions were desalted as described in subsection 3.7.4.

3.7.6 HA-immunoprecipitation

After glass-bead lysis and incubation with ABPs as described in subsections 3.4.1 and 3.4.2, samples were further diluted with NET-buffer to reach a final SDS-concentration of 0.1 %. Subsequently, the labeled lysates were filled onto 5 mL spin columns with a 30 µm pore-size frit (Thermo Scientific, USA) containing 100 µL of pre-washed monoclonal *a*-HA agarose beads (Sigma, clone HA-7). The columns were then sealed with PARAFILM® M (Brand, Germany) on both ends and incubated for 5 h at 4°C constantly rotating at 6 rpm. Hereafter, unbound protein was discarded and the DUB-containing beads were washed twice with NET-buffer and 100 mM NH_4HCO_3 by short centrifugation at $200\times g$. Control samples for unspecific protein binding were generated using the same work flow while omitting addition of ABPs in the labeling step. Finally, samples were subjected to on-bead digestion (subsection 3.7.7).

3.7.7 On-bead Peptide Generation for DUB-enrichment

After DUB-enrichment by HA-IP (3.7.6), samples were digested directly on the HA-agarose beads. Therefore, a carbamidomethylation utilizing chloroacteamide (CAA) and dithiothreitol (DTT) was carried out. 20 mM DTT in 0.1 M NH_4HCO_3 was added until the buffer level reached twice the height of the bead-bed. Then, the samples were incubated for 30 min at 56°C, the solution was removed by spinning down and 55 mM CAA in 0.1 M NH_4HCO_3 was added. The s18amples were then again incubated for 30 min, this time at RT in the dark, and washed twice with NH_4HCO_3. Subsequently, activated trypsin was added to the sample at a ratio of 1:100 (trypsin:protein) and the sample was incubated at 37°C o/N. The next day, the peptides were eluted twice using 0.1 % FA and a small part of the sample was subjected to digestion-control via LC-MS/MS and RawMeat. The remaining samples were cleaned as described in subsection 3.7.4 and then subjected to iTRAQ labeling (3.7.3) if digestion had been successful. For the non-quantitative measurements, samples were directly applied to On-line reverse phase (RP)-C18 peptide clean-up (3.7.8).

3.7.8 On-line Reverse Phase (RP)-C18 Peptide Clean-up

Directly after combination of the iTRAQ-labeled samples from HA-IP an on-line RP-C18 chromatography was carried out to remove unbound iTRAQ reagents, salt and detergents from the sample. Therefore, a self-packed PR-C18 column coupled to an Äkta purifier system with fraction collector Frac-950 was utilized. The column was equilibrated by

consecutive washing with PR buffer B and A. Subsequently, the sample was injected into a 2 mL loop by a syringe and flushed onto the column, followed by further washing with buffer A. For elution, a column volume step gradient from 0 - 100 % RP buffer B (0.1 % TFA, 60 % AcN, filtered, degassed) was used. Finally, acquired fractions were pooled according to the UV-spectrum, excluding the detergents, which were eluted as a single peak after the peptide containing fractions. The desired fractions were then dried for storage.

3.7.9 Mass Spectrometric Data Acquisition and Protein Identification

Directly before measurement, dried samples were dissolved in 6 % AcN in 0.1 % FA, sonicated for 5 min at RT and 0.1 % FA was added to a final concentration of 3 % AcN. Finally, samples were centrifuged at 109,000×g and 4°C for 20 min (Sorvall^{TM} Discovery MS120SE ultra centrifuge, Hitachi) and transferred into glass vials with screw neck (Waters) and subjected to mass spectrometry.

Three different mass spectrometry set-ups were used in this study.

1. LTQ Orbitrap Velos (Pro) with
    a) Liquid chromatography (LC): UltiMate 3000 RSLC nano LC system
    b) pre-column: Acclaim PepMap 100 (75 µm x 2 cm, C 18, 3 µm)
    c) analytical column: Acclaim PepMap RSLC (75 µm x 25 cm, C18, 2 µm)
    d) software: Chromeleon (version 6.8), Xcalibur (version 2.1)
2. LTQ Orbitrap Velos Pro with
    a) LC: Nano Acquity LC system
    b) analytical column: Nano Acquity UPLC column (75 µm x 25 cm, C18 ,1.7 µm BEH130; Waters)
    c) software: Xcalibur (version 2.1)
3. an Orbitrap Fusion^{TM} Tribrid^{TM} with
    a) UltiMate 3000 RSLC nano LC system
    b) pre-column: Acclaim PepMap 100 (75 µm x 2 cm, C 18, 3 µm)
    c) analytical column: Acclaim PepMap RSLC (75 µm x 25 cm, C18, 3 µm)
    d) software: Chromeleon (version 6.8), Xcalibur (version 3.0.63)

The samples were applied onto the pre-column and washed for 3 min or applied directly onto the analytical column. Subsequently, the peptides were separated via a gradient from 3.7 - 31.3 % of solvent B (0.1% FA, 80 % AcN) and then electro-sprayed by a stainless steel

emitter. The mass spectrometer was operated with the parameters described in Table S2 and controlled by Xcalibur and Chromeleon. After detection, raw-files of each experiment were uploaded to Proteome Discoverer (PD, version 1.4.1.14, Thermo Scientific) or Mascot Server (2.4.1, Matrix Sciences) [216, 217]. If SCX-fractions were measured, all fractions were merged in one run. Subsequently a database search was carried out by the Mascot search-engine, either standalone or integrated into PD. The search parameters are listed in Table 13. After successful DB search and protein identification, datasets were either analyzed directly in PD or, if the search was conducted with Mascot, loaded into Scaffold 3.6.5 (Proteome Software, USA).

Table 13. Mascot parameters used for protein identification. In the modification rows, letters in brackets state the modified amino acids: K = lysine, C = cysteine, M = methionine. Letters in brackets behind value denote the analysis setting used in d = DUB-enrichment (Lm-liver), p = proteome, s = Dub-enrichment from PBMCs m = DUB-enrichment in method development.

parameter	value (p/d)	value (s)	value (m)
database	Swissprot	Swissprot	Swissprot
release	2014_01	2015_01	2013_01
taxonomy	*mus musculus* (house mouse)	*homo sapiens*	*mus musculus* (house mouse)
enzyme	trypsin	trypsin	trypsin
max. missed cleavage	1	1	1
fixed modifications	iTRAQ 4-plex (K) iTRAQ (N-term) Methylthio (C)	Carbamidomethyl (C)	Carbamidomethyl (C)
variable modifications	Oxidation (M)	Oxidation (M)	Oxidation (M)
precursor mass tolerance	10 ppm	10 ppm	10 ppm
MS/MS tolerance	0.4 Da	0.4 Da	0.4 Da

3.7.10 Protein Quantification

Protein quantification was carried out for those DUB-enrichment and proteome samples that were iTRAQ labeled (3.7.3). Regulation factors for the proteins were calculated by PD using only peptides that met the parameters described in Table 14. PD generated ratios based on peptide-specific iTRAQ reporter-ion intensities of all 4 channels

Table 14. Proteome Discoverer (PD) parameters used to filter the datasets and to validate the reliability of the data. d = setting used exclusively in DUB-enrichment datasets, p = parameter exclusively used in proteome datasets. If not stated, parameters were identical in all experiments. FDR = false discovery rate.

parameter PD 1.4.1.14	value	parameter Scaffold 3.6.5	value
Peptide confidence	high	identification probability (idp)	99 %
Peptide rank	1	min. peptide idp	95 %
Peptide score	30	min. spectral count	2
No. of peptides	1 (d/s), 2 (p)	No. of peptides (unique)	1
FDR	1 %		
Mascot significance threshold	0.02		
protein grouping	disabled		

using channel 115 (non-infected control sample) as standard. The intensities of the other channels were divided by the standard yielding the following regulation factors: day 1/day 0: 117/115; day 3/day 0: 114/115 and day 9/day 0: 116/115. The complete dataset was then exported to Microsoft Excel and the protein regulation factors were transformed to log2 values, median-normalized and finally analyzed for significantly regulated proteins.

3.8 Determination of Significantly Regulated Proteins

Significantly regulated proteins were determined in cooperation with Prof. Frank Klawonn (HZI). Therefore, a "significance test based on a large number of small samples" described earlier was used [218]. The algorithm is based on the assumptions that regulation factors of proteins follow a normal distribution and that the random variation of protein regulation is independent of the true regulation factor. In the first step, a reliable standard deviation of each samples or time-point was estimated by utilizing the median absolute deviation from the median (MAD) and aggregating this estimation for all proteins. Subsequently, a hypothesis test for the identification of significantly regulated proteins is constructed using the estimated standard deviation σ_0. Thereby, the null hypothesis is that a certain protein is not regulated, having a regulation factor of 0 and a variance of σ_0^2 [218]. To calculated the p-value for each protein to be significantly regulated, a threshold (c_α) was determined using equation 1 where α = significance level for the test, k = number of replicates carried out, m = number of replicates in which a protein is at least found out of k replicates, n_m = number of proteins at least found in m replicates,σ_0 = estimated reliable standard deviation utilizing the MAD, varying around zero. Using the calculated p-values from this test, all proteins with a value smaller than 0.01 were regarded significantly regulated.

$$c_\alpha = \sigma_0 \cdot \Phi^{-1}\left(1 - \left(\frac{\alpha}{2 \cdot n_m \cdot \binom{k}{m}}\right)^{\frac{1}{m}}\right) \quad (1)$$

4 Results

4.1 Detection of Ubiquitination-sites and Deubiquitinating Enzymes with a Role in InlB-mediated Cell Invasion

The receptor-tyrosine kinase c-Met is the entry-portal of Lm to accomplish cell invasion of distinct cell types decorated with c-Met. Differentially regulated ubiquitination could be of crucial importance for this process, however, was not described in the context of c-Met dependent invasion thus far. For that reason, this study intends to investigate the role of intracellular ubiquitination sites at c-Met as well as putative DUBs involved in the deubiquitination of the receptor during activation of c-Met by the Listeria invasin Internalin B (InlB) in comparison to the physiological ligand hepatocyte growth factor (HGF). Before ubiquitination-deficient c-Met mutants could be used in the HeLa S3 model system for Lm invasion, the responsiveness to HGF and InlB was tested.

4.1.1 Recombinant HGF and InlB are Suited to Activate c-Met Dependent Signaling in HeLa S3 Cells

To initially characterize the ability of HeLa S3 cells to be stimulated by either HGF or InlB as well as to ensure the functionality of the recombinant proteins ahead of stimulation experiments, a dilution series from 0.02 to 20 nM of both HGF and InlB were applied to HeLa S3 cells for 5 min and the phosphorylation of c-Met, Erk1/2 and Akt was monitored. For both stimulants, phosphorylation of c-Met at tyrosine (Y)1235 and 1236 was found to occur at a concentration of 0.2 nM, while activating phosphorylation at Erk 1/2 was already detected in non-stimulated cells and enhanced at 0.02 nM HGF or InlB (Figure 18 A). Phosphorylation of a more distal signaling component, Akt, occurred at a concentration of 0.2 nM HGF and 0.02 nM InlB. Those responses render HeLa S3 cells fully functional for the short-term stimulation with recombinant HGF and InlB produced in-house and a concentration of 10 nM was chosen for the following experiments. Responsiveness was examined in the same manner for each new aliquot of HGF and InlB.

Additionally, the intended set-up for transfection experiments of c-Met constructs was checked regarding the activation of all mentioned components after 5, 10 and 30 min of stimulation. c-Met as well as Erk 1/2 and Akt were phosphorylated in a time-dependent manner for both HGF and InlB (Fig 18B). Furthermore, all controls showed diminished or no signals. The last 4 lanes in Figure 18 B represent a pool of wt samples, either

non-stimulated [neg(-)], mock-stimulated with cell-medium including protein buffer for 30 min [neg(buffer)], or stimulated for 5 min with HGF or InlB. Those samples were used to ensure comparability of different blots.

In summary, HeLa S3 cells are readily responding to recombinant, in-house produced HGF and InlB in a time-dependent manner at a stimulant concentration of 10 nM, enabling the monitoring of c-Met activation and localization.

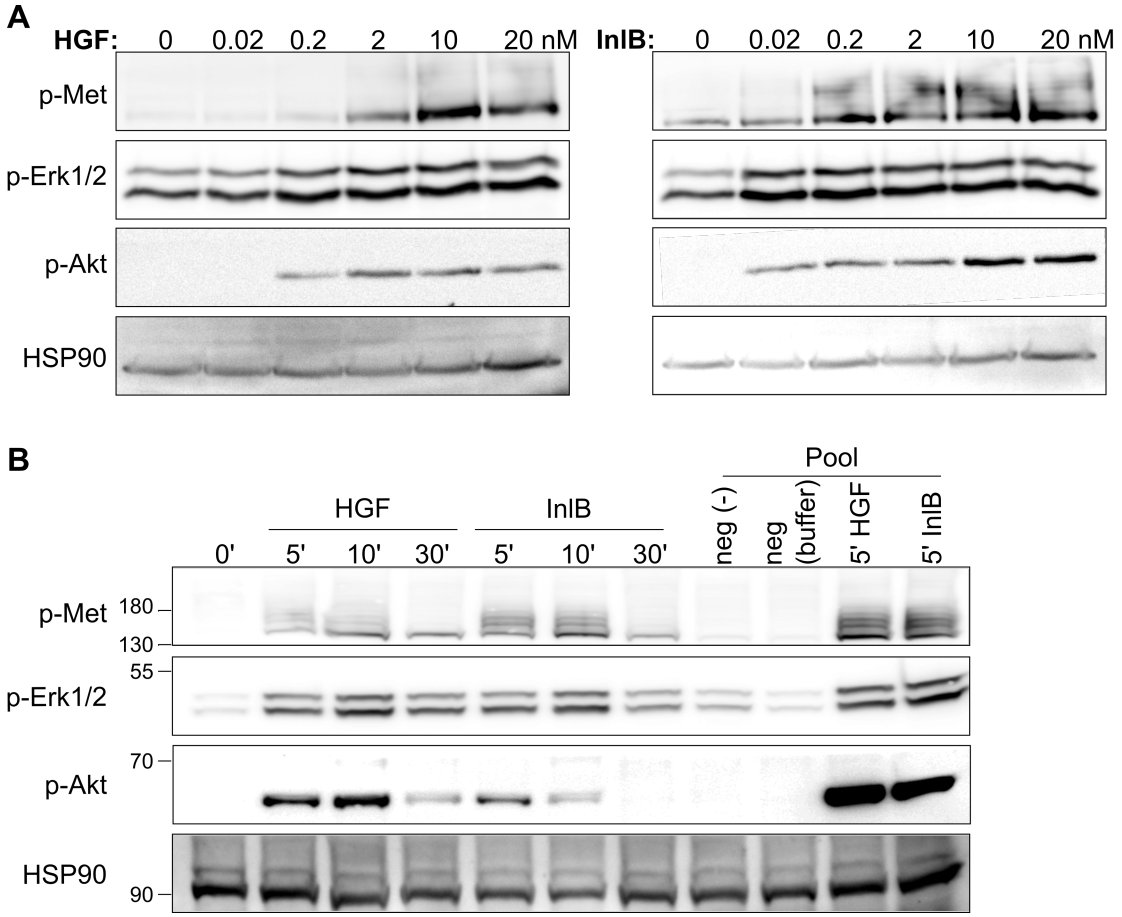

Figure 18. Response of c-Met, Erk 1/2 and Akt kinases upon HGF and InlB stimulation in HeLa S3 cells. (A) Stimulation of HeLa S3 cells with a dilution series of HGF and InlB. (B) Stimulation of HeLa S3 cells with 10 nM HGF and InlB after incubation with transfection reagent (FUGENE) and subsequent starvation.

4.1.2 Influence of Ubiquitination on Receptor Activation, Signaling and Localization of c-Met

In total, 13 ubiquitination sites of c-Met are reported in the Phosphosite Plus DB [219] of which 4 sites are located in extracellular domains of c-Met (Table S1). Of the 9

remaining sites, 2 are in proximity to the c-Cbl binding site around tyrosine 1003 of the receptor. To analyze the role of ubiquitination at those sites, i.e K962 and K1103, ubiquitination-deficient mutants of those sites were produced by replacing the lysine (K) with an arginine (R). Additionally, K1104, the lysine adjacent to K1103, and K1259, which was identified in HGF-stimulated HeLa S3 cells (Fig S1) and recently also detected in mouse tissues [220], was mutagenized.

For mutagenesis, a pcDNA3.1+ c-Met enhanced green fluorescent protein (eGFP) fusion plasmid that was introduced and kindly provided by Małgorzata Szczodrak and Prof. Klemens Rottner (TU Braunschweig) was utilized [221]. Mutants for all Ub-sites mentioned above, as well as a K1103R/K1104R double mutant and a quadruple mutant of all sites were successfully prepared.

Despite of the large size of the plasmid, rendering it difficult to handle and transfect, transfection could be established and the rate ranged between 10 and 30 %. The transfection rates were determined by FACS measurements, taking advantage of the intrinsic eGFP-signal (subsection 3.2.5 & Fig 17). To pre-characterize the mutants regarding their signaling-competence, responses of c-Met, Erk and Akt after HGF and InlB-stimulation were assessed.

4.1.2.1 Pre-characterization of the Influence of c-Met Ubiquitin-deficiency on the Auto-activation of c-Met and Erk1/2 and Akt Kinase Phosphorylation

The first question pursued was, whether the autophosphorylation of c-Met and downstream activation of Erk1/2 and Akt by phosphorylation were influenced after 5, 10 and 30 min of stimulation by HGF and InlB in the mutants as compared to the wt. To evaluate those signaling components, total c-Met content, tyrosine (Y)1235,1236 phosphorylated c-Met, phosphorylated Erk 1/2 (Erk 1: threonine (T)202/204; Erk2: T185/187) and phosphorylated Akt (serine (S)473) were analyzed by immunoblotting.

Auto-activation of c-Met by Phosphorylation: For the normalization of phosphorylated c-Met originating from the transfected constructs, total c-Met as well as endogenous c-Met were determined and the mean signal intensity of endogenous c-Met was subtracted from each sample to yield the amount of expressed c-Met-eGFP construct. This value was then used to normalize the phosphorylated c-Met signal for each sample, eliminating differences in transfection efficiency between the different samples.

The non-transfected control cells [control(wt)] as well as the cells only transfected with a GFP-containing vector [GFP(wt)] showed nearly no phosphorylated c-Met as compared to the non-stimulated internal control in a resting state (Fig 19A). In contrast to that, wt c-Met-eGFP [wt(trans)] and all mutant constructs were already highly phosphorylated in a rested and non-stimulated state. While wt c-Met-eGFP as well as the K1104R, K1259R and K4xR mutants showed a 20 to 50 fold enhanced activation, K962R phospho-levels

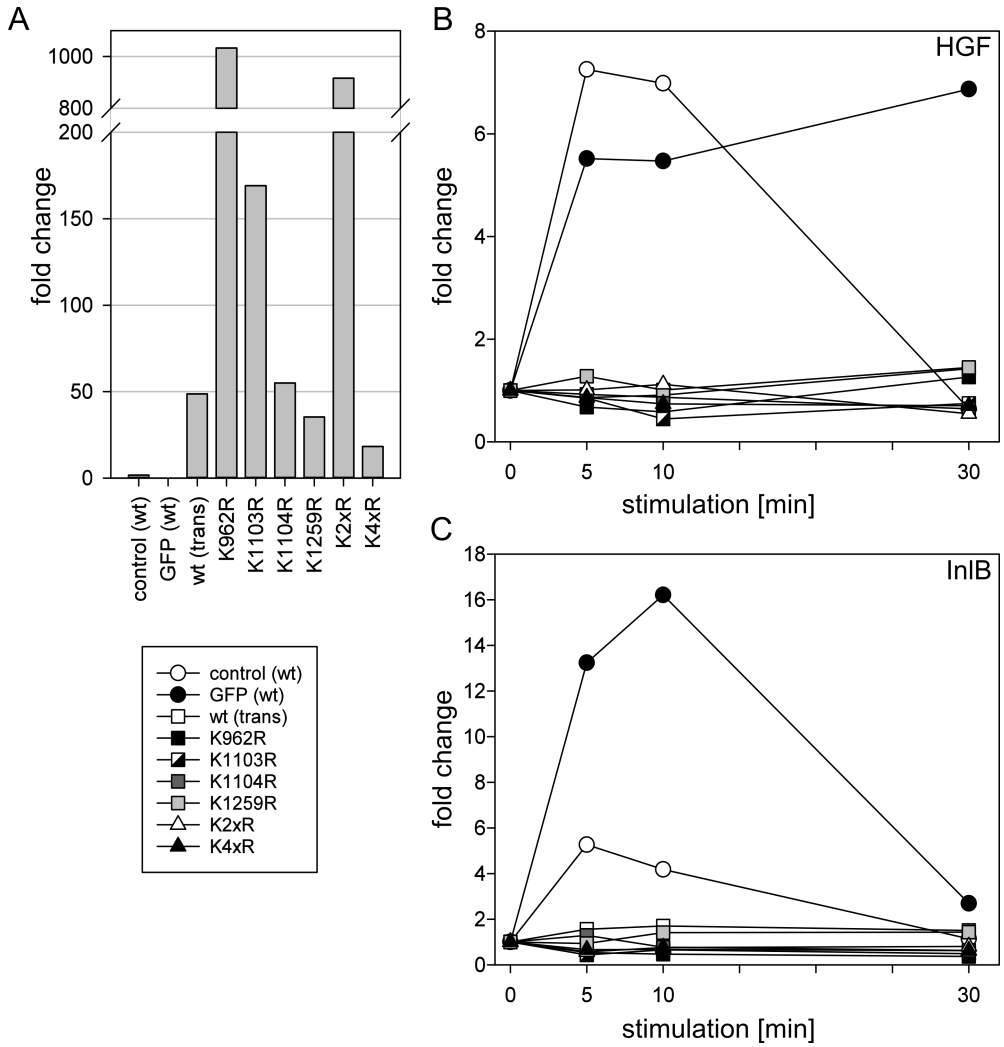

Figure 19. Activity of transfected and endogenous c-Met in rested cells and after stimulation with HGF and InlB. To asses activation of c-Met, phosphorylation at Y1235/1236 was monitored after 5, 10 and 30 min of HGF- or InlB stimulation in comparison to non-stimulated and non-transfected control cells. In graphs, circles indicate activation levels of endogenous c-Met, while squares specify single amino acid-exchange mutants. Triangles were used to mark the double and quadruple mutants. (A) Pre-activation of c-Met without stimulation. The phosphorylated c-Met levels observed in the constructs after starvation and mock-stimulation (30 min incubation with buffer) were compared to a non-stimulated internal control. The resulting fold change in phosphorylated c-Met intensity between control and the non-stimulated but transfected samples of the mutants is shown. (B) Corrected fold changes of phosphorylated c-Met intensities as compared to non-stimulated but transfected control (0') after stimulation of the sample with HGF for 5, 10 and 30 min. To analyze the activation of transfected c-Met only, the samples were normalized to the amount of transfected c-Met determined in anti-c-Met western blots corrected by the mean signal intensities of endogenous c-Met. (C) Corrected fold changes of phosphorylated c-Met intensities as compared to non-stimulated but transfected control (0') after stimulation of the sample with InlB for 5, 10 and 30 min. For normalization, the same method as described in B was applied.

were increased about 160 fold, and K1103R and K2xR about 1000 fold. Following HGF or InlB stimulation (Fig 19B&C), the endogenous wt c-Met (circles) showed increased phosphorylation as expected. In contrast to that, all transfected constructs revealed insensitivity towards the stimulus with fold changes of the signal intensity around 1. This, taken together with the pre-activation, indicates a permanent activation of the transfected c-Met receptor variants for wt and mutants alike, raising the question whether localization of the constructs resembles the wt c-Met or is disturbed leading to differential activation.

Activation of Erk Kinases 1 and 2: Downstream of c-Met, the Erk kinases 1 and 2 are activated upon stimulation with HGF or InlB. To monitor this activation, phosphorylation of Erk 1/2 at T202/204 and T185/187 was analyzed by western blotting. The blot results were normalized against signals of the house-keeper protein HSP90 obtained from the same blots after stripping. Similar to phosphorylated c-Met, Erk 1/2 pre-activation was analyzed by comparison of signal intensity of p-Erk in transfected, non-stimulated samples compared to the internal non-stimulated control signal of endogenous p-Erk. Pre-activation of Erk was found to be relatively low as compared to the pre-activation of c-Met for most of the constructs (Fig 20A). Solely, the quadruple mutant K4xR showed a fold change in intensity of about 100, indicating severe pre-activation. After stimulation of cells containing transfected wt c-Met-eGFP with HGF (Fig 20B) or InlB (Fig 20C), p-Erk signal intensities matched those of wt cells (HGF) or were at least similar (InlB). This might indicate that the transfected c-Met wt protein, although pre-activated, does not influence the downstream signaling after stimulation. The p-Erk signal of cells expressing mutant c-Met, except for K1103R and K4xR, also showed similar behavior as non-transfected cells but revealed a tendency towards a quenched signal after stimulation. For the K4xR mutant, p-Erk signal intensity showed no additional increase after HGF (Fig 20B) or InlB stimulation (Fig 20C). Thus, the transfected cells were rendered insensitive to Erk-activation, which is probably due to the high pre-activation level of the K4xR transfected cells.

Activation of Akt Kinase: The third signaling component monitored for activation was Akt, which is phosphorylated at serine 473 when activated by c-Met induced processes. The phosphorylated form was monitored by western blotting and signal intensities were normalized to the housekeeper protein HSP90. In contrast to c-Met and Erk, Akt showed only mild pre-activation (Fig 21A). The highest fold changes in pre-activation were found for the K2xR and K4xR mutants, with 5 and 3.4 fold, respectively. All other mutants and the transfected wt showed levels comparable to the increase in p-Erk. Notably, after stimulation with HGF, the course of the p-Akt signal of the K2xR mutant was similar to the endogenous signal (Fig 21B, white triangles/circles), although the same mutant showed the highest pre-activation. Additionally, both the wt and K2xR signals peaked

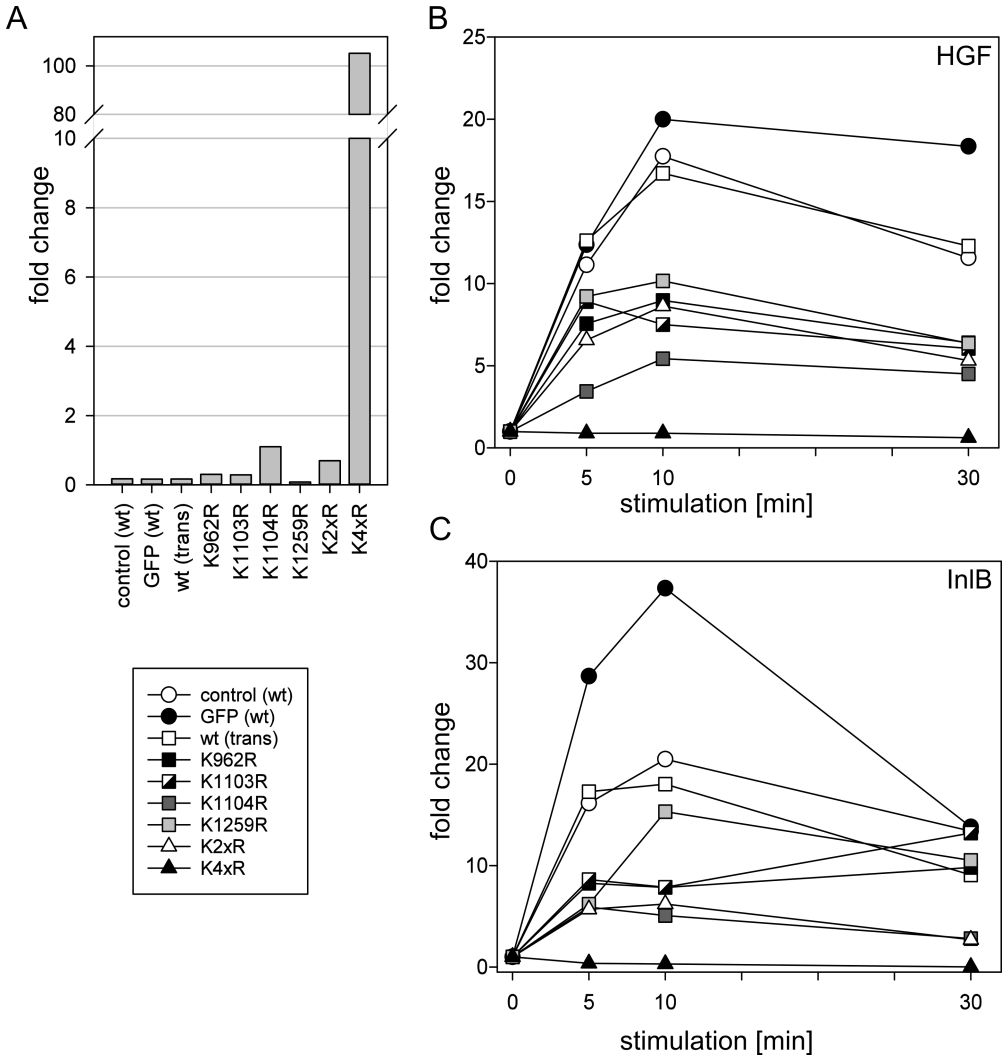

Figure 20. Activation of Erk 1/2 following stimulation of endogenous and transfected c-Met. Phosphorylation of Erk 1/2 at T202/204 and T185/187 was analyzed after stimulation with HGF or InlB for 5, 10 and 30 min in comparison to non-stimulated and non-transfected cells. In graphs, circles indicate endogenous c-Met, while squares specify single amino acid-exchange mutants. Triangles were used to mark the double and quadruple mutants. (A) Pre-activation of Erk without stimulation by HGF or InlB. The p-Erk 1/2 levels observed after starvation and mock-stimulation (30 min incubation with buffer) were compared to a non-stimulated internal control. (B) Fold change of endogenous p-Erk 1/2 intensities as compared to non-stimulated but transfected control (0') after stimulation of the sample with HGF for 5, 10 and 30 min. (C) Fold change of endogenous p-Erk1/2 intensities as compared to non-stimulated but transfected controls (0') after stimulation of the sample with InlB for 5, 10 and 30 min.

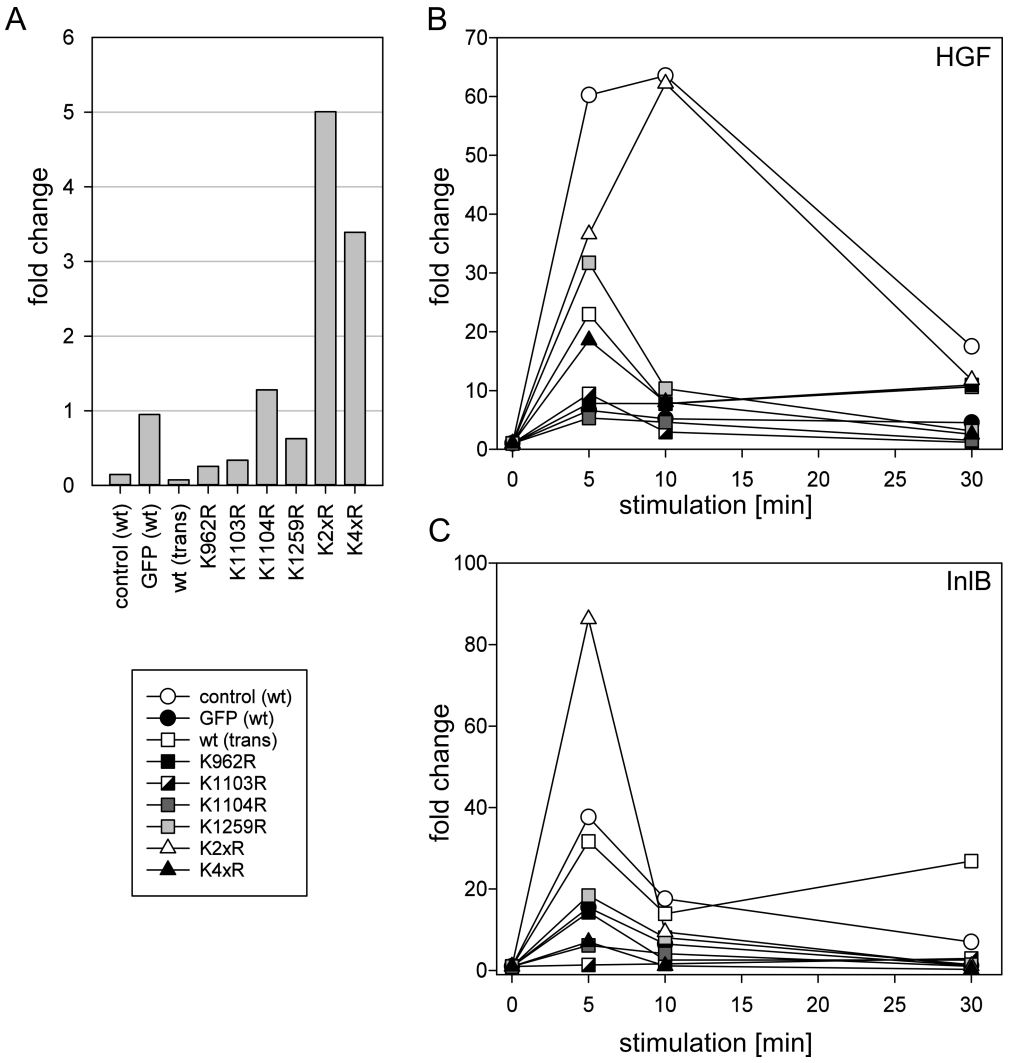

Figure 21. Activation of Akt after stimulation in comparison to non-stimulated and non-transfected cells. Phosphorylation of Akt at S473 was analyzed after stimulation with HGF or InlB for 5, 10 and 30 min in comparison to non-stimulated and non-transfected cells.All values were normalized to the house-keeper protein HSP90, obtained from the same blots as p-Akt. (B&C) Circles indicate endogenous c-Met, while squares specify single amino acid-exchange mutants. Triangles were used to mark the double and quadruple mutants. (A) Pre-activation of p-Akt without stimulation by HGF or InlB. The p-Akt levels observed after starvation and mock-stimulation (30 min incubation with buffer) were compared to a non-stimulated internal control. (B) Fold change of endogenous p-Akt intensities as compared to non-stimulated but transfected control (0') after stimulation of the sample with HGF for 5, 10 and 30 min. (C) Fold change of endogenous p-Akt intensities as compared to non-stimulated but transfected controls (0') after stimulation of the sample with InlB for 5, 10 and 30 min.

at 10 min, while the other samples reached the highest signal intensity at 5 min HGF stimulation. In InlB-stimulated cells (Fig 21C), the mutant signal was found to be even higher than the wt with an increase of about 80 fold over the control time point. All other constructs induced only a quenched phosphorylation of Akt with a peak at 5 min and a steep decline of the signal afterwards regardless of the stimulant. This behavior was also found for both samples only containing endogenous c-Met [control(wt) and GFP(wt)].

In summary, the analysis of phosphorylated c-Met, p-Erk and p-Akt indicated that the down-stream signaling was altered by some of the amino-acid exchanges, especially in the double and quadruple mutants which showed distinct reactions of p-Erk and p-Akt after stimulation. For K4xR, the results hint towards a permanent activation of c-Met and Erk 1/2 with a pre-activation of Akt and thus the signaling cascade downstream of c-Met. In contrast to that, for K2xR a high pre-activation of c-Met was found, with only small influence on p-Erk but a seemingly hyper-activated Akt reaction.

The data needs to be substantiated by biological replicates or further experiments in knock-out cells to make more definite statements regarding the influence of ubiquitin-deficiency on the activation of the signaling cascade. Additionally, the results indicate a differential activation of all transfected c-Met constructs, implying the need to analyze the localization of c-Met in stimulated and non-stimulated cells.

4.1.2.2 Cells Containing Transfected wt c-Met-eGFP Show Differences in Signal-intensities in HeLa S3

To analyze the localization of the site-specific ubiquitination-deficient mutants of c-Met, epifluorescence microscopy was utilized, taking advantage of the intrinsic green fluorescence of the constructs. As a first step, the localization of the wild-type c-Met-eGFP construct was evaluated. Analysis of the samples revealed more than one population of c-Met-eGFP positive cells (Fig 22A). Importantly, those populations and control cells were found in one image and therefore, allowed direct comparison to each other.

Among the cells carrying the transfected wt c-Met-eGFP, the most obvious population were highly expressing cells (Figure 22). In those cells, both endogenous and transfected c-Met localized to the surface of the cells. Additionally, a perinuclear green fluorescent signal, which was described for this vector before [221] and furthermore only incompletely recognized by the anti-c-Met antibody (red channel), was encountered.

The second population of cells showed an intermediate expression of c-Met-eGFP (Fig 22C). Cells with this expression level showed a similar surface-localization as the high-expressing cells with a part of transfected c-Met also localizing to the perinuclear region. In contrast, in non-transfected HeLa S3 cells, which were neither starved nor explicitly stimulated, c-Met localized in pit-like structures (Fig 22D).

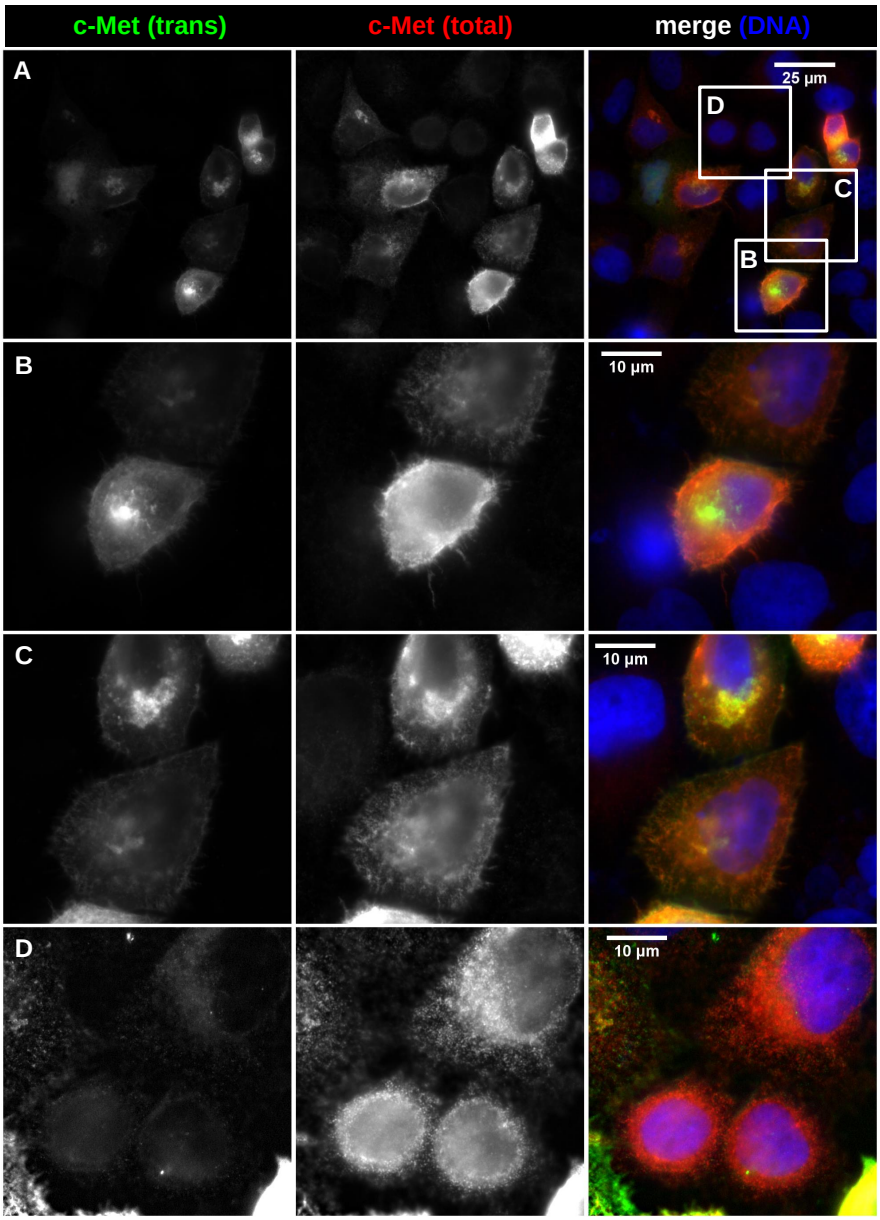

Figure 22. Localization-analysis of wild type c-Met-eGFP in high and intermediate expressing HeLa S3 cells. HeLa S3 cells were transfected with a wild-type c-Met-eGFP plasmid, fixed after 48 h and finally evaluated by epifluorescence microscopy. (A-D) The left panel shows the signal of the transfected c-Met-eGFP fusion (green in merged images). The middle panel shows the signal of total endogenous and transfected c-Met stained with a monoclonal Ab against c-Met (red in merged images). The merged images additionally depict the DNA content of the cells stained by DAPI (blue). (A) Overview of a typical image of transfected HeLa S3 cells. The lettered white squares represent the approximate clippings of the three following panels. (B) Highly expressing transfected cell showing c-Met membrane-localization and perinuclear signal. (C) Cells expressing c-Met-eGFP with an intermediate intensity as compared to the non-transfected cells. (D) Non-transfected control cells from the same image as transfected cells show a typical c-Met localization in vesicle-like structures.

This "unrested" localization of endogenous c-Met is triggered by some components of the FCS used, which are able to activate c-Met.

In summary, two expression levels of wt c-Met-eGFP were found in transfected cells. Both of them showed a surface-localization of c-Met, which does not resemble the observed localization of endogenous c-Met but rather a localization assumed for starved cells. However, as differences in signaling after stimulation were observed, the localization of wt c-Met-eGFP after HGF and InlB stimulation will be analyzed.

4.1.2.3 In Cells with Low Expression Levels, Wild-type c-Met-eGFP and Endogenous c-Met Co-localize

Following stimulation with 10 nM HGF or InlB for 30 min, cell populations were evaluated regarding localization of the transfected, wt c-Met-eGFP compared to the endogenous receptor (Figs 23 & 24).

After 30 min of stimulation with HGF, endogenous c-Met showed perinuclear localization in pit-like structures (Fig 23A, white arrow). In general, transfected cells exhibited an extensive co-localization of endogenous and transfected c-Met as seen by the yellow color in the merged images. The high amount of transfected c-Met is probably influencing the localization of endogenous c-Met, which would explain the localization deviating from the endogenous wt in non-transfected cells.

Highly c-Met expressing cells displayed an unchanged surface localization, as highlighted by the white arrow (Fig 23B), and an additional perinuclear signal for both c-Met variants. The intermediate-expressing cell population showed a two-part localization of c-Met (Fig 23C). A fraction of c-Met localized at the cell-tips (white arrows) while the major part of transfected c-Met was allocated in vesicle-like structures (yellow arrows). During data evaluation, a third transfected cell population was detected (Fig 23D). Some cells expressed the transfected c-Met at low levels just above the auto-fluorescence-signal of HeLa S3 cells. Those cells showed a only slightly enhanced total c-Met content and could only be observed in stimulated cells after 5 to 10 min stimulation (data not shown), probably due to the formation of the pit/vesicle-like structures. In HGF stimulated, low expressing cells, c-Met localized in structures (white arrows) analogous to non-transfected cells (yellow arrows) (Fig 23D). Again, both c-Met variants co-localized in the vesicles indicating comparable dynamics.

After InlB-stimulation for 30 min, the non-transfected cells showed a comparable c-Met localization as the HGF-stimulated cells forming pit-like structures (Fig 24A). Here, too, the highly expressing cells showed a membrane-localization of c-Met (Fig 24B). In contrast, the cells with an intermediate c-Met-eGFP expression level showed only a weak surface-localization (white arrows) and vesicle-like structures (yellow arrows) in which endogenous and transfected c-Met co-localized as seen in the merged image (Fig 24C). Not only among HGF-stimulated but also in InlB-stimulated cells, low level-transfected

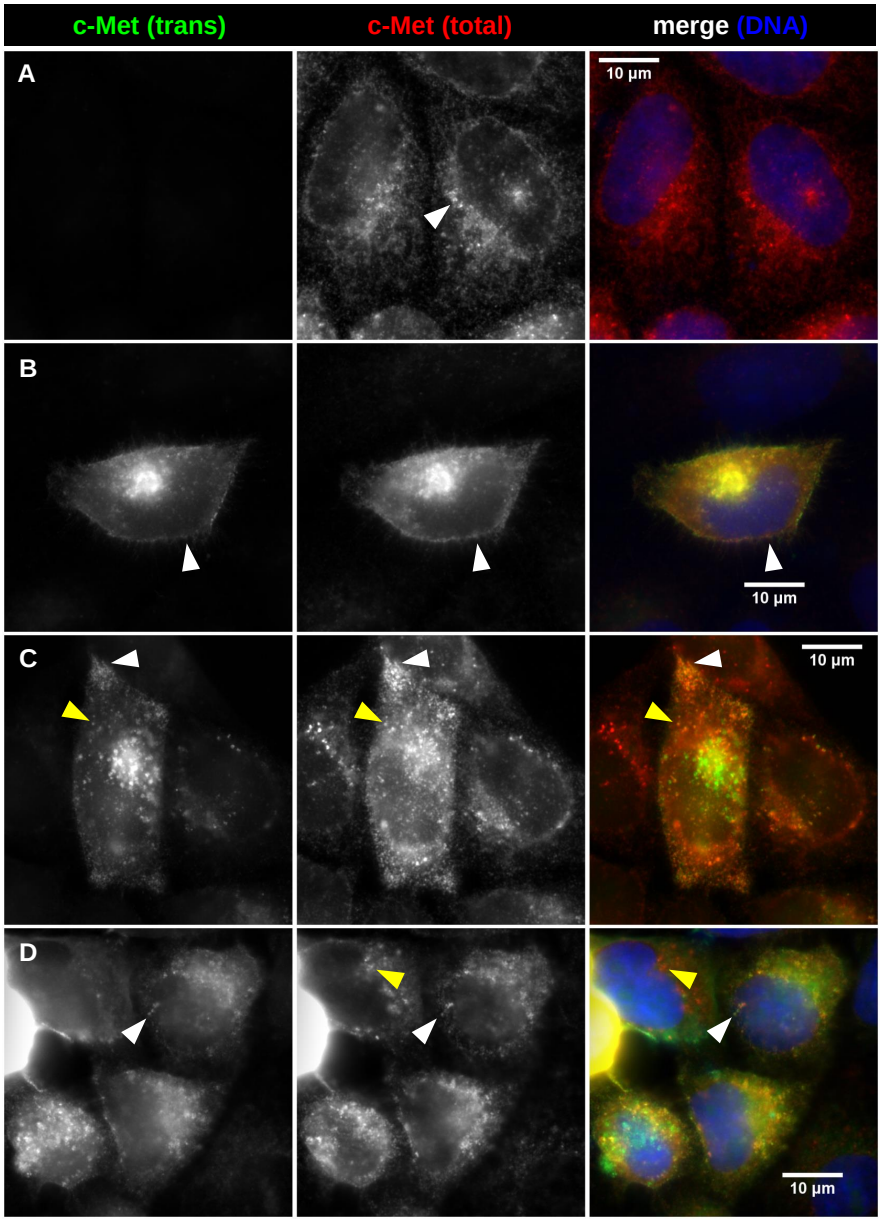

Figure 23. Localization of wild-type c-Met-eGFP in HeLa S3 cells after 30 min HGF-stimulation in high, medium and low-expressing cells. Cells were starved for 24 h and then stimulated with 10 nM HGF for 30 min. After fixation, cells were stained with anti-c-Met antibody and DAPI. (A) c-Met localization in non-transfected HeLa S3 cells stimulated with HGF for 30 min. c-Met was confined to vesicle-like structures as indicated by the white arrow. (B) Typical, highly c-Met-eGFP expressing cell. Although the cells were HGF-stimulated, they do not show the wt phenotype presented in A but surface localization of c-Met (white arrow). (C) Representative cells with a intermediate expression of wt c-Met-eGFP. White arrows indicate localization at the cell-tip. A part of the c-Met receptors also localized vesicular (yellow arrows). (D) Cells with a low expression of c-Met-eGFP. Those cells showed a wild-type like localization of c-Met in vesicular structures (white arrows). Yellow arrows indicate the same structures in a neighboring non-transfected cell.

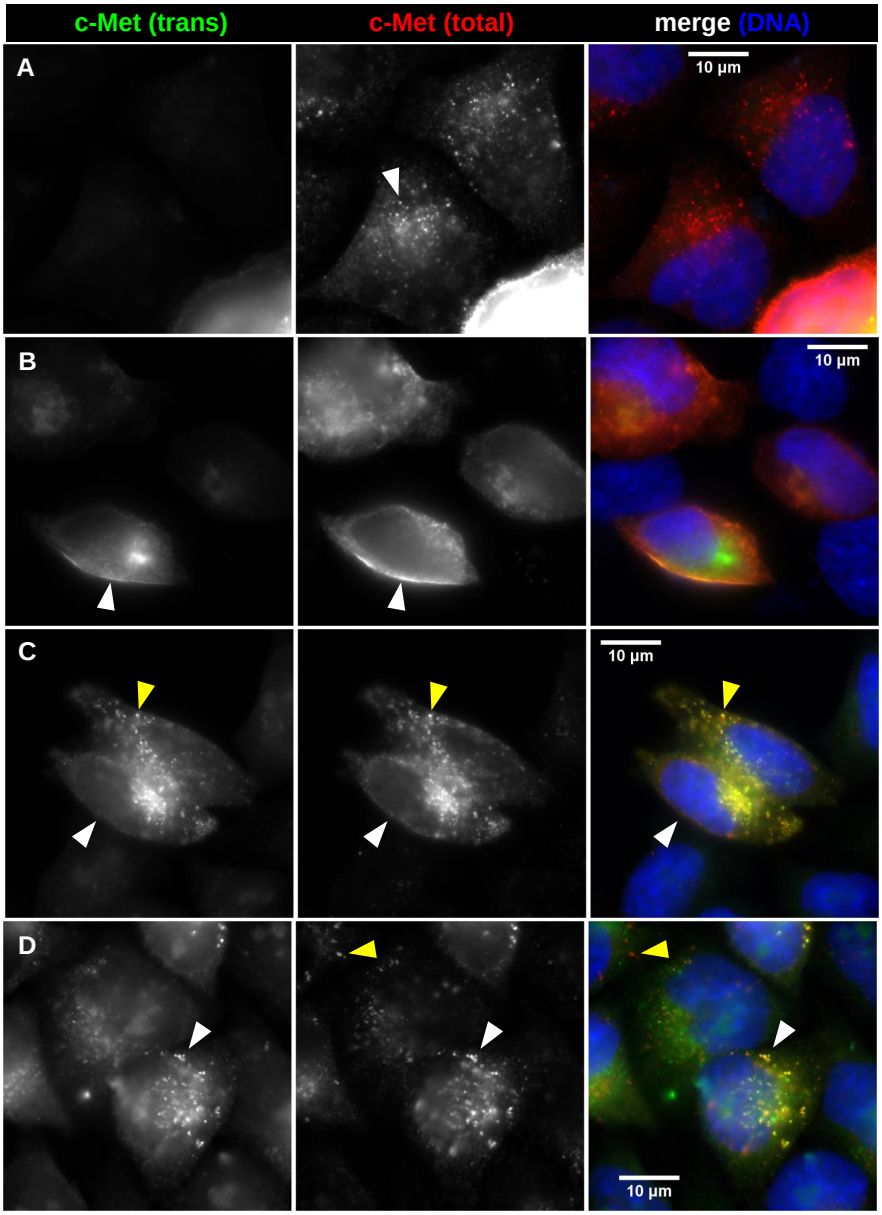

Figure 24. Localization of wild type c-Met-eGFP in HeLa S3 cells after 30 min InlB-stimulation in high, intermediate and low-expressing cells. (A) Distribution of wt c-Met in non-transfected control cells after InlB-stimulation. Cells show pit-like structures with enhanced c-Met signals (white arrow). (B) Representative cell with a high expression-level of wt c-Met-eGFP. The white arrow indicates the surface-localization of endogenous and transfected c-Met. (C) c-Met allocation in cells with an intermediate expression level. Both localizations, surface (white arrow) and in vesicle-like structures (yellow arrows) were found in those cells. (D) Cells with a low expression level of c-Met-eGFP after InlB-stimulation. Both, wild-type (yellow arrows) and transfected cells (white arrow) showed the same localization of c-Met in pit-like structures after InlB-stimulation.

cells were identified (Fig 24D). Those cells displayed a c-Met localization in vesicle-like structures (white arrows) which compared well to c-Met structures in non-transfected cells (yellow arrows).

In summary, cells transfected with wt c-Met-eGFP formed three distinct populations regarding the strength of c-Met expression. While the highly and intermediately expressed c-Met levels were detectable in non-stimulated and stimulated cells, low-expressing cells could only be monitored after stimulation with HGF or InlB. Stimulated cells with high or intermediate levels of c-Met-eGFP showed distinct localizations of c-Met, which were deviating from c-Met localization in non-transfected cells but consistent between HGF and InlB. For both, physiological and pathogenic effector stimulation, cells with low levels of c-Met-eGFP showed wt-like receptor localization. Therefore, this population was analyzed for differences in localization of the ubiquitination-deficient site-directed mutants of c-Met.

4.1.2.4 Ubiquitination-deficiency Does Not Influence c-Met Localization after HGF or InlB Stimulation in HeLa S3 Cells

Subsequent to the characterization of the wild-type c-Met-eGFP construct, the localization of all site-directed mutants of c-Met was investigated to clarify whether the Ub-deficiency has an influence on the receptor-localization after stimulation. In general, all mutants showed a strong co-localization between endogenous and transfected c-Met and displayed expression profiles and localizations described for the wt in the previous subsection (data not shown).

For localization-analysis, only transfected cells with low level of c-Met-eGFP expression were utilized, as the localization of c-Met in those cells closely resembled that of wt c-Met. High and intermediate expressing cells either showed surface or mixed localization as described before for the wt c-Met-eGFP construct (data not shown).

To evaluate the mutants with a exchange of lysine (K) 962, 1103, 1104 or 1259 to arginine (R) as well as the double mutant of K1103R and K1104R (K2xR) and the quadruple mutant (K4xR) for their localization following stimulation, all constructs were transfected and analyzed after 30 min of 10 nM HGF or InlB-stimulation.

Endogenous c-Met localized in vesicle-like structures in proximity to the nucleus after stimulation (Fig 23A & 24A) and all HGF-stimulated mutants showed a similar localization of transfected c-Met in pit-like structures and no additional red signals for the endogenous c-Met population (Fig 25).

In accordance with the observations for the HGF-stimulated cells, all mutants stimulated with InlB at the same concentration for 30 min showed the same vesicular localization (Fig 26). Here, too, localization of endogenous and transfected c-Met was the same, as represented by the yellow color occurring in the merged images. Notably, in most

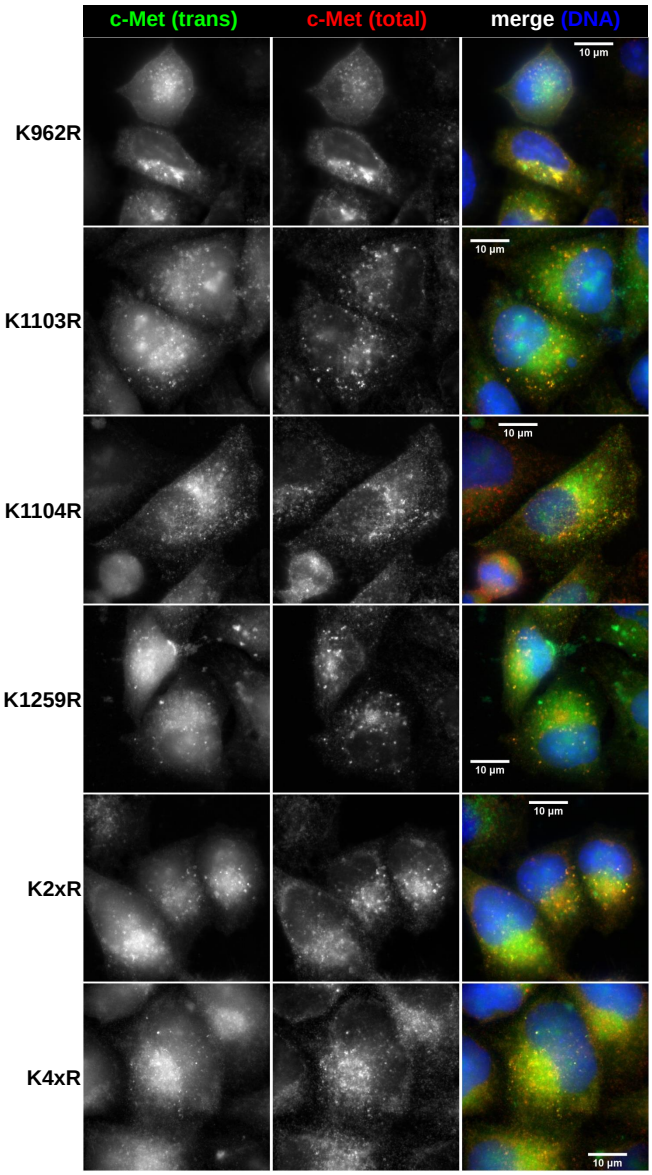

Figure 25. Localization of ubiquitination-deficient c-Met mutants in HGF-stimulated HeLa S3 cells. All cells were stimulated with 10 nM HGF for 30 min and stimulation was arrested by addition of 4 % PFA. Subsequently, cells were stained for c-Met (red channel) and DNA content (blue channel). Additionally, all shown cells expressed the respective mutagenized c-Met receptors at low levels. Yellow color in the merged image indicates co-localization while red indicates exclusive localization of endogenous c-Met. Green signals account for either autofluorescence of HeLa S3 cells or perinuclear c-Met fragments, which were not labeled by the antibody .

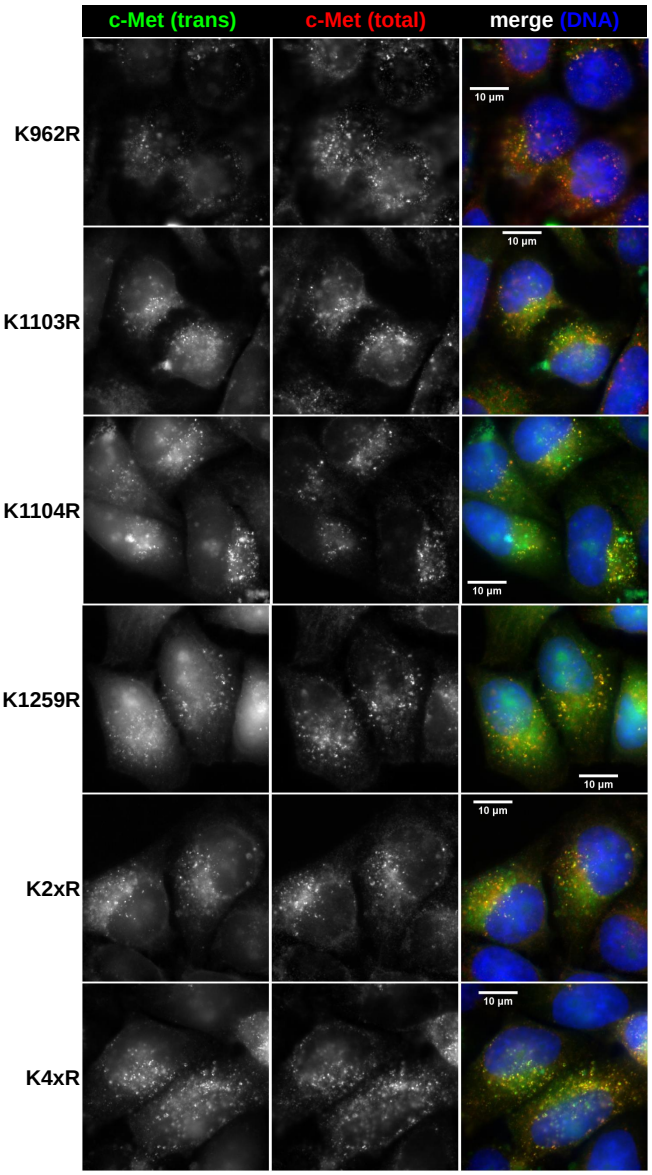

Figure 26. Localization of ubiquitination-deficient c-Met mutants in InlB-stimulated HeLa S3 cells. All cells were stimulated with 10 nM InlB for 30 min and stimulation was arrested by addition of 4 % PFA. Subsequently, cells were stained for c-Met (red channel) and DNA content (blue channel). Additionally, all shown cells expressed the respective mutagenized c-Met receptors at low levels. Yellow color in the merged image indicates co-localization while red indicates exclusive localization of endogenous c-Met. Green signals account for either autofluorescence of HeLa S3 cells or perinuclear c-Met fragments, which were not labeled by the antibody.

cells solely green signals were detected. This might either be due to autofluorescence of the HeLa S3 cells, a degraded c-Met population not detected by the antibody or a portion of free eGFP. However, those signals were not considered for the analyses of c-Met localization.

In summary, all mutants analyzed, i.e. K962R, K1103R, K1104R, K1259R, K2xR and K4xR, showed no obvious differences in localization as compared to wt c-Met when stimulated with 10 nM HGF or InlB for 30 min. The major signals in vesicular structures showed clear yellow color in merged images. As no solely red signals were detected in transfected cells, it is concluded that the receptor internalization of the ubiquitination-deficient c-Met mutants was comparable to the wt and did not show impaired or shifted dynamics. Furthermore, no difference was observed between HGF and InlB as a stimulant. However, attention should be paid to the fact that the experiments were carried out in cells containing endogenous c-Met. Additionally, the influence of c-Met ubiquitination onto the recycling or degradation of the receptor requires further discussion.

4.1.3 Regulation of c-Met Receptor Ubiquitination by DUBs

Not only addition of ubiquitin but also its removal by DUBs contributes to the balance of ubiquitin-mediated processes. For c-Met, no DUB which is directly involved in c-Met deubiquitination was described so far. However, knock-out of USP8 (UBPY) in mice produced a phenotype of impaired c-Met recycling [222] and A549 cells from a panel of DUB knock-outs reacted differentially to HGF stimulation [137]. To tackle this gap in knowledge, potential candidate DUBs were analyzed regarding their co-localization with c-Met. In order to do this, HeLa S3 cells were stimulated with HGF or InlB and subsequently analyzed for c-Met and candidate DUB localization by epifluorescence-microscopy.

4.1.3.1 Regulated Phosphorylation Sites of VCPIP1 & USP8 Do Not Influence DUB Localization after HGF- and InlB-stimulation

To obtain a first clue as to which DUBs might be responsible for c-Met deubiquitination, a phosphoproteome study of HGF-stimulated cells was analyzed for DUBs with significantly regulated phosphosites [223]. The study revealed a downregulation of S768 on the DUB VCPIP1 after stimulation, rendering VCPIP1 a potential candidate for further localization experiments. Additionally, on USP8, S452 was found to be upregulated. Therefore, VCPIP1 and USP8-localization were analyzed in this study.

VCPIP1: The 0 min (neg) control sample illustrates the cell membrane localization of c-Met after resting of the cells (Figure 27). Controls to assess the influence of the buffer in which HGF and InlB were solved, were also conducted and showed no difference

to the negative control (Suppl. Fig S3 & S4). Following stimulation by HGF or InlB, c-Met clustered in vesicle-like structures after 5 min with a peak at 30 min followed by a beginning recycling to the cell membrane at 60 min (Fig 27). In contrast, the VCPIP1 signal (red) was found to be distributed evenly throughout the cells with a signal-increase few bright, dot-like signals in the nuclear compartment.

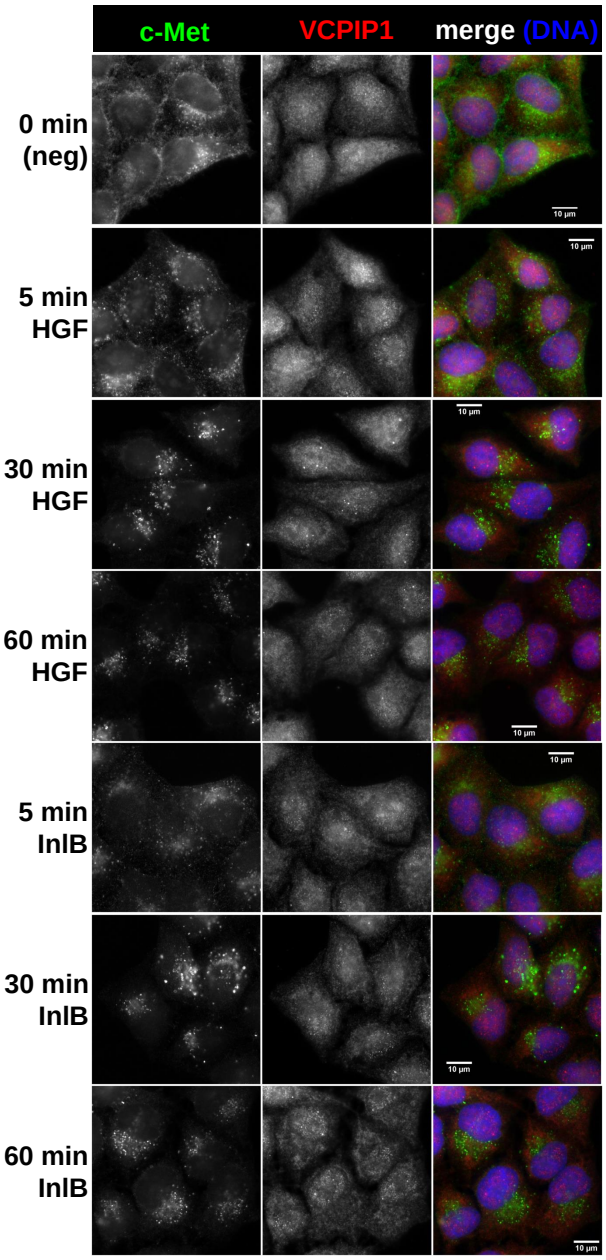

Figure 27. VCPIP1 localization during HGF and InlB stimulation in HeLa S3 cells. HeLa cells were stimulated with 10 nM HGF or InlB for the indicated time periods and subsequently stained for c-Met (green), VCPIP1 (red) and DNA content (blue). Finally, samples were analyzed by epifluorescence microscopy. The white bar represents 10 µm. The negative control [0 min(neg)] shows cells which were only starved, but not stimulated. For both, HGF- and InlB-stimulated cells, the typical c-Met vesicular structures were observed after 30 min of stimulation. For VCPIP1, no major changes in localization and no direct co-localization with c-Met were observed. Additional time points and controls are provided in the Appendix (Figures SS3 & SS4).

The Human Protein Atlas (HPA) [224, 225] denoted a probably cell-membranous localization for VCPIP1, while UniProt gene-ontology (GO) annotation states a cytoplasmic and endoplasmic reticulum localization. During the course of stimulation with HGF or InlB monitored (Fig 27 and Suppl. Figs SS3 & SS4), for VCPIP1 (red channel) neither a change in its localization nor co-localization with c-Met was observed. Those results indicate, that VCPIP1 is an unlikely regulator of c-Met receptor ubiquitination.

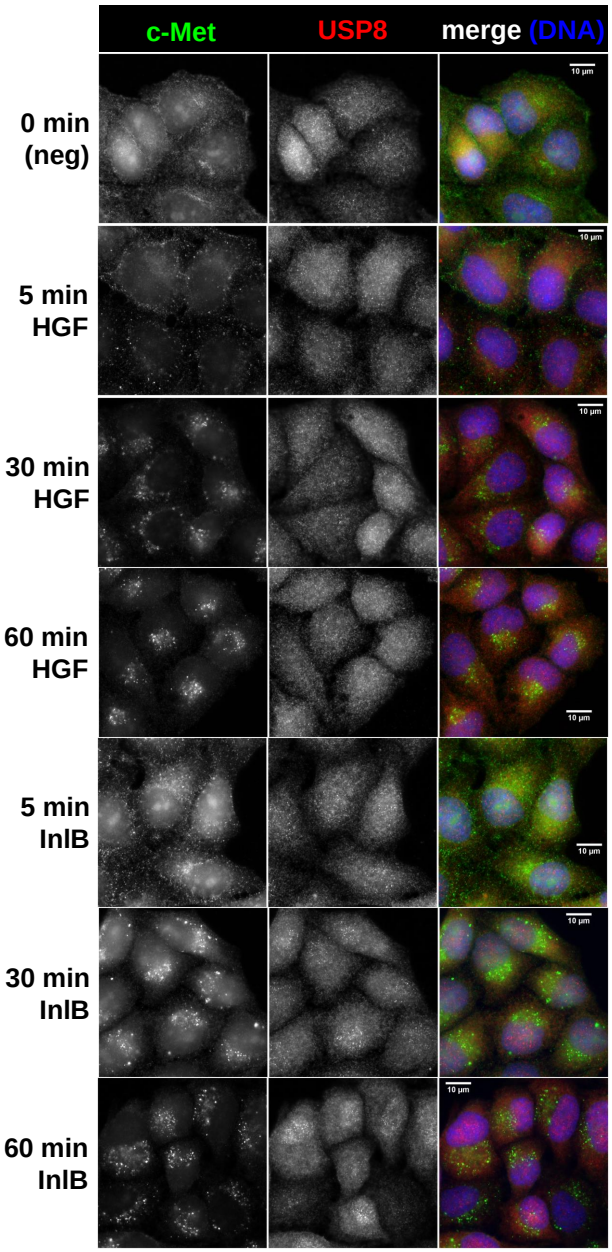

Figure 28. USP8 localization during HGF and InlB stimulation in HeLa S3 cells. HeLa cells were stimulated with 10 nM HGF or InlB for the indicated time periods and subsequently stained for c-Met (green), USP8 (red) and DNA content (blue). The white bar represents 10 µm. The negative control (0 min(neg)) shows cells which were only starved, but not stimulated. For USP8, no major changes in localization and no direct co-localization with c-Met were observed. Additional time points and controls are provided in the Appendix (Figs S5 & S6).

USP8: The second candidate DUB, USP8, was also analyzed for its localization regarding c-Met in the same way as described above for VCPIP1. In general, c-Met showed the typical reaction to activation with its ligand as described before (Fig 28; Suppl. Figs S5 & S6). In contrast, USP8 signals were found to be broadly distributed within the cells with higher intensities in the nuclear compartment, similar to VCPIP1. The HPA specified a localization in Golgi apparatus and cytoplasm, while UniProt GO annotations for subcellular localization hint to a more global distribution, including not only cytoplasm, but also nucleus and various membranes, which matches the localization found in the HeLa S3 cells. Notably, the localization of USP8 did not change during the stimulation with HGF or InlB. Additionally, no visible co-localization to c-Met occurred, although USP8 was described to be involved in RTK-recycling for other receptors.

In summary, neither VCPIP1 nor USP8 displayed a re-localization in response to HGF or InlB stimulation for up to 1 h. Furthermore, although c-Met showed accumulation in vesicles up to 30 min and subsequent recycling to the membrane and thereby excessive reallocation within the cell, no co-localization between the DUBs and c-Met was detected in this setup.

4.1.3.2 c-Met-specific Ubiquitin-isopeptide Probes Define DUB Candidates for c-Met Deubiquitination

As the preceding investigations did not detect a DUB directly interacting with c-Met, a complementary approach to identify further DUB candidates was applied. To this end, the in-house developed concept of Ubiquitin-Isopeptide probes (UIPPs) was applied. These probes harbor a reactive group, which links the probe covalently to active DUBs and uses the peptide sequence of the substrate to generate specificity (Fig S17A) [95]. In case of c-Met, 4 peptide-warheads containing c-Met sequences surrounding the lysines also chosen for mutant-generation (K962, K1103, K1104 and K1259) were produced successfully (Table 10). However, only the c-Met$_{K962}$-UIPP could be produced in a sufficient amount for further analyses due to ligation-difficulties accounted for by the high hydrophobicity of the peptide warheads.

To explore the binding of DUBs towards the c-Met$_{K962}$-UIPP, the probe was incubated with a panel of recombinant DUBs and analyzed by immunoblotting. Four USPs, two UCHs and one OTU-family DUB were able to bind the probe (Fig 29), while all other DUBs utilized showed no activity towards the c-Met$_{K962}$-UIPP (Suppl. Fig S17). Of those, the catalytic domain of USP2 showed the most prominent binding, while CYLD and USP21 showed only relatively faint shifted bands. (Fig 29B). The same is valid for BAP1, USP15 and OTUB1, which exhibited only extremely weak activity towards the c-Met$_{K962}$-UIPP resulting in a hardly visible shifted band (Fig 29C). Therefore, those DUBs were assumed to be not specifically reactive towards the sequence surroundings of

K962 of c-Met. The last binding DUB, UCHL3, showed a good reactivity towards the UIPP (Fig 29C), but as UCHL3 does not process poly-Ub chains *in vitro* [56, 226] and is likely to cleave ubiquitinated peptides [227], it was not considered to be of particular interest.

However, CYLD, USP2 and USP21 were included for further investigation of their binding towards the ubiquitinated c-Met RTK by immunofluorescence microscopy, as the binding to the UIPP suggests a deubiquitinating activity against the c-Met sequence surroundings.

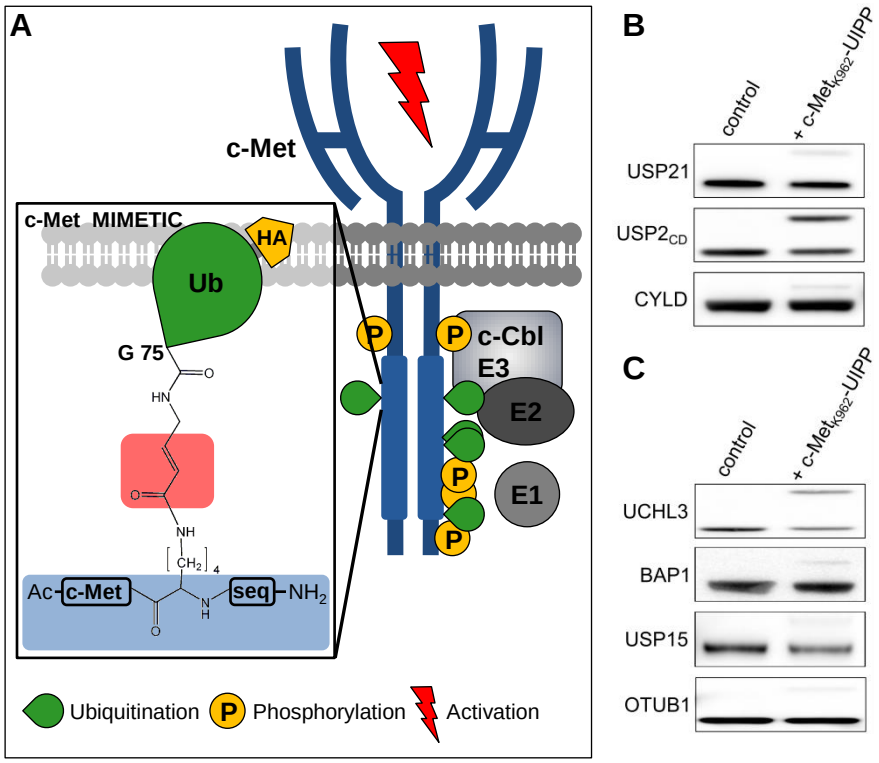

Figure 29. Reactivity of recombinant DUBs towards the c-Met $_{K962}$-UIPP. (A) Scheme of c-Met-UIPP, presenting the structure of the UIPP as well as surroundings and assumed PTM-situation of c-Met after activation. (B) DUBs with a clear shift for c-Met$_{K962}$-UIPP. (C) DUBs that also showed a shift, but were not included in further experiments. (B&C) All DUBs were incubated with the c-Met$_{K962}$-UIPP for 1 h at 37°C. Subsequently, the samples without (control) and with probe were applied to SDS-Page and western blotting. The DUBs were detected by an α-HIS$_6$ antibody. The full panel is presented in Figure S17. A second band above the original one (DUB in control) indicates binding of UIPP and DUB, thus leading to the shift in MW.

4.1.3.3 Two of the Three Candidate DUBs, USP21 and CYLD Show Localization-changes during InlB-stimulation

USP21: The first candidate, USP21 showed a mitochondrial localization (Fig 30 and Suppl. Fig S9). Notably, USP21 was only described as localized in cytoplasm and nucleus (HPA) as well as microtubule-associated and centrosomal [228] in different cell lines before. Beginning as early as 5 min after stimulation, USP21-positive structures formed brighter spots in the perinuclear area of the cell. At 10 to 30 min InlB a relatively small portion of c-Met is found to be re-localizing to this USP21-intense area as indicated by the white arrows in Figure 30. Although the merged image showed yellow and orange coloring in that area, it is not certain whether c-Met and USP21 directly interact with each other. The interaction would have to be validated either by high-resolution microscopy or IP-experiments. However, it is interesting to speculate about the role of the small portion of c-Met which is found in vicinity to USP21 after InlB stimulation.

USP2: For USP2, the observed cytoplasmic localization is in accordance with the data from Human Protein Atlas and UniProt KB. The DUB showed this localization throughout all stimulation experiments without any visible re-localization (Suppl. Fig S7). In contrast, c-Met showed the typical re-localization after stimulation as described before. However, no co-localization between c-Met and USP2 was observed at the monitored time points following InlB stimulation in this study.

CYLD: The third candidate, CYLD, also showed a cytoplasmic and additional nuclear localization within high and lower expressing cells, but no visible co-localization to c-Met (Fig 31 & Suppl. Fig S8). However, starting at 20-30 min of InlB-stimulation, CYLD formed dot-like structures of higher fluorescence in the nucleus (white arrows) while at earlier time points and in the controls, the nuclear CYLD was found to be more evenly distributed (red arrows) (Fig 31). Following the course of stimulation to 60 min, some nuclei showed those structures while others (yellow arrows) revealed a lower intensity in nuclear CYLD signals. In summary, although CYLD does not co-localize with c-Met after InlB-stimulation, its localization is influenced by the stimulation in an InlB-dependent manner after c-Met activation. As CYLD is already known to regulate NF-κB activation in infection and immunity (subsection 1.2.2) and additionally has a severe influence on Lm infection *in vivo* (subsection 1.2.2.1) the relocalization could be a manifestation of a function CYLD exhibits during the early Lm invasion processes. It would be of high interest to characterize the c-Met dependent invasion of Lm into CYLD-knockout cells.

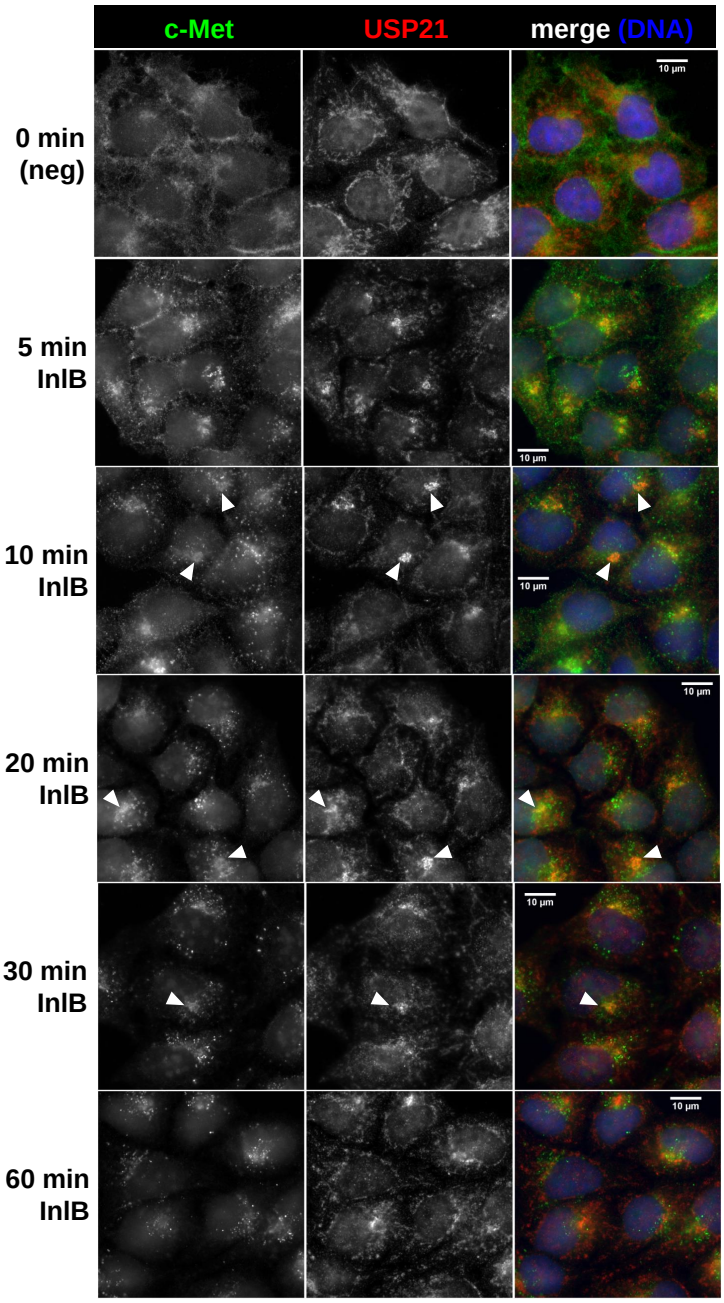

Figure 30. Localization of USP21 at different, sequential time points of InlB stimulation in HeLa S3 cells. All cells were stimulated with 10 nM InlB for the indicated time periods. Subsequently, stimulation was stopped by fixation of cells. Finally, the cells were stained for c-Met (green), USP21(red) and DNA content (blue) and USP21-localization was evaluated. The white bar represents a scale of 10 µm. The 0 min (neg) sample was only rested but not stimulated. White arrows indicate spatial overlap of c-Met and USP21 signals resulting in orange/yellow signals in the merged images. Additional time points and controls are provided in the Appendix (Suppl. Fig S9).

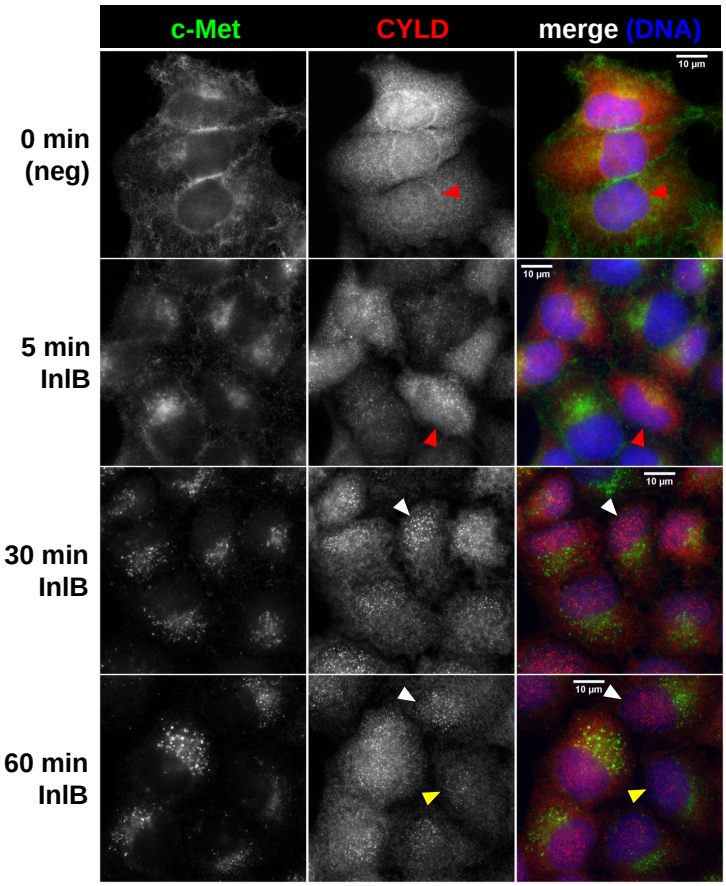

Figure 31. Localization of CYLD at distinct time points of InlB stimulation in HeLa S3 cells. All cells were stimulated with 10 nM InlB for the indicated time periods. Subsequently, stimulation was stopped by fixation of cells. Finally, the cells were stained for c-Met (green), CYLD (red) and DNA content (blue), and CYLD-localization was evaluated. The white bar represents a scale of 10 µm. The 0 min (neg) sample was only rested but not stimulated. Red arrows indicate the nuclear localization before and at the beginning of stimulation. Starting with 30 min of InlB treatment, CYLD accumulates in dot-like structures in the nucleus (white arrows). At 60 min after stimulation, some nuclei show the same accumulation, while others (yellow arrows) show weaker signal intensities. Additional time points and controls are provided in the Appendix (Figure S8).

4.2 Systemic Lm Infection - Hepatic Protein Responses in Murine Listeriosis

Although the infection cycle of *Listeria monocytogenes* (Lm) is a well known, information regarding the systemic host responses towards Lm infections is missing. As Lm is able to cross several tissue barriers and to cause systemic infections, the analysis of a whole organ is of interest to understand the influence of Lm infection on the host proteome. One of the main sites of infection following spread of bacteria through the bloodstream is the liver. All infections and the following experiments to characterize the liver infection (CFUs, FACS, RT-PCR) were carried out by Dr. Nishanth Gopala Krishna in cooperation with Prof. Dirk Schlüter (both University hospital (OVGU), Medical Microbiology, Magdeburg).

This part of the study intends to characterize the hepatic protein response to Lm infection for the first time, to achieve 3 major goals:

1. to evaluate the suitability of this mouse infection model for a mass spectrometric

analysis of the hepatic protein response and to pre-characterize the chosen time-points regarding their immune-cell population and cytokine profiles,

2. to unveil host proteins involved in the pathophysiology of Lm infection and bacterial clearance,

3. to analyze the influence of Lm infection onto the physiological liver processes,

4. and to reveal Ub and UBL-system components implicated in the regulation of Lm infection on the side of conjugation and deconjugation.

4.2.1 Sub-lethal Listeriosis Features Immune Cell Infiltration and Dynamic Cytokine Responses

To reach the first goal, colony-forming units (CFUs), cytokine profiles and immune cell content of murine liver samples were determined. Therefore, mice were inoculated with 1×10^4 bacteria and livers were harvested after 1, 3 or 9 days of infection. In general, the *Listeria* amounts in the livers were well-comparable between the different replicates of each time point. For day 1 p.i., the CFUs resembled the initial Lm amounts accumulating in the liver after infection. Subsequently, the CFUs rose as bacteria were replicating in the liver and then diminished between day 3 and 9 as clearance was setting in (Fig 32A).

4.2.1.1 Characteristics of Leukocyte Populations Define Innate and Adaptive Phases of Infection

During the activation of the host-defenses, immune cells infiltrate the liver tissue. Analysis of innate immune cells (Fig 32B) revealed that only macrophage (MΦ) numbers showed dynamics directly congruent with the CFUs peaking at day 3. On the contrary, inflammatory monocyte (Mo), neutrophil (Neu), dendritic cell (DC) and natural killer cell (NK) counts gradually increased throughout the monitored time-points. NK cells represented the largest set of innate immune cells with about 36 % of all detected innate cells and displayed an early accumulation. While monocytes and neutrophils also accumulated directly after inoculation, DC numbers increased mainly between day 3 and 9 p.i.

As it is described for Lm infection, that monocytes differentiate into DCs after encounter of Lm and prime $CD8^+$ T cells [229], the late cell dynamics of monocytes and DCs are sensible. Besides the innate cells, major adaptive immune cells were also monitored as presented in Figure 32C. All three sets of cells, B cells, $CD4^+$ T cells and $CD8^+$ T cells accumulated rapidly between day 3 and 9, marking the onset of adaptive responses towards the Lm infection. In general, all of those cell populations presented higher numbers than the innate cells and showed comparable amounts of about 5×10^6 cells per population.

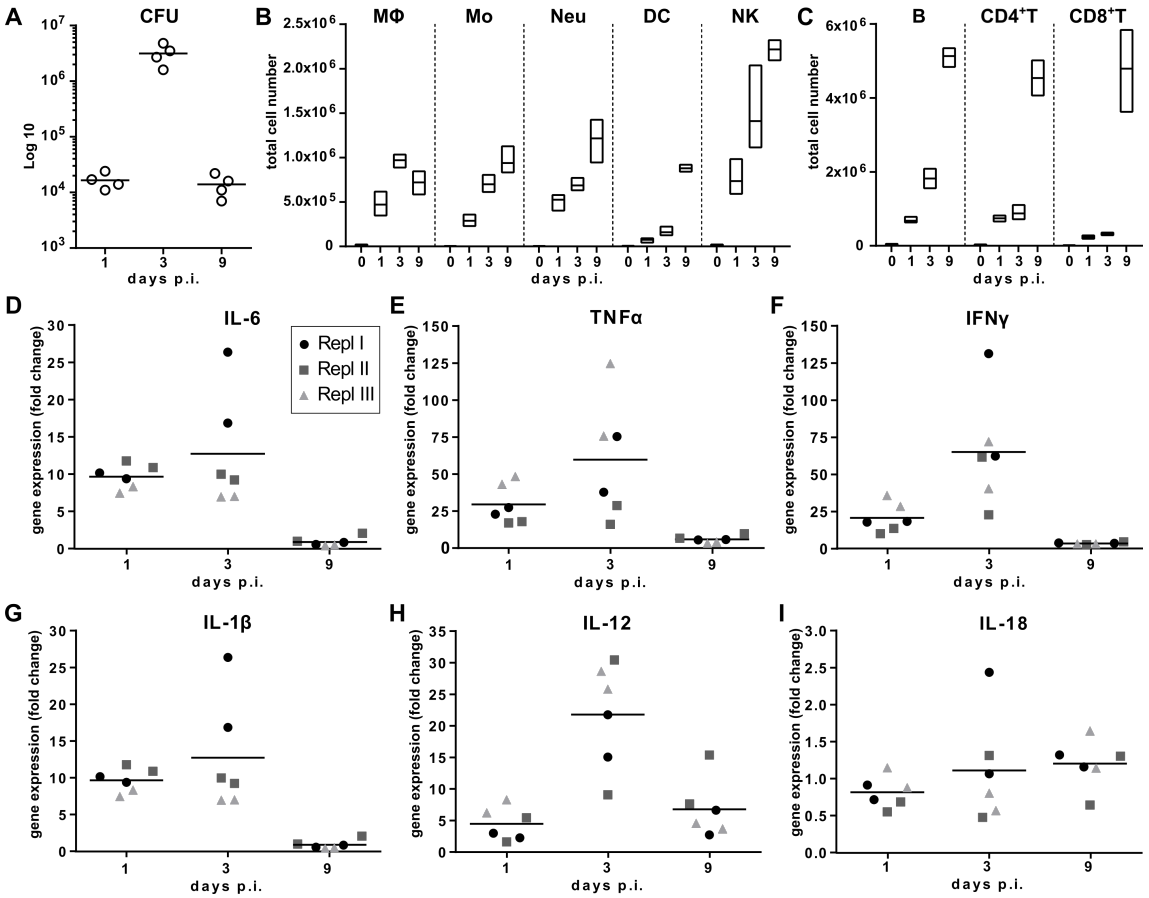

Figure 32. Characterization of the course of Lm infection in murine liver samples. (A) CFUs after inoculation during the course of infection. (B & C) Major immune cell sets in infected livers after inoculation. Cells were isolated and CD45 positive cell populations were analyzed by FACS. Bars represent the extreme values with the line representing the mean of 4 measurements. (B) The liver samples were examined for macrophages (MΦ), inflammatory monocytes (Mo), neutrophils (Neu), dendritic cells (DC) and natural killer cells (NK) numbers. MΦ numbers peaked at day 3 and then decreased towards day 9. In contrast to that, DC numbers increased mainly at the latest time point. All other innate cell populations increased throughout the stages of infection and showed the strongest increase at day 1 as compared to uninfected mice. (C) The liver samples were also monitored for B cells, CD4 positive and CD8 positive T cells. Those adaptive cells also accumulated throughout the infection, with a saltatory increase between day 3 and day 9 especially for effector T cells and reached higher amounts than the innate cell populations. (D-I) Cytokine expression patterns in the liver following Lm infection. The expression was determined by RT-PCR and is depicted as the increase in the level of mRNA over uninfected controls. All single measurements are given as well as the mean. (D) IL-6 expression was high at day 1 and 3 p.i. and then decreased as anticipated for a regulator of acute-phase response. (E-H) The expression of TNFα, IFNγ, IL-1β and IL-12 reached a peak at day 3 p.i., representing the typical response towards an infection. (I) IL-18 expression showed only slight increase of expression at all time points.

4.2.1.2 Cytokine Profiles of Sub-lethally Infected Livers are Highly Dynamic

Apart from the infiltrating cells, cytokine expression profiles (Fig 32D-I) were utilized to further characterize the state of the experimental system. As anticipated for a regulator of the acute-phase response, expression levels of IL-6 were highest at day 1 and 3 p.i. with a mean increase of about 10 and 11 fold, at day 1 and 3 respectively and dropped back to the level of uninfected control liver samples at day 9 (Fig 32D). In contrast to that, TNFα, IFNγ, IL-1β and IL-12 showed a more bell-shaped fold-change of expression, which was already elevated at day 1, peaked at day 3 and diminished then towards day 9. The only cytokine in the panel which showed only slight expression changes was IL-18 (Fig 32I). At a more general perspective it became visible, that all cytokine expression profiles varied considerably, if the individual measurements were considered. Thus, beside the mean, all single results of the liver samples also used for proteomic analysis are presented (Fig 32D-I).

In summary, the raised data illustrate the suitability to reproduce a typical Lm infection in the experimental set-up. Furthermore, the chosen time points could be characterized regarding influences of cytokines and infiltrating cell populations as well as the amount of bacteria present in the system (Table 15). The first stage of infection (day 1.p.i.) showed strongly increased counts of macrophages, monocytes, neutrophils and NK cells together with a general elevation in cytokine levels with an emphasis on IL-6 expression. The following stage, day 3 p.i., was defined by the peak of cytokine expression, as well as further strong increase of innate immune cells as well as beginning B cell accumulation. In contrast to those, the late stage (day 9 p.i.) was determined by T cell recruitment e.g. by DCs and therefore, the onset of the adaptive immune response. In addition to the functional characterization, the cytokine profiles hinted towards variability between the three conducted replicates, emphasizing the need for a stringent statistical analysis for proteome experiments.

Table 15. Properties of the analyzed time-points forming distinct stages of Lm infection.

stage	day p.i.	behavior of bacterial numbers	major immune cell populations involved	cytokines
early	1	increasing	MΦ, Mo, Neu, NKs	increase; esp. IL-6, IL1β
peak	3	peak	innate cells, B cells	peak in expression
late	9	decreasing	DCs, T and B cells	decrease

4.2.2 The Liver Proteome of Mice with Sub-lethal Listeriosis is Systematically Deregulated

To analyze the protein response to Lm infection in the liver, the proteome of three stages of infection was studied. Therefore, 12 mice livers were collected to allow three replicates of a comparative analysis of control and Lm-infected mice. To quantify the protein responses, an iTRAQ-labeling approach was utilized. Following nHPLC-MS/MS measurement, proteins were identified by searching against SwissProt database. Finally, protein significance was determined by utilizing a stringent approach that uses the median absolute deviation (MAD) from the median to estimate the standard-deviation of the protein regulation factors and subsequently assign a p-value to each protein [218]. Protein regulations were considered significant if the p-value was smaller than 0.01 and the protein was either identified in all 3 or in 2 out of 3 replicates.

To assess quality and properties of the dataset, box and 3D-scatter plots were prepared utilizing R software (Fig S10A&B). The box plots illustrate the noise inherent to each of the samples. For all samples, 50 % of all regulation factors ranged between an RF of -0.5 and 0.5 indicating a decent noise level. The day-wise 3D-scatter plots present the correlation between the replicates. A perfect correlation would produce a line between the smallest and the biggest coordinates of the system. For all days, the RF-distribution followed this diagonal, which indicates a positive correlation in particular for day 3. The individual Pearson correlation factors are given in Figure S10C. The occurring variations were taken into account for the analysis of the proteomic dataset.

Overview of the Proteomic Dataset: The dataset yielded 3666 quantified proteins, of which 67.3 % were identified in all replicates and another 15.1 % in two replicates (Fig 33A). In total, 82.4 % of all proteins were considered for the determination of significant regulations while the 644 proteins only identified in one replicate were excluded from further analyses. Utilizing stringent statistics, 522 significantly regulated proteins were extracted from the data. Figure 33B reveals a peak of regulation (n=471 proteins) at day 3 p.i. which was expected from the cytokine profiles and CFUs. In general, up- and downregulations occurred at a comparable frequency at all stages with a slight emphasis on upregulation at day 1 (58 %) and downregulation at day 3.p.i. (55 %). Of the 522 significantly regulated proteins, only a small number (n = 15) had a changed abundance across all time points (Fig 33C). The majority of proteins displayed regulation dynamics with a significant change only at one or two stages of the monitored infection (73.2 % and 23.9 %, respectively). Furthermore, Figure 33C underlined the differences between day 1 and day 9, as no proteins were simultaneously and exclusively regulated at these two days.

To furthermore validate the iTRAQ-based regulation factors, peptides from proteins with high regulation factors were reviewed and two examples are presented (Fig 33D&E).

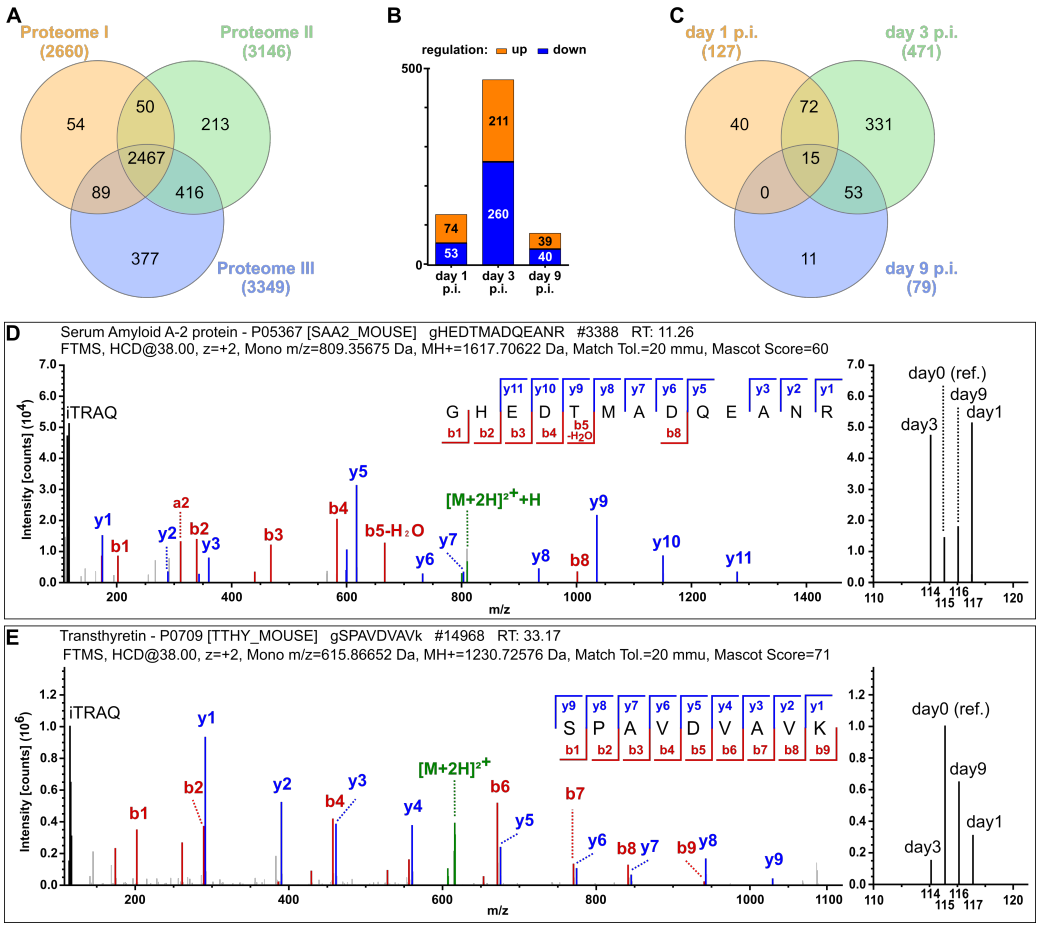

Figure 33. Protein quantification and regulation dynamics of Lm infected mice liver samples. (A) Overview of quantified proteins in individual replicates. The Venn-diagram shows the numbers of proteins quantified and the overlap between the replicates. In total, 3666 proteins were quantitatively identified. Of them, 2467 (67.3 %) were found in all three replicates and another 555 in 2 out of 3. Those proteins were then further investigated for significant regulation. (B) Significant regulations along the stages of infection. Up- and downregulation occurred at similar frequencies. With 471 proteins, a peak of regulation was observed at day 3. (C) Dynamics of regulated proteins throughout the time points. Only a small fraction of the proteins (n = 15) was regulated independently of the infection stages. In contrast, for the majority of proteins, the abundance only changed at one (73.2 %) or two stages of infection (23.9 %). (D & E) Exemplary MS/MS-spectra illustrate the determination of regulation by iTRAQ. (D) The peptide from Serum amyloid A-2 protein (SAA2) was reliably identified by y- and b-ions. The iTRAQ-reporter ions shown at the enlarged section on the right indicated a strong upregulation on day 1 and 3 p.i., which is in accordance with the calculated protein regulation factors. (E) An exemplary peptide from Transthyretin (TTHY) showed a downregulation at all time points compared to the reference (day 0). As illustrated, the identification of the peptide sequence was complete.

The peptide of Serum amyloid A-2 protein (SAA2) was well identified by both b- and y-ion series and iTRAQ-reporters revealed an upregulation at day 1 and 3 p.i. as compared to the reference (day 0, uninfected). The illustrated intensities of the reporters matched the calculated protein regulation factors (RF) of 2.08 (day 1 p.i.) and 2.66 (day 3 p.i.), respectively. In contrast to that, the peptide of Transthyretin (TTHY), which was also exhaustively identified, showed a downregulation at all time points compared to the reference (Fig 33E). The strongest regulation occurred at day 3 p.i. which was also concurrent to the protein RF of 1.44. Both of the reviewed proteins belonged to the functional class of acute-phase response proteins (APP).

Proof-of-concept: APPs which are produced in hepatocytes constitute the first organism-wide inflammatory response [158]. In conjunction with the complement system, which is an early response to bacterial infection, these proteins are eminently suitable to serve as proof-of-concept proteins (POC-proteins).

Therefore, the data set was queried for proteins described as APPs in literature and additionally for proteins which had a functional description in the UniProt KB [230] implicating a role in acute-phase response or complement activation, e.g. the GO annotation for a biological process. Of 54 POC-proteins included in that way, 32 were regulated significantly in the anticipated directions (Table S4).
In summary, it can be stated that the regulation of the APPs is in perfect accordance with the literature and relatable to the cytokine profiles of IL-1, IL-6, TNFα and IFNγ (Fig 32), therefore confirming our set-up again as a suitable approach to analyze liver responses distinct to Lm infection.

4.2.2.1 Protein Regulation Dynamics Correlate to Lm Pathophysiology and Clearance in Murine Livers

To obtain an insight into the major regulations of each stage of infection, the top 10 regulated proteins were extracted and reviewed regarding their role in infection.

Early Stage of Infection - Pathophysiology: For the first time point, which represented the early stage in infection, mainly regulation of inflammatory and pathophysiological processes was expected. Indeed, three APPs ranked among the top regulated proteins; SAA2, α-1-acid glycoprotein 2 (A1AG2) and Haptoglobin were found heavily upregulated on day 1 and 3 p.i. (Table 16). Additionally, A1AG2 was also significantly increased at day 9 and therefore was classified stage-independently regulated proteins. For two of the tree, SAA2 and A1AG2, it was reported that their heightened presence decreases Lm CFUs in murine liver [231]. Furthermore, Neutrophil gelatinase-associated lipocalin, Lactotransferrin, Protein S100-A9 and Interferon-induced guanylate-binding protein 2 were also found to be upregulated both at day 1and day 3. All of these proteins

were recently described to be increased upon Lm infection [232] and inhibit Lm growth [233–235].

Of the 10 extracted proteins presented in Table 16 only 2 showed changes in abundance solely at the early stage of infection. Pancreatic alpha-amylase and Protein disulfide-isomerase A2 were both highly upregulated with an RF of 2.61 and 1.77, respectively.

Table 16. Top 10 regulated proteins of the early stage of infection (day 1 p.i.). Proteins classified as proof-of-concept data are marked with a hash mark (#) after the protein name. Direction of regulation is indicated by symbols (●= not significant ▼= downregulated, ▲=upregulated).

Gene name	ID	Protein name	d1/d0 mean RF	d3/d0 mean RF	d9/d0 mean RF	Role in Infection
Amy2	AMYP	Pancreatic α-amylase	▲ 2.61	●	●	Salivary alpha amylase is endotoxin-responsive [236]
Saa2	SAA2	Serum amyloid A-2 protein #	▲ 2.08	▲ 2.66	●	decreases Lm CFUs in murine liver [231] acute-phase protein [237]
Pdia2	PDIA2	Protein disulfide-isomerase A2	▲ 1.77	●	●	needed for *Chlamydia* entry [238]
Lcn2	NGAL	Neutrophil gelatinase-associated lipocalin	▲ 1.70	▲ 2.15	●	k.o. increases susceptibility to bacterial infections [233]
Ltf	TRFL	Lactotrans-ferrin	▲ 1.63	▲ 0.89	●	inhibits Lm growth [234]
Orm2	A1AG2	α-1-acid glycoprotein 2 #	▲ 1.63	▲ 3.28	▲ 1.35	decreases Lm CFUs in murine liver [231] acute-phase protein [237]
S100a9	S10A9	Protein S100-A9	▲ 1.61	▲ 1.29	●	antimicrobial peptide to Lm [235]
Gbp2	GBP2	Interferon-induced guanylate-binding protein 2	▲ 1.53	▲ 1.34	●	IFNγ-dependently upregulated upon Lm infection (Gram-pos.) [232]
Hp	HPT	Haptoglobin #	▲ 1.51	▲ 2.26	●	acute-phase protein [237]
Ifit3	IFIT3	Interferon-induced protein with tetratrico-peptide repeats 3	▲ 1.50	▲ 1.55	●	protective role in virus infection [239]

While Pancreatic alpha-amylase was not described to play a role in infection so far, for closely related salivary alpha-amylase, endotoxin-responsiveness was shown [236]. Interestingly, for protein disulfide-isomerases it was demonstrated, that *Chlamydia* is dependent on the host-enzyme function for successful invasion [238].

Table 17. Top 10 regulated proteins of peak stage of infection (day 3 p.i.). Proteins classified as proof of concept data are marked with a hash mark (#) after the protein name. Direction of regulation is indicated by symbols (●= not significant ▼= downregulated, ▲=upregulated).

Gene name	ID	Protein name	d1/d0 mean RF	d3/d0 mean RF	d9/d0 mean RF	Role in Infection
Orm2	A1AG2	Alpha-1-acid glycoprotein 2 #	▲ 1.63	▲ 3.28	▲ 1.35	decreases Lm CFUs in murine liver [231]
Cyp3a16	CP3AG	Cytochrome P450 3A16	●	▼ -2.93	▼ -2.78	
Apcs	SAMP	Serum amyloid P-component #	▲ 1.37	▲ 2.69	●	acute-phase protein [240]
Saa2	SAA2	Serum amyloid A-2 protein #	▲ 2.08	▲ 2.66	●	decreases Lm CFUs in murine liver [231]
Hpx	HEMO	Hemopexin #	▲ 1.21	▲ 2.53	●	modulates responsiveness to IFNγ via STAT1 [241]
Isyna1	INO1	Inositol-3-phosphate synthase 1	▲ 0.55	▲ 2.51	▲ 1.39	
Crybb3	CRBB3	Beta-crystallin B3	▲ 1.08	▲ 2.51	▲ 1.01	
Tmsb10	TYB10	Thymosin beta-10	▲ 1.22	▲ 2.49	▲ 2.81	
A2mp	A2MP	Alpha-2-macroglobulin-P #	●	▲ 2.33	●	acute-phase protein [158]
Cyp4a12a	CP4CA	Cytochrome P450 4A12A	●	▲ 2.33	▲ 1.91	

Peak Stage: For the peak stage of infection (day 3 p.i.) the top 10 regulation list (Table 17) contained 5 POC-proteins including Serum amyloid P-component, Hemopexin and Alpha-2-macroglobulin as well as both of the APPs present among the top proteins from day 1, SAA2 and A1AG2. The other five proteins included three proteins, Beta-crystallin B3 (CRBB3), Thymosin beta-10 (TYB10) and Inositol-3-phosphate synthase 1 (INO1), which were all upregulated stage-independently with a peak regulation at day 3 for CRBB3 and TYB10 (RF = 2.51). All three of these proteins were not described to

be involved in infection until now. Nevertheless, inositol which is the final metabolite of the cascade INO1 belongs to, is an important factor to facilitate survival for various pathogens [242] and furthermore INO1 was recently shown to be upregulated on mRNA-level in Lm infected liver [243].

In contrast to that, the last two proteins from the top 10 list (Fig 17) belonged to the same protein family, the cytochrome P450 system and yet were divergently regulated. While Cytochrome P450 3A16 (Cyp3a16) displayed a severe decrease in protein abundance with RFs of -2.93 at day 3 and -2.78 at day 9 p.i., Cytochrome P450 4A12A (Cyp4a12a) was found to be strongly increased at day 3 (RF = 2.33) and also at day 9 p.i. (RF = 1.91).

Late Stage - Clearance: For the late stage of infection analyzed, proteins involved in clearance of bacteria were expected. Indeed, in Table 18, two proteins were found that are implicated in clearance or sustained inflammatory signaling. For Glutathione S-transferase P 1 (GSTP1) a strong increase in protein abundance was found (RF = 2.03). Recently, GSTP1 was shown to be involved in suppression of excessive pro-inflammatory signaling and attenuation of inflammation. [244, 245]. On the other hand, Thymosin beta-10 (TYP10), which was associated with apoptosis of macrophages and neighboring cells [246], was highly increased in abundance with a peak at day 9.p.i (RF =2.81). In contrast to that, Thymosin beta-4, with no evident role in infection, was downregulated on day 3 and 9 with an RF of -1.17 and -1.92, respectively. In comparison to the two preceding stages of infection, the top 10 protein list of day 9 contained a high number of downregulated proteins (Table 18). Along with TYB10 and GSTP1 already described above, only Cyp4a12a was found to be increased compared to the uninfected control. Cyp4a12a as well as Cyp2d9, Cyp3a41a and Cyp3a16, which also appeared in the top regulated proteins list of day 3, belong to the CYP 450 system and are therefore involved in the biotransformation of endogenous substrates and xenobiotics.

In contrast to Cyp4a12a, the other 3 CYPs were strongly decreased at day 9. Apart from the CYPs, three other proteins, that might play a role in biotransformation processes, were found among the top 10 regulated proteins. All of those, i.e. GSTP1, Amine sulfotransferase 3A1 and Dimethylaniline monooxygenase 3 were found to be strongly downregulated.

In summary, the analysis of the Top-regulated proteins revealed both proof-of-concept proteins as well as proteins which might serve as candidates for further investigation and knock-out studies. Additionally, dynamic protein regulations highlighted distinct processes at each stage of infection. While at day 1, Lm growth-inhibiting proteins were found among the top regulated, at day 3, proteins which could be beneficial for Lm, e.g. INO1 and so far non-characterized proteins showed highest regulations. In contrast, the late stage (d9) was characterized by strong downregulation of biotransformation enzymes as well as proteins implicated in Lm clearance and sustained inflammatory

signaling. Especially the regulation of cytochromes hints towards a severe deregulation of physiological liver processes.

Table 18. Top 10 regulated proteins of the late stage of infection (day 9 p.i.). Proteins classified as proof of concept data are marked with a hash mark (#) after the protein name. Direction of regulation is indicated by symbols (●= not significant ▼= downregulated, ▲=upregulated).

Gene name	ID	Protein name	d1/d0 mean RF	d3/d0 mean RF	d9/d0 mean RF	Role in Infection
Tmsb10	TYB10	Thymosin beta-10	▲ 1.22	▲ 2.49	▲ 2.81	Upregulation associated with apoptosis in *M.bovis* infection [246]
Cyp3a16	CP3AG	Cytochrome P450 3A16	●	▼ -2.93	▼ -2.78	
Sult3a1	ST3A1	Amine sulfotransferase	●	▼ -2.01	▼ -2.35	
Tomm20	TOM20	Mitochondrial import receptor subunit TOM20 homolog	●	▼ -2.14	▼ -2.11	importer of *N.gonorrhea*PorB [247]
Fmo3	FMO3	Dimethylaniline monooxygenase [N-oxide-forming] 3	●	▼ -2.01	▼ -2.03	TLR4-dependently downregulated by LPS stimulation [248]
Gstp1	GSTP1	Glutathione S-transferase P 1	●	▲ 2.12	▲ 2.03	Anti-inflammatory role in LPS stimulation [244]
Tmsb4x	TYB4	Thymosin beta-4	●	▼ -1.17	▼ -1.92	reduced by LPS-administration and in patients with septic shock (blood levels) [249]
Cyp4a12a	CP4CA	Cytochrome P450 4A12A	●	▲ 2.33	▲ 1.91	
Cyp3a41a	CP341	Cytochrome P450 3A41	●	▼ -1.75	▼ -1.88	
Cyp2d9	CP2D9	Cytochrome P450 2D9	●	▼ -1.23	▼ -1.88	

4.2.2.2 Sub-lethal Listeriosis Deregulates Hepatic Biotransformation Enzymes

Previous data-analysis indicated a severe deregulation of physiological processes in the liver especially among the enzymes facilitating biotransformation of endogenous and exogenous substances e.g. hormones and drugs. Led by the appearance of biotransformation enzymes in the Top-10 lists, the data set was analyzed for protein families belonging to these metabolic pathways. In total, the data set contained 42 cytochrome P450 enzymes (CYPs) of which 25 were significantly regulated (Tables 19 & SS5). Of all found CYPs, only three were significantly upregulated. Cyp4a12a and Cyp2d9 showed a strong increase in protein abundance at day 3 and 9. For both of those, gender-specific regulations were described previously [250, 251]. For the third upregulated CYP, Cyp7b1, nothing in regard to its regulation or role in infection is known so far. Interestingly, the second isoenzyme Cyp7a1 was not significantly regulated but showed tendencies to be downregulated (Table S5), hinting towards an opposite reaction.

However, the majority of CYPs as well as other enzymes implicated in biotransformation (Tables S6 & S7) were identified to be dynamically downregulated. For Cyp1a2, Cyp3a11 and Cyp2b10, this behavior was already described for mRNA under endotoxin stimulation [252] and could be substantiated in this study. For Cyp1a2 it was shown previously, that the levels of the protein family containing Cyp1a1 and Cyp1a2 are stable, if an Lm infection of the brain was present [253]. While Cyp1a2 was downregulated, Cyp1a1 was not identified.

Sustained Downregulation of CYPs: A group of 4 CYPs, Cyp2a4, Cyp2b9, Cyp3a16 and Cyp3a41a showed a sustained downregulation with RFs peaking at day 9 p.i or only slight increase of protein abundance after the peak of regulation at day 3 (Table 19, marked with '&'). Especially Cyp3a16 and Cyp3a41a presented high RFs of -2.93 (d3) and -2.78 (d9) as well as -1.75 (d3) and -1.88 (d9), respectively. Interestingly, both of them belong to the Cyp3a subfamily, which was described for their role in detoxification of xenobiotics [256]. In contrast to that, Cyp3a25 was showing only a minor change of abundance at the peak stage of infection while Cyp3a13 was not regulated at all.

Deregulation of Non-CYP Phase I and II Enzymes: Aside from the CYP450 enzymes, further biotransformation enzymes of both phase I and phase II were recorded in the data set. Of phase I, 12 enzymes, 6 of them regulated, could be detected (Table S6). Dimethylaniline monooxygenase 2&3, aldehyde dehydroxygenase 1&4 and amine oxidase A&B were significantly downregulated. While the aldehyde dehydroxygenases and amine oxidases showed only a decrease at day 3 p.i., the dimethylaniline monooxygenases displayed a sustained regulation comparable to some cytochromes mentioned above.

Additionally, 36 phase II enzymes were quantified, i.e. glutathione S-, UDP-glucuronosyl-, and acetyltransferases (Table S7). Among them, 12 proteins showed a significantly chan-

Table 19. Cytochrome P450 family members showing significant regulation in Lm liver infection. Direction of regulation is indicated by symbols (●= not significant ▼= downregulated, ▲=upregulated). Asterisk indicates a p-value of 0.05 deviating from the standard of 0.01. Hash mark = not significantly regulated in referred study. & = proteins show sustained regulation.

Gene name	d1/d0 mean RF	d3/d0 mean RF	d9/d0 mean RF	Regulation in (Lm) infection
Cyp4a12a	●	▲ 2.33	▲ 1.91	LPS: decreased in male mice [250]
Cyp2d9	●	▲ 1.23	▲ 1.88	Lm: decrease in male mice (mRNA) [254], LPS: decreased (mRNA) [252]; upregulated in female mice [251]
Cyp7b1	●	●	▲ 0.83	
Cyp2a4 &	▼ -0.92	▼ -1.52	▼ -1.57	
Cyp8b1	▼ -0.71	▼ -0.97	●	
Cyp2a5	▼ -0.62	▼ -1.29	●	
Cyp1a2	▼ -0.42	▼ -1.60	●	LPS: STAT1 independent decrease (mRNA) [252], Lm: stable (Cyp1a1/2; brain inf.) [253]
Cyp2c50	●	▼ -1.83	●	
Cyp3a11	●	▼ -1.04	●	LPS: STAT1 independent decrease (mRNA) [252]
Cyp2c29	●	▼ -1.00	●	LPS: STAT1 independent decrease (mRNA) [252]
Cyp4f14	●	▼ -0.75	●	
Cyp2f2	●	▼ -0.68	●	
Cyp3a25	●	▼ -0.65	●	
Cyp2c70*	●	▼ -0.60	●	
Cyp3a16&	●	▼ -2.93	▼ -2.78	
Cyp2c37	●	▼ -2.08	▼ -1.78	
Cyp2c40	●	▼ -1.95	▼ -1.81	
Cyp4a14	●	▼ -1.69	▼ -1.46	LPS: downregulation [255]
Cyp2b9 &	●	▼ -1.60	▼ -1.57	
Cyp4a10	●	▼ -1.47	▼ -1.09	LPS: STAT1 independent induction (mRNA), protein content reduced [252], downregulation (gram-negative bacteria) [255]
Cyp2c54	●	▼ -1.23	▼ -0.95	
Cyp3a41a &	●	▼ -1.75	▼ -1.88	
Cyp39a1	●	▼ -0.73	▼ -0.86	
Cyp2b10	●	▼ -0.89	▼ -0.99	LPS: STAT1 independent decrease (mRNA) [252] #
Cyp17a1	●	●	▼ -1.70	

ged protein abundance and the majority of those were downregulated at day 3 and 9. Only two proteins, glutathione S-transferase P1 (GstP1) and Mu3 (GstM4), were upregulated. While regulation of GstP1 could also be due to its mentioned role in inflammatory responses [244, 245], for GstM4, no such context was described yet.

In summary, a large fraction of biotransformation enzymes was found deregulated in Lm-infected livers, hinting towards a profound influence of the infection on drug metabolism and clearance.

4.2.2.3 Proteins Abundances of UBLs and Regulating Enzymes are Scarcely Influenced

One goal of this proteomic study was to observe the dynamic regulation of proteins involved in changes in ubiquitin and Ub-like modifiers.

UBLs: As a first step to unravel the impact of Ub-dependent processes, the data set was analyzed for Ub and UBLs as well as their modifying enzymes. Of the known UBL modifiers, 5 were identified and quantified.

Ubiquitin-like protein ISG15, which was already described to be increased in abundance in *Listeria* infection [34], showed a significant upregulation with an RF of 1.05 at the peak stage of infection. Additionally, the ISG15 ligase TRIM25 as well as the conjugating enzyme UB2L6 were identified. While TRIM25 was reliably quantified and showed no changes, UB2L6 was found in only one out of three replicates and there showed an increase in abundance through all time points.

Furthermore, NEDD8 was quantified as well as its conjugating enzyme UBC12. Both of them showed no consistent regulation during all stages of infection. For UFM1, another UBL-modifier, the protein itself as well as the E3 UFM1-protein ligase Ufl1 and one of two known UFM1-specific proteases Ufsp2 [36] were quantified reliably throughout all three replicates, but showed no changes in protein abundance.

The Small ubiquitin-related modifiers 2 and 3 (SUMO 2/3) were identified only in one out of three replicates and showed no apparent changes in abundance in this replicate. Additionally, SUMO-conjugating enzyme UBC9, which was recently shown to be degraded during Lm infection in mouse liver [25], as well as SUMO-activating enzyme subunit 1 and 2 (SAE1/2) and E3 SUMO-protein ligase RanBP2 were quantified, but showed no significant regulation. Additionally, ATG12 was identified in 2 of 3 replicates (non-regulated) as well as its activating enzyme ATG3 and the conjugating enzyme ATG7, which were both non-regulated.

Ubiquitin itself was identified in all replicates but was not quantified due to disabled protein grouping in the data analysis. Manual evaluation of ubiquitin revealed mean regulation factors of 0.64 (d1), 0.58 (d3) and 0.32 (d9), hinting towards slightly elevated Ub-levels.

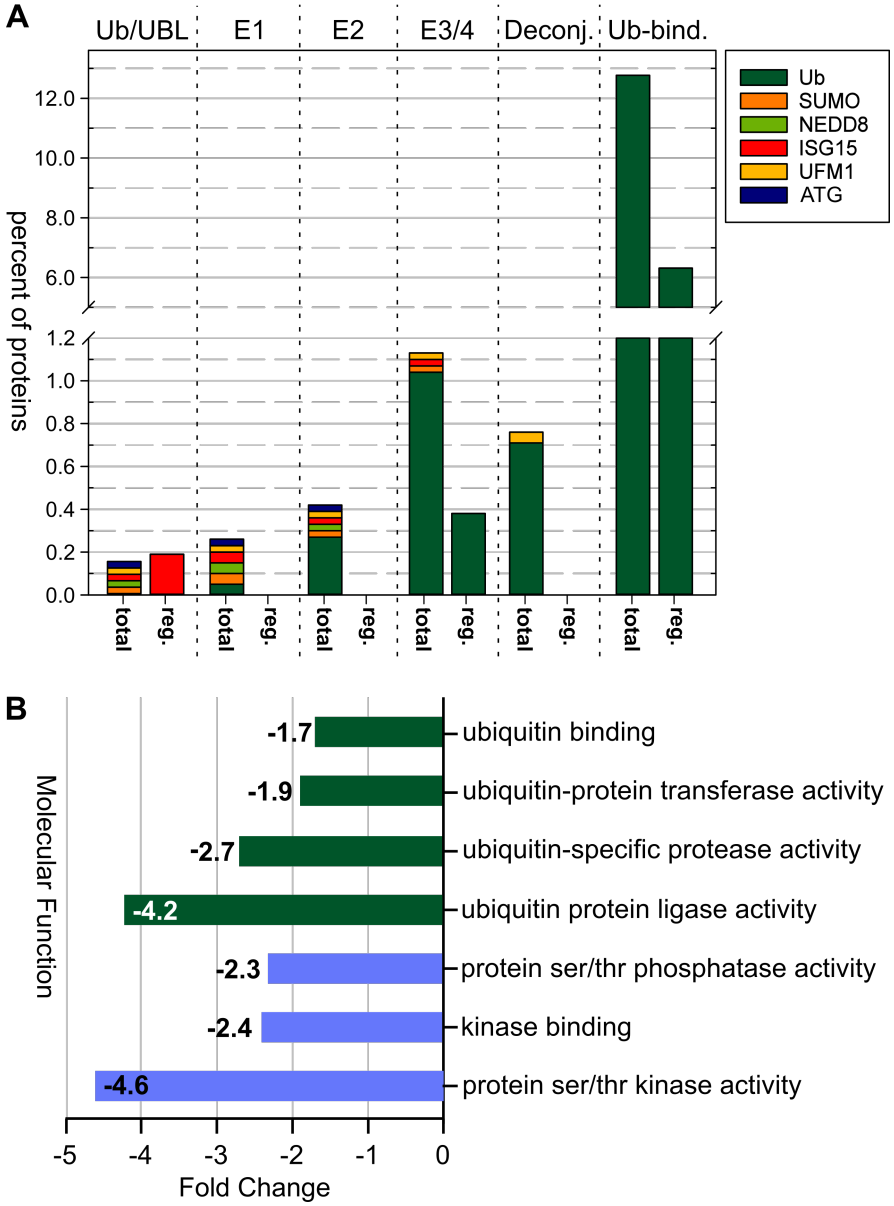

Figure 34. Percentage of quantified proteins related to Ub and UBLs in the data set and occurrence among the regulated proteins. (A) Percentage of Ub-related proteins among all quantified as well as all regulated proteins. Specificities of proteins in the groups are indicated by a color code. Proteins with dual specificity for Ub and UBL were counted once for the UBL and not listed in the Ub-category (green). (B) Underrepresentation of protein-functions among the regulated data points as annotated by GO terms. Analysis of GO terms category "Molecular Function" utilizing FunRich [257] revealed a depletion of protein activities implicated in signaling in significantly regulated proteins compared to the whole data set. Besides phosphorylation-dependent processes (blue), proteins with ubiquitin protein ligase (E3 ligases), ubiquitin-specific protease (DUBs) and ubiquitin protein transferase activities (E2 conjugating enzymes) as well as ubiquitin-binding proteins were underrepresented as indicated by the negative fold changes (regulated/all proteins).

Ub-related Proteins: To obtain an overview over the quantified and regulated Ub-related proteins, the protein numbers for the UBLs themselves, E1, E2, E3/4 and deconjugating enzymes, as well as UB-binding proteins, were determined for the whole data set (total) and regulated proteins (reg.) (Fig 34A). In contrast to the UBLs, for E1 activating and E2 conjugating enzymes, no proteins were found regulated, while in the whole data set 0.38 and 0.41 % of the proteins belonged to those categories and even showed different specificities against Ub, SUMO, NEDD8, UFM1 and ATG (Fig 34A). For E3/4 ubiquitin ligases, the majority of proteins found (1.04 %) had a described specificity for Ub as had both of the regulated ligases RNF213 and RNF135. For deconjugating enzymes, again, no regulated members where found. The most abundant Ub-related group contained proteins which were implicated in Ub-binding. In this group, all proteins that either contain a Ub-binding domain, bind Ub in processes of conjugation or deconjugation or were tagged as "Ub-binding" by UniProt KB were included. In sum, Ub-binding proteins constituted 12.8 % of all quantified proteins and 6.3 % of the regulated proteins (Fig 34A). Although the percentages for the different groups were relatively small, it was prominent that an even smaller portions of the regulated proteins belonged to the analyzed groups, if any.

To verify this observation and to examine whether the observed effect was specific for Ub-related proteins or more general, an enrichment analysis for GO terms using FunRich [257] was carried out. The analysis revealed a general decrease of protein activities implicated in PTM regulation in the GO category "Molecular Function" for regulated proteins *vs.* the whole data set (Fig 34B). Proteins with activities regulating phosphorylation, e.g. "protein ser/thr kinase activity" showed even stronger decrease (blue bars) than Ub-related functions (green bars). Furthermore, also "kinase-binding" proteins and proteins with "prot ser/thr phosphatase activities" were underrepresented.

Regarding ubiquitination, proteins with "ubiquitin protein ligase activity" (E3/4) were 4.2 fold decreased in the regulated proteins and proteins with "ubiquitin protein transferase activities" were also depleted (1.9 fold). Furthermore, proteins that non-covalently bind ubiquitin were also underrepresented as illustrated by an -1.7 fold change of the function "ubiquitin binding" (Fig 34B).

In summary, the significantly regulated proteins showed a strong decrease in protein numbers performing functions that belong to the ubiquitin-machinery and in ubiquitin binding as well as in phospho-regulating activities and kinase binding compared to the numbers in the whole data set. Although about 100 proteins which are associated with ubiquitination or ubiquitin-related modifiers were quantified, only two of those proteins were found to be significantly regulated, indicating a high importance and key role of those two Ub-ligases in Lm infection. To further elucidate the functions and roles of the candidate ligases, network analyses were carried out for both of them.

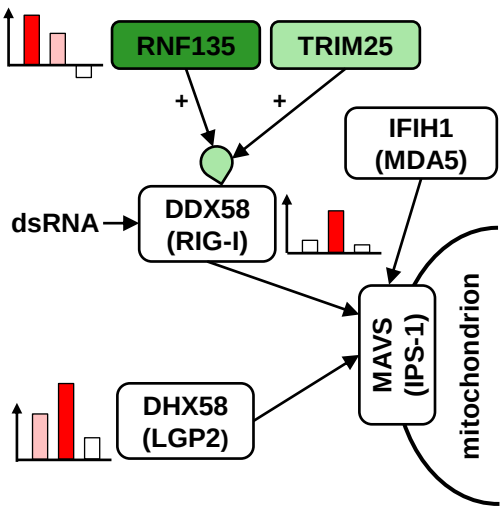

Figure 35. RNF135 - Integration into the RIG-I pathway in Lm liver infection. All proteins presented were quantified in this study and significant regulation is indicated by red bars. RNF135 was found to be significantly upregulated at the early stage of infection (RF = 0.66). The substrate of RNF135, Probable ATP-dependent RNA helicase DDX58 (RIG-I), was also found and displayed a significant increase in abundance at day 3 (RF = 0.55). Furthermore, several proteins interacting with DDX58 were identified, i.e. MAVS (IPS-1), IFIH1 (MDA5) and DHX58 (LGP2). DHX58 was also found to be upregulated with an RF of 1.05 (d3). Furthermore, a second Ub-ligase of DDX58, TRIM25, was quantified and showed stable protein abundance. Tear-shape: ubiquitin; +: activation; green color: implicated in ubiquitin-related process.

Ub-ligase RNF135: The first protein, the E3 ubiquitin protein ligase RNF135/Riplet was found to be significantly upregulated at the early stage of infection (RF = 0.66). RNF135 was recently described to ubiquitinate the probable ATP-dependent RNA helicase DDX58 by K63-linked chains and to thereby activate DDX58 [258,259]. To assess the role of RNF135 regulation in this study, protein interactions were determined using STRING (version 10) [260] and subsequently, associated data points were extracted (Fig 35). Indeed, DDX58 was quantified in the data set and showed a significant upregulation at day 3 (RF = 0.55), thereby revealing a later response than RNF135. Apart from RNF135 and DDX58, E3 ubiquitin protein ligase TRIM25, which was also described to ubiquitinate and activate DDX58 [261], was detected with unchanged protein abundance throughout the infection. Additionally, two further RIG-I like receptors, Interferon-induced helicase C domain-containing protein 1 (IFIH1)/Melanoma Differentiation-Associated protein 5 (MDA5) and Probable ATP-dependent RNA helicase DHX58/LGP2, were identified. While IFIH1 was unchanged, DHX58 showed an increased protein amount at day 3 (RF = 1.05). Furthermore, Mitochondrial antiviral-signaling protein (MAVS)/IPS-1, which acts downstream of the RIG-I like receptors, was identified but showed no regulation (Fig 35). In summary, proteins directly and indirectly influenced by RNF135 were identified and their regulation in Lm infection could be described in the complex setting of whole liver. It is feasible that RNF135 activates DDX58 by ubiquitination and together with DHX58 modulates the immune response in a Lm specific manner.

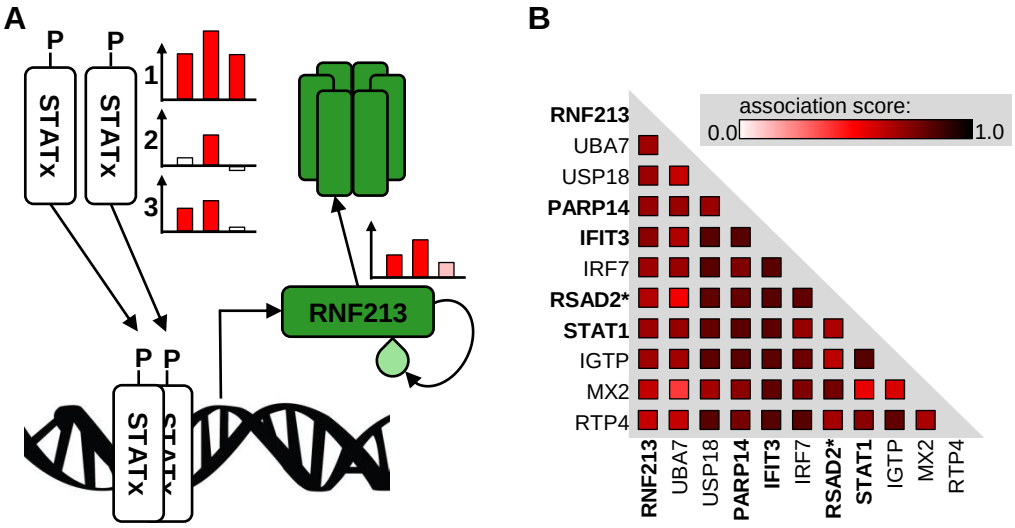

Figure 36. Schematic representation regulation of RNF213 expression as well as an analysis for putative pathway components of the E3 ubiquitin protein ligase. All proteins presented were quantified in this study and significant regulation is indicated by red bars. (A) Mechanism of transcriptional regulation of RNF213. The ubiquitin ligase RNF213 was found to be upregulated at day 1 and 3. Recently, it was described that RNF213 transcription was regulated by STATs, presumably STAT1. STAT1, 2 and 3 were identified and showed an increased protein abundance as indicated. After transcription, RNF213 is known to ubiquitinate itself and to form homo-dimers to perform its ATPase function. (B) Co-expressing proteins according to String DB analysis. All listed proteins were reported to be co-expressed with RNF213 and the association score between them is indicated by the colored boxes. Proteins in bold print were quantified in the data set. The asterisk indicates that RSAD2 was only found in one replicate. All present proteins were found to be regulated with similar dynamics as RNF213.

Ub-ligase RNF213: The second protein RNF213/Mysterin, which is also an E3 ubiquitin protein ligase, presented a significantly increased protein abundance at day 1 (RF = 0.64) and day 3 p.i. (RF = 0.99) (Fig 36A). It was recently described that RNF213, which is not only a ubiquitin ligase but also a big AAA+ ATPase, on the one hand ubiquitinates itself and on the other hand forms homo-dimers while converting ATP to ADP [262, 263]. Furthermore, it was described, that RNF213 was probably transcriptionally regulated by a member of the STAT-proteins [264]. In this study, STAT1, 2, 3, 5a, 5b and 6 were identified, but only STAT 1,2 and 3 presented changes in protein abundances (Fig 36A).

To identify potential interaction-partners or substrates, the RNF213 interactome was analyzed via STRING [260]. No direct interaction partners or substrates were found, but co-expressing proteins were identified (Fig 36B). All proteins listed showed a high

association score, indicating co-expression across different conditions in micro-arrays. It is therefore tempting to speculate, that those proteins are either direct substrates of RNF213 or at least participate in the same pathways. Indeed, from 10 predicted proteins, 4 were identified in this study: PARP14, IFIT3, STAT1 and RSAD2. Notably, all of the identified proteins were also found to be significantly upregulated. IFIT3 and STAT1 showed even higher changes in protein abundance at the peak of regulation with a 2.92 and 3.4 fold increase. PARP14 showed a displaced dynamic with a significant regulation only at day 1 p.i. (RF = 0.63). For RSAD2, regulation was not determined as significant as the protein was only found in one out of three replicates. Nevertheless, all of these proteins might be interaction partners or putative substrates of RNF213.

In summary, it was obvious that proteins belonging to the ubiquitin cascade were underrepresented in the regulated data set. Nevertheless, two candidate E3 ubiquitin ligases, RNF135 and 213, were found to be significantly upregulated and around both of them, a network of additional, quantified proteins emerged. Surprisingly, RNF135 was described in association with anti-viral responses although the background here was a bacterial infection.

4.2.3 Deubiquitinating Enzymes in Hepatic Listeriosis

In contrast to all other groups of Ub-related proteins, for DUBs, tools are available to enrich active members of this enzyme family and thereby not only gain in-depth information on their abundance but also activity. To overcome the limited coverage and information content of the proteome data, the activity-based probe (ABP) HAUb-VME was utilized to analyze and enrich DUBs.

In brief, DUBs were enriched by HA-immunoprecipitation and finally, a iTRAQ-labeling approach was utilized for quantitative analyses by LC-MS/MS measurements. For the DUB-analysis, lysates from the same liver pieces as used for proteome and cytokine-profiles were utilized, allowing direct comparison across the data sets. In addition to that, the DUB-enrichment via ABPs allowed for an insight into the activity-status of the DUBs.

In total, 52 DUBs were quantified in the analysis, which amounts to 62.8 % of all annotated DUBs in mouse as compared to 26 identified DUBs in the proteome approach. In Table 20, numbers of identified DUBs assigned to the DUB-families and the percentage of coverage are presented. In summary, DUBs from five families were found, among them 31 members of the largest DUB-family, the USPs, and 4 out 5 UCHs. Furthermore, 16 OTU-domain containing and 1 MJD-domain containing DUBs were quantified. Although JAMM DUBs are metalloproteases and do not directly interact with the ABPs, 58.3 % of the annotated JAMM DUBs (7/12) were identified in the data set. This interaction could be due to complex formation or unspecific interactions. MCP-induced protein 1, which is

Table 20. Numbers of quantitatively identified DUBs in hepatic Lm infection in comparison to the numbers of annotated DUBs. USP: Ubiquitin-specific proteases, UCH: Ubiquitin c-terminal hydrolases, OTU: Ovarian tumor domain containing, MJD: Machado-Josephin Disease domain containing, JAMM: Jab1/MPN/Mov34 metalloenzyme domain containing, MCPIP: MCP-induced protein (single protein).

DUB-family	# annotated	# identified	coverage
USP	49	31	63.3 %
UCH	5	4	80 %
OTU	16	11	68.8 %
MJD	3	1	33.3 %
JAMM	12	7	58.3 %
(MCPIP)	1	0	0 %
$\sum$	86	54	62.8 %

the only member of MCPIP-"family" with proven DUB-activity, was not detected.

Of the 52 identified DUBs, 46 were quantified in 2 out of 3 replicates. The 6 DUBs identified in only one replicate, UCHL1, OTULIN, USP1, USP37, USP42 and USP46 were clearly identified, adding to the number of expressed DUBs in the liver, but were excluded from the analysis of significant regulations. In total, 46 DUBs were used for further analyses (Fig 37). In general, the heat map indicated a high level of noise between the replicates as the regulation factors differed markedly in some cases, e.g. USP12, USP16 and USP48, UCHL5 and OTUB1. Although the dataset is median-normalized, the regulation factors, especially in replicate I, showed a tendency to be increased as illustrated by the predominating red color (Fig 37). For the analysis of statistically significant regulations, the same stringent algorithm as utilized for the proteomic experiments and described in section 3.8 was used [218]. As the positive regulation factors show a wider spread than the negative factors, upregulations presented in the heat map. e.g. for USP25, USP9X and VCPIP1, were eye-catching but not determined to be significant.

Significantly Regulated Candidate DUBs: Nevertheless, two DUBs were found to be significantly downregulated (Fig 37). UCHL3 showed a significantly decreased probe-binding at day 1 p.i. in all three replicates. The mean regulation factor of -0.51 indicated a 1.4 fold decrease in bound UCHL3 as compared to the uninfected control. Recently, UCHL3 mRNA was shown to be significantly decreased in Lm-infected livers at day 3 p.i. indicating a change in abundance rather than in activity [243].

USP2, the second candidate DUB, showed a significant decrease in binding of about

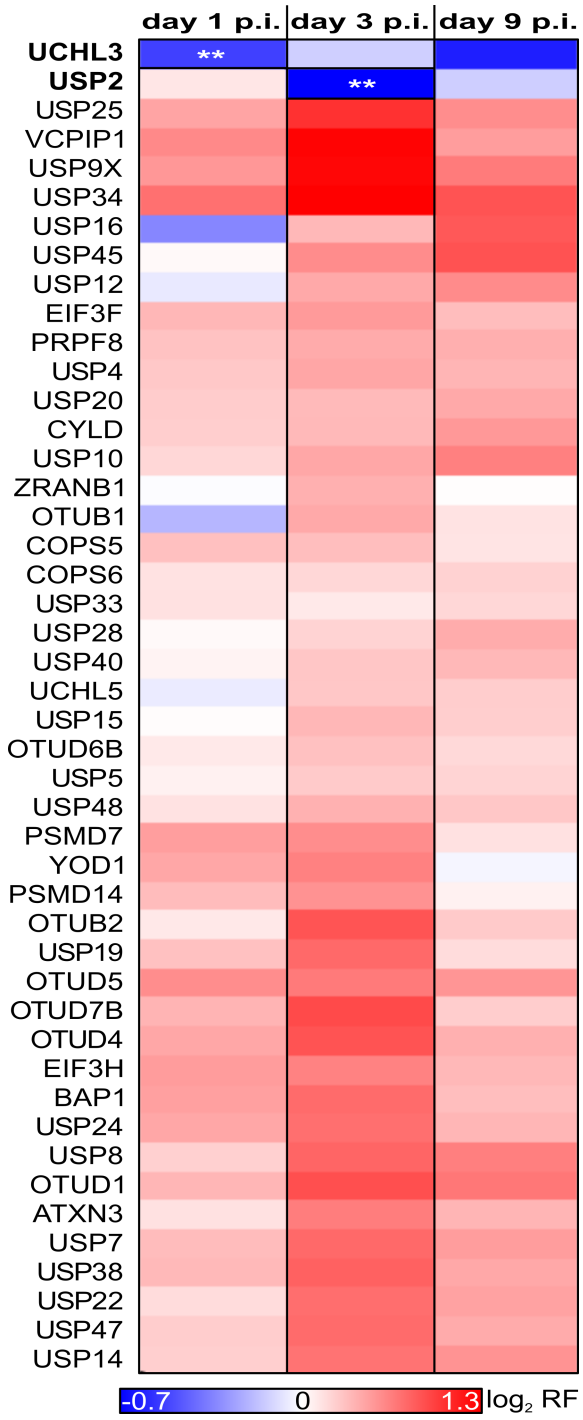

Figure 37. Regulation of active DUBs quantified in hepatic Lm infection. The columns show the regulation factors of each distinct DUB in a day-wise manner. Downregulation is represented in blue, upregulation in red, gray signifies that DUBs were not found and significance in regulation is indicated by two asterisks (p-value < 0.01). Protein names of regulated proteins are displayed in bold. Although the data were median-normalized before the extraction of DUBs, the regulation factors are considerably higher for up- than for downregulation. Nevertheless, two DUBs, USP2 and UCHL3 showed significant regulations. USP2 was found to be downregulated at day 3 p.i. with a mean RF of -0.68 which corresponds to a 1.6 fold decrease. UCHL3, in contrast, showed an 1.4 fold decreased protein abundance at day 1 p.i. (mean RF = -0.51). Apart from those two, a cluster of DUBs containing VCPIP, USP9X, USP25 and USP34 was conspicuous, revealing putative candidates for upregulation, but was not statistically significant. A heat map showing all regulation factors is found in the Supplementary data (Fig S12).

1.6 fold (mean RF = -0.68) at day 3. The regulation factors of day 1 and 9 showed inconclusive results with a tendency to slight upregulation at day 1. Notably, USP2 mRNA was described to first increase at 4 and 24 hours after infection and then decrease at later time points [243], which could explain the results illustrated in the heat map (Fig 37).

To evaluate the candidate DUBs, UCHL3 and USP2, the protein-amount was determined via western blotting. Therefore, frozen lysates from the liver pieces were thawed, applied to SDS-PAGE and subsequently transferred to PVDF-membrane to detect UCHL3 or USP2 and, after stripping, actin to normalize the samples. For USP2, no signal could be detected at the anticipated molecular weight.

UCHL3: A generic blot of UCHL3 and corresponding actin is presented in Figure 38A. The western blot analysis was repeated three times for each of the replicates. The evaluation of those data confirmed the downregulation of UCHL3 at day 1 p.i. revealed by the mass spectrometric analysis. Even though the values showed considerable variations between the individual experiments, the mean regulation factor revealed a decrease in abundance also at days 3 and 9 (Fig 38B). Especially for days 1 and 9 p.i., the western blot confirms the results displayed in the heat map (Fig 37) and furthermore clarifies that the decrease of UCHL3 was due to downregulation of the protein rather than change in activity.

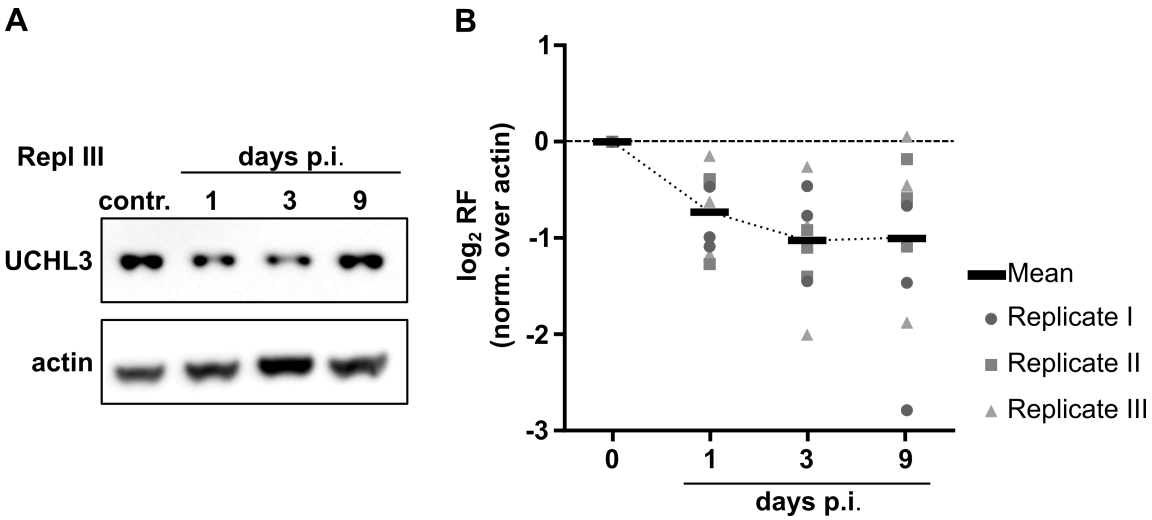

Figure 38. UCHL3 protein abundance and regulation in Lm infected liver. Liver lysates of all three replicates were utilized for western blotting against UCHL3 and actin to quantify UCHL3 throughout the infection(A) Prototypic blot of UCHL3 and actin for replicate III. (B) Regulation of UCHL3 throughout the infection. The distinct experiments are indicated by different symbols and the day-wise mean is indicated by a black bar. All values were normalized using actin and then regulation factors over the naive control were calculated. The dotted line represents the trend of mean regulation.

In summary, of 52 DUBs which were identified due to DUB-enrichment in Lm infected liver samples in comparison to 18 DUBs in the proteome samples, two were significantly influenced in their binding behavior to HAUb-VME. Both, UCHL3 and USP2 showed a decrease in binding at day 1 and 3 p.i., respectively. For UCHL3 western blot analyses confirmed and nominalized information about the regulation and revealed a decrease in abundance rather than activity. Thus, this study adds 2 novel candidates to the repertoire of DUBs which are effected by *Listeria* infection and probably have profound impact on the immune response similar as described for the deubiquitinase CYLD.

4.3 Clinical Manifestations - Deubiquitinating Enzymes in Sepsis Patients

4.3.1 Analysis of Deubiquitinase Activities in Sepsis Patients

Manifestations of listeriosis include meningoencephalitis, focal infections and sepsis, which have an especially high prevalence among the elderly and immunocompromised patients [164]. Although intensive care units (ICUs) utilize a varying diagnostic repertoire to reveal sepsis in patients, the mortality is up to 30 % of all cases.

Since sepsis is an infection with a systemic response, immune cells circulating in the blood should be able to represent the immunological state of the organism better than body fluids as cells can respond to signaling molecules and other cells and adapt their status accordingly. Furthermore, PBMCs are easily extracted from whole blood of patients. However, cells contain a complex repertoire of proteins and other components making it unfeasible to monitor all changes between the individual samples. To asses a cellular representation of the immune status, this study focused on the idea of a targeted biomarker approach utilizing one prominent enzyme class. DUBs are implicated in regulation of immunity and bacterial infection especially in immune cells (subsection 1.2.2) and tools to monitor DUB-activity are readily available. Hence, this study aims to clarify whether DUBs are suitable for the discrimination between healthy, SIRS and sepsis patients.

Therefore, PBMCs from patients showing different conditions as well as control samples were collected. Thereby, samples for the following patient states were collected: OP control, systemic inflammatory response syndrome (SIRS), sepsis, severe sepsis and septic shock. OP control group patients had had a surgery but did not show signs of SIRS or bacterial infection. All patient samples as well as patient information were acquired from the surgical ICU of the university medical center Magdeburg in cooperation with Dr. Uwe Lodes.

Utilizing the collected samples, this study pursued three goals:

1. to clarify whether DUB patterns can be extracted from this material,
2. to validate if the pattern have predictive power for the different stages of sepsis vs. healthy controls,
3. and to identify single DUBs which are predictive for certain states of sepsis-progression.

4.3.1.1 Characterization of Samples and Available Patient Information

In total, 59 samples of 50 ICU patients were collected over the course of one and a half years, and the mortality rate was 30 % averaged for patients showing any septic state.

Notably, 2 patients exhibiting SIRS later developed severe symptoms and died, while in the OP control class, all patients survived. If patients were sampled more than once, they showed individual sepsis periods at each sampling point. The numbers of samples belonging to each class, OP control, SIRS, sepsis, severe sepsis and septic shock, were highly divergent with 24 septic shock samples and only 6 samples in the SIRS and sepsis class each. Furthermore, 10 severe sepsis and 13 OP control class samples were collected (Fig 39A).

To obtain a further insight in the patient characteristics, age and medication of the patients was analyzed and is presented below (Fig 39B&C).

Age: 32 samples were collected from male patients with a mean age of 65.8 years and 27 from female patients with a mean age of 69.6 years (Fig 39B). The weighted mean difference of ages accounting for the gender-specific life expectancy gap was calculated using the 2010-2012 life tables published by the German Federal Office of Statistics [265] and amounted to 2.8 years, meaning that women in the sample group on average get 2.8 years older than men. The actual difference between both mean ages (3.9 years) was larger than it could be expected and hints towards a deviation from the anticipated age-distribution (+1 year). If only the samples for which patterns could be acquired were taken into account (black dots), the effect was even more prominent, with a sample difference of 4.9 years as compared to expected difference in age of 2.9 years. Whenever more than one sample from a patient was collected, the same age was also plotted more then once, thereby treating the samples as independent from each other.

Medication: Although *Listeria monocytogenes* (Lm) is a causative agent of septicemia, Lm could not be identified in the samples. Only in 10 patient samples, pathogens could be identified and only 3 of them yielded a precise identification of the bacteria implicated in sepsis. Nevertheless, the administration of antibiotics in all patients was summarized (Fig 39C). In total, 44 patients received up to 4 antibiotics. The two most frequently used substances were Meropenem against Gram-negative bacteria (23) and Vancomycin against Gram-positives (17). Additionally, further antibiotics targeting Gram-positive (Erythromycin and Linezolid), Gram-negative (Cefuroxim) and both kinds of pathogens (Piperacillin/Tazobactam, Sultamicillin, Ciprofloxacin, Gentamicin and Trimethoprim/Sulfamethoxazol) were given. Furthermore, the antimycotica Caspofungin and Flucanazol, as well as Metronidazol targeting anaerobic bacteria and protozoa were administered. The patients undergoing selective intestine decontamination (SID) received multiple antibiotics, which were not individually listed in the ICU reports. The use of antibiotics targeting Gram-positive bacteria in general hints towards the presence of Lm, which is suspected especially in Sultamicillin treated patients. On a closer look, Sultamicillin is essentially Ampicillin, which is the standard treatment for Lm, fused to a β-lactamase inhibitor. Additionally, in some patients, Gentamicin was administered,

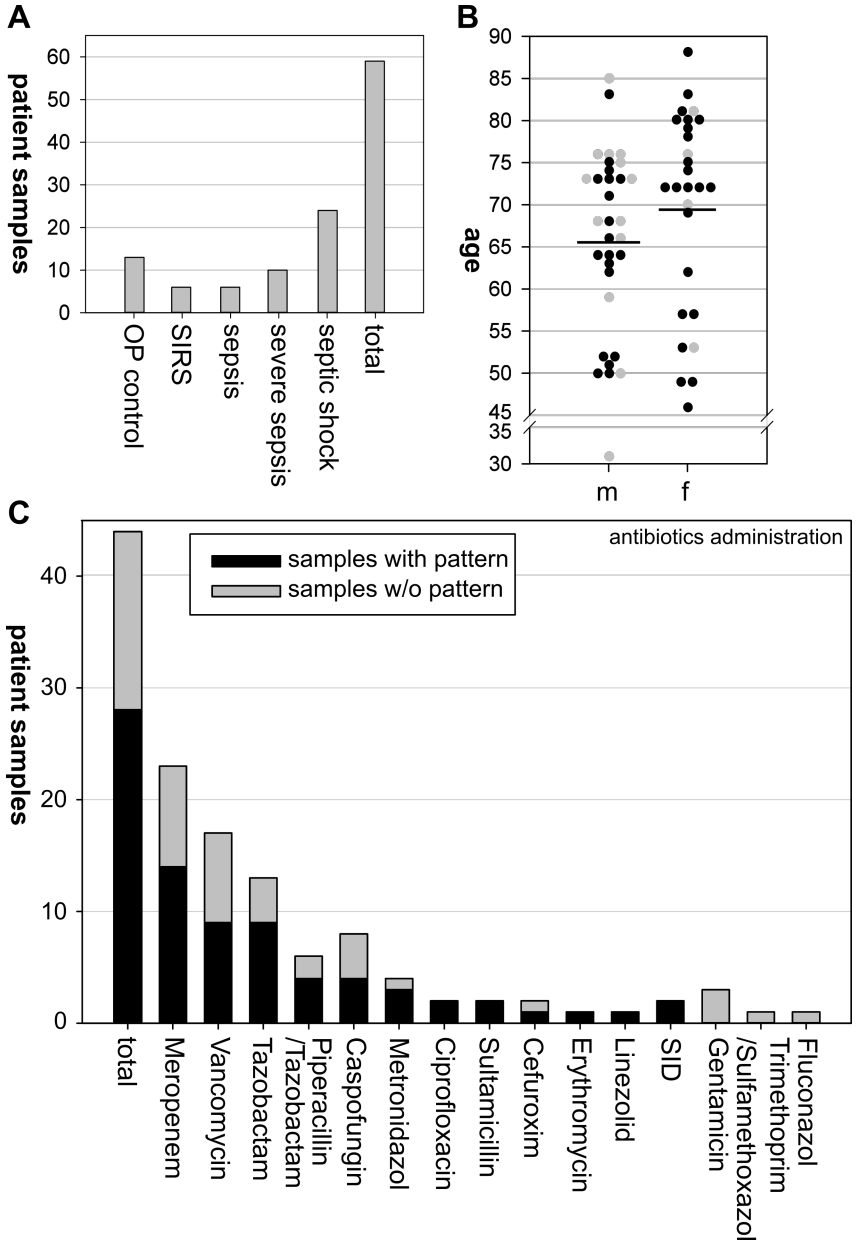

Figure 39. Summary of patient characteristics sampled during their hospitalization at the ICU. (A) Sample numbers for each sampling category and success in extracting DUB patterns across the classes. Of 59 samples collected, most were from patients with septic shock. (B) Age distribution of male and female patients. 19 male and 23 female patients were sampled. The mean ages were 64.6 and 69.6, respectively and are represented by the lines. (C) Antibiotic administration among the sampled patients. In total, 23 patients were treated with antibiotics with the most common ones being Meropenem and Vancomycin. Patients are included in several bars, if they received multiple antibiotics. The patients undergoing selective intestine decontamination (SID) received multiple antibiotics, which were not individually listed in the ICU reports.

which is also highly effective against Lm and the second antibiotic routinely used for Lm infection. Apart from the antibiotics, about 80 different drugs were administered to the patients, ranging from opioid pain killers to anti-hypertensive drugs. Together with a multitude of causes for submission into the ICU, this emphasizes the diversity among the patients and subsequently samples.

To acquire and evaluate DUB patterns from the collected samples, a reproducible work flow which is presented below was designed in cooperation with the working group Medical Microbiology of Prof. Dirk Schlüter (University hospital (OVGU), Medical Microbiology, Magdeburg).

4.3.1.2 Acquisition of IB-based DUB Patterns

The work flow developed for DUB patterns of sepsis patients is schematically represented in Figure 40. In detail, blood samples from ICU-patients were collected in sterile 15 ml blue-cap reaction tubes which contained 7 ml of RPMI to dilute the samples. Subsequently, the blood-RPMI mixture was added to a Ficoll cushion and PBMCs were isolated by utilizing gradient centrifugation. After erythrocyte lysis, if necessary, pellets were stored at -80°C until analyzed. After glass bead lysis, distinct protein amounts were incubated with HAUb-VME and samples were then applied to SDS-gel electrophoresis using precast 4-12 % BIS/TRIS gradient gels and western blotting. Finally, after detection, 16-bit tiff-images of all blots were acquired and used for further evaluation (Fig 40).

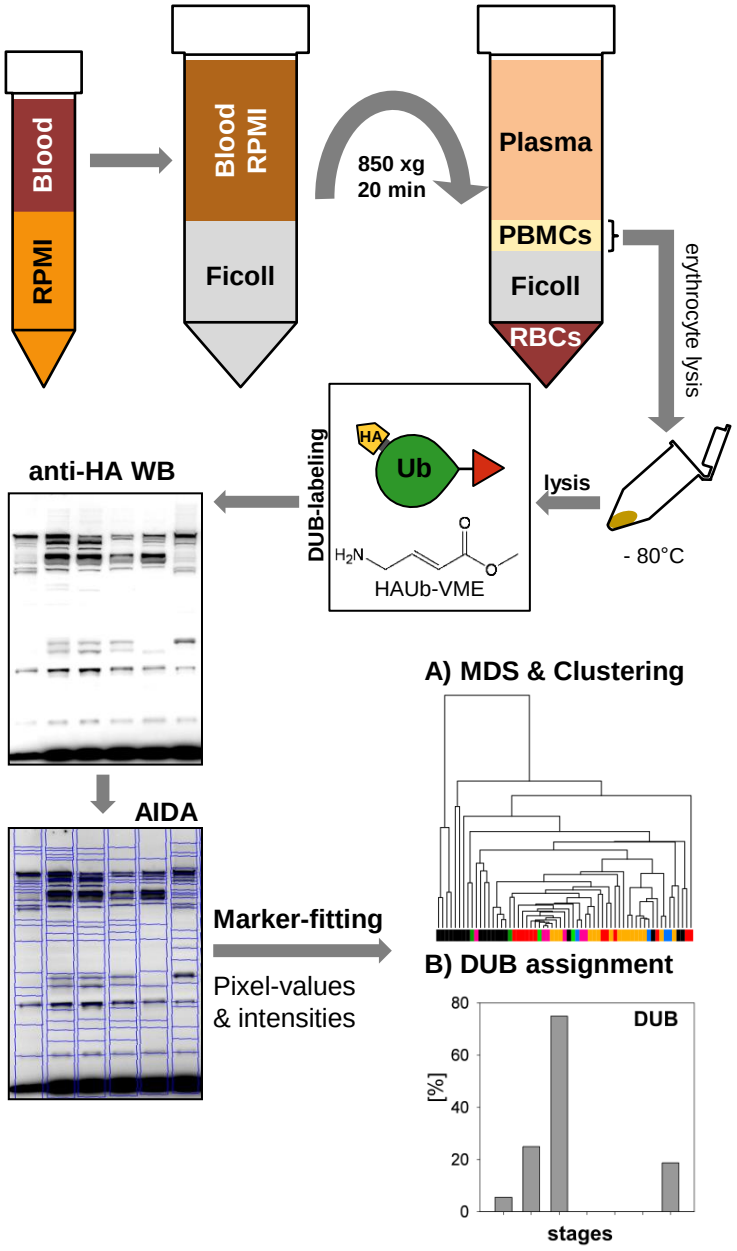

Figure 40. Work flow for the generation of DUB patterns from PBMC samples and analysis of the results utilizing the marker-fitting approach. PBMCs were extracted from a 50 % mixture of RPMI and patient blood by Ficoll gradient centrifugation and PBMC-pellets were stored at -80 °C for the following analysis. Cells were lysed utilizing glass-bead lysis and subsequently a distinct protein amount was labeled with 0.025 µg of HAUb-VME per µg protein for 1 h at 37°C. The signals were recorded using an anti-HA antibody and ECL Prime detection reagent on an LAS 3000 recording device. The obtained western blots were analyzed using Advanced Image Data Analyzer (AIDA) software. Subsequently, extracted data of each pattern was first normalized utilizing the marker bands of the blot, and finally multidimensional scaling (MDS) and hierarchical clustering were carried out. Additionally, this information was utilized to assign DUBs to the distinct bands of the patterns on the basis of their molecular weight.

Manual Inspection: The application of the work flow (Fig 40) successfully yielded DUB patterns for a large part of the samples. After acquisition of the first of them, the results were manually inspected (Fig 41). Strikingly, the samples 10/01 and 11/01 (OP controls) as well as sample 12/01 (SIRS) showed more complex and intense patterns than the other samples, while sample 14/01, which was classified as SIRS samples but was collected from a patient, which developed a septic shock shortly after sampling, displayed a less prominent, even weak pattern. Moreover, samples from patients with septic shock seemed to display only weak, if any, bands in the high molecular weight region, while for the sepsis sample (15/01) the pattern was weaker than for the controls, but the upper MW bands were clearly visible.

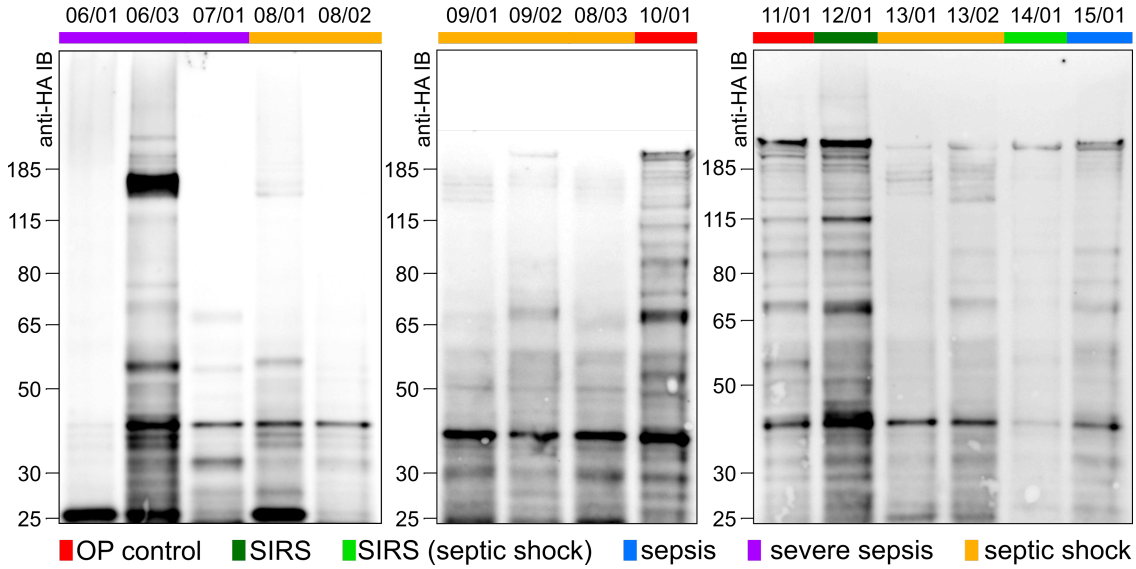

Figure 41. Exemplary DUB patterns for patients 6 to 15. For all blots, the same amount of total protein was applied and DUB activities were visualized utilizing HAUb-VME incubation of samples and subsequent detection with an anti-HA antibody. The color-code beneath the sample numbers illustrates the sample class. Samples with XX/02 and XX/03 are from the same patient (XX), but represent different episodes of sepsis during the course of treatment.

In summary, DUB patterns could be acquired for a large part of the collected samples and manual inspection of the first results hinted towards probable differences between the patterns of different sample classes. However, as this observation was based on only few samples and the blots also revealed a certain heterogeneity of the patterns even in one sample class, it became obvious, that a standardized data extraction and evaluation method was urgently needed.

Pattern Extraction: To extract the DUB patterns from the anti-HA western blots in a standardized manner, images were loaded to Advanced Image Data Analyzer (AIDA) software in 1D evaluation mode and lanes were marked by vertical or arbitrary rectangles of about 115 pixel width in a way that all signals of one lane were included even in non-vertical lanes (arbitrary mode). Then, the baseline of the intensity profile created by AIDA was determined automatically by the following parameters: Baseline Determination-Search level: 1, smoothed: 0 pixels. The profile of each lane was explored for visible maxima manually and those selected were then marked as peak together optical inspection of the original blot utilizing the parameters "position by center" and "avoid overlap" so that the position was located in the center of the respective band.

Finally, absolute pixel values for all peaks as well as background-subtracted intensities were exported to Microsoft Excel. Additionally, positions (absolute pixels) for the marker bands (PageRuler prestained plus) were also extracted for each blot using the same settings but omitting intensities.

4.3.1.3 Normalization of Patterns by a Marker-fitting Approach

To be able to compare individual DUB patterns as well as samples from different western blots, normalization was carried out by an R-software routine developed together with Prof. Frank Klawonn (HZI and Ostfalia University of Applied Sciences) and is described hereafter. For each blot, the lowermost band represented unbound HAUb-VME which has a distinct mass. To normalize the individual lanes, all determined pixel values of the HAUb-VME band were shifted to the theoretical pixel value determined by the mass of HAUb-VME (10.2567 Da) and all bands above were shifted accordingly, leading to an alignment of all lanes by the highest pixel value of the blot. Additionally, all intensities were normalized by the median intensity of the respective blot to account for differences in development.

To compare the DUB patterns between different blots, the normalized pixel lines were converted into a molecular weight value using the marker bands. The marker consisted of 9 bands with 10, 15, 25, 30, 50, 65, 80, 115 and 185 kDa, which yielded an individual pixel line. The mass ranges between these points were extrapolated by linear conjunction of two neighboring marker bands as shown in Supplementary Figure SS11. In that way, molecular weights in kDa were determined for each band in the blot and subsequently, the molecular weights were back-transformed to a pixel line utilizing a golden standard to project all DUB patterns into the same pixel range for comparison. The golden standard marker used in this study was derived from the markers of all analyzed blots regardless whether healthy control or sepsis samples (Fig 42). Furthermore, all bands with a molecular weight smaller than 25 kDa were discarded from further analyses since the smallest DUB is about 30 kDa in size when labeled.

In addition to the samples from the ICU patients, a set of healthy 19 control PBMC

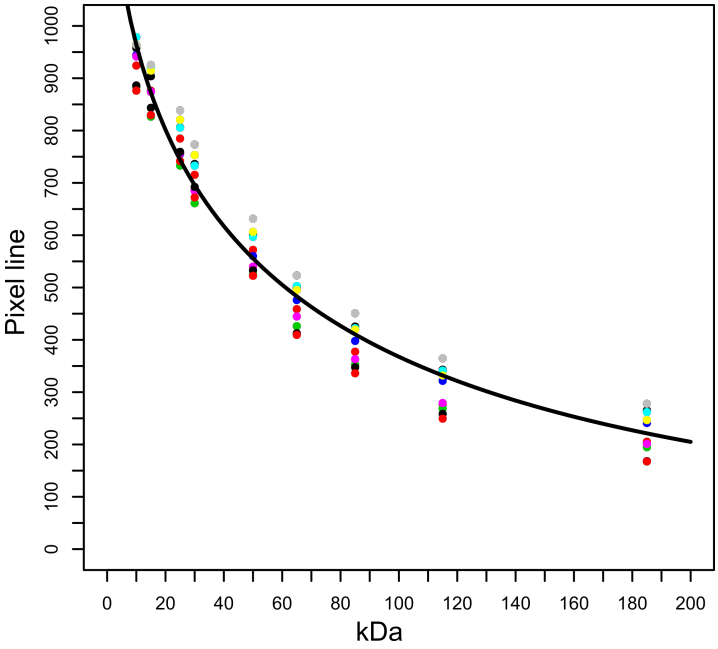

Figure 42. Golden standard for the normalization of DUB patterns. The marker bands of all blots (colored dots) were used to determine a mean marker curve (black line), which in turn was utilized to generate normalized pixel values for the comparison of DUB patterns from different samples.

samples was generated from buffy coats provided by the Deutsches Rotes Kreuz (NSTOB, Springe). Therefore, samples were prepared in the same manner as described for the samples from Magdeburg. These samples are termed "healthy controls" as compared to the OP control samples from patients which underwent surgery and were hospitalized in the ICU.

To visualize all normalized DUB patterns, all of them were plotted onto a theoretical blot and colored according to their class affiliations. Intensities were not integrated in this illustration, therefore only showing the presence or absence of bands among the patterns (Fig 43).

In general, samples were not evenly distributed among the classes and patterns could only be acquired for about 70 % of the ICU and 78 % of all samples (Table 21). The best represented classes were septic shock (24) and OP control (13) which yielded 16 and 11 patterns, respectively. The other categories contained fewer samples and only 4 patterns for SIRS and sepsis and 6 patterns for severe sepsis could be collected. Especially for patients showing a SIRS, sample numbers are problematic as two of the patients developed sepsis after the taking of the blood sample. Therefore, the SIRS samples were split in two classes, SIRS and SIRS (septic shock), latter containing the two mentioned samples. In summary, the obtained samples formed a very heterogeneous and biased collection that proved difficult to analyze.

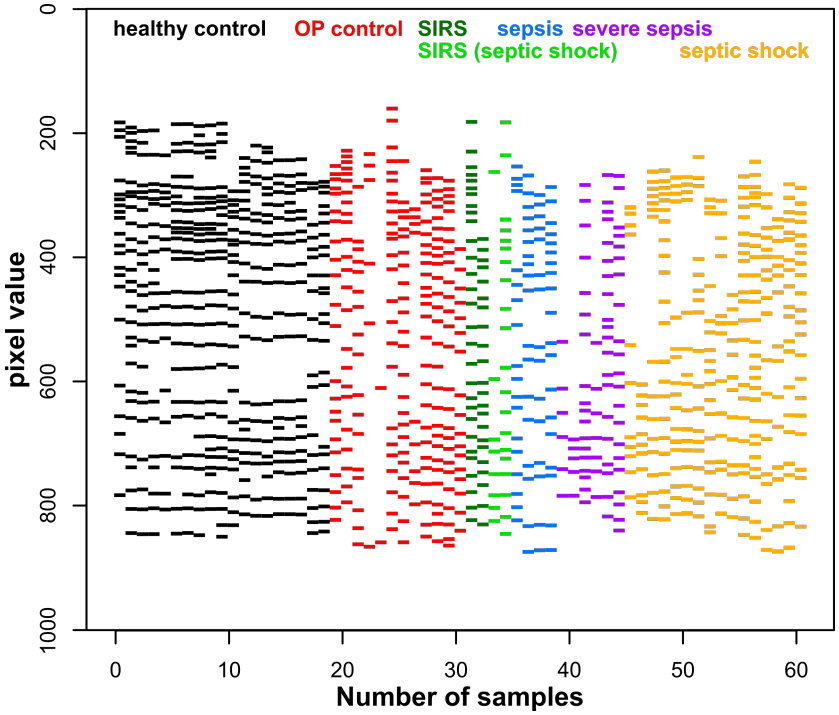

Figure 43. Summary of all normalized DUB patterns acquired. All bands of each pattern are displayed irrespective of the intensities. The different sample classes are indicated by a color code: black = healthy controls, red = OP controls, dark green = SIRS, light green = SIRS at the day of blood sampling with following septic shock, blue = sepsis, purple = severe sepsis and orange = septic shock.

Table 21. Summary of sample numbers and acquired patterns in each sample class.

class	# samples	# patterns	percent of patterns
healthy controls	19	19	100 %
OP controls	13	12	92.3 %
SIRS	4	2	66.7 %
SIRS (septic shock)	2	2	100 %
sepsis	6	4	66.7 %
severe sepsis	10	6	60 %
septic shock	24	16	66.7 %
$\sum$	78	61	78.2 %

4.3.2 Discriminating between SIRS and Sepsis

After normalization as described above, the distance between the different DUB patterns was calculated by pair-wise comparison of all single bands of two patterns as devised by Frank Klawonn. At first, a threshold had to be determined which defined two bands as identical. In this study, 3 different thresholds, i.e 3.5, 7 and 10 pixels were tested. Then, every band in pattern A was looked up in pattern B for a match. If a match was found, the distance of both patterns increased about the difference of both normalized intensities. If more than one match was found, the band with the smallest variance was used and if no match was found, the distance increased by the full normalized intensity of the band in pattern A. After determination of the distance for all bands and the addition to yield the A to B pattern distance, the same calculations were carried out *vice versa*. Finally,distances of both calculations were added up to the total pattern distance. In that way, a distance matrix was created for all patterns.

This matrix was then utilized for multidimensional scaling as well as hierarchical clustering of the samples with the 3 above mentioned thresholds 3.5, 7 and 10 pixels. The dendrograms resulting from the clustering algorithm were additionally reordered as described by Novoselova et al. to ensure that samples from the same class are adjacent provided that the tree structure allowed this reordering [266].

Clustering and MDS with a 3.5 Pixel Threshold: As a first step, results were analyzed by clustering and multidimensional scaling (MDS) utilizing a 3.5 pixel-threshold (Fig 44). After reordering, the hierarchical clustering resulted in several smaller clusters but no clear distinction between the sample classes. For the healthy controls, two main clusters formed with only few samples not found in those clusters. In contrast, OP control samples (red) were found in one cluster with several additional samples spread over the dendrogram. Samples of the third larger sample class, septic shock, were split into one larger (7 samples) and two smaller clusters (3 samples each) and further single samples. The 3 classes with smaller sample numbers, SIRS, sepsis and severe sepsis showed only pair-wise clustering, if any. Especially the 4 SIRS samples analyzed spread across the whole dendrogram as shown by the green squares.

The MDS analysis showed a similar picture with no clear separation of sample classes (Fig 44B). In general, all samples spread around zero in a continuous way. Especially the healthy controls (black dots) showed a scattered distribution in the lower half of the coordinate system. Additionally, some samples were found relatively close to the zero point of the system indicating small distances between those samples. On that account, the clustering and MDS was repeated with logarithmic scaling of the distances. Although the effect of accumulation of samples around zero is diminished in the logarithmic MDS, only the spread of the samples increased, but again, no clear separation of classes was found. The logarithmic hierarchical clustering showed more small clusters as compared to

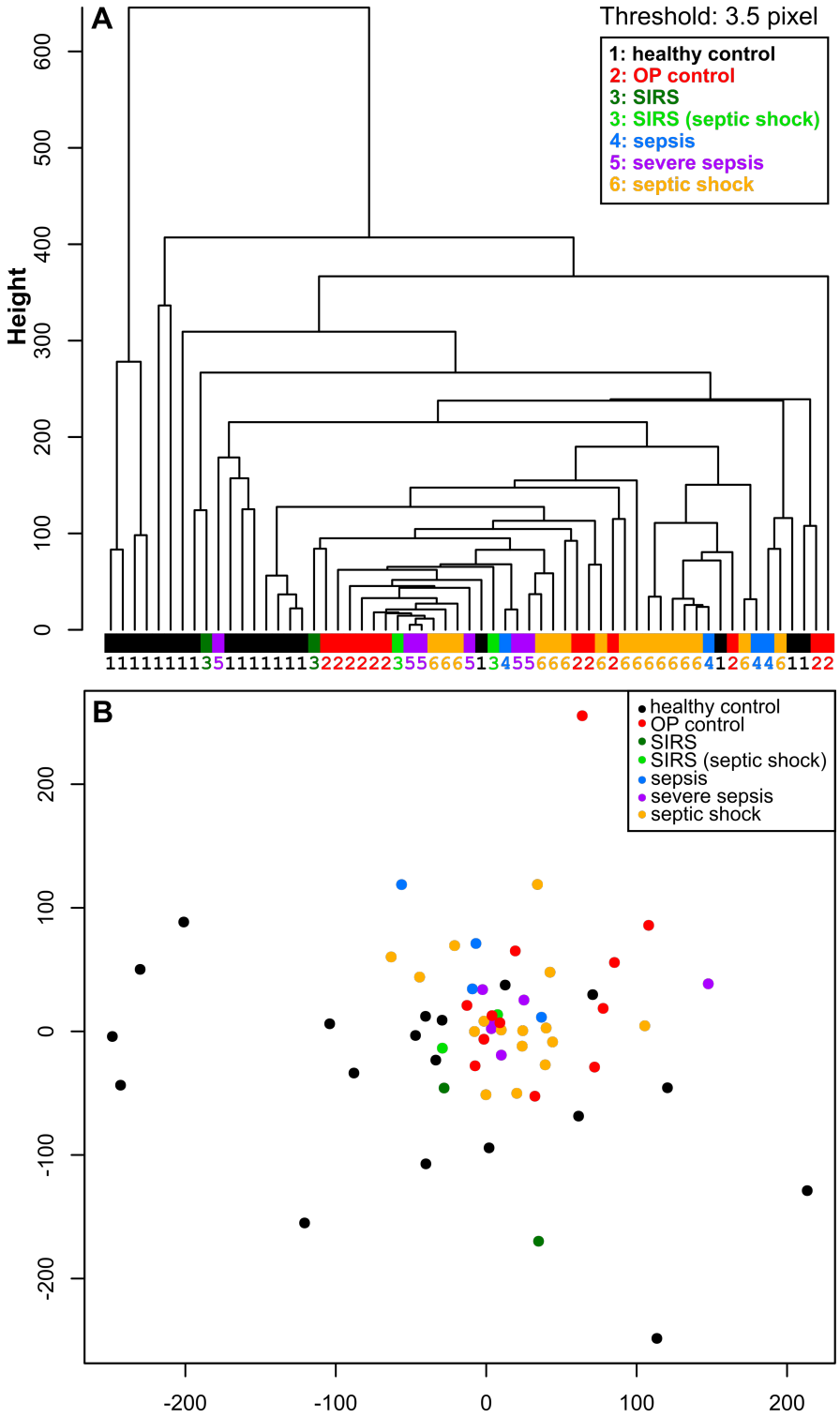

Figure 44. Hierarchical clustering and MDS for a threshold of 3.5 pixel. (A) Hierarchical clustering of all 61 samples. For this threshold, sample classes were not clearly separated. While the bigger classes, i.e. controls and septic shock were found in few bigger clusters, the samples of the other classes were either found in pairs or scattered across the dendrogram. (B) MDS of the all samples. In accordance with the clustering, no definite grouping of samples was detected. It is striking to note, that the healthy controls scattered very broadly compared to the other samples.

the non-logarithmic counterpart, especially for the controls. The only sample class that benefited from the logarithmic scale was the severe sepsis class, which showed distinct clusters as compared to the spread in the non-logarithmic cluster (Fig S15).

In summary, neither clustering nor MDS with a threshold of 3.5 pixel revealed considerable clustering of the samples of one sample class or a distinct separation from other classes.

7 and 10 Pixel Thresholds: Subsequently, the threshold was doubled to 7 pixels and analyses were repeated as described before (Fig S13). As reported for the threshold of 3.5 pixels, the new value also was not able to generate a class-separation for the samples. The MDS for the 7-pixel threshold also showed no distinction between the classes although the spread of the samples changed notably. The clustering result of the log-values (Fig S15) again revealed a favorable result for the healthy control class (2 clusters and 1 single sample), while for the other classes were disrupted.

Finally, a 10-pixel threshold was applied to the samples (Fig S14A). However, a clear clustering of classes was not visible with this threshold. The MDS also showed no significant differences between the classes (Fig S14B). The same held true for the logarithmically scaled MDS. The logarithmic clustering again showed a enhanced clustering of the healthy controls very similar to the results for the log 7-pixel threshold (Fig S15).

In summary, the different thresholds of 3.5, 7 and 10 pixels as well as the logarithmic and linear scaling of the distances between the samples revealed distinct clustering and MDS results for the samples. Thereby, mainly the control classes (healthy and OP controls) and the septic shock class built groups within the different dendrograms. However, no class could be discriminated clearly from the others on the basis of this clustering approach. Nevertheless, it is conceivable, that samples can be categorized in two groups according to their behavior in clustering. If a sample clusters within a distinct group of samples, a diagnosis or prognosis based on the patterns might be possible for those patients, allowing the use of patterns as biomarkers at least for part of the patients. On the other hand, the second group would contain the samples where no prediction was possible based on the results of the cluster analysis.

For the MDS analysis, no concise grouping of the classes could be exposed throughout the analyses. Therefore, with the aid of the obtained results so far, it is not possible to determine features of DUB patterns that allow the differentiation between the sample classes. However, there are further possibilities of evaluation, which should be examined.

4.3.3 Identification of Prominent Deubiquitinase Signals

As the protein amount acquired from ICU samples was limited and not sufficient to carry out a DUB-identification based on enrichment by probes (HA-IP), a theoretical approach to identify DUBs with a potential regulatory role in sepsis-progression was developed in cooperation with Prof. Frank Klawonn. Therefore, the molecular masses from all cysteine-class DUBs, were extracted from UniProt KB and the mass of HAUb-VME (10.2567 Da) was added to account for the shift in mass due to labeling of the DUBs. Then, for each individual experiment, the masses were transformed into pixel lines utilizing the extrapolated marker curves (Fig S11) and then the resulting pixel lines were compared to the found pixel lines of the DUB patterns. If the difference of the two pixel lines was smaller than 3.5 pixels, the DUB was classified as assigned.

MS-aided Support of DUB Assignment: To additionally strengthen the theoretical DUB-assignment, HA-IPs from pooled ICU-patient samples (6, 8 and 4 samples) and healthy control samples (5 donors, PBMCs) were carried out. Due to the relatively small protein amounts available, DUB-identifications for the sepsis-pools were scarce and therefore results were summarized resulting in 14 identified DUBs. As a base for the theoretical DUB-assignment and to visualize the results from the HA-IP approaches, a virtual blot was generated by utilizing the golden standard marker (Fig 45A). The molecular weights were transformed into pixel lines and then displayed as virtual bands. The gray lane represents 81 DUB-signals which are possible in theory as those DUBs can be labeled by HAUb-VME. The second lane (black) was compiled from those DUBs which were identified by an HA-IP either in this study or previously [96, 210]. The third, green lane of the virtual blot summarizes all DUBs identified in a pool of 5 healthy control PBMC samples. In total, 43 DUBs were found in this sample, of which 37 were also theoretically detectable by HAUb-probes (Fig S16).

The red lane (Fig 45A) summarizes the DUBs identified in 3 HA-IPs of lysate pools from sepsis-patient PBMCs. The 3 pools consisted of 18 samples in total and samples belonged to either sepsis, severe sepsis or septic shock class, and were mixed throughout all pools. In sum, the mass spectrometric analyses identified only 14 DUBs in all of these pools (Fig 45A), while 19 DUBs were identified in a fourth pool, containing also OP control and SIRS samples (data not shown).

Although single samples from ICU patients are not sufficient for HA-IP approaches and pools do not reflect the DUB composition of individual samples, the data points acquired from healthy control samples and sepsis sample pools validate the theoretical approach as they confirm the presence of certain DUBs in the different sample groups.

To get an overview of the DUB-assignments, the mean and median DUB-assignment per band in DUB patterns was analyzed (Fig 45B).

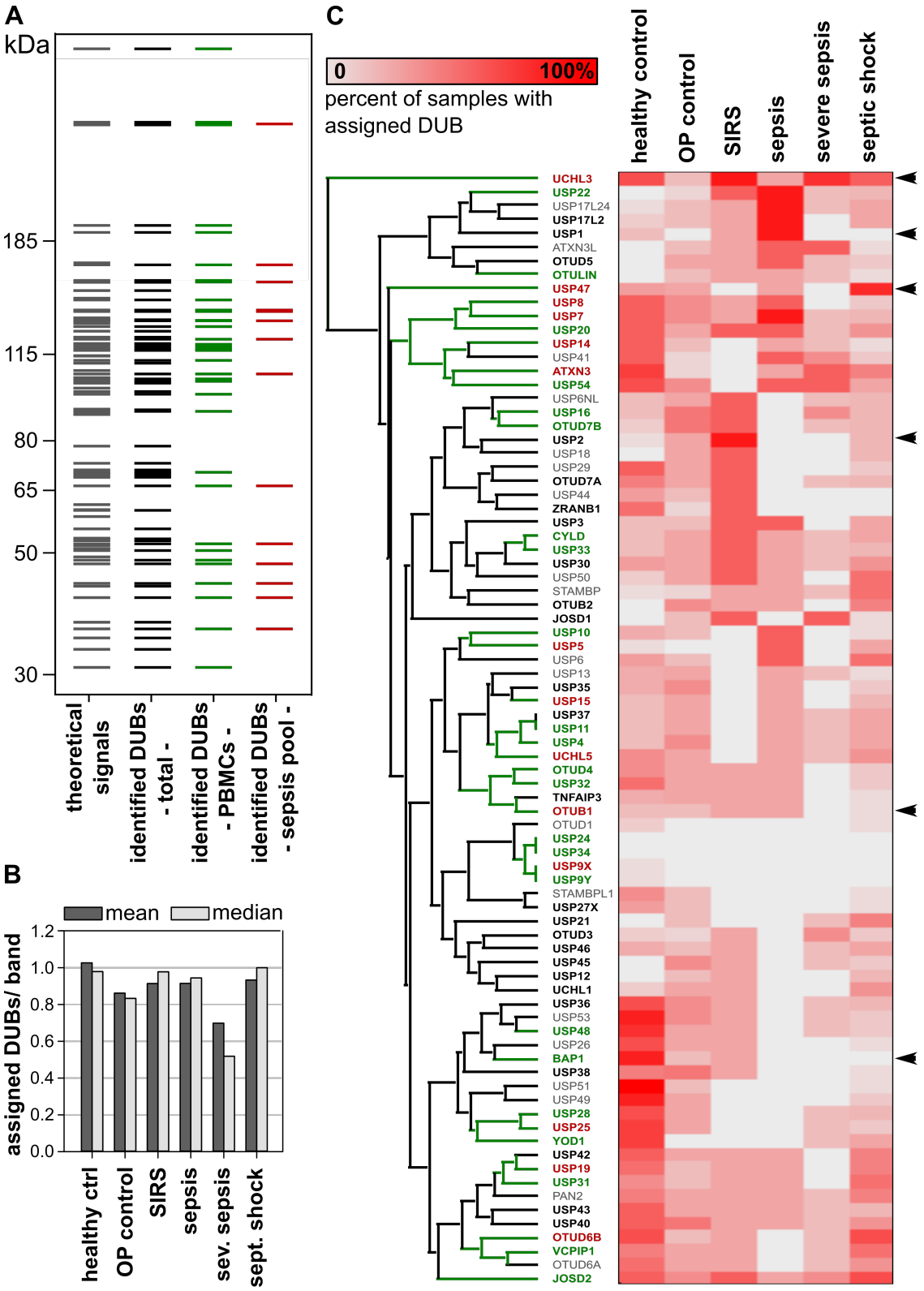
A
kDa
185
115
80
65
50
30
theoretical signals
identified DUBs - total -
identified DUBs - PBMCs -
identified DUBs - sepsis pool -
B
mean
median
assigned DUBs/ band
1.2
1.0
0.8
0.6
0.4
0.2
0.0
healthy ctrl
OP control
SIRS
sepsis
sev. sepsis
sept. shock
C
0
100%
percent of samples with assigned DUB
healthy control
OP control
SIRS
sepsis
severe sepsis
septic shock
UCHL3
USP22
USP17L24
USP17L2
USP1
ATXN3L
OTUD5
OTULIN
USP47
USP8
USP7
USP20
USP14
USP41
ATXN3
USP54
USP6NL
USP16
OTUD7B
USP2
USP18
USP29
OTUD7A
USP44
ZRANB1
USP3
CYLD
USP33
USP30
USP50
STAMBP
OTUB2
JOSD1
USP10
USP5
USP6
USP13
USP35
USP15
USP37
USP11
USP4
UCHL5
OTUD4
USP32
TNFAIP3
OTUB1
OTUD1
USP24
USP34
USP9X
USP9Y
STAMBPL1
USP27X
USP21
OTUD3
USP46
USP45
USP12
UCHL1
USP36
USP53
USP48
USP26
BAP1
USP38
USP51
USP49
USP28
USP25
YOD1
USP42
USP19
USP31
PAN2
USP43
USP40
OTUD6B
VCPIP1
OTUD6A
JOSD2

Figure 45. Theoretical assignment of DUBs to the activity-patterns according to their probe-modified molecular weight. The molecular weight of all known DUBs of the cysteine protease families in an HAUb-VME labeled state was determined and transformed to pixel lines using the marker of each experiment. Then, values were compared with the pixel lines of the bands from DUB patterns, and the DUB was marked as assigned, if the pixel lines varied about less than 3.5 pixels. (A) Theoretical blot of DUB patterns. To visualize the theoretically possible DUB patterns, a theoretical blot was generated utilizing SigmaPlot13. Based on the pixel value of the golden Standard marker, pixel values were determined for different samples. The gray lane illustrates the theoretical DUB pattern for all DUBs which were theoretically tag-able with HAUb-VME and contains most signals. The second, black lane depicts signals from all DUBs that were identified in either of the HA-IPs carried out in this study, regardless of cell types. In the green lane, all DUBs are presented, which were identified in a pool of PBMCs from 5 healthy donors. Finally, the red lane shows the theoretical pattern of mass spectrometrically identified DUBs from 3 pools of sepsis samples (18 in total). (B) Mean and median assigned DUB numbers per band in DUB patterns. The numbers of assigned DUBs for each group was normalized by the band count of each pattern to reveal differences in assignment. (C) DUB-assignment for individual DUBs and sample classes. The heat map illustrates the percentage of assignment for each specific DUB listed utilizing a color code from 0 % (gray) to 100 % (bright red). Dendrogram and DUB names were color-coded according to the presence of each DUB in the theoretical blots. If a DUB was found in more than one sample type, the color-code presents first sepsis pools by red coloring of DUB name and then PBMCs in green by the colored branch. Assigned DUBs, that were confirmed by any HA-IP experiment but not found in PBMCs or sepsis samples were marked black, and only theoretically HAUb-VME detectable DUBs are presented in gray. Black arrows on the right side indicate interesting DUB-assignments presented in more detail in Figure 46.

For the healthy control samples, 1.02 DUBs per band were assigned, indicating a theoretical DUB identification rate of 100 %. That is not the case, as DUBs were not assigned to bands with lower molecular weights, while due to the resolution limits in gel separation, more than one DUB was assigned to bands with high molecular weight. Interestingly, this mirrors the results from in-gel digestions of HA-IP samples in which those bands also contained more than one DUB. Thus, the mean assignment is a valid measure for the matching of DUB-masses and bands but does not directly reflect the completeness of assignment. The mean and median assignments for the OP control were 0.86 and 0.83 respectively and thus 20 % lower than for the healthy controls. SIRS, sepsis and septic shock samples showed a mean assignment between 0.91 and 0.93 but a slightly higher median (0.94 to 1). The only sample class with diverging assignment of DUBs per band was the severe sepsis class. There, only 0.7 DUBs (mean) or 0.52 DUBs (median) were assigned per band. As the class did not show any suspicious band distribution (Fig 43), the cause of this drop in DUB-assignment is not easily rationalized.

DUBs Identified by Theoretical Assignment: To further elucidate the DUBs assigned to each sample class patterns were visualized in a heat map. To this end, the percentage of samples in one class to which a particular DUB was assigned to was calculated and subsequently clustered (Fig 45C) to reveal plausible patterns in DUB-assignment. Notably, USP34 and USP24 were not assigned while USP9X and USP9Y were assigned, albeit rarely. A closer look revealed, that those four DUBs have molecular weights way above 300kDa. Although USP9X/Y were identified through the HA-IP in sepsis samples pools, assignment to bands is problematic due to the high molecular weights and the relatively low resolution of the used SDS-gels in this range. In contrast to that, the molecular weights of all other DUBs were found to be well within the boundaries of the assignable area.

Especially for the healthy control, SIRS and sepsis classes, groups of frequently assigned DUBs were found, while OP control and septic shock samples revealed a more uniformly distributed assignment, which might at least partly result form higher sample numbers in these classes. In the healthy controls, a group of DUBs containing USP54, USP7, USP8, USP 20, ATXN3 and USP41 was assigned. Interestingly this group should result in only 4 distinct bands in a blot, since USP7 and USP8 (about 138 kDa) as well as USP41 and ATXN3 (about 51 kDa) would be nearly inseparable. USP54 presence should result in a high MW band of 197 kDa and USP20 yield a 112 kDa band. Additionally, all members of this group except for USP41 were previously identified in PBMCs (green names), but 4 of the DUBs were also found in sepsis pools (red).

A second group of commonly assigned DUBs in the healthy controls included USP36, USP53, USP48, USP26 and BAP1 as well as USP49 and USP51. Here again, some DUBs were practically inseparable, i.e USP48 and 53 (129 kDa) and USP49/51 (89 kDa), while USP26 and BAP1 presence should result in individual signals. For the SIRS and severe sepsis classes only single DUBs showed high percentage of assignment, while in the sepsis class, a group of DUBs was uncovered. This group contained both forms of the USP17 family as well as USP1 and USP22, of which only USP22 was previously identified in PBMCs. Astonishingly, none of those DUBs were previously identified in the HA-IP approaches of sepsis samples.

DUB Candidates for Prediction of Sepsis-progression: Beyond these groups, few individual DUBs showed high assignment in distinct sample classes (Fig 46A-F). Of the DUBs assigned in samples of all classes, UCHL3 showed the highest values (Fig 46A). In the healthy control, SIRS, severe sepsis and septic shock classes the assignment was above 50 %. In the two remaining classes, the values were lower (16.7 and 25 %), but nevertheless high as compared to other assignments. In contrast, BAP1 mass was assigned to 72.2 % of the healthy control samples as well as to 16.7 and 25 % percent of OP control and SIRS samples, but no assignment was found for the sepsis states (Fig 46B). A similar assignment was found for USP2 (Fig 46C) with highest matching in SIRS samples

(75 %). Furthermore USP2 was assigned to a lower extent in OP control, healthy control and septic shock samples, but not in sepsis or severe sepsis.

Another DUB, USP1, showed a peak of assignment in sepsis (75 %) and additionally, similar but lower assignments in SIRS and septic shock (25 and 30 %) and also low assignment in the healthy control samples. In contrast, OTUB1 showed a generally low but constant assignment of 15 to 25 % in healthy controls, OP controls, SIRS and sepsis, but no assignment in severe sepsis and only 5 % in septic shock samples. Last, but not least, USP47 showed the highest assignment (68.8 %) in septic shock samples, while it was not assigned to SIRS and severe sepsis samples and about 25 % assignment in the other classes.

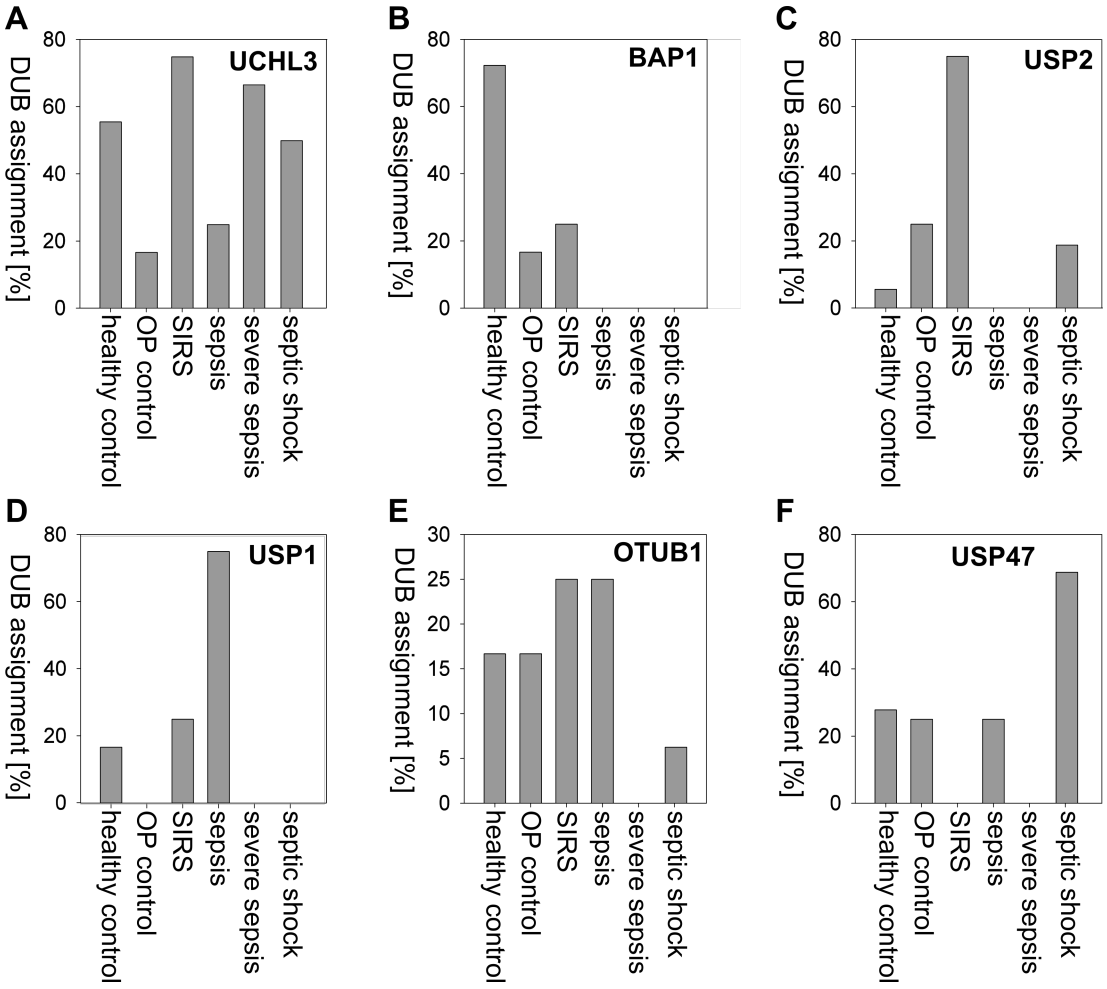

Figure 46. Percentage of assignments for individual DUBs in distinct sample classes. These assignment were calculated by the number of assignments in one class divided by the number of samples. Presented DUBs were selected for their occurrence in the different sample classes.

In summary, the theoretical DUB assignment revealed both distinct groups of DUB assignments as well as single DUBs with specific assignment patterns. Most interestingly, among those DUBs, candidates which in combination reflect each sepsis state, were defined. Although the assignment is purely theoretical, most of the candidates were identified either in PBMCs or sepsis samples by MS-measurements. Therefore, the next step has to be the validation of these candidates in a quantitative manner to assess whether they can indeed differentiate healthy, SIRS and sepsis patients and even different sepsis states.

4.4 Development of Activity-based Probes to Analyze Deubiquitinating Enzyme Activity

4.4.1 Characterization of HAUb-VFEA for the Screening of DUB Activities in Comparison to HAUb-VME

Activity-based probes are valuable tools in proteomic research which are able to bind distinct groups of active enzymes covalently and enable the extraction of those proteins from complex biological samples through the included affinity-tag or monitoring of their activities.

The novel probe HAUb-VFEA is a classical ABP for DUBs using a C-terminal reactive group for covalent attachment and a hemagglutinin (HA)-Tag for purification [96] and was developed and prepared in-house (section 3.3) in cooperation with Dr. Raimo Franke (HZI). The structures of both warheads are illustrated in Supplementary Figure S2. Recently, HAUb-VFEA (HAUb-MF) was used to characterize the active DUB-complement of 5 cancer cell lines (manuscript in preparation) [96, 210]. Although the capability of this probe to bind DUBs was described and evaluated, a comparison to the gold-standard, the C-terminal electrophilic HAUb-VME, introduced in 2002 [88] and used in a number of studies [90, 94, 104, 106, 267–269], was missing until now. Most importantly, it is also not clarified, if the current gold-standard HAUb-VME only reacts with active DUBs and which levels of DUB-activity HAUb-VFEA is able the discriminate.

4.4.1.1 Activity in Cell-lysates of the EL-4 Cell Line

As EL-4 cells are frequently utilized for the characterization of newly devised probes, HAUb-VFEA was also characterized in comparison to HAUb-VME in this cell line. Therefore, EL-4 cells were lysed and subsequently, 9.35 mg of lysates were labeled with HAUb-VME or HAUb-VFEA or incubated without probe. After enrichment of DUBs, samples were analyzed by LC-MS/MS measurements.

In total, 46 active DUBs were identified by mass-spectrometry in labeled samples as compared to 11 in the non-enriched controls (Table 22). Of the former, 45 were bound

Table 22. DUBs captured in EL-4 lysates by HAUb-VME and HAUb-VFEA. DUBs are sorted according to their families. $\sum$ = total numbers of DUBs.

	control	HAUb-VME	HAUb-VFEA
USP	9	30	29
UCH	2	4	4
OTU	/	8	2
MJD	/	3	1
$\sum$	11	45	36

by HAUb-VME while 36 were detected by HAUb-VFEA. The main portion of bound DUBs for both probes belonged to the USP-family and the differences in binding were minimal (30 to 29) in this family. For the UCH-family, both probes even bound the same members. In contrast to that, HAUb-VME extracted 8 OTU and 3 MJD-family DUBs while HAUb-VFEA captured only 2 OTU DUBSs and 1 MJD-family DUB (Table 22).

To illustrate the distribution of identified DUBs, the unique spectra recorded were normalized to the molecular weight of the individual DUBs and subsequently utilized to create a heat map displayed in Figure 47. The data points used to create this figure are collected in Supplementary Table S8. In general, a strong enrichment of DUBs as compared to the control IP could be shown as fewer DUBs were identified in the control with lower numbers of unique spectra. For the USP and UCH-family, the heat map confirmed the relatively small differences described above also in terms of enrichment as depicted by similar color saturation caused by similar numbers of unique spectra for HAUb-VME and HAUb-VFEA. Additionally, four DUBs, USP17L2, USP34, USP42 and USP45 were identified for the first time as binding an ABP by both probes alike.

Differences in identification were only found for USP10 and USP30, which were only identified by HAUb-VME and USP3 which was solely identified in the HAUb-VFEA samples. Beyond identification, HAUb-VFEA showed slightly stronger enrichment of USP8, USP15 and USP19 and lower spectrum counts for USP25, USP37 and USP48 as well as CYLD, UCHL1 and Ataxin 3 (ATXN3) as compared to HAUb-VME.

In contrast to the small differences within the USP and UCH families, HAUb-VFEA enriched only few members of the OTU and MJD groups, either with low numbers of unique spectra or identification only in one or two replicates.

Nevertheless, the ability of HAUb-VFEA to enrich DUBs from complex cell lysates was clearly demonstrated. HAUb-VFEA also exhibited a tendency towards USP- and UCH-family DUBs, where it bound DUBs as broadly as VME.

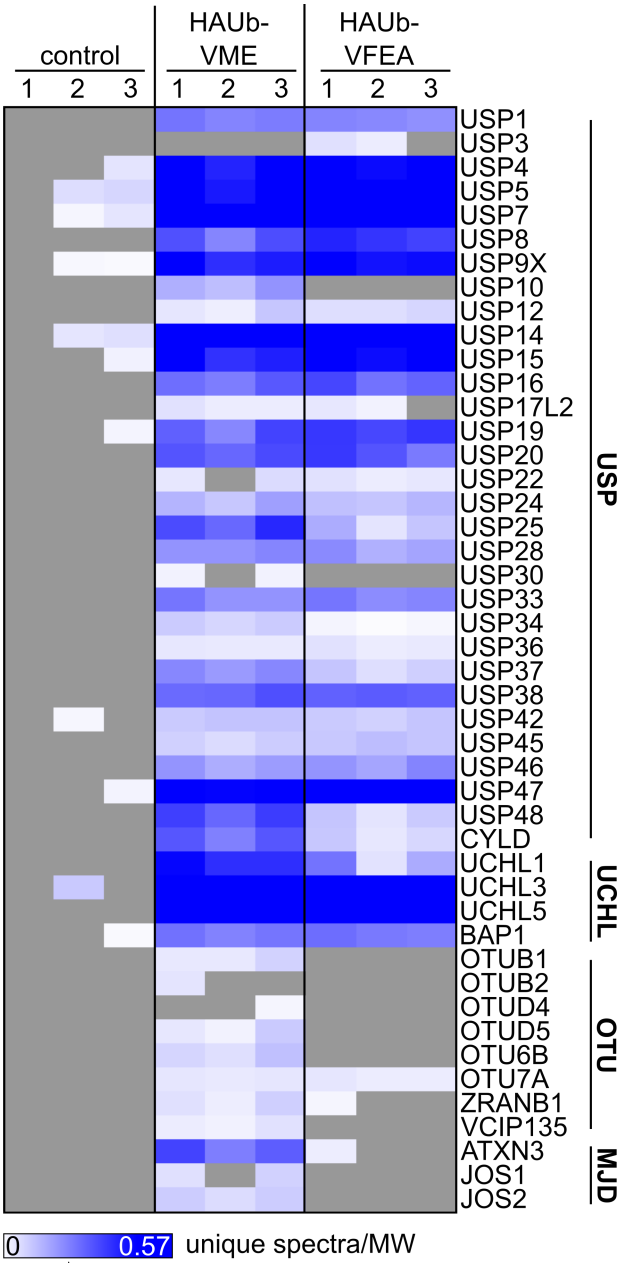

Figure 47. Unique spectra of DUBs captured by HAUb-VME and HAUb-VFEA. HAUb-VME, HAUb-VFEA and pure agarose beads (control) were used to extract DUBs from EL-4 cell lysates. Subsequently, the samples were analyzed by mass spectrometry and unique spectra were extracted. Unique spectra normalized by molecular weight are presented in the heat map with a color range from white (0) to dark blue (0.57) while gray indicates that the particular DUB was not identified in the replicate. Application of both probes revealed enrichment of DUBs as compared to the control as well as distinct DUB patterns. HAUb-VME showed a broader spectrum of DUB-binding and for some DUBs, i.e. USP25, USP37, USP48, CYLD, UCHL1, ATXN3, higher numbers of unique spectra as compared to HAUb-VFEA. In contrast, HAUb-VFEA produced an increased spectral count for USP8, USP8, USP15 and USP19 and solely identified USP3. In general, 4 DUBs, USP17L2, USP34, USP42 and 45 were not described to be labeled by ABPs before and were enriched by both probes. The family affiliations of all DUBs are given at the right side of the figure.

4.4.1.2 Activity Towards Recombinant Enzymes

As a validation for the results of the MS-approach, the shift in molecular weight for a panel of recombinant DUB was monitored to verify the binding behavior towards the tested DUBs (Fig 48). For the majority of DUBs, the reactivity of the probes was comparable to the MS measurements. For example, USP28, USP47 and BAP1 showed comparable signals in both a approaches with similar reactivity of HAUb-VME and

VFEA. Furthermore, the blots of USP25, CYLD and UCHL1 confirmed pronounced binding to HAUb-VME in comparison to VFEA, while USP10, OTUB1 and JOS1 were solely targeted by HAUb-VME.

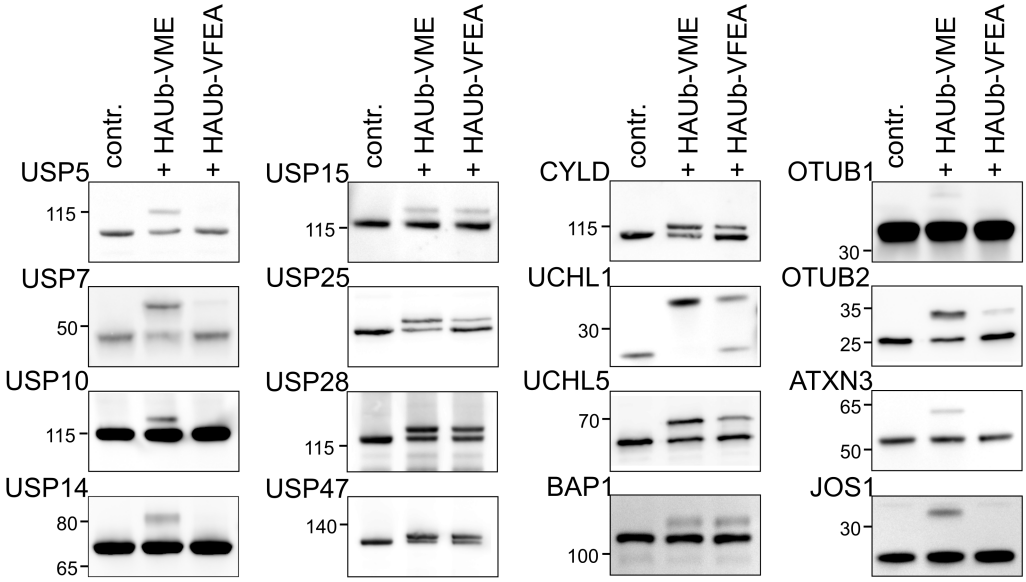

Figure 48. Comparative shift assays of recombinant DUBs labeled with HAUb-VME and HAUb-VFEA. Recombinant DUBs were labeled with HAUb-VME or HAUb-VFEA and the shift in mass was subsequently analyzed by α-HIS_6 western blotting. Each individual blot shows the DUB alone, and in complex with the two probes, always detecting the respective DUB which carried the HIS_6-Tag. All DUBs were also identified in the MS-approach where they reacted with at least one of the used probes.

Nevertheless, for a number of DUBs the results from the western blots differ from the cell line screening results. For example, UCHL5 showed lower reactivity towards HAUb-VFEA in the western blots while nearly equal numbers of normalized unique spectra were generated from the HA-IP approach. Furthermore, ATXN3 showed no binding of HAUb-VFEA in the blot, but the MS measurement provided a signal in one of the replicates. In contrast to that, OTUB2 bound to HAUb-VFEA in the western blot but showed no enrichment in the MS approach.

However, the strongest deviations were found for USP5, USP7 and 14. While all three of those DUBs showed similar numbers of normalized spectra in the heat map for both of the probes, they were not bound by HAUb-VFEA in the shift assays.

Since K63 Ub-chains were previously described as substrates for USP5 and USP7 [270–272], both DUBs were incubated with K63 tetra-Ub chains as described in subsection 3.4.4 to assess the DUB activity and to evaluate the binding behavior of USP5 and USP7 towards the probes in the presence of the natural substrate (Fig 49). Notably, HAUb-VFEA-binding was highly intensified by addition of K63 tetra-Ub chains in USP5,

while HAUb-VME-binding showed only a slight increase in presence of the substrate (Fig 49A). In contrast, for USP7 no differential probe-binding upon substrate addition was observed and no binding occurred towards HAUb-VFEA as noticed before. The DUB activity was then assessed by monitoring the cleavage of K63 tetra-Ub chains during 60 min of incubation (Fig 49B). While USP5 was found to be highly active and had cleaved nearly all of the Ub-tetramers directly after mixing (0 min), USP7 showed only very weak activity. Only the later time points, 30 and 60 min displayed faint bands at the height of Ub-trimers (Ub3) and Ub-dimers (Ub2).

In summary, HAUb-VFEA was confirmed to be a broad ABP for DUBs with a preferred binding of USP and UCH family DUBs. Incubation of recombinant DUBs with both probes and comparison to the HA-IP data ultimately demonstrated a substrate-dependent binding of HAUb-VFEA to USP5 which might indicate a difference in "activity-sensing" in HAUb-VFEA as compared to HAUb-VME.

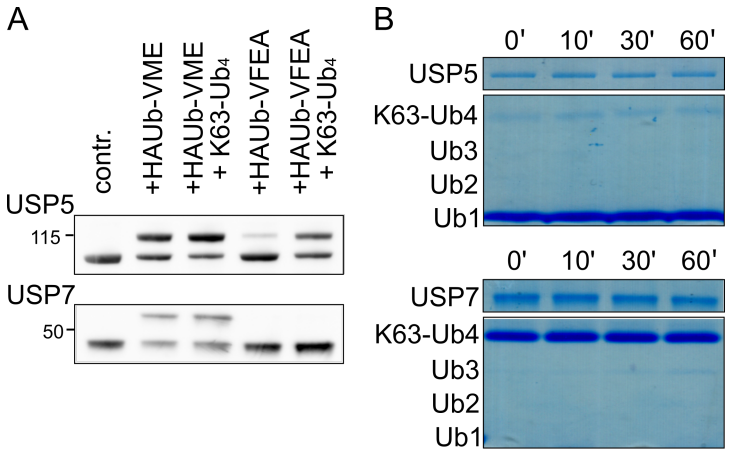

Figure 49. Characterization of recombinant USP5 and USP7 regarding activity and probe-binding properties. (A) Probe-binding of USP5 and USP7 in presence of K63 tetra-Ub chains. USP5 and USP7 were incubated with HAUb-VME and HAUb-VFEA in the presence and absence of their natural substrate and the shift caused by probe-binding was investigated by α-HIS_6western blot. For USP5, substrate-dependent binding of HAUb-VFEA was found to be enhanced as compared to HAUb-VME. In contrast to that, addition of K63 tetra-Ub chains had no influence on probe binding. (B) K63 tetra-Ubiquitin chain cleavage assay of USP5 and USP7. Both DUBs were incubated with K63 tetra-Ub chains for the indicated times and samples were evaluated by Coomassie-staining of prepared gels. USP5 showed nearly complete Ub-chain cleavage directly after mixing (0'), while USP7 showed virtually no activity against the Ub-chains. The amount of applied enzymes is presented in the upper Coomassie-strips.

4.4.2 Ubiquitin-Isopeptide Probes to Mimic Ubiquitin-substrate Conjugation

In contrast to the classical C-terminal ABPs, the so-called Ubiquitin-Isopeptide probes (UIPPs) were designed to mimic ubiquitin moieties attached to a substrate or incorporated into Ub-chains of different linkages. Therefore, a peptide of the target protein, the substrate of ubiquitination, was attached to the warhead to enable the binding of DUBs by recognition of the specific sequence surrounding of the Ub-site. A part of the UIPP-set, the probes imitating K48 and K63-ubiquitin chains were published to introduce the concept of UIPPs [95]. Following this, additional UIPPs were also produced in this study in cooperation with Dr. Raimo Franke (HZI). Thus, peptides of interesting targets were synthesized, coupled to the reactive warhead VA and finally ligated to HA-ubiquitin. Utilized peptide sequences are listed in Table 10. Ultimately, two different sets of UIPPs were designed with distinct goals:

1. The first set, mimicking poly-Ub chains was intended to investigate chain-linkage specificity of DUBs.

2. The second set, which was designed to recreate ubiquitinated sites at the RTK c-Met, is to be utilized to identify DUBs which regulate deubiquitination of c-Met.

The first set is described hereafter, while results for the c-Met UIPPs is found in subsection 4.1.3.2 of this study.

4.4.2.1 Ubiquitin-chain Mimicking UIPPs

To mimic differentially linked poly-ubiquitin chains, probes utilizing the sequence surroundings of K6-, K11-, K27-, K29-, K33-, K48- and K63-ubiquitin chains were ligated. While K6- and K11-ligation did not yield enough material, the other probes were successfully produced. The set of Ub linkage-specific probes, now containing K27-, K29- and K33-UIPPs as well as the initially characterized K48- and K63-UIPPs [95] were used to investigate recombinant DUBs for their binding specificities. To this end, the DUBs were incubated with UIPPs and HAUb-VME for 1 h and subsequently analyzed via SDS-PAGE and western blotting. To detect the recombinant, HIS_6-tagged DUBs, an α-HIS_6antibody was used.

In general, three groups of DUB-reactivities resulted from the screen with recombinant enzymes and corresponding western blots are shown in Figure 50. The first group of DUBs (Fig 50, upper left) showed a broad reactivity towards all UIPPs and HAUb-VME and contained USP15, USP21 and USP47 as well as UCHL3. Notably, both USP15 and UCHL3 showed a weaker signal for the K63-UIPP as compared to the other probes. The second group at the lower left of Figure 50 was inactive against the UIPPs, but reacted with HAUb-VME. This reactivity, observed for USP10 and USP14 as well as

ATXN3, ATXN3L and YOD1, hints towards a general specificity of those enzymes either for specific substrates or poly-Ub chains.

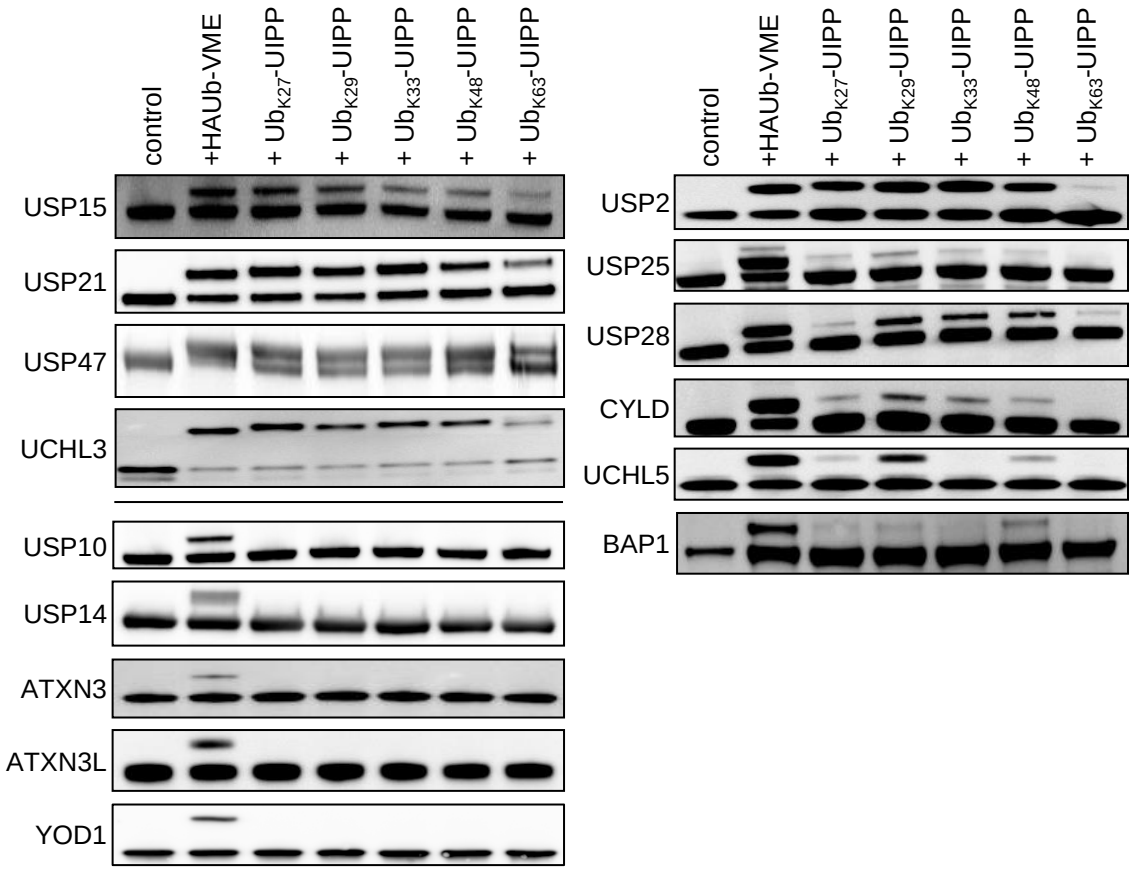

Figure 50. Reactivity and specificity of Ub-chain linkage-specific UIPPs towards recombinant DUBs. The recombinant DUBs were incubated with HAUb-VME and the panel of UIPPs mimicking K27, K29, K33, K48 and K63-linkage and subsequently analyzed by α-HIS$_6$ western blotting. HAUb-VME was also used for labeling as comparison to classical C-terminal electrophilic warheads.Three groups of DUB-reactivities towards UIPPs were detected; DUBs were either broadly (upper left), non-reactive (lower left) or differentially reactive (right).

Most interestingly, DUBs in the third group (Fig 50, upper right) showed distinct activities towards a specific subset of the UIPPs. USP2 for example was highly reactive towards all of the UIPPs except for the K63-UIPP, where only a weak signal was found. In contrast to that, USP25 showed weak reactivity towards UIPPs in general and a stronger shift for the K29-UIPP, but no binding towards the K63-UIPP at all. The third

USP-family member in this group, USP28 reacted strongly with the K29-, K33-, and K48-UIPPs, but only weakly with K27- and K29-UIPPs, while CYLD, the fourth USP, bound preferentially to the K29-chain mimic, but not to the K63-UIPP and only poorly to the other UIPPs.

The two remaining DUBs in this group, both belonging to the UCH family exhibited the most distinct binding patterns. UCHL5 showed pronounced binding of the K29-UIPP and only slight reactivity towards K27- and K48-UIPPs. The other probes yielded no signal at all, hinting to inactivity towards those UIPPs. On the other hand, BAP1 displayed moderate binding of the K48-UIPP and very weak signals for K27- and K29-mimics. Notably, most of these DUBs showed enhanced activities towards the K29-UIPP and a diminished binding towards the K63-Ub-chain-mimicking probe.

The question whether the described binding preferences are truly a mirror of substrate specificities or influenced by the steric properties of the isopeptide-constructs needs to be discussed.

5 Discussion

This study aimed to survey the influence of the human ubiquitin system on bacterial pathogenesis and host responses on three distinct levels of complexity. As a model, the well-described Gram-positive pathogen *Listeria monocytogenes* (Lm) was chosen for the characterization of activities of deubiquitinating enzymes (DUBs) as a crucial part of the ubiquitin system and host-reaction towards infection.

On a cellular level, ubiquitination and counter-regulating DUB activities involved in the initial signal transduction after bacterial-host contact on non-phagocytic cells were investigated using the example of the InlB/c-Met axis of Lm invasion.

In a subsequent step, the systematic proteome and DUB-responses to Lm infection were surveyed in a murine animal model of listerial liver infection. While InlB-mediated invasion of hepatocytes is also a major mechanism in this infection model, host-responses are much more sophisticated than on cellular level, including infiltrating immune cells and their orchestrated immune response. On this level, the influence of Lm on physiological as well as Ub-regulatory proteins was analyzed in particular.

On the third and most complex level of investigation, the diagnostic and prognostic value of DUB activities in sepsis was tested in a pilot-study on PBMC samples of ICU-patients and healthy controls. To optimize the access to DUB activities on all of those levels, novel activity-based DUB-probes were developed.

Hereafter, different aspects of this thesis will be discussed in the frame of the increasing complexity of the investigated systems.

5.1 Ubiquitin-dependent Mechanisms during Cell Invasion via the c-Met/InlB Axis

In the first part of this thesis, ubiquitination of the receptor-tyrosine kinase c-Met as the most proximal component of InlB-mediated Lm cell-entry was investigated. Furthermore, candidate DUBs regulating ubiquitination of c-Met or InlB-mediated invasion in general were determined (section 4.1).

Of the 6 generated ubiquitination-deficient K to R mutants of c-Met utilized for the analysis, all showed permanent receptor activation upon transfection into HeLa S3 cells judging from the immunoblot results obtained as did the transfected wt control (subsection 4.1.2). However, downstream of c-Met, Erk1/2 and Akt kinases displayed

altered activation following stimulation with HGF or InlB, especially for the K2xR (K1103/04R) double mutant which showed Akt hyperactivation and the quadruple mutant K4xR, for which results hint towards a permanent activation of the c-Met signaling axis (subsection 4.1.2).

In contrast to the signaling,intracellular localization of the mutant receptor variants did not differ from wild-type c-Met after stimulation with HGF or InlB (subsection 4.1.2.4).

In addition to the ubiquitination-deficient mutants, candidate DUBs were analyzed for their localization after receptor stimulation. Of the five candidate DUBs USP8, VCPIP1, USP2, USP21 and CYLD, only two displayed changes in cellular localization (subsection 4.1.3). Interestingly, an extensive co-localization between any DUB and c-Met, as would be necessary for its global deubiquitination, was not observed.

5.1.1 Is De-ubiquitination of c-Met of Relevance for Ligand-mediated Receptor-endocytosis?

Checkpoint-driven Receptor Endocytosis and Recycling: At first glance, the results mentioned above are unexpected, as the leading model of ligand-mediated endocytosis of RTKs follows the idea that ubiquitination facilitates the formation of protein complexes leading to receptor internalization [273]. Hereafter, this model is referred to as checkpoint-driven receptor endocytosis and recycling (Fig 51A).

As it was shown that Lm induces c-Met ubiquitination during cell invasion comparable to HGF-stimulated receptors [135] and no differences were observed between HGF- and InlB-mediated c-Met activation, the following discussion will aim at general receptor-endocytosis mechanisms rather than HGF- or InlB-specific explanations.

In the framework of the checkpoint-driven receptor endocytosis model, ubiquitination is necessary but also sufficient for endocytosis of the activated receptor, representing the first checkpoint. Indeed, for c-Met as well as other RTKs, mono- and polyubiquitination introduced by the Cbl family of E3-ligases was found to be sufficient for receptor endocytosis following ligand stimulation [133, 134, 136]. However, evidence for the necessity of RTK-ubiquitination is not direct for c-Met and others [273]. Instead, mutation of the c-Cbl recruiting phosphosite Y1003 of c-Met was shown to lead to increased receptor stability and thus, it was inferred that ubiquitination of c-Met results in receptor internalization and degradation [275, 276]. In contrast, other studies reported that this effect is c-Cbl dependent but Ub-independent, indicating that c-Cbl serves as a mere adapter in the process [277, 278].

Nevertheless, the endosomal sorting complex required for transport (ESCRT)-machinery responsible for RTK-recycling was shown to be dependent upon receptor ubiquitination when forming the early ESCRT-complexes I and II. In contrast, ESCRT-III was described to lack ubiquitin-binding domains. At this point a second checkpoint is introduced

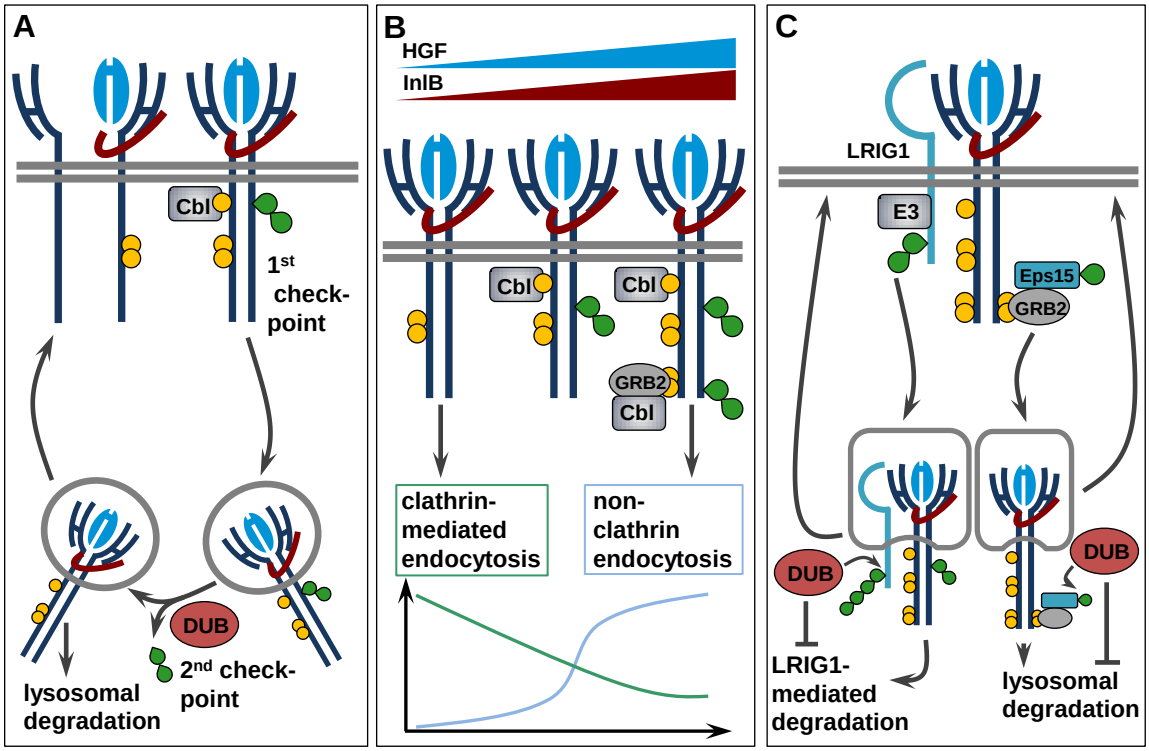

Figure 51. Involvement of ubiquitination and DUBs in suggested mechanisms of c-Met recycling and degradation. (A) Checkpoint-driven receptor recycling model. (B) Threshold-controlled endocytosis model adapted from Sigismund et al. [274]. (C) Recycling or degradation facilitated by indirect mechanisms.Cbl: Casitas B-lineage Lymphoma E3-ligase, Eps15: Epidermal growth factor receptor substrate 15, GRB2: Growth factor receptor-bound protein 2, LRIG1: Leucine-rich repeats and immunoglobulin-like domains protein 1.

into the classical model by considering the deubiquitination of c-Met at the ESCRT-III stage as a prerequisite for sorting, degradation and probably also recycling of the receptor [273, 278, 279]. Here, direct interaction between the ubiquitinated receptor and a DUB would be necessary. For other RTKs, e.g. EGFR and PGDFR, the DUB AMSH was described as the direct regulator of ubiquitination and therefore degradation [280]. In contrast, USP8/UBPY knock-out studies established only indirect effects on receptor stabilization [222, 281]. For both DUBs, further investigations of their roles in c-Met endocytosis are required, as it is not clear when and to what extend direct receptor deubiquitination takes place [273].

The observations of this study regarding ubiquitination as well as candidate DUB localization strongly contradict the checkpoint-driven receptor endocytosis model. In conjunction with previous indecisive results published, an alternative model for receptor-endocytosis, which fits the present results better, is required.

Threshold-controlled Endocytosis: One alternative model could be a threshold-controlled endocytosis of c-Met (Fig 51B). Recent results revealed that for EGFR, at least in some cell lines, ubiquitination and Ub-dependent internalization occur in a ligand concentration-dependent manner [274]. At low concentrations of ligand, EGFR was found to be activated and internalized in a clathrin-dependent manner, while above a certain threshold, ubiquitination of the receptor set in. Simultaneously, clathrin-independent endocytosis was activated, also driving receptor-degradation [274, 282]. For c-Met, no such concentration dependency was described until now. However, in light of the wt-like endocytosis of the Ub-deficient c-Met mutants analyzed in this study, it is tempting to speculate on a similar model for c-Met. In line with that, such a model could not only explain these results but also unify the contradicting claims of the clathrin-dependency of ligand-mediated c-Met endocytosis. While Clathrin-mediated endocytosis (CME) is described to be the major endocytosis-mechanism for c-Met [283], Clathrin-independent mechanisms were proposed depending on the model system and probably also ligand-concentrations [221]. Even though EGFR and c-Met are not comparable in all aspects of endocytosis [273], both are ubiquitinated by the Cbl E3 Ub-ligase, hinting at similarities regarding ubiquitination.

In contrast to the first model, the concept of threshold-controlled endocytosis does not require deubiquitination of the receptor other than the proteasomal deubiquitination activity to distinguish between receptors targeted for recycling or degradation. Polo and colleagues rather suggest that the endocytic mechanism *per se* dictates the receptor fate [282]. Thus, the model would also be in line with the "missing" direct interaction of a DUB and receptor found in this study.

Indirect Ubiquitin-mediated Endocytosis and Degradation: Another alternative model would be a ubiquitin-dependent but indirect endocytosis and degradation mechanism (Fig 51C). Recent studies of RTK endocytosis suggested that accessory proteins and not the RTK itself can be targeted by ubiquitination and subsequently facilitate receptor endocytosis.
For example, Leucine-rich repeats and immunoglobulin-like domains protein 1 (LRIG1) was recently described to interact with EGFR and c-Met. While acting in concert with EGFR, LRIG1 amplified direct EGFR ubiquitination and lysosomal degradation. However, interaction with c-Met led to LRIG1 ubiquitination and recruitment of both receptors for lysosomal degradation without an influence on c-Met ubiquitination [284, 285].

Thus, LRIG1 could be a candidate mediating Ub-dependent c-Met-degradation or recycling in absence of direct c-Met ubiquitination. Furthermore, Oh and colleagues identified USP8 as the DUB which regulates LRIG ubiquitination, thereby strengthening the role of USP8 in RTK-endocytosis as an indirectly acting DUB [273, 285]. However, LRIG1-coordinated RTK-endocytosis is until now described as ligand-independent only and therefore might not play an important role during ligand stimulation.

In contrast, Epidermal growth factor receptor substrate 15 (Eps15) was shown to

be monoubiquitinated following EGF stimulation even at low EGF concentrations and thereby orchestrating lysosomal degradation of EGFR [286]. As Eps15 was also found to interact with c-Met *via* the adapter protein GRB2, it is likely that an ubiquitination of Eps15 also occurs after c-Met stimulation. Interestingly, Eps15 contains an ubiquitin-binding domain, but interacts with c-Met through GRB2-binding *via* a coiled-coil domain [287].

Thus, Eps15 would be in position to regulate ligand-mediated endocytosis of c-Met through its ubiquitination without the necessity of receptor ubiquitination. Savio and colleagues introduced USP9X as a regulator of Eps15 ubiquitination. As USP9X is expressed in epithelial cells and implicated in protein trafficking, it is possible that USP9X also deubiquitinates endocytic proteins following c-Met activation [288].

In general, both alternative endocytosis models are better suited to explain the results of this study than the classical checkpoint-driven model which requires ubiquitination of c-Met for internalization and afterwards direct deubiquitination by a DUB to determine receptor fate. The best fit to the results of this study is achieved by a combination of an indirect mechanism for lower HGF or InlB concentrations (Fig 51B) paired with a threshold-controlled endocytosis mechanism (Fig 51C), which eliminates the need for a DUB to work directly at the receptor for deubiquitination.

Still, the precise role of Cbl-mediated ubiquitination of c-Met is unknown and needs to be elucidated to exclude a role in endocytosis. Additionally, a second cluster of Ub-sites is found in the multi-adaptor binding site of c-Met. As this cluster was not tackled by site-directed mutagenesis in this study, the possibility that those sites are exclusively responsible for Ub-mediated receptor-endocytosis cannot be ruled out with certainty.

5.1.2 DUBs Involved in Regulation of Lm Invasion

Many pathogens, e.g. viruses, fungi, parasites and Gram-negative bacteria acquired or developed own DUBs with specificity for Ub or UBLs to influence and control host processes [60]. Furthermore, some Gram-negative bacteria also express Ub-ligase-like effectors, which facilitate ubiquitination of host-proteins [289]. Thus, some pathogens, e.g. *Salmonella* and *E.coli* are able to hijack ubiquitination and deubiquitination alike while others were only described to express either Ub-ligase like effectors or DUBs [60, 289]. Interestingly, for Gram-positive bacteria neither DUBs nor ligase-like effectors were described until now.

Hence, for Gram-positive bacteria in general and Lm in particular, the only way to manipulate the host Ub-system is seemingly by influencing host DUBs and ligases *via* bacterial effectors. As discussed above, DUBs might not play a prominent role in direct deubiquitination of c-Met, but nevertheless were found to effect Lm infection and invasion [66, 80]. In this study, candidate DUBs were analyzed for direct co-localization

with c-Met. Localization of CYLD and USP21 were found to be changed following InlB-mediated c-Met stimulation (Fig 52A).

USP21: USP21 was found to co-localize with a portion of activated c-Met after 10 to 30 min of InlB stimulation in HeLa S3 cells. It was recently described that endosomal c-Met continues to participate in signaling and that the dynamics of endocytosis contribute to the signaling output of the receptor [132,290]. Endosomal signaling is required for full Erk1/2 activation as well as for STAT3 nuclear accumulation [291, 292]. Menard and colleagues most recently found that following c-Met activation by HGF, the receptor either localizes in peripheral endosomes (PE) or in perinuclear endosomes (PNE) [293]. If USP21 directly or indirectly interacts with signaling-competent c-Met species with perinuclear localization only, this spatial separation could lead to an altered signaling (Fig 52B). Conceivable results of direct deubiquitination would include an impact on adaptor molecule-binding as described for Ub-mediated complexes in immune cells [13]. Furthermore, priming of the c-Met containing endosome for ESCRT-III-mediated degradation by removing Ub-chains from c-Met would also be possible [279]. In contrast, deubiquitinating activity against adapter molecules of c-Met, i.e. an indirect mechanism, could alter the signaling output in a non-predictable manner.

CYLD: The deubiquitinase CYLD was found to relocate to speckles in the nucleus of InlB-activated HeLa S3 cells after 30 to 60 min of activation (Fig 52A). Interestingly, CYLD was previously described to attenuate anti-Lm immune responses *via* disturbance of the IL-6/STAT3-mediated fibrin production in hepatocytes [66] and inhibition of RIPK2 in macrophages [74]. In this study, CYLD was also found to localize in the nucleus, thereby deviating from the mainly described target location of CYLD i.e. the cytoplasm.

However, HPA denotes CYLD as nuclear localized, thereby confirming the obtained results [225]. The relocalization observed might be due to recruitment of CYLD towards a nuclear protein complex of unknown composition following c-Met activation. No such nuclear interactions are described for CYLD so far, but of the known interactors, Tumor necrosis factor receptor-associated factors 6 (TRAF6) [62], B cell lymphoma 3 (BCL3) [294], STAT3 and transforming growth factor beta-activated kinase 1 (TAK1) [63] are localized in the nucleus at least partly and therefore could be targets of nuclear CYLD. As STAT3 was already described as a direct substrate of CYLD and c-Met activates STAT3 as a part of perinuclear endosomal signaling [292], it is tempting to speculate that in this case CYLD also regulates STAT3 (Fig 52). However, it would be equally possible that CYLD deubiquitinates an as yet unknown protein, e.g. an activated kinase, to regulate nuclear functions.

At a first glance, it is unlikely that CYLD directly interacts with c-Met although it was identified as a candidate by utilizing a c-Met-mimicking UIPP. However, the interaction

might be restricted to a narrow temporal or spatial window of c-Met stimulation. Notably, a 60 kDa C-terminal fragment of c-Met was reported to re-localize to the nucleus independently of receptor stimulation in some cell lines like MDA-MB231 and also HeLa [295, 296]. It might well be possible that CYLD is recruited to nuclear c-Met fragments which either are not immediately detectable by the antibody utilized in this study or influencing the signaling of those fragments by deubiquitination even at low concentrations.

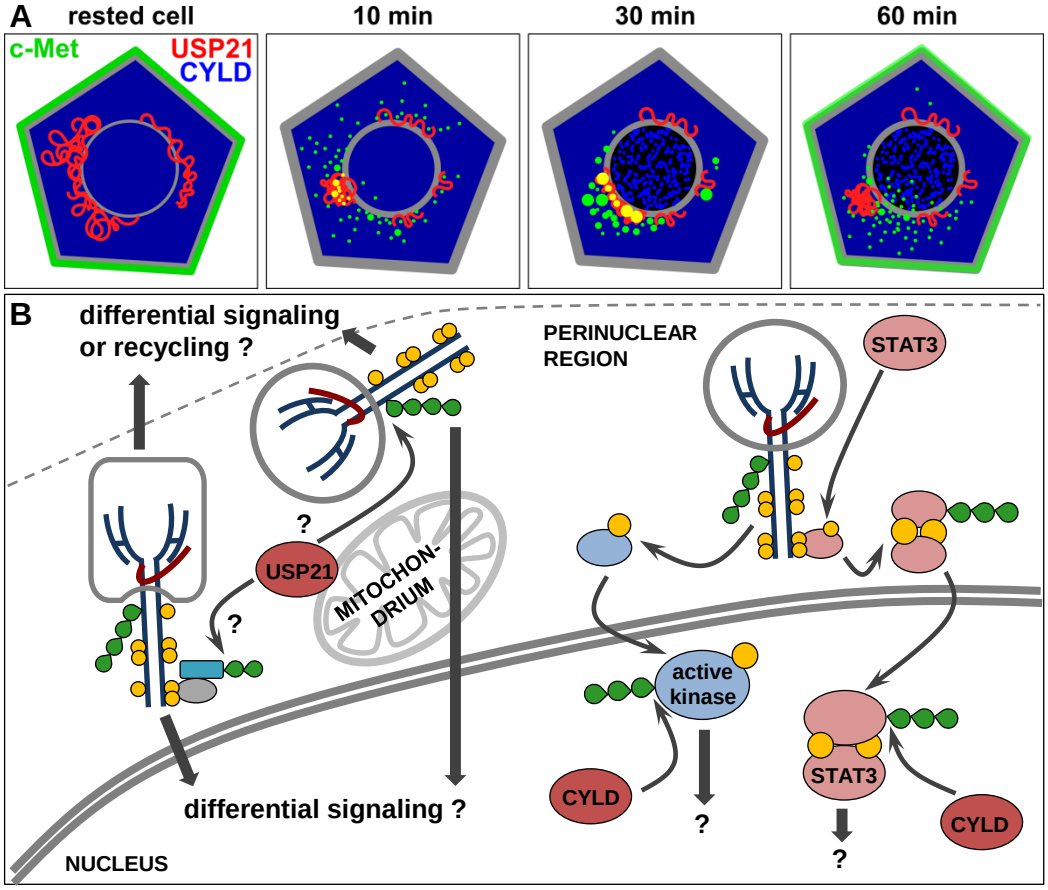

Figure 52. Potential roles of USP21 and CYLD in InlB-mediated c-Met stimulation. (A) Schematic representation of c-Met, CYLD and USP21 localizations in HeLa S3 cells as observed in this study. c-Met: green, USP21: red, CYLD: blue. (B) Representation of USP21 and c-Met as well as potential interaction partners in the perinuclear area and nucleus of the cell.

5.2 Regulation of Ubiquitination in Systemic, Sub-lethal Listeriosis

While the direct roles of both ubiquitination and DUBs seem to be only minor in ligand-mediated receptor endocytosis and thereby cell invasion, in Lm infection CYLD is well-established as a negative regulator of immunity [66, 74, 75]. This study revealed the regulation of two completely new DUB candidates which were not described in the context of Lm infection before. Both DUBs, USP2 and UCHL3, were downregulated in a systematic, activity-based DUB-screening in murine liver (subsection 4.2.3) . Interestingly, both DUBs were also found to interact with a c-Met mimicking UIPP, which might indicate an interaction with c-Met (subsection 4.1.3.2).

Additionally, the analysis of the liver proteome of Lm infected mice identified and quantified a number of proteins implicated in the regulation of Ub- and UBL-mediated processes. Of those, only the UBL ISG15 and two Ub-ligases, RNF213 and RNF135, were found to be significantly regulated.
Those unexpectedly low numbers of regulations (subsection 4.2.2.3) on the one hand indicate the partial needlessness of protein regulation to recalibrate a PTM system that is mainly based on activation and deactivation of proteins. On the other hand, the few regulated proteins thus gain in importance and are likely key-modulators in Ub-mediated cellular responses to Lm infection.

5.2.1 Ubiquitination and ISGylation Orchestrate the "Anti-viral" Immune Response in Hepatic Lm Infection

Notably, RIG-I-like receptor(RLR) signaling is usually activated as a defense response to viruses and is a sensor for viral 5´-triphosphorylated RNA species [297]. However, DDX58 itself and the two additional RIG-I-like receptors DHX58 (LGP2) and Interferon-induced helicase C domain-containing protein 1 (IFIH1/MDA5) are also able to detect RNA from few intracellular bacteria. *Legionella pneumophila, Shigella flexneri, Salmonella typhimurium* and *Listeria monocytogenes* RNAs were found to activate DDX58 or IFIH1, however, the downstream-signaling remains unknown [298–303]. This study uncovered the upregulation of DDX58 as well as a stable expression of IFIH1. Furthermore, it uncovered a whole battery of proteins described for antiviral immune-responses downstream of DDX58, which were also activated in the Lm infection setting of this study, e.g. IFITs , OAS1, PML and ISG15, and mostly not described in anti-bacterial responses until now (Fig 53).

DHX58 (LGP2): Notably, DHX58 (LGP2), which was previously described as an inhibitory factor of DDX58 was also found upregulated in this study. This result strengthens the study of Pollpeter and colleagues, who indicated an activating role for

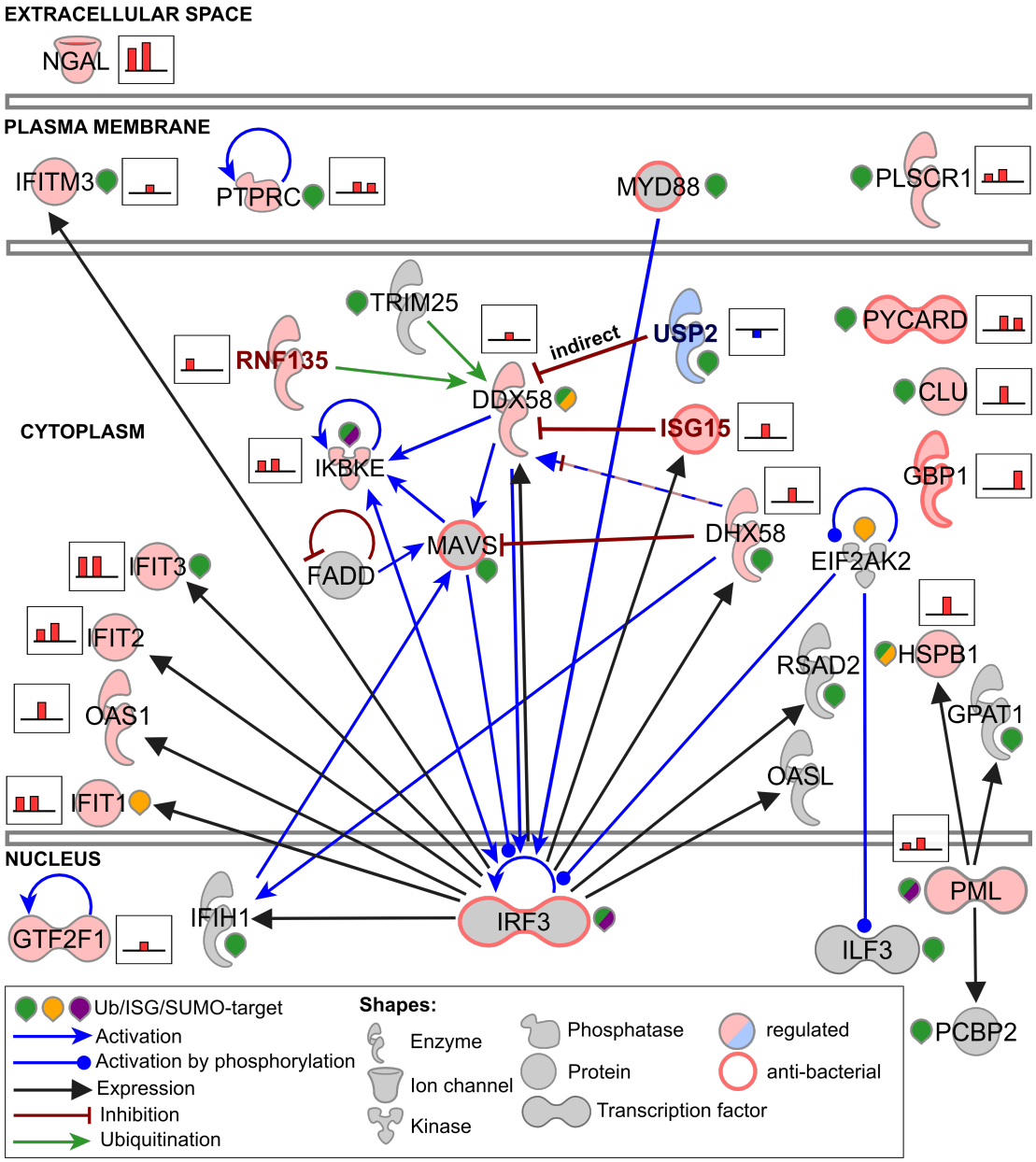

Figure 53. Identified and regulated proteins involved in "anti-viral" signaling during hepatic Lm infection. A pathway was built by Ingenuity® Pathway Analysis (IPA®) [304] using all identified proteins from the dataset which were annotated with the GO-term "response to virus". Lm is known to activate DDX58 (RIG-I) by intracellular nucleic acids. All proteins illustrated were identified in the study, proteins depicted as light red/blue shapes were found significantly regulated. Light red outlines indicate an additional annotation of the proteins as described in anti-bacterial immunity. CLU: clusterin, FADD: FAS-associated death domain protein, GBP1: Guanylate-binding protein 1, GPAT1: Glycerol-3-phosphate acyltransferase 1, GTF2F1: General transcription factor IIF subunit 1, HSPB1: Heat shock protein beta-1, IFIT1/2/3: Interferon-induced protein with tetratricopeptide repeats 1/2/3, IFITM3: Interferon-induced transmembrane protein 3, IKBKE: Inhibitor of nuclear factor kappa-B kinase subunit epsilon, ILF3: Interleukin enhancer-binding factor 3, IRF3: Interferon regulatory factor 3, MAVS: Mitochondrial antiviral-signaling protein, MYD88: Myeloid differentiation primary response protein MyD88, NGAL: Neutrophil gelatinase-associated lipocalin, OAS1: 2'-5'-oligoadenylate synthase 1, OASL. 2'-5'-oligoadenylate synthase-like protein, PCBP2: Poly(rC)-binding protein 2, PLSCR1: Phospholipidscramblase 1, PTPRC: Receptor-type tyrosine-protein phosphatase C, PYCARD: Apoptosis-associated speck-like protein containing a CARD-domain (ASC), RSAD2: Radical S-adenosyl methionine domain-containing protein 2.

LGP2 in Lm infection [305]. It is tempting to speculate that the activation of LGP2 is *Listeria*-specific, as it was not described for other bacterial pathogens before.

RNF135 and USP2: Most interestingly, the Ub-ligase RNF135 and the DUB USP2 were both previously described to regulate DDX58 (RIG-I) activity. The E3 Ub-ligase RNF135 was shown to ubiquitinate DDX58 at the repressor-domain and thereby to induce activation of DDX58 and association with TRIM25 and TANK-binding kinase 1 (TBK1) [258, 259]. In this study, RNF135 was found upregulated at day 1 post infection indicating an early DDX58-activation by ubiquitination, which then probably led to increased DDX58 expression through a positive feedback loop *via* IRF3.

In contrast, USP2b was recently described to remove K63-linked Ub-chains from TBK1, thereby inhibiting TBK1 kinase activity [306]. As USP2b was found to be the major isoform of USP2 in murine liver [307], it is assumable that USP2 detected in this study is indeed the isoform USP2b.

USP2 was found significantly down-regulated at day 3 p.i. and thereby most likely supports the activation of DDX58 *via* TBK1-deubiquitination during the peak phase of infection. A recent mRNA study from B. Izar reported a significant increase of USP2-cDNA in the first 4 h of infection in murine liver and a subsequent decrease at later time points [243].

All of those results hint towards a fundamental and tightly timed regulation of RLR-signaling following Lm infection by ubiquitination. The acquired datasets of this study (subsections 4.2.2.3 & 4.2.3) thus revealed two proximal regulators of RIG-I signaling as well as their temporal regulation in Lm infection (Fig .53).

ISGylation & Ubiquitination: The ubiquitin-like molecule ISG15 is one of the proteins expressed following IRF3-activation and rapidly upregulated following type I IFN response to viral infection [5]. As found in this study and also previously described, ISG15 is increasingly expressed during Lm infection. Interestingly, ISG15-knockout cells were described to be more susceptible to Lm but not to *S. flexneri* or *S. typhimurium* and those two pathogens also did only weakly induce ISG15 expression [34]. Thus, it seems that ISGylation is of special benefit in the defense of Lm infection in contrast to other pathogens and ISG15 expression is activated in an Lm-specific manner. One candidate could be the aforementioned DHX58/LGP2, which could influence the detailed activation of RLR-signaling, as it seems also to be Lm-specific.

ISG15 was also found to modify DDX58 and thereby inhibit its activity in a negative feedback-loop [308], as well as several other proteins which are part of RLR-signaling or the "anti-viral" response in general (described as ISGylated in UniProt KB or PTMScout [230,309], see Fig 53). Therefore, it is likely that ISG15 exhibits this feedback functionality also during Lm infection, thereby further shaping the RLR-signaling.

Apart from ISGylation, for many of the identified and quantified proteins presented in Figure 53, ubiquitination or SUMOylation sites were experimentally detected and reported in the PTMScout database [309]. Even though no ligases or proteases are described for those sites and the conditions of occurrence might not be clear, their presence implicates a certain degree of Ub-mediated protein regulation. Especially for regulated proteins in the pathway, Ub-conjugation could be of importance to facilitate protein degradation to enable shut-down of the host-defense pathway in the clearing phase of infection.

Therefore, it would be of high interest to analyze UBL-modifications in Lm infection on a systematic level by means of proteomics.

5.2.2 Novel Ub-modifying Proteins in Lm Infection

Apart from RNF135 and USP2, two additional Ub-regulating proteins, the Ub-ligase RNF213 and the Deubiquitinase UCHL3, were found to be significantly regulated. However, neither of those was described in context of infection before and putative roles in Lm infection are therefore purely theoretical.

RNF213: As pointed-out in the results section (4.2.2.3), RNF213 is described as an Ub-ligase with dual function as ATPase and was found significantly upregulated at day 1 and 3 after infection. The STRING DB analysis of the RNF213-interactome revealed only proteins which were co-expressed together with the ligase and no direct interaction partners. However, co-expressed proteins could be substrates of RNF213 or act jointly in a pathway. Among those co-expressed proteins, USP18 and UBA7 are listed. Both of those proteins not identified in this study are implicated in conjugation of ISG15 as activating and deISGylating proteins respectively, at least in human [41, 310]. This strongly hints towards a combined ubiquitination and ISGylation function of RNF213. Additionally, STAT1, IFIT3, IRF7, MX2, RSAD2 and IGTP, which were also co-expressed, are all implicated in interferon-related immune responses according to their assigned GO terms at the UniProt KB (GO version 142). In light of the affiliation of the co-expressed protein, RNF213 might be a novel regulator of infection-induced ISGylation with a broader activity window than RNF135.

UCHL3: UCHL3, which was found to be significantly downregulated during Lm liver infection in this study, is not well described in literature. UCHL3-knockout mice exhibit an elevated stress response and germ cell apoptosis [311,312]. As UCHL3 is closely related to the DUB UCHL1, it might be that UCHL3 exhibits similar functions, as described in other cases [312,313]. If that is the case, probable functions would be regulation of the innate immune response and signaling *via* the Akt, Erk1/2 pathways also influencing Lm invasion [80, 314, 315]. However, all those assumptions are highly speculative.

5.3 The Time-resolved Hepatic Proteome of Lm Infection - Research Reference and Clinical Guide

Apart from the Ubiquitin-related processes, the proteome of Lm-infected livers of course revealed a manifold of protein regulations, both previously described and novel in the context of Lm infection. This study was carried out in a mouse model system, however mouse and human genomes are highly similar (97.5 %) and orthologous genes feature a sequence similarity of 78.5 % [316, 317]. On the proteome level, mouse ranks in the third place regarding the number of orthologous proteins (87 %) as determined by the inParanoid tool, which compares proteome datasets [318]. Thus, it is highly likely that results inferred from the model system are also of importance for research in the human system.
Even though a cell type-resolved proteome of murine liver uncovered about 11.500 proteins, an earlier quantitative study of the whole liver proteome could only detect about 2200 proteins [319, 320]. However, even fewer comparative studies of non-infected and infected liver on the proteome level were carried out and this study represents the first time-resolved proteome of Lm infected murine liver. He and colleagues recently published the liver proteome of *Toxoplasma gondii*-infected mice, containing 3600 quantified proteins in two comparative conditions. They uncovered about 300 regulated proteins, with a p-value < 0.05 [321].

The liver proteome analyzed in this thesis resulted in 3666 quantified proteins of which 522 were found to be significantly regulated with a p-value < 0.001, amounting to 14 % of the total proteins (subsection 4.2.2). Furthermore, the analysis involved 3 time-points of infection as well as a control, indicating a superior resolution of the proteome regarding the course of infection and detection of significant protein regulation. Thus, this study constitutes a base to guide further research on the influence of Lm infection on organs *in vivo*.

Among the regulated proteins determined, many were identified to be proof-of-concept data as described in the results section (4.2.2). A GO-annotation enrichment analysis of the regulated proteins *vs.* the whole dataset utilizing the Gene Ontology enRIchment anaLysis and visuaLizAtion tool (GOrilla) confirmed the general regulation of proteins annotated as belonging to immune- and defense responses, e.g. acute-phase response, as well as the cytokine response especially to IFN-β (Fig 54). From the significantly enriched categories, two might be of special interest for further investigations (yellow star, Fig 54). Firstly, proteins exhibiting a "defense response to virus" could be of high interest to better characterize the Lm-dependent immune response, as discussed extensively above (5.2.1).

Proteins Involved in "Response to stress" are Interesting Candidates for Further Research: A second category of interest is "response to stress". There, proteins which

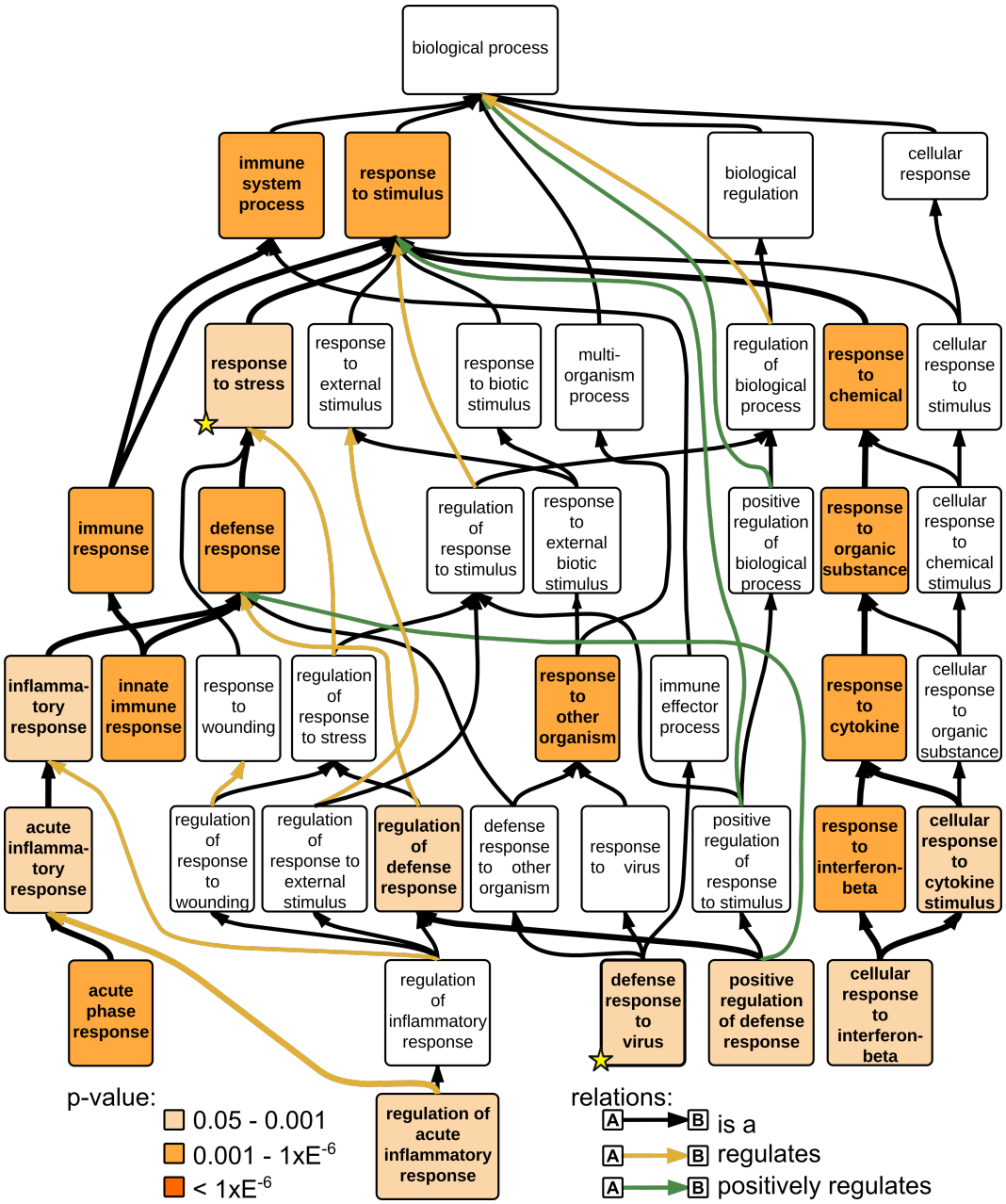

Figure 54. Enriched GO terms regarding biological processes involved in immune responses and immune regulation. Regulated proteins were analyzed for their GO annotation in the category biological processes and enrichment against the whole dataset was calculated utilizing GOrilla tool (GO version 142) [322]. The p-values illustrated are corrected for multiple testing. Processes discussed in more detail are marked with a yellow star.

are involved in "any process that results in a change in state or activity of a cell or an organism [...] as a result of a disturbance in organismal or cellular homeostasis [...]" are annotated [323]. Thus, subtracting the proteins annotated as involved in a defense response from those responsive to stress should reveal novel candidate proteins, which were previously not defined to be involved in defense responses, but were found regulated in this study, hinting towards involvement in Lm infection and clearance or deregulation by Lm.

For example, the protein disulfide isomerase 2 (PDIA2) found among the top-regulated proteins at day 1 p.i. as well as PDIA3, PDIA4 and PDIA6 (all upregulated) were also annotated as stress responders. Host PDIs in general were reported to be implicated in *Chlamydia* cell entry and infection with the mouse polyomavirus [238, 324].

Furthermore, overexpression of ISG15 was recently shown to lead to PDI clustering [34], linking PDIs and ISGylation.

As a second example, the actin-bundling protein Plastin-2, which was also annotated in this group and upregulated in this study, was found to be essential for the control of pneumococcal infection in mice, and plastin was even described to be involved in listerial actin assembly [325, 326].

Among proteins annotated as stress responders, many were found to be additionally annotated as implicated in actin-cytoskeleton remodeling or apoptosis, both processes well known to be influenced by Lm [327, 328]. This observation emphasizes the potential of the proteome dataset obtained in this study as a basis for future research.

Apart from immune-related processes, metabolic processes were also found to be highly enriched, indicating the severe influence of listeriosis on the physiology and metabolism of liver (Suppl. Fig S18). For example, cellular respiration (oxidation-reduction process), as well as cellular lipid and fatty acid metabolism were found to be deregulated during Lm infection among other processes. Of special interest in the context of Lm infection is the regulation of steroid metabolic processes and amino-acid metabolism and catabolism. Furthermore, the epoxygenase P450 pathway was found to be enriched 4 times among the regulated proteins, hinting towards a severe deregulation in drug metabolism (discussed below).

In general, the dataset defines the temporal liver proteome response during sub-lethal listeriosis for the first time and thus provides a valuable atlas of protein regulations as well as novel candidate proteins for future research.

5.3.1 Influence of Biotransformation Enzyme Regulation on Drug Metabolism of Listeriosis Patients

In total, this study identified about 100 proteins implicated in phase I and II biotransformation, of which 46 % were significantly regulated (subsection 4.2.2.2). The most prominently deregulated group of drug-metabolizing enzymes was the cytochrome P450

family with over 60 % of significantly regulated proteins. This severe and sustained downregulation found for many of the CYPs likely disrupts the hepatic drug-metabolism as well as metabolism of endogenous substances. Especially in elderly and immunocompromised listeriosis patients, impairment of the drug-metabolism might lead to severe side-effects not only in listeriosis treatment but also in treatment of unrelated conditions.

However, regulation of CYPs is not easily extrapolated from mouse to human, since distinct differences between the murine and human CYP-family were described [329]. Nevertheless, for 16 of the 25 regulated CYPs quantified in this study, human orthologs could be determined (Table 23). For 9 of those CYPs a single homolog was predicted in human, while for another 2 CYPs prediction varied depending on the search routine used, resulting in 2 homologs each (HomoloGene [330] / inParanoid [318]). Nelson and colleagues suggested that for the one-to-one homologies, direct transfer of functions from mouse to human might be meaningful [329].

For, e.g. Cyp2f2 and its human ortholog CYP2F1, it has be shown that both detoxify naphthalenes although toxicity differs between men and mice [331]. For the human homologs of Cyp7b1, Cyp8b1 and Cyp39a1, a role in bile-acid metabolisms was implicated as curated in the ReactomeKB [332]. Similarly, Ccp4a10 (human CYP4A11) and Cyp4a12a (human CYP4A22) are also not involved in xenobiotic conversion, but rather in fatty acid metabolism and Cyp17a1 is described to participate in steroid metabolism [333].

In contrast to the CYPs discussed above, the human homologs of Cyp1a2, Cyp2b10, Cyp2c29 and Cyp4f14 are involved in activation or degradation of xenobiotics.

Cyp1a2 (CYP1A2): CYP1A2 was described to be the human homolog of the murine Cyp1a2 with a sequence homology of 73 % on amino acid level as determined by using NCBI HomoloGene database [330]. Zanger and colleagues reviewed the Top-200 prescribed drugs in the U.S. and found that 9 % of those are partially or exclusively processed by CYP1A2. Among the metabolized drugs described were antidepressants, anti-psychotics, cardiovascular drugs, antiemetics, preventing vomiting, and muscle relaxants [334]. Especially the latter three categories of medication might be readily expected in the elderly or chronically ill patients. For example, tizanidine, metabolized by CYP1A2, was described in managing spasticity in multiple sclerosis and other conditions [335, 336]. The most interesting example for this study probably is theophylline, an anti-asthmatic drug, which is mainly metabolized by CYP1A2 and has a narrow therapeutic range [334, 337]. For this substrate, intoxication is commonly described both following drug interactions and infections. Furthermore, a prolonged half-time could be observed in sepsis patients with multiple organ dysfunction syndrome [337–340]. Thus, theophylline exemplifies the direct and grave sequelae of CYP-impairment.

Table 23. Human CYP homologs of murine cytochrome P450 enzymes. Homology and sequence identity on protein level were determined using NCBI HomoloGene database [330]. Substrates and functions are inferred from UniProt KB entries and ReactomeKB if not otherwise stated [230, 332]. Subscript letters indicate orthologs determined on gene (g) or protein (p) level.

mouse Cyp(s)	human ortholog	aa seq. identity [%]	substrates/function of human CYP
Cyp1a2	CYP1A2	73	9 % / Top-200 prescribed drugs in the U.S [334]
Cyp2a4, Cyp2a5	CYP2A6	84, 85	cyclophosphamide, ifosphamide (anti-cancer drugs), phenacetin [341]
	CYP2A7	82, 84	drug metabolism
	CYP2A13	87, 89	drug metabolism
Cyp2b10	CYP2B6	79	4 % / Top-200 prescribed drugs in the U.S [334]
Cyp2c29	$CYP2C8_g$	71	more than 100 drugs [342]
	$CYP2C18_p$	77	antipyrine, diclofenac, verapamil [343]
Cyp3a16, Cyp3a41a, Cyp3a11	CYP3A5	70, 72, 73	37 % / Top-200 prescribed drugs in the U.S [334]
Cyp4f14	$CYP4F12_g$	75	astemizole, terfenadine, ebastine (antihistamines) [344, 345], fingolimod [346]
	$CYP4F2_p$	80	vitamin E, K1; leukotrienes [347–349]
Cyp2f2	CYP2F1	82	naphtalene (polyaromatic hydrocarbon) [331]
Cyp7b1	CYP7B1	67	bile acid metabolism
Cyp8b1	CYP8B1	75	bile acid metabolism
Cyp39a1	CYP39A1	76	bile acid metabolism
Cyp4a10	CYP4A11	78	fatty acid metabolism
Cyp4a12	CYP4A22	75	fatty acid metabolism
Cyp17a1	CYP17A1	67	steroid metabolism

Cyp2b10 (CYP2B6): Human CYP2B6, the ortholog of Cyp2b10, also plays a major role in drug-metabolism by metabolizing a range of drugs [334]. In contrast to CYP1A2, none of the substrates described so far for CYP2B6 is catabolized exclusively by this Cyp. Consequently, impairment of CYP2B6 would probably not abolish the metabolization of one of the substrates, but could, depending on the mechanism, lead to slower activation, degradation of drugs or formation of an intermediate product.

Cyp2c29 (CYP2C8 & CYP2C18): Cyp2c29 and its human homolog on gene-level CYP2C8 show 71 percent of sequence identity and CYP2C8 was recently described to process more than 100 drugs [342]. However, the most probable ortholog on protein level as determined by the inParanoid tool [318] is CYP2C18, which displayed a sequence identity of 77 %. Therefore, it is not clear which of the human proteins would be influenced in listeriosis. Nevertheless, both human CYPs metabolize a multitude of xenobiotics with analgesics and antihypertensives among the known substrates [342, 343].

In contrast to the one-to-one homologs discussed above, for some CYPs no direct homologs could be determined due to gene-duplication or deletion on either, murine or human, side.

CYP2A - subfamily: The human CYP2A subfamily contains 3 members, 2A6, 2A7 and 2A13, which were all determined to be orthologous or paralogous to the 2 murine CYPs 2a4 and 2a5 identified in this study [341]. Thus, no direct relation between the individual proteins could be established. Additionally, the time point-resolved regulation detected in this study indicated differential regulation dynamics of the murine Cyps. However, all of the human isoforms were found to be involved in metabolism of xenobiotics.

A similar picture was also seen in the CYP3A subfamily. There also, the results of this thesis revealed differential regulations of the murine Cyps, which also compromised the transferability towards the human system.

While the interference with pharmacokinetics and drug disposition by both Lm infection and infection in general, is known for many years, it is still not well understood and probably underestimated [337, 350].

W. Renton recently reviewed this topic and specified several scenarios in which the effect of CYP-impairment could have detrimental results [337], all of which fully fit this study. Clinical significance will emerge, e.g. when clearance of drugs with a narrow therapeutic index, like theophylline, is primarily dependent on a single CYP, or when not only the CYP-phase of detoxification but also other phases or substrate-transport are disturbed, of which the latter is likely in Lm infection. Furthermore, increasing incidence of Lm infection in the elderly and immunocompromised as well as chronically ill patients leads to an averagely higher number of drugs present in the infected patients as compared to otherwise healthy outbreak patients [109]. Consequently, inhibition or

induction of CYPs due to other drugs and cross-reactions might additionally add to their deregulation.

A further clinically relevant aspect is the high polymorphism of the CYPs, leading to individual variations resulting in "good" and "bad" metabolizing alleles of many CYPs [351]. Especially for the before-mentioned drugs with a low number of metabolizing CYPs, an allele leading to a slow metabolism could, in combination with infection, lead to an impaired activation of clearance of those drugs [337].

In general, it became evident that although the deregulation of the drug-metabolism observed in this study is obvious and systemic, the impaired functions in human are not easily deducible from the mouse data due to non-unique relationships between murine and human CYPs. Nevertheless, the dataset readily presents clues for further investigation in an adequate system, e.g. humanized mice or artificial human chip-based microtissues [352] and draws attention to the general deregulation of physiological processes and the probable clinical implications.

5.4 DUBs as Biomarkers in Diagnosis and Progression of Sepsis

This study aimed to examine whether DUB activities of blood lymphocytes are suitable molecular markers for diagnosis or progression of sepsis in order to aid the search for urgently needed but still missing clinically utilizable markers which are able to outperform the subjective scoring systems in place at the moment [353].

DUB activity patterns were obtained for 71 % of all samples and analyzed by statistic-aided pattern evaluation. However, it was not possible to derive a clear statement about the predictive power of those patterns (subsection 4.3.2), despite the promisingly looking early results (Fig 41 & subsection 4.3.1.2).

In fact, the approach to characterize DUB activities as a biomarker was both ambitious and highly experimental, as no comparable studies were conducted so far. In general, only few studies interpreted DUB activity patterns in a comparative way [102, 103]. Ovaa and colleagues profiled USPs in virus-infected and malignant human cells, revealing activity patterns dependent on tissue origin and activation status of immune cells and high heterogeneity between patterns [102]. On this basis, Rolen and colleagues profiled 25 cervical tumor biopsies and their healthy counterparts, revealing up- or downregulation of 6 DUB activities. However, the authors did not utilize the full DUB pattern for discrimination of cancer and healthy samples and denoted that the sample number was too low to make a point regarding association of USP-activities with clinical stages of the biopsies [103]. Nevertheless, the results of both studies validate the feasibility of the approach of DUB activity-profiling used in this study.

5.4.1 Sample and Pattern Heterogeneity Hampered the Assessment of Predictive Power

Due to limited sample access, a set-up which included all blood-leukocyte samples received from the surgical ICU was chosen for this pilot study, which was organized as a case-control study.

Among them, samples from patients with septic shock and septic conditions in general were dominating while SIRS samples were considerably underrepresented, especially as two of the SIRS-classified patients developed a septic shock afterwards. For the OP control samples, which represent the second control group beside SIRS, numbers are also smaller than for the case groups (Tab 24). This imbalance poses one serious difficulty for the evaluation of this pilot study, as case-control study results are most reliable if case and control numbers are similar or if controls even outnumber cases 4 to 1 [354].

Table 24. Patient characteristics leading to high sample heterogeneity. The septic group includes all samples from patients with sepsis, severe sepsis and septic shock. *: Two of the patients, whose blood was drawn to serve as a SIRS sample developed a septic shock afterwards, reducing the number of certain SIRS samples with a pattern to 2.

	septic	SIRS	OP
# samples (f/m)	40 (19/21)	6 (1/5)	13 (7/6)
# samples w/ patterns	26	4 (2*)	12
avg. age	64.9	69.3	68.8
age span	31 - 88	57 - 85	46 - 80
avg.# of drugs administered	11.2	8.3	6.9
span of drugs	5 - 21	4 - 13	3 - 11
avg.# of antibiotics administered	2.0	0.7	0.3
span of antibiotics	0 - 4	0 - 2	0 - 2
% samples from patients w/ tumor	52.5	83.3	76.9

Apart from the sample imbalance, several other factors might have influenced the predictive power of the results (see Tab 24):

- The ratio of samples from female and male patients differed for the SIRS group (1:5) as compared to septic and control samples with an approximate 1:1 ratio. This indicates that the SIRS group is not representative regarding the gender-distribution.
- Case and control samples were not age-matched and the average ages differed noticeably among the groups. The average age in the septic group was 4.4 years

higher in the SIRS and 3.9 years higher in the OP control group, probably due to lower sample numbers in the later groups. If age had an influence on the activity patterns, it would have distorted the results for the different groups.

- The average numbers of administered drugs were higher in the septic group as compared to SIRS and OP control. This trend even held true if antibiotics were not included.
- The fraction of patients with a tumor removal was about 50 % in the septic group, but above 75 % in the other groups, hinting towards a confounding association between sepsis occurrence and the primary disease of the patients. Of the case patients without tumor, 17 displayed a primary inflammatory disease, e.g. peritonitis, which might positively correlate with the development of sepsis.

In summary, all of the above mentioned characteristics probably influenced the DUB activity patterns without being recognized, thus raising the sample heterogeneity to a level difficult to manage with the small group sizes currently available.

5.4.2 Does the Cellular Composition of the Sample Influence the Resulting Pattern?

As mentioned briefly above, previous studies of DUB activity patterns revealed distinct patterns dependent on cell or tissue types as well as cellular activation status [102,103,210]. Thus, it might be possible that the cellular composition of the patient PBMCs influenced the manifestation of the DUB activity patterns in the different samples.

Indeed, for erythrocytes, a putative contaminant of PBMCs, distinct but simple DUB activity patterns were observed (data not shown). For other cell types present in PBMCs of patients, no DUB activity patterns are available at present.

However, the compiled immune status of each patient recorded at the OVGU Magdeburg contained data for different cell populations also present in PBMCs and therefore should provide an impression of the average variation of prominent cell types.

Interestingly, the measured values were found to vary considerably, often leaving the reference ranges, thus indicating changes in all cell populations as compared to the healthy state. In contrast, the overall means as well as the individual means for the septic, SIRS and OP-groups were found to lie in close proximity to each other as well as well inside of the reference range for most of the cell types (Fig 55). The highest differences were detected for total leukocytes, which showed highly increased numbers in the septic group compared to mild increase in SIRS and OP-groups. However, even those variations were small compared to the total variations between the extreme measured values of each cell type.

Those considerable inter-patient variations mirrored by the immune status values suggest that the cellular composition of the PBMCs is highly dynamic and distinct between

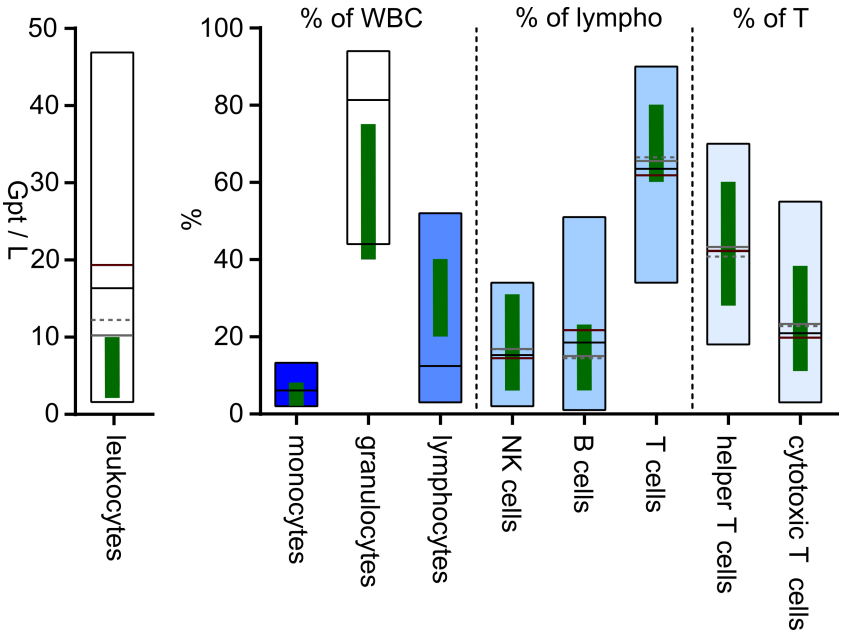

Figure 55. Variation of cell types in patient samples determined as part of the patient immune status. The floating bars contain all measured values from smallest to the largest. All cell types marked in blue are also part of the PBMCs. The green bar represents the reference range for each cell type, the black line represents the overall mean, the dark red (septic), gray (SIRS) and gray dashed lines represent the mean for each sample group, provided that they deviated visibly from each other. Gpt / L: Gigaparticle per liter, WBC: white blood cells (leukocytes).

individual patients rather than only between the patient groups. If the DUB activity patterns were distinct between different (immune) cell types as suggested previously [102, 103], this versatile composition of PBMCs would have a massive impact on the DUB activity patterns acquired.

Thus, higher numbers of control samples would have been needed to obtain average patterns typical for control or SIRS samples, which could then be compared with septic patterns.

In summary, different factors were discussed, which likely have an influence onto the inconclusive results of this pilot study. Some of them, e.g. differences in age, medication and tumor-abundance could be avoided by careful selection of case-patients and sampling of additional suitable control (SIRS and OP) samples. The role of individual cell types in the manifestation of DUB activity patterns, in contrast, could be clarified at least for healthy donors by generation of cell type specific reference patterns.

In contrast to the pattern-based evaluation discussed above, the complementary approach for the theoretical identification of active DUBs contributing to patterns by

MS-aided bioinformatics proposed a panel of candidate DUBs, UCHL3, BAP1, USP2, USP1, OTUB1 and USP47 (subsection 4.3.3), which might have predictive power and should be validated. Possible next steps, thus, will be elucidated in the outlook section of this thesis.

5.5 Probe-development

As part of this study, novel activity-based probes (ABPs) were designed and produced to close gaps in the current repertoire of DUB-specific ABPs (see introductory section 1.3) regarding the activity-based reactivity of C-terminal probes and substrate specificity of context-introducing probes.

The characterization of the novel C-terminal probe HAUb-VFEA revealed a slightly weaker reactivity as compared to the gold-standard HAUb-VME (subsection 4.4.1) but additionally uncovered a potential substrate-dependent binding of DUBs, hinting towards a distinct "activity-sensing" in HAUb-VFEA (Fig 49), which will be discussed below.

Additionally, two sets of Ubiquitin-isopeptide probes (UIPPs) were designed to examine their value in the determination of linkage specificities of DUBs as well as to detect DUBs that potentially regulate ubiquitination at the RTK c-Met. Therefore, both variants of the UIPP-concept described in the introduction (1.3.2) were utilized.

The linkage specificity screening revealed the reactivity of 10 DUBs towards UIPPs mimicking K27, K29, K33, K48 and K63 (subsection 4.4.2.1). Of the 4 designed substrate-specific UIPPs targeting c-Met Ub-sites, only the c-Met$_{K962}$-UIPP was produced and, during screening of recombinant DUBs, uncovered 3 candidate DUBs, of which 2, USP21 and CYLD, were found to be at least putative interactors of c-Met (subsection 4.1.3.2).

Nevertheless, the uses and limits of the UIPP-concept will also be illuminated in more detail.

5.5.1 Activity-based Capture of DUBs?

Generally, probes utilized for the labeling and enrichment of DUBs as described in the introduction, are referred to as activity-based probes, but the definition of this term remains ambiguous. Cravatt and colleagues outline ABPs as probes reporting on the reactivity and structure of enzyme active sites, working on the bases on catalytic activity, while Fonović and Bogyo only state that ABPs covalently modify the active sites of enzymes [86,355]. More recently, Heal and colleagues described ABPs as directly detecting the formation of a catalytically active site, and Yang and Liu described detection of enzymes by ABPs as dependent on a protein's enzymatic or binding activity under certain conditions [82, 356].

In summary, those reviews imply, that enzymes, in order to be reactive towards ABPs, need to fulfill the following requirements:

- The enzymes targeted must possess an active site, which is aligned in a manner allowing for catalytic activity.
- An active-site amino-acid which allows an attack and covalent binding of the probe needs to be present. In case of the cysteine-protease DUBs labeled in this study, the nucleophilic attack of the ABP targets the active-site cysteine.

Indeed, several publications showed that exchange of the active-site cysteine of DUBs abolished binding to HAUb-VME completely [80,97,357]. However, it was also shown that HAUb-VME and Ub-aldehyde are capable of inducing a realignment of DUB active-sites into the active conformation [267,358]. In general, the activity of DUBs is regulated by a manifold of mechanisms, e.g. by PTMs, substrate binding, conformational changes induced by own domains or binding proteins and even target binding (reviewed in [359]), but it is not clear, which of those mechanisms would influence ABP-binding.

Activity Sensing of HAUb-VFEA: The novel ABP HAUb-VFEA further characterized in this study did only weakly react with recombinant USP5 and not at all with USP7 (Fig 49). While USP7 was shown to be inactive, USP5 showed activity towards K63 poly-Ub chains and, when pre-incubated with the poly-Ub chains, showed an increased reactivity with HAUb-VFEA but not HAUb-VME.

This binding behavior of HAUb-VFEA *in vitro* points towards a substrate dependent binding mode in which the K63 poly-Ub chain probably realigns the active center of USP5 to activate the enzyme as described previously [360]. Only then is HAUb-VFEA able to bind to the now active DUB, thus representing the concept of activity-based probes more consequently then HAUb-VME, which was also found reactive towards USP5 in absence of the substrate.

A similar consideration holds true for USP7, which was in an activatable state but inactive in the assays of this study and not labeled by HAUb-VFEA *in vitro*, while *in situ* it was readily reacting with the probe as demonstrated by the HA-IP from EL-4 cell lysate (Fig 47).

In summary, HAUb-VME-binding to DUBs rather mirrors the general competence to be active, independent of the actual activity, as it is able to rearrange the enzymes' active-sites by itself as described before, while HAUb-VFEA seems to react only with DUBs, whose active-site does not require further rearrangement. However, at this point, it is not clear whether HAUb-VFEA is also able to discriminate DUB activity regulated by PTMs or additional binding proteins.

5.5.2 Uses and Limitations of the Ubiquitin-Isopeptide Probe Concept

5.5.2.1 Determination of DUB Linkage Specificity

For 10 DUBs, linkage specificities were detected utilizing the UIPPs designed and produced in this study. In general, the review of previous studies probing the linkage specificities of DUBs with ABPs and Di-Ub chains and comparison to the results of this study revealed a higher degree of consistency between the different studies utilizing ABPs than between ABP and Di-Ub based results (Tab 25).

Table 25. Linkage specificities reported for DUBs in this study as compared to previous results. The column "UIPP specificity" presents the results of this study. Results from Iphöfer et al. and McGouran et al. were obtained utilizing ABPs [95, 97]. Results from Ritorto et al. [272] and others rely on cleavage of Di-Ub, except for those marked with a p, which were also ABP-based [98, 270, 361]. ***: high reactivity, **: medium reactivity, *: low reactivity.

DUB	UIPP-specificity	McGouran et al.	Iphöfer et al.	Ritorto et al. (Di-Ub)	others
USP15	all	K27**, K29**, K33*, K48*, K63*	K48 = K63	low linkage specificity	K11, K63
USP21	all	/	/	low linkage specificity	K6, K11, K29, $K48_p$, $K63_p$
USP47	all	K27**, K29**, K33*, K48*, K63*	K48 = K63	/	
UCHL3	all	K27**, K29*, K33*, K48*, K63*	K48 > K63	low or no activity	
USP2	K27***, K29***, K33***, K48***, K63*	/	/	low linkage specificity	K6, K11, K29, $K48_p$, $K63_p$
USP25	K27*, K29**, K33*, K48*	K27*, K29**, K33*, K48*, K63*	/	low linkage specificity $K27^{-}$, $K29^{-}$	
USP28	K27*, K29***, K33***, K48***, K63*	K27*, K29**, K33*, K48*, K63*	(low) K48 > K63	low linkage specificity $K63^{high}$	
CYLD	K27*, K29**, K33*, K48*	/	/	low linkage specificity $K63^{high}$	K6, K63
UCHL5	K27*, K29***, K48*	all *	K48 > K63	low or no activity	
BAP1	(low) K27*, K29*, K48*	/	(low) K48 < K63	low or no activity	

For the DUBs with a broad specificity, e.g. USP15, USP21 and USP47, this observation might not be relevant, as they react both with ABPs and Di-Ubs. However, UCHL3 for instance seems to be only minimally reactive towards Di-Ub [272, 361], at least in *in vitro* assays, while it readily reacts with all UIPPs used in this study including the c-Met mimicking UIPP. Furthermore, UCHL3 could be retrieved from cell lysates with UIPPs as well as other Di-Ub ABPs [95, 97], which strongly hints towards activity *in vivo*.

Similar observations were also made for USP25 and USP28. While Di-Ub-based assays indicate that K27 and K29 chains are not a substrate of USP25, both this study and McGouran and colleagues suggest low reactivity against K27 and higher activity against K29-chains in unison, although the latter study used an IP approach while the results of this study are based on recombinant enzymes. USP28, in contrast, showed high reactivity against K63 and moderate activity against all chain-types tested, while the UIPP and Di-Ub ABP results suggest rather low activity against K63 chains (Tab 25).

Additionally, it became apparent that the *in vitro* assay results and former IP results generated with UIPPs were not congruent. In detail, UCHL5 and BAP1 did not react with the K63-UIPP in those assays but were identified following a UIPP-IP carried out previously [95]. This might be due to additional specificity-facilitating proteins or factors in complex cell lysates and is not be thought of as an inconsistency *per se*, especially since for both DUBs reactivity against Di-Ubs *in vitro* was also found to be very low [272].

In summary, it is not obvious whether specificity data obtained by ABPs or Di-Ub cleavage assays are more reliable for prediction of DUB-linkage specificities. Markedly, the results differ obviously and partially even contradict each other. However, while Di-Ub cleavage assays are restricted to *in vitro* assays with both recombinant substrate and enzymes, Di-Ub-mimicking ABPs allow to profile DUB-specificity both *in vitro* and in a more natural environment, i.e. cell lysate. Thus, it is likely that results obtained by ABPs, when agreeing *in vitro* and *in situ*, are the more reliable estimates of linkage specificity.

5.5.2.2 Mimics of Substrate Specific Ub-sites

In contrast to the UIPPs used to profile linkage specificity, this study also described UIPPs mimicking ubiquitinated c-Met to capture the deubiquitinating enzyme. During design and production of the set of 4 peptides, limitations of the approach regarding peptide-synthesis and warhead ligation became perceptible.

Peptide Properties: A challenge during synthesis and ligation of the warhead peptides was posed by the overall properties of the peptides. Both in solid-state peptide synthesis and the ligation of the UIPPs, high hydrophobicity is problematic [362]. While the peptide of the successfully ligated c-Met_{K962}-UIPP contained 4 highly hydrophilic amino

acids apart from the warhead-modified lysine (*) (Fig 56A) and thus possessed a good solubility in aqueous solution, the peptide warhead of the c-Met$_{K1259}$-UIPP was more hydrophobic (Fig 56B) and not easily soluble in water as determined by PepCalc [363]. Although it would be possible to add solvents like dimethyl sulfoxide (DMSO) to the peptide up to 1 % final concentration, the protocol for ligation would need to be verified or even revised regarding solvent addition beyond that. Alternatively, a different chemical approach of UIPP production could reduce the problems in peptide handling if it allows harsher conditions during ligation of warhead and peptide.

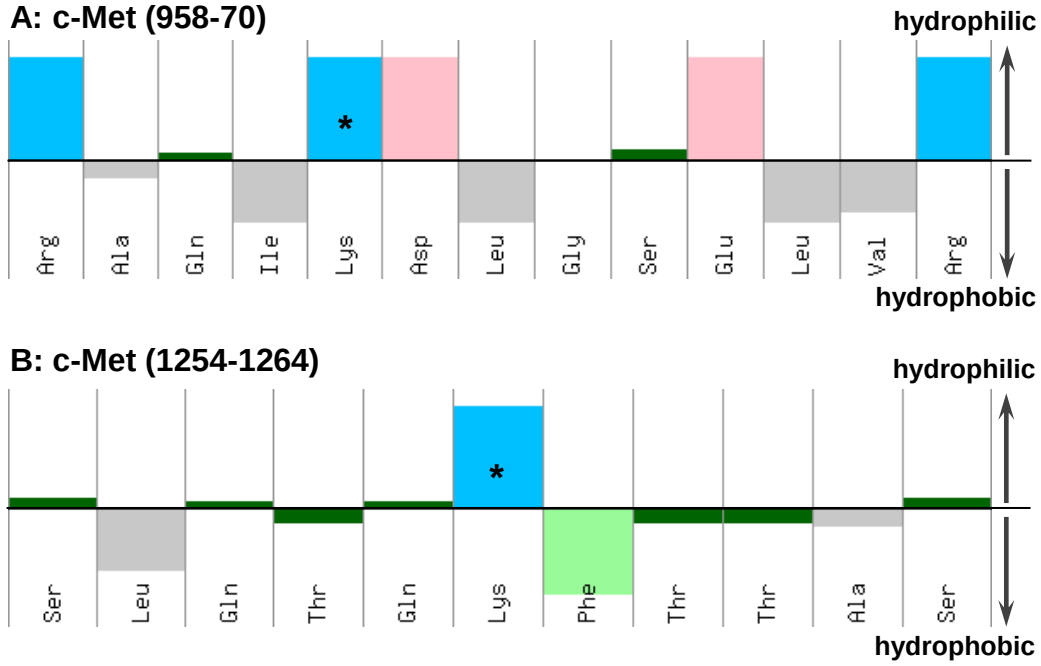

Figure 56. Amino acid properties of peptides synthesized for c-Met-UIPPs. The images were generated using PepCalc [363]. Light blue: basic, rose: acidic, gray: aliphatic, dark green: polar, light green: aromatic amino acids. For each amino acid the height and direction of the colored bar represents the impact on hydropathy. The star (*) denotes the position of the warhead, influencing the properties of the lysine.

Additional Lysines in Chosen Peptide Sequences: In general, it is possible to synthesize all conceivable peptides of substrate proteins. However, if the sequence of interest contains additional lysines apart from the ubiquitinated one, an orthogonal protecting group would be required during synthesis for protection of the lysine side-chain [95]. While this approach is generally feasible, it complicates synthesis. Thus, in this study, additional lysines were changed to alanine. This approach needs careful considerations, as amino acid exchanges can influence peptide properties and interfere with formation of secondary

structures, which likely occurs in UIPPs [95].

Despite the limitations and challenges in UIPP design and synthesis, the concept is up to now the only activity-based approach which allows the production of substrate-mimicking DUB ABPs in contrast to Di-Ub mimics [83]. Pao and colleagues recently presented an approach utilizing a recombinant E2 enzyme, which was modified to harbor a warhead-linked Ub, but this technique relies on recombinant production of the substrate protein [364]. The UIPP concept in contrast is depending on the success of the solid-phase peptide synthesis, which can be challenging, but is carried out in a well-defined artificial environment as compared to protein expression.

6 Summary

This study aimed to close gaps in the knowledge about the involvement of deubiquitinating enzymes (DUBs) and ubiquitination (Ub) in *Listeria monocytogenes*(Lm) infection. On that account, three main research questions were posed concomitant with three levels of complexity of the model systems and samples investigated to solve these questions:

1. Are ubiquitination and DUB-activities involved in InlB/c-Met-mediated cell invasion of *Listeria*? At the cellular level, the involvements of c-Met ubiquitination and DUB-activities in InlB-mediated invasion were investigated in HeLa S3 cells. In total, 6 "ubiquitination-resistant" lysine to arginine mutants of c-Met were generated, including single mutants of lysines 962, 1103, 1104 and 1259 as well as a double (K1103/04R) and a quadruple mutant. The immunoblot-based pre-characterization of those mutants revealed differential Erk1/2 and Akt phosphorylation especially for the double and quadruple mutants, hinting towards changes in down-stream signaling. In contrast to that, the cellular receptor-dynamics and localization following physiological (HGF) or pathogenic (InlB) activation were found to be wt-like for all mutants.

As first DUB-candidates responsible for direct deubiquitination of c-Met, USP8 and VCPIP1, which were previously found differentially phosphorylated after c-Met activation, were microscopically analyzed but showed no colocalization.

To identify other DUBs, which are potentially able to remove Ub from c-Met, a novel concept of substrate-specific activity-based probes, called UIPPs, was utilized. As a first step, the concept was validated by a profiling of the specificity of DUBs with 5 UIPPs resembling K27, K29, K33, K48 and K63-linked Di-Ubs. The results obtained for 10 recombinant DUBs were in accordance with results from other activity-based Di-Ub probe concepts published previously. Following, four c-Met specific UIPPs were designed and one of those, the UIPP mimicking c-Met ubiquitinated at K962, was successfully produced. A screening of recombinant DUBs for reactivity with this UIPP revealed 7 reactive DUBs, of which 3 were further analyzed microscopically.

Of those, USP21 was detected in the vicinity of a distinct portion of c-Met following receptor activation. The second candidate, CYLD, re-localized within the nuclei during c-Met activation of the cells, but did not visibly co-localize with c-Met.

As CYLD was described to be of importance in Lm infection, it seems likely that it is also involved in c-Met-mediated signaling during Lm invasion and furthermore also in the physiological pathway.

In general, the results support a model of receptor endocytosis driven by an, at least partly, Ub-independent mechanism which only utilizes ubiquitination of c-Met accessory proteins for determination of the receptor fate. This kind of mechanism, described previously for the EGF-receptor, would also be independent of direct c-Met deubiquitination, rendering a DUB-activity redundant at this point.

2. Does Lm infection deregulate Ub-mediated processes and DUB-activities *in vivo*?

This question was investigated utilizing whole livers from a murine infection model of systemic, sub-lethal listeriosis. At first, the suitability of the model system for proteomic analyses was determined and the chosen time-points were characterized.

Expression profiles for 6 cytokines (IL-1β,IL-6, IL-12, IL-18, TNFα and IFNγ) as well as the profiles of the major populations of infiltrating innate and adaptive immune cells validated the suitability of the system and furthermore defined the individual time-points regarding their immune status. Thus, the set-up represented three distinct stages of infection:

- the early stage (day 1 p.i.), characterized by rising cytokine amounts and infiltrating innate cells (macrophages, monocytes, neutrophils and NK cells),
- the peak stage (day 3 p.i.), characterized by peaking cytokine profiles as well as bacterial numbers and
- the late stage (day 9 p.i.), characterized by decreasing cytokine amounts and the infiltration of B and T cells.

Based on the characterized model system, a workflow for proteomics of liver samples was established and allowed a comparative time course analysis of liver proteome responses utilizing 12 individual mice in 3 independent replicates.

Despite of the inter-mouse variability of the samples, 3666 proteins were quantified throughout the study. Of those, 522 were determined as significantly regulated at least at one time-point, while only 15 were found to be permanently regulated. These results indicate an extensive and highly dynamic regulation of the liver proteome during Lm infection.

The proteins found regulated in this study included both, proof-of-concept data as well as novel candidates for further research, e.g. knock-out studies, to elucidate the candidates' roles in Lm infection. Thus, the dataset can be regarded as a comprehensive resource for basic research in Lm infection in terms of host reactions as well as candidate proteins for functional studies.

Most interestingly, an extensive and sustained deregulation of the cytochrome P450 (CYP) enzyme family implicated in drug metabolism was demonstrated. Of 42 detected CYPs, 25 were significantly regulated and 4 of those did not show recovery of protein

amounts even at day 9 p.i. Additionally, non-CYP phase I and phase II drug-metabolizing enzymes were also deregulated. 50 % of the phase I and 33 % of the phase II enzymes identified were also found to be heavily deregulated during Lm infection. As with the CYPs, most of those proteins were down-regulated, jointly suggesting a substantial impairment of the liver-mediated drug-metabolism in listeriosis.

Of the murine CYPs, 9 were found to possess direct human homologs which play major roles in drug activation and degradation. Thus, the results are a valuable starting point for analyses in humanized mice or other systems and furthermore underline the importance of continuous monitoring of listeriosis patients to prevent drug intoxication. While other physiological processes were both extensively identified and found regulated in this study, protein groups playing a role in regulation of ubiquitination or Ub-binding were also substantially identified, representing 15 % of all proteins, but only sparsely regulated. Of the 6.7 % of regulated proteins belonging to the aforementioned categories, 6 % were found to be Ub-binding. Of course, for Ub and UBLs as post-translational modifications, changes in protein-abundance are not mandatory prerequisites for changes in activity. Hence, the significant regulation of the two Ub-ligases RNF135 and RNF213 detected in this study might be of high importance, as they both were found to distinctly and dynamically upregulated during Lm infection.

Apart from the general proteomic analysis, DUBs were enriched and analyzed by the activity-based probe (ABP) HAUb-VME to characterize DUB-regulation during Lm infection. The immunoprecipitation approach resulted in the quantification of 52 DUBs of which two, USP2 and UCHL3, were found to be significantly downregulated. Both were not described for Lm infection so far, rendering both as promising and novel candidates for further research.
Markedly, both the Ub-ligase RNF135 and the DUB USP2 are implicated in regulation of ISG15-dependent RIG-I like receptor (RLR) immune-signaling which was found regulated during Lm infection in a pathogen-specific way. The regulation of RLR-signaling is based on ISGylation and ubiquitination, which should therefore be directly analyzed to complement the current knowledge of Ub-mediated signaling in Lm infection.

As mentioned above, DUBs were enriched utilizing the gold-standard probe HAUb-VME. At the moment, it is unaccounted for whether the ABP is only reactive towards active DUBs. To overcome this uncertainty, HAUb-VME and the novel probe HAUb-VFEA were comparatively profiled for their reactivity with DUBs in cell lysates and against recombinant enzymes. Both showed broad DUB binding, but HAUb-VFEA bound to a lower total number of DUBs in both approaches. However, *in vitro* assays utilizing the recombinant DUBs USP5 and USP7 and their natural substrate K63-poly-Ub chains revealed that HAUb-VME reacted with both DUBs irrespective of their actual cleavage-activity. In contrast, HAUb-VFEA only bound to the active DUB in presence of the substrate.

Thus, HAUb-VFEA proved to be a more selective as well as consistent in activity-sensing towards recombinant DUBs, suggesting HAUb-VFEA as a valuable profiling tool for DUB-activities.

3. Can DUB activities serve as molecular biomarkers for the diagnosis or prognosis of sepsis? The third part of this thesis tried to answer the question whether DUB-activities of blood PBMCs are potential biomarkers for the diagnosis or prognosis of sepsis.

To this end, PBMC-samples from ICU patients showing signs of either sepsis, severe sepsis or septic shock were collected and compared to patients with SIRS, surgery only and healthy control samples. First, an approach was established to portray the individual immune status of each patient by a cellular DUB-activity profiling. Additionally, evaluation routines were developed, which allowed standardized comparison of the DUB-patterns between patients and to theoretically identify the single DUB-activities in a mass spectrometry aided approach.

The immunoblot-based analysis yielded 26 patterns from septic patients (sepsis, severe sepsis or septic shock) as well as 4 from patients with SIRS, 12 from OP controls and 19 from healthy control samples. First results did show promising differences, however, the overall pattern analyses did not yield clear discrimination between any of the examined groups. In general, the patterns showed a high heterogeneity and the study evaluation was compromised by the relatively few samples available, especially for the SIRS and sepsis groups. Nevertheless, a suggestion for an alternative approach, identifying two groups of patients for analyses, is possible. The first group would contain those patients which show patterns very similar to a prototypic pattern e.g. of sepsis, that thus can be assigned to one distinct class. The second group, in contrast, would comprise those patients which could not be assigned with this method. This evaluation could at least allow classification or prediction of the sepsis state for a part of the patients sampled.

In contrast to the inconclusive results outlined above, the MS-aided theoretical DUB assignment resulted in a number of candidate DUBs, which were predicted with differing frequencies for the sample classes. Those DUBs, i.e. USP1, USP2, USP47, UCHL3, BAP1 and OTUB1, should be validated for their predictive power by utilizing a combined approach of specific antibodies and ABP-labeling to determine their activity status (see outlook).

In essence, this study contributes to the understanding of DUB-activities involved in Lm invasion and infection at different degrees of complexity. On the cellular level, two novel DUB candidates were found which might be involved in c-Met-mediated cell invasion of Lm but in any case do contribute to our understanding of physiological c-Met signaling. Furthermore, the proteome and DUB-activity results obtained from the sub-lethal murine infection model of listeriosis add novel candidate Ub-ligases and DUBs involved in the

regulation of immune signaling to the current knowledge and additionally characterize the influence of Lm infection on the host physiology, thus serving as a resource for further research. While DUB-activity patterns in general could not be established as biomarkers for sepsis diagnosis or progression in samples from ICU-patients, a theoretical approach of DUB assignment aided by mass spectrometry suggested 6 DUB-candidates, which should be further investigated and putatively provide predictive power.

7 Outlook

7.1 Listerial Deconjugase- and Ligase-activities

While in Gram-negative bacteria and other pathogens like viruses and protozoa, numerous Ub-ligase-like effectors and UBL-deconjugation enzymes are expressed [60, 289], no such enzymes are described for Gram-positive bacterial pathogens. With respect to the similar intracellular live style in close contact with the host, it seems unlikely that *Listeria* does not possess enzymes of those functions while Gram-negatives like *Salmonella* and *Legionella* do. Moreover, recent results demonstrated that Lm wields influence on distinct ubiquitin-like modifiers, e.g. SUMO [25].

Thus, it would be of high interest to examine the Lm proteome for ligase-like effectors or DUBs. While for ligase-like effectors, no screening system is described and candidates from other pathogens required laborious manual validation [365,366], screening for DUBs would be readily realizable by using ABPs.

Utilizing ABPs, it would be possible to directly screen lysates harvested from bacteria in general and under distinct conditions, e.g. nutrient deprivation or high temperatures, for DUBs. In this way, permanently active deconjugases as well as those activated in special conditions only would be assessable.

To investigate DUB-activities related to infection, screening of cellular lysates of infected cells would also be a promising approach, as exemplified by Misaghi and colleagues, who identified a *Chlamydia trachomatis* DUB active only during infection utilizing HAUb-VME [367]. For Lm, a similar approach, either using HeLa S3 cells or even primary hepatocyte spheroids is conceivable [368]. Additionally, it would also be feasible to infect those cells with fluorescently or magnetic bead-labeled Lm and then isolate bacteria from the infected cells [369, 370]. Subsequently, the isolated bacteria could then be directly profiled for active DUBs without the inference from host proteins. Furthermore, taking advantage of the modular setup of ABPs, the specificity element could be changed from ubiquitin to other UBLs, e.g. NEDD8 or SUMO, without changing the warhead. Thereby, it would be possible not only to detect DUBs but also activities of deconjugating enzymes of other UBLs under the same conditions.

Obviously, putative deconjugating activities need to be identified for further characterization. The ABP-approach would allow identification of a putative bacterial DUB by utilizing an HA-IP workflow. Next steps would include the determination of the candidates' role in Lm infection utilizing Lm knockout strains as well as the recombinant

expression of the candidates for *in vitro* assays, e.g. determination of cleavage specificities and putative substrates.

Should putative listerial deconjugating enzymes not possess a cysteine-based activity, reactivity towards ABPs would, of course, be unlikely. In that case, a feasible way to investigate deconjugating activities would be the incubation of recombinant Ub-chains with bacterial lysates to obtain first hints.

7.2 From DUB Patterns to Identified DUB Biomarkers

The heterogeneity among the available samples complicated the analysis of the predictive power of DUB-activity patterns and did not allow the clear allocation of all samples to the different classes based on clustering of their patterns. Nevertheless, the clustering did reveal samples which were similar to each other and clustered together.

To lessen the influence of sample heterogeneity on the predictive power of the patterns, an approach based on standard patterns obtained for each sample class might be suitable. Thereby, the extracted data would have to be processed class-wise, calculating the mean or summed intensities of the patterns pixel-wise, thus calculating a standard pattern which represents the average properties of a pattern. As a first step, a statistical algorithm is needed for building the standard patterns as well as to calculate the difference of an individual pattern from all standard patterns, and then assign it to the class with the smallest difference. "Summed" standard patterns which are built from the signals with the highest intensities might be suitable for the discrimination, as they show distinct differences between the classes (Fig 57). Another possibility would be the use of "median" or "mean" standard patterns. For all of these approaches, testing of the available samples utilizing the leave-one-out method [371] would allow the determination of a threshold for a good assignability to a class, minimizing both false-positives and -negatives.

The DUB-activity patterns generated in this study represent the entirety of activity-competent DUBs in each of the samples. However, identification of individual DUBs is not easily realizable by this approach without the utilization of a great number of antibodies. In contrast, mass spectrometry allows identification of enriched DUBs but relatively high amounts of protein are needed.

The MS-aided theoretical DUB-assignment (subsection 4.3.3), a combination of both approaches, resulted in a number of candidate DUBs which could be of use as diagnostic and progressive markers in sepsis.

The logical next step of those theoretical results is of course the validation utilizing samples from patients exhibiting different sepsis states. The most straight-forward approach would be immunoblotting of the candidate DUBs to confirm their presence in the respective samples. However, in this way, the activity information for the DUBs would be lost.

To preserve this information, labeling of the total DUB-activities utilizing ABPs could be carried before western blotting. In contrast to the screening approach which generated the patterns, staining with a DUB-specific antibody would reveal the activity pattern of this single DUB only. As described recently [372], the blot would show two bands at different molecular weights if a DUB becomes inactive and thus nonreactive towards the ABP. Increased concentrations of active DUB, in contrast, would result in one band with increasing signal intensity at a molecular weight corresponding to

the DUB including covalently linked ABP.

First of all, the 6 candidate DUBs identified in this thesis should be tested utilizing a combination of ABPs and DUB-specific antibodies. If those candidates do not suffice to cover all stages of sepsis conveniently, the results of the theoretical assignment indicate additional DUBs. A bioinformatics approach could be used to determine the DUBs most predictive for each stage, based on the identification rates which were determined for all DUBs. Thus, additional DUB-activities can be proposed for inclusion into the panel.

In general, the results from the validation could furthermore be combined with other

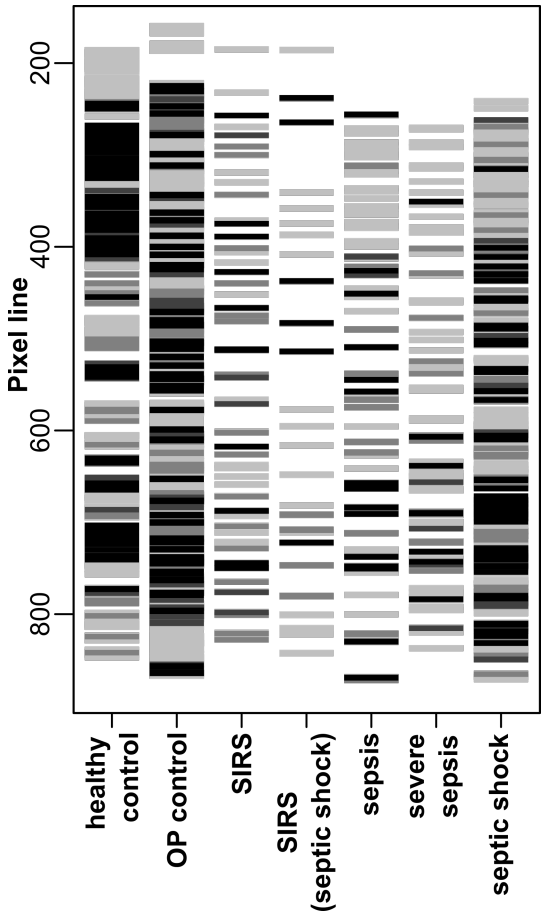

Figure 57. Schematic representation of standard "summed" patterns for all sample classes. Standard “summed” patterns were built from the class-wise sum of bands of the respective samples. Bands with an intensity higher than 3 times the median intensity of the samples are depicted in black, higher than 2x in dark gray, higher than the median in gray and all below in light gray. The merged band patterns depict a summed distribution of signal-intensities which might emerge in a pattern of each sample class. Comparison of an individual patient-pattern to those standard patterns could then allow a classification of the samples.

prospective biomarkers to yield more robust results [179].

The most promising biomarkers for the combination with DUB-activities would be those, which might complement the putative predictive powers of DUB-activities. As the experimental design used in this study is based on drawing venous blood from patients, most of the current biomarker candidates could be detected in the serum which is also extracted during gradient centrifugation without great effort.

For example, a combination of DUBs with C-reactive protein or procalcitonin could be considered for support of diagnosis, while angiopoietins, proadrenomodullin or endocans would aid the prognostic powers. If a general boost in predictive power is needed, a combination with sTREM-1 or sCD14 would also be feasible, as these molecules are accessible in serum after proteolytic cleavage, too.

7.3 ^{18}O labeling as a Method for Quantitative Determination of Ubiquitin Modifications in Patient Samples

DUBs increasingly come into the focus of attention in clinical research which led to a number of adapted approaches and workflows for systematic DUB-analyses in such samples. In contrast, analysis of ubiquitination events, which would complement the knowledge of Ub-mediated processes, is currently mainly carried out for single candidate proteins. One major constraint in realizing an unbiased screening approach for ubiquitination sites are the insufficient quantitation methods for the predominant workflow for identification of ubiquitinated peptides. By this approach, called ubiquitin-remnant enrichment, ubiquitinated peptides are enriched utilizing an antibody and subsequently analyzed by mass spectrometry to yield information about the localization of Ub-sites and their dynamics [373].

The Ub-remnant method itself is well established [374], however, it is incompatible with chemical labeling strategies like iTRAQ and tandem-mass tags (TMT), as the antibody will not recognize the iTRAQ- or TMT-modified ubiquitinated peptides (Fig 58A) [374]. Labeling after enrichment of Ub-peptides is possible in theory, but the additional label at the di-glycine residue complicates the analysis of those peptides, resulting in a low number of Ub-sites even at high sample amounts in a recent study [375].

Thus, for clinical samples, which cannot be labeled metabolically, e.g. primary cells and tissues, only label-free quantification is available at the moment. However, this technique is not very reliable for quantification based on single peptides [376] which is common in Ub-remnant datasets. To introduce robust Ub-remnant analyses for such samples, a different labeling technique has to be utilized.

One feasible concept is the utilization of C-terminal ^{18}O labeling. This labeling strategy introduces heavy oxygen into the C-terminus of peptides by utilizing trypsin in heavy water to exchange both available ^{16}O molecules and creates a mass shift of 4 Da [8, 377].

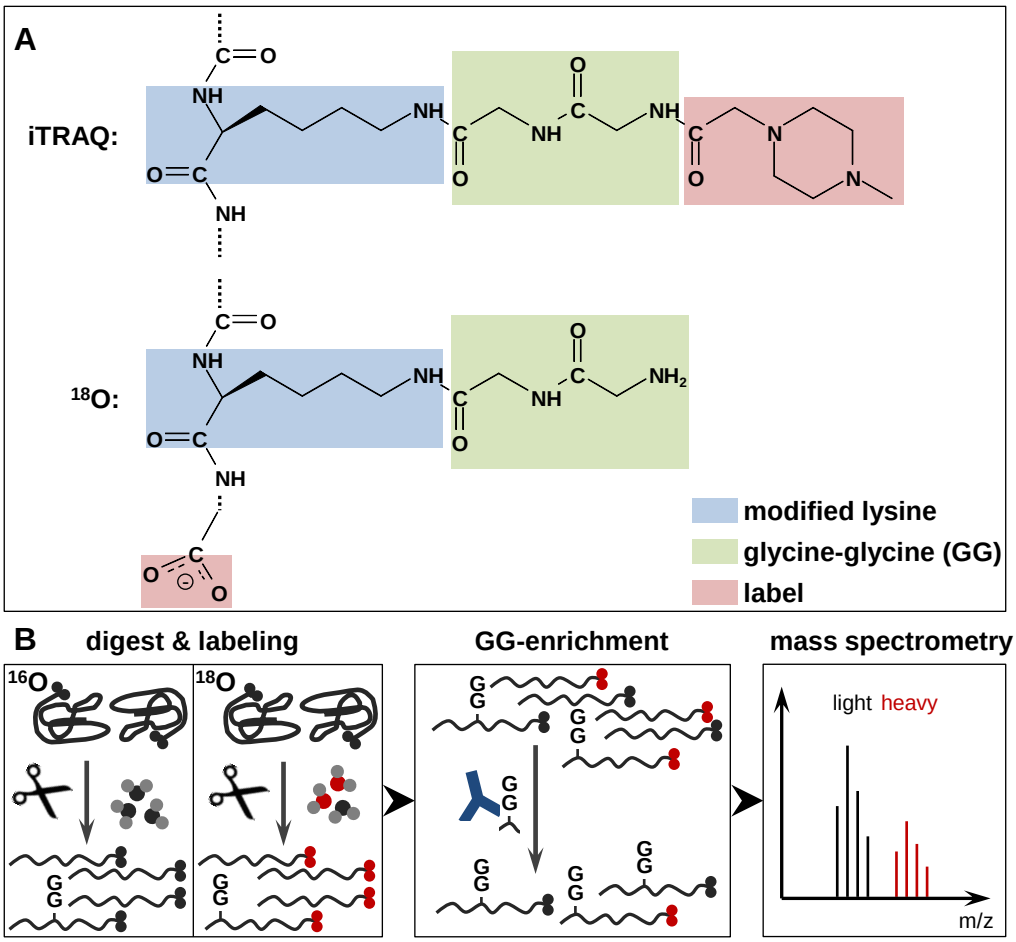

Figure 58. Advantages of 18O-labeling for the quantitative analysis of enriched ubiquitinated peptides. (A) Status of the ubiquitinated (GG-modified) lysine of a peptide following iTRAQ or ^{18}O-labeling. The modified lysine is highlighted in light blue, both glycines which remain after ubiquitination in light green. The iTRAQ or ^{18}O-labels are highlighted in red. (B) Schematic representation of a mass spectrometric workflow for ^{18}O-labeling and subsequent enrichment of ubiquitinated peptides (GG-enrichment). Oxygen 18 is presented as a red circular shape, oxygen 16 in gray, both in water molecules and in-cooperated in the C-terminus of peptides.

In contrast to iTRAQ- or TMT-labeling, the di-glycine residue of ubiquitinated peptides is not modified further by this method, presumably allowing for labeling ahead of the Ub-remnant enrichment and more convenient mass spectrometric detection (Fig 58B).

However, a disadvantage of 18O labeling is that only two conditions may be compared in one experiment. Nevertheless, as labeling with heavy water is relatively cheap as compared to all other labeling techniques [377], the approach would still be viable with a higher amount of samples and certainly for the model systems presented in this study.

For clinical samples, the most crucial limitation would be the sample amount. To isolate ubiquitinated peptides successfully, at least 1 mg of total protein is needed [378]. This would amount to approximately 1-2x10^7 PBMCs, which would be achievable for most of the patient sepsis samples received so far, but leaving little scope for additional DUB-activity analyses due to different cell lysis protocols. Doubling the amount of blood drawn to 14 ml would certainly suffice for the analysis and be acceptable even for ICU patients.

In summary, ^{18}O labeling would be particularly promising for the analyses of patient samples, as it would allow to both quantitatively analyze the proteome and the ubiquitination sites in parallel. Thus, establishing and utilizing this technique especially for clinical samples could make valuable information on changes in ubiquitination available for clinical issues.

Bibliography

[1] Vierstra, R. D. The expanding universe of ubiquitin and ubiquitin-like modifiers. *Plant Physiol.* **160**, 2–14 (2012).

[2] Hochstrasser, M. Origin and function of ubiquitin-like proteins. *Nature* **458**, 422–9 (2009).

[3] Iyer, L. M., Burroughs, A. M. & Aravind, L. The prokaryotic antecedents of the ubiquitin-signaling system and the early evolution of ubiquitin-like beta-grasp domains. *Genome Biol.* **7**, R60 (2006).

[4] Hershko, A. & Ciechanover, A. The ubiquitin system. *Annu. Rev. Biochem.* **67**, 425–79 (1998).

[5] Morales, D. J. & Lenschow, D. J. The antiviral activities of ISG15. *J. Mol. Biol.* **425**, 4995–5008 (2013).

[6] Lenkinski, R. E., Chen, D. M., Glickson, J. D. & Goldstein, G. Nuclear magnetic resonance studies of the denaturation of ubiquitin. *Biochim. Biophys. Acta - Protein Struct.* **494**, 126–130 (1977).

[7] Pickart, C. M. & Eddins, M. J. Ubiquitin: structures, functions, mechanisms. *Biochim. Biophys. Acta* **1695**, 55–72 (2004).

[8] Ye, Y. & Rape, M. Building ubiquitin chains: E2 enzymes at work. *Nat. Rev. Mol. Cell Biol.* **10**, 755–64 (2009).

[9] Braun, S. & Madhani, H. D. Shaping the landscape: mechanistic consequences of ubiquitin modification of chromatin. *EMBO Rep.* **13**, 619–30 (2012).

[10] Akutsu, M., Dikic, I. & Bremm, A. Ubiquitin chain diversity at a glance. *J. Cell Sci.* **129**, 875–880 (2016).

[11] Li, W. & Ye, Y. Polyubiquitin chains: functions, structures, and mechanisms. *Cell. Mol. Life Sci.* **65**, 2397–406 (2008).

[12] Alfano, C., Faggiano, S. & Pastore, A. The Ball and Chain of Polyubiquitin Structures. *Trends Biochem. Sci.* (2016).

[13] Grabbe, C., Husnjak, K. & Dikic, I. The spatial and temporal organization of ubiquitin networks. *Nat. Rev. Mol. Cell Biol.* **12**, 295–307 (2011).

[14] Shaid, S., Brandts, C. H., Serve, H. & Dikic, I. Ubiquitination and selective autophagy. *Cell Death Differ.* **20**, 21–30 (2012).

[15] Herhaus, L. & Dikic, I. Expanding the ubiquitin code through post-translational modification. *EMBO Rep.* **16**, 1071–83 (2015).

[16] Enchev, R. I., Schulman, B. A. & Peter, M. Protein neddylation: beyond cullin-RING ligases. *Nat. Rev. Mol. Cell Biol.* **16**, 30–44 (2014).

[17] Nie, M. & Boddy, M. Cooperativity of the SUMO and Ubiquitin Pathways in Genome Stability. *Biomolecules* **6**, 14 (2016).

[18] Xu, P. *et al.* Quantitative proteomics reveals the function of unconventional ubiquitin chains in proteasomal degradation. *Cell* **137**, 133–45 (2009).

[19] van der Veen, A. G. & Ploegh, H. L. Ubiquitin-Like Proteins. *Annu. Rev. Biochem.* **81**, 323–357 (2012).

[20] Ulrich, H. D. The fast-growing business of SUMO chains. *Mol. Cell* **32**, 301–5 (2008).

[21] Wei, W. *et al.* A stress-dependent SUMO4 sumoylation of its substrate proteins. *Biochem. Biophys. Res. Commun.* **375**, 454–459 (2008).

[22] Taherbhoy, A. M., Schulman, B. A. & Kaiser, S. E. Ubiquitin-like modifiers. *Essays Biochem.* **52**, 51–63 (2012).

[23] Eifler, K. & Vertegaal, A. C. O. Mapping the SUMOylated landscape. *FEBS J.* **282**, 3669–3680 (2015).

[24] Herrmann, J., Lerman, L. O. & Lerman, A. Ubiquitin and ubiquitin-like proteins in protein regulation. *Circ. Res.* **100**, 1276–1291 (2007).

[25] Ribet, D. *et al.* Listeria monocytogenes impairs SUMOylation for efficient infection. *Nature* **464**, 1192–1195 (2010).

[26] Oudshoorn, D., Versteeg, G. A. & Kikkert, M. Regulation of the innate immune system by ubiquitin and ubiquitin-like modifiers. *Cytokine Growth Factor Rev.* **23**, 273–282 (2012).

[27] Jones, J. *et al.* A Targeted Proteomic Analysis of the Ubiquitin-Like Modifier Nedd8 and Associated Proteins. *J. Proteome Res.* **7**, 1274–1287 (2008).

[28] Schmidt, M. H. H. & Dikic, I. Ubiquitin and NEDD8: Brothers in Arms. *Sci. STKE* **2006**, pe50 (2006).

[29] Oved, S. Conjugation to Nedd8 Instigates Ubiquitylation and Down-regulation of Activated Receptor Tyrosine Kinases. *J. Biol. Chem.* **281**, 21640–21651 (2006).

[30] Zuo, W. *et al.* c-Cbl-Mediated Neddylation Antagonizes Ubiquitination and Degradation of the TGF-β Type II Receptor. *Mol. Cell* **49**, 499–510 (2013).

[31] Bogunovic, D., Boisson-Dupuis, S. & Casanova, J.-L. ISG15: leading a double life as a secreted molecule. *Exp. Mol. Med.* **45**, e18 (2013).

[32] D'Cunha, J., Knight, E., Haas, A. L., Truitt, R. L. & Borden, E. C. Immunoregulatory properties of ISG15, an interferon-induced cytokine. *Proc. Natl. Acad. Sci. U. S. A.* **93**, 211–5 (1996).

[33] Liu, C., Chang, R., Yao, X., Qiao, W. T. & Geng, Y. Q. ISG15 expression in response to double-stranded RNA or LPS in cultured Fetal bovine lung (FBL) cells. *Vet. Res. Commun.* **33**, 723–33 (2009).

[34] Radoshevich, L. *et al.* ISG15 counteracts Listeria monocytogenes infection. *Elife* **4** (2015).

[35] Zhao, C., Collins, M. N., Hsiang, T.-Y. & Krug, R. M. Interferon-induced ISG15 pathway: an ongoing virus-host battle. *Trends Microbiol.* **21**, 181–6 (2013).

[36] Sung, H. K. H. B. *et al.* Two novel ubiquitin-fold modifier 1 (Ufm1)-specific proteases, UfSP1 and UfSP2. *J. Biol. Chem.* **282**, 5256–5262 (2007).

[37] Cai, Y. *et al.* UFBP1, a Key Component of the Ufm1 Conjugation System, Is Essential for Ufmylation-Mediated Regulation of Erythroid Development. *PLOS Genet.* **11**, e1005643 (2015).

[38] Huang, D. T. *et al.* E2-RING expansion of the NEDD8 cascade confers specificity to cullin modification. *Mol. Cell* **33**, 483–95 (2009).

[39] Wada, H., Kito, K., Caskey, L. S., Yeh, E. T. & Kamitani, T. Cleavage of the C-terminus of NEDD8 by UCH-L3. *Biochem. Biophys. Res. Commun.* **251**, 688–92 (1998).

[40] Mendoza, H. M. *et al.* NEDP1, a highly conserved cysteine protease that deNEDylates Cullins. *J. Biol. Chem.* **278**, 25637–43 (2003).

[41] Malakhov, M. P., Malakhova, O. A., Il Kim, K., Ritchie, K. J. & Zhang, D. E. UBP43 (USP18) specifically removes ISG15 from conjugated proteins. *J. Biol. Chem.* **277**, 9976–9981 (2002).

[42] Eifler, K. & Vertegaal, A. C. O. SUMOylation-Mediated Regulation of Cell Cycle Progression and Cancer. *Trends Biochem. Sci.* **40**, 779–93 (2015).

[43] Huang, C.-J., Wu, D., Khan, F. A. & Huo, L.-J. DeSUMOylation: An Important Therapeutic Target and Protein Regulatory Event. *DNA Cell Biol.* **34**, 652–60 (2015).

[44] Hipp, M. S., Kalveram, B., Raasi, S., Groettrup, M. & Schmidtke, G. FAT10, a ubiquitin-independent signal for proteasomal degradation. *Mol. Cell. Biol.* **25**, 3483–91 (2005).

[45] Komander, D. & Rape, M. The Ubiquitin Code. *Annu. Rev. Biochem.* **81**, 203–229 (2012).

[46] Heride, C., Urbé, S. & Clague, M. J. Ubiquitin code assembly and disassembly. *Curr. Biol.* **24**, R215–20 (2014).

[47] Hutchins, A. P., Liu, S., Diez, D. & Miranda-Saavedra, D. The repertoires of ubiquitinating and deubiquitinating enzymes in eukaryotic genomes. *Mol. Biol. Evol.* **30**, 1172–87 (2013).

[48] Reyes-Turcu, F. E. & Wilkinson, K. D. Polyubiquitin binding and disassembly by deubiquitinating enzymes. *Chem. Rev.* **109**, 1495–508 (2009).

[49] Liang, J. *et al.* MCP-induced protein 1 deubiquitinates TRAF proteins and negatively regulates JNK and NF-kappaB signaling. *J. Exp. Med.* **207**, 2959–73 (2010).

[50] Nijman, S. M. B. *et al.* A genomic and functional inventory of deubiquitinating enzymes. *Cell* **123**, 773–86 (2005).

[51] Coyne, E. S. & Wing, S. S. The business of deubiquitination - location, location, location. *F1000Research* **5**, 1–9 (2016).

[52] Clague, M. J. *et al.* Deubiquitylases from genes to organism. *Physiol. Rev.* **93**, 1289–315 (2013).

[53] Reyes-Turcu, F. E., Ventii, K. H. & Wilkinson, K. D. Regulation and cellular roles of ubiquitin-specific deubiquitinating enzymes. *Annu. Rev. Biochem.* **78**, 363–97 (2009).

[54] Kessler, B. M. & Edelmann, M. J. PTMs in conversation: activity and function of deubiquitinating enzymes regulated via post-translational modifications. *Cell Biochem. Biophys.* **60**, 21–38 (2011).

[55] Komander, D., Clague, M. J. & Urbé, S. Breaking the chains: structure and function of the deubiquitinases. *Nat. Rev. Mol. Cell Biol.* **10**, 550–63 (2009).

[56] Komander, D. *et al.* Molecular discrimination of structurally equivalent Lys 63-linked and linear polyubiquitin chains. *EMBO Rep.* **10**, 466–73 (2009).

[57] Hospenthal, M. K., Freund, S. M. V. & Komander, D. Assembly, analysis and architecture of atypical ubiquitin chains. *Nat. Struct. Mol. Biol.* **20**, 555–565 (2013).

[58] Wertz, I. E. *et al.* De-ubiquitination and ubiquitin ligase domains of A20 downregulate NF-kappaB signalling. *Nature* **430**, 694–9 (2004).

[59] Ndubaku, C. & Tsui, V. Inhibiting the deubiquitinating enzymes (DUBs). *J. Med. Chem.* **58**, 1581–1595 (2015).

[60] Nanduri, B., Suvarnapunya, A. E., Venkatesan, M. & Edelmann, M. J. Deubiquitinating enzymes as promising drug targets for infectious diseases. *Curr. Pharm. Des.* **19**, 3234–47 (2013).

[61] Trompouki, E. *et al.* CYLD is a deubiquitinating enzyme that negatively regulates NF-κB activation by TNFR family members. *Nature* **424**, 793–796 (2003).

[62] Yoshida, H., Jono, H., Kai, H. & Li, J.-D. The tumor suppressor cylindromatosis (CYLD) acts as a negative regulator for toll-like receptor 2 signaling via negative cross-talk with TRAF6 AND TRAF7. *J. Biol. Chem.* **280**, 41111–21 (2005).

[63] Ahmed, N. *et al.* The E3 ligase Itch and deubiquitinase Cyld act together to regulate Tak1 and inflammation. *Nat. Immunol.* **12**, 1176–83 (2011).

[64] Wertz, I. E. It takes two to tango: a new couple in the family of ubiquitin-editing complexes. *Nat. Immunol.* **12**, 1133–1135 (2011).

[65] Tsagaratou, A., Kontoyiannis, D. L. & Mosialos, G. Truncation of the deubiquitinating domain of CYLD in myelomonocytic cells attenuates inflammatory responses. *PLoS One* **6**, e16397 (2011).

[66] Gopala, N. *et al.* CYLD Enhances Severe Listeriosis by Impairing IL-6/STAT3-Dependent Fibrin Production. *PLoS Pathog.* **9**, e1003455 (2013).

[67] Shembade, N., Ma, A. & Harhaj, E. W. Inhibition of NF-kappaB signaling by A20 through disruption of ubiquitin enzyme complexes. *Science* **327**, 1135–9 (2010).

[68] Catrysse, L., Vereecke, L., Beyaert, R. & van Loo, G. A20 in inflammation and autoimmunity. *Trends Immunol.* **35**, 22–31 (2014).

[69] Xuan, N. T. *et al.* A20 expression in dendritic cells protects mice from LPS-induced mortality. *Eur. J. Immunol.* **45**, 818–828 (2015).

[70] Zou, W. *et al.* Microarray analysis reveals that Type I interferon strongly increases the expression of immune-response related genes in Ubp43 (Usp18) deficient macrophages. *Biochem. Biophys. Res. Commun.* **356**, 193–9 (2007).

[71] Lim, J. H., Ha, U.-H., Woo, C.-H., Xu, H. & Li, J.-D. CYLD is a crucial negative regulator of innate immune response in Escherichia coli pneumonia. *Cell. Microbiol.* **10**, 2247–56 (2008).

[72] Lim, J. H. *et al.* Tumor suppressor CYLD acts as a negative regulator for non-typeable Haemophilus influenza-induced inflammation in the middle ear and lung of mice. *PLoS One* **2**, e1032 (2007).

[73] Lim, J. H. *et al.* Tumor suppressor CYLD regulates acute lung injury in lethal Streptococcus pneumoniae infections. *Immunity* **27**, 349–60 (2007).

[74] Wex, K. *et al.* Receptor-Interacting Protein Kinase-2 Inhibition by CYLD Impairs Antibacterial Immune Responses in Macrophages. *Front. Immunol.* **6**, 650 (2015).

[75] Wurm, R. *et al.* Protective dendritic cell responses against listeriosis induced by the short form of the deubiquitinating enzyme CYLD are inhibited by full-length CYLD. *Eur. J. Immunol.* **45**, 1366–76 (2015).

[76] Coombs, N. *et al.* Helicobacter pylori affects the cellular deubiquitinase USP7 and ubiquitin-regulated components TRAF6 and the tumour suppressor p53. *Int. J. Med. Microbiol.* **301**, 213–24 (2011).

[77] Bomberger, J. M. *et al.* A Pseudomonas aeruginosa toxin that hijacks the host ubiquitin proteolytic system. *PLoS Pathog.* **7**, e1001325 (2011).

[78] Akimana, C., Al-Khodor, S. & Abu Kwaik, Y. Host factors required for modulation of phagosome biogenesis and proliferation of Francisella tularensis within the cytosol. *PLoS One* **5**, e11025 (2010).

[79] Edelmann, M. J., Kramer, H. B., Altun, M. & Kessler, B. M. Post-translational modification of the deubiquitinating enzyme otubain 1 modulates active RhoA levels and susceptibility to Yersinia invasion. *FEBS J.* **277**, 2515–2530 (2010).

[80] Bassères, E. *et al.* The ubiquitin C-terminal hydrolase UCH-L1 promotes bacterial invasion by altering the dynamics of the actin cytoskeleton. *Cell. Microbiol.* **12**, 1622–33 (2010).

[81] Jeffery, D. A. & Bogyo, M. Chemical proteomics and its application to drug discovery. *Curr. Opin. Biotechnol.* **14**, 87–95 (2003).

[82] Yang, P. & Liu, K. Activity-based protein profiling: Recent advances in probe development and applications. *ChemBioChem* **16**, 712–724 (2015).

[83] Ekkebus, R., Flierman, D., Geurink, P. P. & Ovaa, H. Catching a DUB in the act: novel ubiquitin-based active site directed probes. *Curr. Opin. Chem. Biol.* **23**, 63–70 (2014).

[84] Loch, C. M., Cuccherini, C. L., Leach, C. A. & Strickler, J. E. Deubiquitylase, deSUMOylase, and deISGylase activity microarrays for assay of substrate preference and functional modifiers. *Mol. Cell. Proteomics* **10**, M110.002402 (2011).

[85] Artavanis-Tsakonas, K. *et al.* Identification by functional proteomics of a deubiquitinating/deNeddylating enzyme in Plasmodium falciparum. *Mol. Microbiol.* **61**, 1187–95 (2006).

[86] Cravatt, B. F., Wright, A. T. & Kozarich, J. W. Activity-based protein profiling: from enzyme chemistry to proteomic chemistry. *Annu. Rev. Biochem.* **77**, 383–414 (2008).

[87] Borodovsky, A. *et al.* A novel active site-directed probe specific for deubiquitylating enzymes reveals proteasome association of USP14. *EMBO J.* **20**, 5187–96 (2001).

[88] Borodovsky, A. *et al.* Chemistry-based functional proteomics reveals novel members of the deubiquitinating enzyme family. *Chem. Biol.* **9**, 1149–59 (2002).

[89] Hemelaar, J. *et al.* Chemistry-based functional proteomics: mechanism-based activity-profiling tools for ubiquitin and ubiquitin-like specific proteases. *J. Proteome Res.* **3**, 268–76 (2004).

[90] Love, K. R. *et al.* Ubiquitin C-Terminal Electrophiles Are Activity-Based Probes for Identification and Mechanistic Study of Ubiquitin Conjugating Machinery. *ACS Chem. Biol.* **4**, 275–287 (2009).

[91] Ekkebus, R. *et al.* On terminal alkynes that can react with active-site cysteine nucleophiles in proteases. *J. Am. Chem. Soc.* **135**, 2867–70 (2013).

[92] Sommer, S., Weikart, N. D., Linne, U. & Mootz, H. D. Covalent inhibition of SUMO and ubiquitin-specific cysteine proteases by an in situ thiol-alkyne addition. *Bioorg. Med. Chem.* **21**, 2511–7 (2013).

[93] McGouran, J. F. *et al.* Fluorescence-based active site probes for profiling deubiquitinating enzymes. *Org. Biomol. Chem.* **10**, 3379–83 (2012).

[94] Claessen, J. H. L. *et al.* Catch-and-release probes applied to semi-intact cells reveal ubiquitin-specific protease expression in Chlamydia trachomatis infection. *Chembiochem* **14**, 343–52 (2013).

[95] Iphöfer, A. *et al.* Profiling ubiquitin linkage specificities of deubiquitinating enzymes with branched ubiquitin isopeptide probes. *Chembiochem* **13**, 1416–20 (2012).

[96] Iphöfer, A. *Novel activity-based probes for functional analysis of deubiquitinating enzymes.* Ph.D. thesis, TU Braunschweig (2012).

[97] McGouran, J. F., Gaertner, S. R., Altun, M., Kramer, H. B. & Kessler, B. M. Deubiquitinating Enzyme Specificity for Ubiquitin Chain Topology Profiled by Di-Ubiquitin Activity Probes. *Chem. Biol.* **20**, 1447–55 (2013).

[98] Li, G., Liang, Q., Gong, P., Tencer, A. H. & Zhuang, Z. Activity-based diubiquitin probes for elucidating the linkage specificity of deubiquitinating enzymes. *Chem. Commun. (Camb).* **50**, 216–8 (2014). arXiv:NIHMS150003.

[99] Haj-Yahya, N. *et al.* Dehydroalanine-based diubiquitin activity probes. *Org. Lett.* **16**, 540–543 (2014).

[100] Mulder, M. P. C., El Oualid, F., Ter Beek, J. & Ovaa, H. A native chemical ligation handle that enables the synthesis of advanced activity-based probes: Diubiquitin as a case study. *ChemBioChem* **15**, 946–949 (2014).

[101] Flierman, D. *et al.* Non-hydrolyzable Diubiquitin Probes Reveal Linkage-Specific Reactivity of Deubiquitylating Enzymes Mediated by S2 Pockets. *Cell Chem. Biol.* 1–11 (2016).

[102] Ovaa, H. *et al.* Activity-based ubiquitin-specific protease (USP) profiling of virus-infected and malignant human cells. *Proc. Natl. Acad. Sci. U. S. A.* **101**, 2253 (2004).

[103] Rolén, U. *et al.* Activity profiling of deubiquitinating enzymes in cervical carcinoma biopsies and cell lines. *Mol. Carcinog.* **45**, 260–269 (2006).

[104] Altun, M. *et al.* Activity-based chemical proteomics accelerates inhibitor development for deubiquitylating enzymes. *Chem. Biol.* **18**, 1401–12 (2011).

[105] de Jong, A. *et al.* Ubiquitin-Based Probes Prepared by Total Synthesis To Profile the Activity of Deubiquitinating Enzymes. *ChemBioChem* **13**, 2251–2258 (2012).

[106] Gredmark, S., Schlieker, C., Quesada, V., Spooner, E. & Ploegh, H. L. A functional ubiquitin-specific protease embedded in the large tegument protein (ORF64) of murine gammaherpesvirus 68 is active during the course of infection. *J. Virol.* **81**, 10300–9 (2007).

[107] Hamon, M., Bierne, H. & Cossart, P. Listeria monocytogenes: a multifaceted model. *Nat. Rev. Microbiol.* **4**, 423–34 (2006).

[108] Pillich, H., Chakraborty, T. & Mraheil, M. A. Cell-autonomous responses in Listeria monocytogenes infection. *Future Microbiol.* **10**, 583–597 (2015).

[109] Hernandez-Milian, A. & Payeras-Cifre, A. What is new in listeriosis? *Biomed Res. Int.* **2014**, 358051 (2014).

[110] RKI. Infektionsepidemiologisches Jahrbuch meldepflichtiger Krankheiten für 2014 **36**, 142–143 (2015).

[111] Pizarro-Cerdá, J., Kühbacher, A., Cossart, P. & Kuhbacher, A. Entry of listeria monocytogenes in mammalian epithelial cells: An updated view. *Cold Spring Harb. Perspect. Med.* **2**, 1–18 (2012).

[112] Disson, O. & Lecuit, M. In vitro and in vivo models to study human listeriosis: mind the gap. *Microbes Infect.* **15**, 971–80 (2013).

[113] Jung, C. *et al.* Involvement of CD44v6 in InlB-dependent Listeria invasion. *Mol. Microbiol.* **72**, 1196–207 (2009).

[114] Braun, L., Ghebrehiwet, B. & Cossart, P. gC1q-R/p32, a C1q-binding protein, is a receptor for the InlB invasion protein of Listeria monocytogenes. *EMBO J.* **19**, 1458–1466 (2000).

[115] Jonquieres, R., Pizarro-Cerda, J. & Cossart, P. Synergy between the N- and C-terminal domains of InlB for efficient invasion of non-phagocytic cells by Listeria monocytogenes. *Mol. Microbiol.* **42**, 955–965 (2001).

[116] Dortet, L., Veiga, E., Bonazzi, M. & Cossart, P. CD44-independent activation of the Met signaling pathway by HGF and InlB. *Microbes Infect.* **12**, 919–927 (2010).

[117] Martins, M. *et al.* Listeria monocytogenes triggers the cell surface expression of Gp96 protein and interacts with its N terminus to support cellular infection. *J. Biol. Chem.* **287**, 43083–93 (2012).

[118] Travier, L. & Lecuit, M. Listeria monocytogenes ActA: A new function for a 'classic' virulence factor. *Curr. Opin. Microbiol.* **17**, 53–60 (2014).

[119] Yoshikawa, Y. *et al.* Listeria monocytogenes ActA-mediated escape from autophagic recognition. *Nat. Cell Biol.* **11**, 1233–1240 (2009).

[120] Cossart, P. Illuminating the landscape of host - pathogen interactions with the bacterium Listeria monocytogenes. *PNAS* **108**, 19484–19491 (2011).

[121] Niemann, H. H. Structural insights into Met receptor activation. *Eur. J. Cell Biol.* **90**, 972–981 (2011).

[122] Stamos, J., Lazarus, R. A., Yao, X., Kirchhofer, D. & Wiesmann, C. Crystal structure of the HGF beta-chain in complex with the Sema domain of the Met receptor. *EMBO J.* **23**, 2325–35 (2004).

[123] Niemann, H. H. *et al.* Structure of the human receptor tyrosine kinase Met in complex with the Listeria invasion protein InlB. *Cell* **130**, 235–46 (2007).

[124] Li, N., Xiang, G. S., Dokainish, H., Ireton, K. & Elferink, L. A. The Listeria protein internalin B mimics hepatocyte growth factor-induced receptor trafficking. *Traffic* **6**, 459–473 (2005).

[125] Reinl, T. *et al.* Quantitative phosphokinome analysis of the Met pathway activated by the invasin internalin B from Listeria monocytogenes. *Mol. Cell. Proteomics* **8**, 2778–95 (2009).

[126] Trusolino, L., Bertotti, A. & Comoglio, P. M. MET signalling: principles and functions in development, organ regeneration and cancer. *Nat. Rev. Mol. Cell Biol.* **11**, 834–848 (2010).

[127] Boccaccio, C. *et al.* Induction of epithelial tubules by growth factor HGF depends on the STAT pathway. *Nature* **391**, 285–8 (1998).

[128] Mungunsukh, O. *et al.* A tandem repeat of a fragment of Listeria monocytogenes internalin B protein induces cell survival and proliferation. *Am. J. Physiol. Lung Cell. Mol. Physiol.* **299**, L905–14 (2010).

[129] Gessain, G. *et al.* PI3-kinase activation is critical for host barrier permissiveness to Listeria monocytogenes. *J. Exp. Med.* **212**, 165–83 (2015).

[130] Gouin, E. *et al.* The Listeria monocytogenes InlC protein interferes with innate immune responses by targeting the I{kappa}B kinase subunit IKK{alpha}. *Proc. Natl. Acad. Sci. U. S. A.* **107**, 17333–8 (2010).

[131] Singleton, P. A. *et al.* CD44 regulates hepatocyte growth factor-mediated vascular integrity. Role of c-Met, Tiam1/Rac1, dynamin 2, and cortactin. *J. Biol. Chem.* **282**, 30643–57 (2007).

[132] Barrow-McGee, R. & Kermorgant, S. Met endosomal signalling: In the right place, at the right time. *Int. J. Biochem. Cell Biol.* **49**, 69–74 (2014).

[133] Haglund, K. *et al.* Multiple monoubiquitination of RTKs is sufficient for their endocytosis and degradation. *Nat. Cell Biol.* **5**, 461–466 (2003).

[134] Carter, S., Urbé, S. & Clague, M. J. The met receptor degradation pathway: requirement for Lys48-linked polyubiquitin independent of proteasome activity. *J. Biol. Chem.* **279**, 52835–9 (2004).

[135] Veiga, E. & Cossart, P. Listeria hijacks the clathrin-dependent endocytic machinery to invade mammalian cells. *Nat. Cell Biol.* **7**, 894–900 (2005).

[136] Haglund, K. & Dikic, I. The role of ubiquitylation in receptor endocytosis and endosomal sorting. *J. Cell Sci.* **125**, 265–75 (2012).

[137] Buus, R., Faronato, M., Hammond, D. E., Urbé, S. & Clague, M. J. Deubiquitinase Activities Required for Hepatocyte Growth Factor-Induced Scattering of Epithelial Cells. *Curr. Biol.* **19**, 1463–1466 (2009).

[138] Joffre, C. *et al.* A direct role for Met endocytosis in tumorigenesis. *Nat. Cell Biol.* **13**, 827–37 (2011).

[139] Muller, P. A. J. *et al.* Mutant p53 enhances MET trafficking and signalling to drive cell scattering and invasion. *Oncogene* **32**, 1252–65 (2013).

[140] Parachoniak, C. A., Luo, Y., Abella, J. V., Keen, J. H. & Park, M. GGA3 Functions as a Switch to Promote Met Receptor Recycling, Essential for Sustained ERK and Cell Migration. *Dev. Cell* **20**, 751–763 (2011).

[141] Shen, Y., Naujokas, M., Park, M. & Ireton, K. InIB-dependent internalization of Listeria is mediated by the Met receptor tyrosine kinase. *Cell* **103**, 501–10 (2000).

[142] Reinl, T. *Phosphoproteom-Analysen humaner Kinasen : Charakterisierung des c-Met-Signalweges nach Aktivierung durch InlB von Listeria monocytogenes.* Ph.D. thesis, Helmholtz Center for Infection Research (2008).

[143] Banerjee, M. *et al.* GW domains of the Listeria monocytogenes invasion protein InlB are required for potentiation of Met activation. *Mol. Microbiol.* **52**, 257–71 (2004).

[144] Doran, K. S., Banerjee, A., Disson, O. & Lecuit, M. Concepts and mechanisms: Crossing host barriers. *Cold Spring Harb. Perspect. Med.* **3** (2013).

[145] Jacquet, C. *et al.* A molecular marker for evaluating the pathogenic potential of foodborne Listeria monocytogenes. *J. Infect. Dis.* **189**, 2094–100 (2004).

[146] Waite, J. C. *et al.* Dynamic imaging of the effector immune response to listeria infection in vivo. *PLoS Pathog.* **7**, e1001326 (2011).

[147] Williams, M. A., Schmidt, R. L. & Lenz, L. L. Early events regulating immunity and pathogenesis during Listeria monocytogenes infection. *Trends Immunol.* **33**, 488–95 (2012).

[148] Stavru, F., Archambaud, C. & Cossart, P. Cell biology and immunology of Listeria monocytogenes infections: novel insights. *Immunol. Rev.* **240**, 160–184 (2011).

[149] Disson, O. *et al.* Conjugated action of two species-specific invasion proteins for fetoplacental listeriosis. *Nature* **455**, 1114–1118 (2008).

[150] Gründler, T. *et al.* The surface proteins InlA and InlB are interdependently required for polar basolateral invasion by Listeria monocytogenes in a human model of the blood-cerebrospinal fluid barrier. *Microbes Infect.* **15**, 291–301 (2013).

[151] Cossart, P. & Toledo-Arana, A. Listeria monocytogenes, a unique model in infection biology: an overview. *Microbes Infect. Inst. Pasteur* **10**, 1041–1050 (2008).

[152] Cousens, L. P. & Wing, E. J. Innate defenses in the liver during Listeria infection. *Immunol. Rev.* **174**, 150–159 (2000).

[153] Blériot, C. *et al.* Liver-resident macrophage necroptosis orchestrates type 1 microbicidal inflammation and type-2-mediated tissue repair during bacterial infection. *Immunity* **42**, 145–58 (2015).

[154] Indramohan, M., Sieve, A. N., Break, T. J. & Berg, R. E. Inflammatory monocyte recruitment is regulated by interleukin-23 during systemic bacterial infection. *Infect. Immun.* **80**, 4099–4105 (2012).

[155] Carr, K. D. *et al.* Specific depletion reveals a novel role for neutrophil-mediated protection in the liver during Listeria monocytogenes infection. *Eur. J. Immunol.* **41**, 2666–2676 (2011). arXiv:NIHMS150003.

[156] Schmidt, R. L., Filak, H. C., Lemon, J. D., Potter, T. A. & Lenz, L. L. A LysM and SH3-domain containing region of the Listeria monocytogenes p60 protein stimulates accessory cells to promote activation of host NK cells. *PLoS Pathog.* **7**, e1002368 (2011).

[157] Viegas, N. *et al.* IFN-γ production by CD27+ NK cells exacerbates Listeria monocytogenes infection in mice by inhibiting granulocyte mobilization. *Eur. J. Immunol.* **43**, 2626–2637 (2013).

[158] Bode, J. G., Albrecht, U., Häussinger, D., Heinrich, P. C. & Schaper, F. Hepatic acute phase proteins - Regulation by IL-6- and IL-1-type cytokines involving STAT3 and its crosstalk with NF-κB-dependent signaling. *Eur. J. Cell Biol.* **91**, 496–505 (2012).

[159] Ebe, Y. *et al.* The role of Kupffer cells and regulation of neutrophil migration into the liver by macrophage inflammatory protein-2 in primary listeriosis in mice. *Pathol. Int.* **49**, 519–532 (1999).

[160] Shi, C. *et al.* Monocyte trafficking to hepatic sites of bacterial infection is chemokine independent and directed by focal intercellular adhesion molecule-1 expression. *J. Immunol.* **184**, 6266–74 (2010).

[161] Tam, M. A. & Wick, M. J. Dendritic cells and immunity to Listeria: TipDCs are a new recruit. *Trends Immunol.* **25**, 335–339 (2004).

[162] Zenewicz, L. A. & Shen, H. Innate and adaptive immune responses to Listeria monocytogenes: a short overview. *Microbes Infect.* **9**, 1208–15 (2007). arXiv:NIHMS150003.

[163] Busch, D. H., Pilip, I. M., Vijh, S. & Pamer, E. G. Coordinate regulation of complex T cell populations responding to bacterial infection. *Immunity* **8**, 353–62 (1998).

[164] Preußel, K. *et al.* Risk Factors for Sporadic Non-Pregnancy Associated Listeriosis in Germany - Immunocompromised Patients and Frequently Consumed Ready-To-Eat Products. *PLoS One* **10**, e0142986 (2015).

[165] Engel, C. *et al.* Epidemiology of sepsis in Germany: results from a national prospective multicenter study. *Intensive Care Med.* **33**, 606–618 (2007).

[166] Charchaflieh, J., Rushbrook, J., Worah, S. & Zhang, M. Activated Complement Factors as Disease Markers for Sepsis. *Dis. Markers* **2015** (2015).

[167] Seymour, C. W. *et al.* Assessment of Clinical Criteria for Sepsis. *JAMA* **315**, 762 (2016).

[168] Bone, R. C. Definitions for sepsis and organ failure and guidelines for the use of innovative therapies in sepsis. The ACCP/SCCM Consensus Conference Committee. American College of Chest Physicians/Society of Critical Care Medicine. *CHEST J.* **101**, 1644 (1992).

[169] Levy, M. M. *et al.* 2001 SCCM/ESICM/ACCP/ATS/SIS International Sepsis Definitions Conference. *Crit Care Med.* **31**, 1250–1256 (2003).

[170] Martin, G. S. Sepsis, severe sepsis and septic shock: changes in incidence, pathogens and outcomes. *Expert Rev. Anti. Infect. Ther.* **10**, 701–706 (2012).

[171] Su, L. *et al.* Identification of novel biomarkers for sepsis prognosis via urinary proteomic analysis using iTRAQ labeling and 2D-LC-MS/MS. *PLoS One* **8**, e54237 (2013).

[172] Liu, J., Li, J. & Deng, X. Proteomic analysis of differential protein expression in platelets of septic patients. *Mol. Biol. Rep.* **41**, 3179–3185 (2014).

[173] Czura, C. "Merinoff symposium 2010: sepsis"-speaking with one voice. Tech. Rep. 1-2 (2011).

[174] Vincent, J. L., Opal, S. M., Marshall, J. C. & Tracey, K. J. Sepsis definitions: Time for change. *Lancet* **381**, 774–775 (2013).

[175] Jawad, I., Lukšić, I. & Rafnsson, S. B. Assessing available information on the burden of sepsis: global estimates of incidence, prevalence and mortality. *J. Glob. Health* **2**, 010404 (2012).

[176] Deutschman, C. S. & Tracey, K. J. Sepsis: Current dogma and new perspectives. *Immunity* **40**, 463–475 (2014).

[177] Stevenson, E. K., Rubenstein, A. R., Radin, G. T., Wiener, R. S. & Walkey, A. J. Two decades of mortality trends among patients with severe sepsis: a comparative meta-analysis*. *Crit. Care Med.* **42**, 625–31 (2014).

[178] Skibsted, S., Bhasin, M. K., Aird, W. C. & Shapiro, N. I. Bench-to-bedside review: Future novel diagnostics for sepsis - a systems biology approach. *Crit. Care* **17**, 231 (2013).

[179] Biron, B. M., Ayala, A. & Lomas-Neira, J. L. Biomarkers for sepsis: What is and what might be? *Biomark. Insights* **10**, 7–17 (2015).

[180] Dunne, W. M. Laboratory Diagnosis of Sepsis? No SIRS , Not Just Yet. *J Clin Microbiol* **53**, 2404–2409 (2015).

[181] KNAUS, W. A., DRAPER, E. A., WAGNER, D. P. & ZIMMERMAN, J. E. APACHE II. *Crit. Care Med.* **13**, 818–829 (1985).

[182] Le Gall, J.-R. A New Simplified Acute Physiology Score (SAPS II) Based on a European/North American Multicenter Study. *JAMA J. Am. Med. Assoc.* **270**, 2957 (1993).

[183] Vincent, J. L. *et al.* The SOFA (Sepsis-related Organ Failure Assessment) score to describe organ dysfunction/failure. On behalf of the Working Group on Sepsis-Related Problems of the European Society of Intensive Care Medicine. *Intensive Care Med.* **22**, 707–10 (1996).

[184] Strand, K. & Flaatten, H. Severity scoring in the ICU: A review. *Acta Anaesthesiol. Scand.* **52**, 467–478 (2008).

[185] Agrawal, A., Singh, P. P., Bottazzi, B., Garlanda, C. & Mantovani, A. Pattern recognition by pentraxins. *Adv. Exp. Med. Biol.* **653**, 98–116 (2009).

[186] Jaye, D. L. & Waites, K. B. Clinical applications of C-reactive protein in pediatrics. *Pediatr. Infect. Dis. J.* **16**, 735–46; quiz 746–7 (1997).

[187] Henriquez-Camacho, C. & Losa, J. Biomarkers for sepsis. *Biomed Res. Int.* **2014**, 547818 (2014).

[188] ten Oever, J., Netea, M. G. & Kullberg, B. J. Utility of immune response-derived biomarkers in the differential diagnosis of inflammatory disorders. *J. Infect.* (2015).

[189] Wacker, C., Prkno, A., Brunkhorst, F. M. & Schlattmann, P. Procalcitonin as a diagnostic marker for sepsis: a systematic review and meta-analysis. *Lancet Infect. Dis.* **13**, 426–435 (2013).

[190] Agarwal, R. & Schwartz, D. N. Procalcitonin to guide duration of antimicrobial therapy in intensive care units: a systematic review. *Clin. Infect. Dis.* **53**, 379–87 (2011).

[191] Ricciuto, D. R. *et al.* Angiopoietin-1 and angiopoietin-2 as clinically informative prognostic biomarkers of morbidity and mortality in severe sepsis. *Crit. Care Med.* **39**, 702–710 (2011).

[192] Mussap, M., Cibecchini, F., Noto, A. & Fanos, V. In search of biomarkers for diagnosing and managing neonatal sepsis: the role of angiopoietins. *J. Matern. Fetal. Neonatal Med.* **26 Suppl 2**, 24–6 (2013).

[193] Suberviola, B. *et al.* Prognostic value of proadrenomedullin in severe sepsis and septic shock patients with community-acquired pneumonia. *Swiss Med. Wkly.* (2012).

[194] Kali, A. & Shetty, K. Endocan: A novel circulating proteoglycan. *Indian J. Pharmacol.* **46**, 579 (2014).

[195] Endo, S. *et al.* Usefulness of presepsin in the diagnosis of sepsis in a multicenter prospective study. *J. Infect. Chemother.* **18**, 891–7 (2012).

[196] Kweon, O. J., Choi, J.-H., Park, S. K. & Park, A. J. Usefulness of presepsin (sCD14 subtype) measurements as a new marker for the diagnosis and prediction of disease severity of sepsis in the Korean population. *J. Crit. Care* **29**, 965–70 (2014).

[197] Shubin, N. J., Monaghan, S. F., Heffernan, D. S., Chung, C.-S. & Ayala, A. B and T lymphocyte attenuator expression on CD4+ T-cells associates with sepsis and subsequent infections in ICU patients. *Crit. Care* **17**, R276 (2013).

[198] Chang, K. C. *et al.* Blockade of the negative co-stimulatory molecules PD-1 and CTLA-4 improves survival in primary and secondary fungal sepsis. *Crit. Care* **17**, R85 (2013).

[199] Liu, X., Ren, H. & Peng, D. Sepsis biomarkers: An omics perspective. *Front. Med. China* **8**, 58–67 (2014).

[200] Bomsztyk, K. *et al.* Experimental acute lung injury induces multi-organ epigenetic modifications in key angiogenic genes implicated in sepsis-associated endothelial dysfunction. *Crit. Care* **19**, 225 (2015).

[201] Dhas, D. B. B., Ashmi, A. H., Bhat, B. V., Kalaivani, S. & Parija, S. C. Comparison of genomic DNA methylation pattern among septic and non-septic newborns - An epigenome wide association study. *Genomics data* **3**, 36–40 (2015).

[202] Cao, Z. & Robinson, R. A. S. The role of proteomics in understanding biological mechanisms of sepsis. *Proteomics - Clin. Appl.* **8**, 35–52 (2014).

[203] Kalenka, A. *et al.* Changes in the serum proteome of patients with sepsis and septic shock. *Anesth. Analg.* **103**, 1522–6 (2006).

[204] Cuello, F. *et al.* Redox state of pentraxin 3 as a novel biomarker for resolution of inflammation and survival in sepsis. *Mol. Cell. Proteomics* **13**, 2545–57 (2014).

[205] Stringer, K. A. *et al.* Metabolic consequences of sepsis-induced acute lung injury revealed by plasma 1H-nuclear magnetic resonance quantitative metabolomics and computational analysis. *Am. J. Physiol. Lung Cell. Mol. Physiol.* **300**, L4–L11 (2011).

[206] Schneider, C. A., Rasband, W. S. & Eliceiri, K. W. NIH Image to ImageJ: 25 years of image analysis. *Nat. Methods* **9**, 671–5 (2012).

[207] Schindelin, J. *et al.* Fiji: an open-source platform for biological-image analysis. *Nat. Methods* **9**, 676–82 (2012).

[208] Böyum, A. Isolation of mononuclear cells and granulocytes from human blood. Isolation of monuclear cells by one centrifugation, and of granulocytes by combining centrifugation and sedimentation at 1 g. *Scand. J. Clin. Lab. Invest. Suppl.* **97**, 77–89 (1968).

[209] Zhang, J. *et al.* Isolation of lymphocytes and their innate immune characterizations from liver, intestine, lung and uterus. *Cell. Mol. Immunol.* **2**, 271–280 (2005).

[210] Kummer, A. Active-Site Directed Probes for Protein Profiling - Application to Deubiquitinating Enzymes. *Master Thesis* (2011).

[211] Kang, D., Gho, Y. S., Suh, M. & Kang, C. Highly Sensitive and Fast Protein Detection with Coomassie Brilliant Blue in Sodium Dodecyl Sulfate-Polyacrylamide Gel Electrophoresis. *Communications* **23**, 1511–1512 (2002).

[212] Laemmli, U. K. Cleavage of structural proteins during the assembly of the head of bacteriophage T4. *Nature* **227**, 680–5 (1970).

[213] Towbin, H., Staehelin, T. & Gordon, J. Electrophoretic transfer of proteins from polyacrylamide gels to nitrocellulose sheets: procedure and some applications. 1979. *Proc Natl Acad Sci U S A.* **76**, 4350–4354 (1979).

[214] Livak, K. J. & Schmittgen, T. D. Analysis of relative gene expression data using real-time quantitative PCR and the 2(-Delta Delta C(T)) Method. *Methods* **25**, 402–8 (2001).

[215] Ross, P. L. *et al.* Multiplexed protein quantitation in Saccharomyces cerevisiae using amine-reactive isobaric tagging reagents. *Mol. Cell. Proteomics* **3**, 1154–69 (2004).

[216] Koenig, T. *et al.* Robust prediction of the MASCOT score for an improved quality assessment in mass spectrometric proteomics. *J. Proteome Res.* **7**, 3708–3717 (2008).

[217] Perkins, D. N., Pappin, D. J., Creasy, D. M. & Cottrell, J. S. Probability-based protein identification by searching sequence databases using mass spectrometry data. *Electrophoresis* **20**, 3551–67 (1999).

[218] Klawonn F. Significance tests to identify regulated proteins based on a large number of small samples. *Kybernetica* **48**, 478–493 (2012).

[219] Hornbeck, P. V. *et al.* PhosphoSitePlus, 2014: mutations, PTMs and recalibrations. *Nucleic Acids Res.* **43**, D512–20 (2015).

[220] Wagner, S. a. *et al.* Proteomic analyses reveal divergent ubiquitylation site patterns in murine tissues. *Mol. Cell. Proteomics* 1578–1585 (2012).

[221] Szczodrak, M. *c-Met Dynamics and its Functional Connection to Signalling and Actin Reorganisation.* Ph.D. thesis, MHH Hannover (2008).

[222] Niendorf, S. *et al.* Essential role of ubiquitin-specific protease 8 for receptor tyrosine kinase stability and endocytic trafficking in vivo. *Mol. Cell. Biol.* **27**, 5029–39 (2007).

[223] Berger, E. *Time - resolved characterization of the HGF / Met response and the influence of L . monocytogenes InlB on the physiological phosphoproteome.* Ph.D. thesis, TU Braunschweig (2013).

[224] Uhlén, M. *et al.* A human protein atlas for normal and cancer tissues based on antibody proteomics. *Mol. Cell. proteomics MCP* **4**, 1920–1932 (2005).

[225] Berglund, L. *et al.* A genecentric Human Protein Atlas for expression profiles based on antibodies. *Mol. Cell. Proteomics* **7**, 2019–27 (2008).

[226] Popp, M. W., Artavanis-Tsakonas, K. & Ploegh, H. L. Substrate filtering by the active site crossover loop in UCHL3 revealed by sortagging and gain-of-function mutations. *J. Biol. Chem.* **284**, 3593–3602 (2009).

[227] Komander, D. Mechanism, Specificity and Structure of the Deubiquitinases. In Groettrup, M. (ed.) *Conjug. Deconjugation Ubiquitin Fam. Modif.*, chap. Chapter 6, 69–87 (Springer, 2010).

[228] Urbé, S. *et al.* Systematic survey of deubiquitinase localization identifies USP21 as a regulator of centrosome- and microtubule-associated functions. *Mol. Biol. Cell* **23**, 1095–103 (2012).

[229] Pamer, E. G. Immune responses to Listeria monocytogenes. *Nat. Rev. Immunol.* **4**, 812–823 (2004).

[230] The UniProt Consortium. UniProt: a hub for protein information. *Nucleic Acids Res.* **43**, D204–212 (2014).

[231] Hawkins, J. S., Wu, Q., Wang, Y. & Lu, C. Y. Deficits in serum amyloid A contribute to increased neonatal mortality during murine listeriosis. *Pediatr. Res.* **74**, 668–74 (2013).

[232] Degrandi, D. *et al.* Extensive Characterization of IFN-Induced GTPases mGBP1 to mGBP10 Involved in Host Defense. *J. Immunol.* **179**, 7729–7740 (2007).

[233] Xu, M.-J. *et al.* Liver is the major source of elevated serum lipocalin-2 levels after bacterial infection or partial hepatectomy: A critical role for IL-6/STAT3. *Hepatology* **61**, 692–702 (2015).

[234] Palumbo, D., Iannaccone, M., Porta, A. & Capparelli, R. Experimental antibacterial therapy with puroindolines, lactoferrin and lysozyme in Listeria monocytogenes-infected mice. *Microbes Infect.* **12**, 538–545 (2010).

[235] Zou, X., Sorenson, B. S., Ross, K. F. & Herzberg, M. C. Augmentation of Epithelial Resistance to Invading Bacteria by Using mRNA Transfections. *Infect. Immun.* **81**, 3975–3983 (2013).

[236] Grigoleit, J.-S., Kullmann, J. S., Oberbeck, R., Schedlowski, M. & Engler, H. Salivary α-amylase response to endotoxin administration in humans. *Psychoneuroendocrinology* **38**, 1819–23 (2013).

[237] Trautwein, C., Boker, K. & Manns, M. P. Hepatocyte and immune system: acute phase reaction as a contribution to early defence mechanisms. *Gut* **35**, 1163–1166 (1994).

[238] Abromaitis, S. & Stephens, R. S. Attachment and Entry of Chlamydia Have Distinct Requirements for Host Protein Disulfide Isomerase. *PLoS Pathog.* **5**, e1000357 (2009).

[239] Hsu, Y.-L., Shi, S.-F., Wu, W.-L., Ho, L.-J. & Lai, J.-H. Protective roles of interferon-induced protein with tetratricopeptide repeats 3 (IFIT3) in dengue virus infection of human lung epithelial cells. *PLoS One* **8**, e79518 (2013).

[240] Garlanda, C., Bottazzi, B., Bastone, A. & Mantovani, A. Pentraxins at the crossroads between innate immunity, inflammation, matrix deposition, and female fertility. *Annu. Rev. Immunol.* **23**, 337–366 (2005).

[241] Fagoonee, S. *et al.* Lack of Plasma Protein Hemopexin Dampens Mercury-Induced Autoimmune Response in Mice. *J. Immunol.* **181**, 1937–1947 (2008).

[242] Reynolds, T. B. Strategies for acquiring the phospholipid metabolite inositol in pathogenic bacteria, fungi and protozoa: making it and taking it. *Microbiology* **155**, 1386–1396 (2009).

[243] Izar, B. *The hepatic response following infection with Listeria monocytogenes.* Ph.D. thesis, Justus-Liebig-University Gießen (2013).

[244] Xue, B. *et al.* Regulation of lipopolysaccharide-induced inflammatory response by glutathione S-transferase P1 in RAW264.7 cells. *FEBS Lett.* **579**, 4081–7 (2005).

[245] Luo, L. *et al.* Recombinant protein glutathione S-transferases P1 attenuates inflammation in mice. *Mol. Immunol.* **46**, 848–57 (2009).

[246] Gutiérrez-Pabello, J. A., McMurray, D. N. & Adams, L. G. Upregulation of thymosin beta-10 by Mycobacterium bovis infection of bovine macrophages is associated with apoptosis. *Infect. Immun.* **70**, 2121–7 (2002).

[247] Müller, A. *et al.* VDAC and the bacterial porin PorB of Neisseria gonorrhoeae share mitochondrial import pathways. *EMBO J.* **21**, 1916–29 (2002).

[248] Zhang, J. *et al.* Hepatic flavin-containing monooxygenase gene regulation in different mouse inflammation models. *Drug Metab. Dispos.* **37**, 462–468 (2009).

[249] Badamchian, M. *et al.* Thymosin beta(4) reduces lethality and down-regulates inflammatory mediators in endotoxin-induced septic shock. *Int. Immunopharmacol.* **3**, 1225–33 (2003).

[250] Theken, K. N. *et al.* Activation of the acute inflammatory response alters cytochrome P450 expression and eicosanoid metabolism. *Drug Metab. Dispos.* **39**, 22–9 (2011).

[251] Nyagode, B. a., Williams, I. R. & Morgan, E. T. Altered inflammatory responses to Citrobacter rodentium infection, but not bacterial lipopolysaccharide, in mice lacking the Cyp4a10 or Cyp4a14 genes. *Inflammation* **37**, 893–907 (2014).

[252] Pan, J. *et al.* Lipopolysaccharide-mediated modulation of cytochromes P450 in STAT1 null mice. *Drug Metab. Dispos.* **31**, 392–397 (2003).

[253] Garcia Del Busto Cano, E. & Renton, K. W. Modulation of hepatic cytochrome P450 during Listeria monocytogenes infection of the brain. *J. Pharm. Sci.* **92**, 1860–8 (2003).

[254] Armstrong, S. & Renton, K. Mechanism of Hepatic Cytochrome P450 Modulation during Listeria monocytogenes Infection in Mice. *Mol. Pharmacol.* (1993).

[255] Richardson, T. A. *et al.* Hepatic and renal cytochrome p450 gene regulation during citrobacter rodentium infection in wild-type and toll-like receptor 4 mutant mice. *Drug Metab. Dispos.* **34**, 354–60 (2006).

[256] Scheer, N. *et al.* Deletion of 30 murine cytochrome p450 genes results in viable mice with compromised drug metabolism. *Drug Metab. Dispos.* **42**, 1022–30 (2014).

[257] Pathan, M. *et al.* FunRich: An open access standalone functional enrichment and interaction network analysis tool. *Proteomics* **15**, 2597–601 (2015).

[258] Oshiumi, H., Matsumoto, M., Hatakeyama, S. & Seya, T. Riplet/RNF135, a RING finger protein, ubiquitinates RIG-I to promote interferon-beta induction during the early phase of viral infection. *J. Biol. Chem.* **284**, 807–17 (2009).

[259] Oshiumi, H., Miyashita, M., Matsumoto, M. & Seya, T. A distinct role of Riplet-mediated K63-Linked polyubiquitination of the RIG-I repressor domain in human antiviral innate immune responses. *PLoS Pathog.* **9**, e1003533 (2013).

[260] Jensen, L. J. *et al.* STRING 8–a global view on proteins and their functional interactions in 630 organisms. *Nucleic Acids Res.* **37**, D412–6 (2009).

[261] Gack, M. U. *et al.* TRIM25 RING-finger E3 ubiquitin ligase is essential for RIG-I-mediated antiviral activity. *Nature* **446**, 916–920 (2007).

[262] Liu, W. *et al.* Identification of RNF213 as a susceptibility gene for moyamoya disease and its possible role in vascular development. *PLoS One* **6**, e22542 (2011).

[263] Morito, D. *et al.* Moyamoya disease-associated protein mysterin/RNF213 is a novel AAA+ ATPase, which dynamically changes its oligomeric state. *Sci. Rep.* **4**, 4442 (2014).

[264] Kobayashi, H. *et al.* Biochemical and Functional Characterization of RNF213 (Mysterin) R4810K, a Susceptibility Mutation of Moyamoya Disease, in Angiogenesis In Vitro and In Vivo. *J. Am. Heart Assoc.* **4**, e002146– (2015).

[265] German Federal Office of Statistics. Life Tables 2010-2012 (2012). URL `https://www-genesis.destatis.de/genesis/online`.

[266] Novoselova, N., Wang, J. & Klawonn, F. Optimized leaf ordering with class labels for hierarchical clustering. *J. Bioinform. Comput. Biol.* **13** (2015).

[267] Boudreaux, D. A., Maiti, T. K., Davies, C. W. & Das, C. Ubiquitin vinyl methyl ester binding orients the misaligned active site of the ubiquitin hydrolase UCHL1 into productive conformation. *Proc. Natl. Acad. Sci. U. S. A.* **107**, 9117–9122 (2010).

[268] Edelmann, M. J. *et al.* Structural basis and specificity of human otubain 1-mediated deubiquitination. *Biochem. J.* **418**, 379–90 (2009).

[269] Catic, A. *et al.* Screen for ISG15-crossreactive deubiquitinases. *PLoS One* **2**, e679 (2007).

[270] Virdee, S., Ye, Y., Nguyen, D. P., Komander, D. & Chin, J. W. Engineered diubiquitin synthesis reveals Lys29-isopeptide specificity of an OTU deubiquitinase. *Nat. Chem. Biol.* **6**, 750–757 (2010).

[271] Faesen, A. C. *et al.* The differential modulation of USP activity by internal regulatory domains, interactors and eight ubiquitin chain types. *Chem. Biol.* **18**, 1550–61 (2011).

[272] Ritorto, M. S. *et al.* Screening of DUB activity and specificity by MALDI-TOF mass spectrometry. *Nat. Commun.* **5**, 4763 (2014).

[273] Goh, L. K. & Sorkin, A. Endocytosis of Receptor Tyrosine Kinases. *Cold Spring Harb. Perspect. Biol.* **5**, a017459–a017459 (2013).

[274] Sigismund, S. *et al.* Threshold-controlled ubiquitination of the EGFR directs receptor fate. *EMBO J.* **32**, 2140–2157 (2013).

[275] Abella, J. V. *et al.* Met/Hepatocyte growth factor receptor ubiquitination suppresses transformation and is required for Hrs phosphorylation. *Mol. Cell. Biol.* **25**, 9632–45 (2005).

[276] Peschard, P. *et al.* Mutation of the c-Cbl TKB domain binding site on the Met receptor tyrosine kinase converts it into a transforming protein. *Mol. Cell* **8**, 995–1004 (2001).

[277] Petrelli, A. *et al.* The endophilin-CIN85-Cbl complex mediates ligand-dependent downregulation of c-Met. *Nature* **416**, 187–190 (2002).

[278] Clague, M. J. Met receptor: a moving target. *Sci. Signal.* **4**, pe40 (2011).

[279] Henne, W. M., Buchkovich, N. J. & Emr, S. D. The ESCRT Pathway. *Dev. Cell* **21**, 77–91 (2011).

[280] McCullough, J., Clague, M. J. & Urbé, S. AMSH is an endosome-associated ubiquitin isopeptidase. *J. Cell Biol.* **166**, 487–492 (2004).

[281] Row, P. E., Prior, I. A., McCullough, J., Clague, M. J. & Urbé, S. The ubiquitin isopeptidase UBPY regulates endosomal ubiquitin dynamics and is essential for receptor down-regulation. *J. Biol. Chem.* **281**, 12618–12624 (2006).

[282] Polo, S., Di Fiore, P. P. & Sigismund, S. Keeping EGFR signaling in check: Ubiquitin is the guardian. *Cell Cycle* **13**, 681–682 (2014).

[283] Pizarro-Cerda, J., Bonazzi, M. & Cossart, P. Clathrin-mediated endocytosis: What works for small, also works for big. *BioEssays* **32**, 496–504 (2010).

[284] Gur, G. *et al.* LRIG1 restricts growth factor signaling by enhancing receptor ubiquitylation and degradation. *EMBO J.* **23**, 3270–81 (2004).

[285] Oh, Y. M. *et al.* USP8 modulates ubiquitination of LRIG1 for Met degradation. *Sci. Rep.* **4**, 4980 (2014).

[286] Savio, M. G. *et al.* USP9X Controls EGFR Fate by Deubiquitinating the Endocytic Adaptor Eps15. *Curr. Biol.* **26**, 173–83 (2016).

[287] Parachoniak, C. A. & Park, M. Distinct recruitment of Eps15 via Its coiled-coil domain is required for efficient down-regulation of the met receptor tyrosine kinase. *J. Biol. Chem.* **284**, 8382–94 (2009).

[288] Murray, R. Z., Jolly, L. A. & Wood, S. A. The FAM Deubiquitylating Enzyme Localizes to Multiple Points of Protein Trafficking in Epithelia, where It Associates with E-cadherin and β-catenin. *Mol. Biol. Cell* **15**, 1591–1599 (2004).

[289] Maculins, T., Fiskin, E., Bhogaraju, S. & Dikic, I. Bacteria-host relationship: ubiquitin ligases as weapons of invasion. *Cell Res.* **26**, 499–510 (2016).

[290] Hammond, D. E. Endosomal Dynamics of Met Determine Signaling Output. *Mol. Biol. Cell* **14**, 1346–1354 (2003).

[291] Kermorgant, S., Zicha, D. & Parker, P. J. PKC controls HGF-dependent c-Met traffic, signalling and cell migration. *Eur. Mol. Biol. Organ. J.* **23**, 3721–3734 (2004).

[292] Kermorgant, S. & Parker, P. J. Receptor trafficking controls weak signal delivery: A strategy used by c-Met for STAT3 nuclear accumulation. *J. Cell Biol.* **182**, 855–863 (2008).

[293] Ménard, L., Parker, P. J. & Kermorgant, S. Receptor tyrosine kinase c-Met controls the cytoskeleton from different endosomes via different pathways. *Nat. Commun.* **5**, 3907 (2014).

[294] Massoumi, R., Chmielarska, K., Hennecke, K., Pfeifer, A. & Fässler, R. Cyld inhibits tumor cell proliferation by blocking Bcl-3-dependent NF-kappaB signaling. *Cell* **125**, 665–77 (2006).

[295] Matteucci, E., Bendinelli, P. & Desiderio, M. A. Nuclear localization of active HGF receptor Met in aggressive MDA-MB231 breast carcinoma cells. *Carcinogenesis* **30**, 937–45 (2009).

[296] Chaudhary, S. C. *et al.* A putative pH-dependent nuclear localization signal in the juxtamembrane region of c-Met. *Exp. Mol. Med.* **46**, e119 (2014).

[297] Hornung, V. *et al.* 5'-Triphosphate RNA is the ligand for RIG-I. *Science* **314**, 994–7 (2006).

[298] Monroe, K. M., McWhirter, S. M. & Vance, R. E. Identification of host cytosolic sensors and bacterial factors regulating the type I interferon response to Legionella pneumophila. *PLoS Pathog.* **5**, e1000665 (2009).

[299] Abdullah, Z. *et al.* RIG-I detects infection with live Listeria by sensing secreted bacterial nucleic acids. *EMBO J.* **31**, 4153–64 (2012).

[300] Jehl, S. P., Nogueira, C. V., Zhang, X. & Starnbach, M. N. IFNγ inhibits the cytosolic replication of Shigella flexneri via the cytoplasmic RNA sensor RIG-I. *PLoS Pathog.* **8**, e1002809 (2012).

[301] Dixit, E. & Kagan, J. C. *Intracellular Pathogen Detection by RIG-I-Like Receptors*, vol. 117 (Elsevier Inc., 2013), 1 edn. URL `http://dx.doi.org/10.1016/B978-0-12-410524-9.00004-9`.

[302] Hagmann, C. A. *et al.* RIG-I detects triphosphorylated RNA of Listeria monocytogenes during infection in non-immune cells. *PLoS One* **8**, e62872 (2013).

[303] Schmolke, M. *et al.* RIG-I detects mRNA of intracellular Salmonella enterica serovar typhimurium during bacterial infection. *MBio* **5**, 1–9 (2014).

[304] Qiagen. Ingenuity(R) Pathway Analysis (IPA(R)) (2016). URL `www.qiagen.com/ingenuity`.

[305] Pollpeter, D., Komuro, A., Barber, G. N. & Horvath, C. M. Impaired cellular responses to cytosolic DNA or infection with listeria monocytogenes and vaccinia virus in the absence of the murine LGP2 protein. *PLoS One* **6** (2011).

[306] Zhang, L., Zhao, X., Zhang, M., Zhao, W. & Gao, C. Ubiquitin-specific protease 2b negatively regulates IFN-β production and antiviral activity by targeting TANK-binding kinase 1. *J. Immunol.* **193**, 2230–7 (2014).

[307] Haimerl, F., Erhardt, A., Sass, G. & Tiegs, G. Down-regulation of the deubiquitinating enzyme ubiquitin-specific protease 2 contributes to tumor necrosis factor-alpha-induced hepatocyte survival. *J. Biol. Chem.* **284**, 495–504 (2009).

[308] Kim, M.-J., Hwang, S.-Y., Imaizumi, T. & Yoo, J.-Y. Negative feedback regulation of RIG-I-mediated antiviral signaling by interferon-induced ISG15 conjugation. *J. Virol.* **82**, 1474–83 (2008).

[309] Naegle, K. M. *et al.* PTMScout, a Web resource for analysis of high throughput post-translational proteomics studies. *Mol. Cell. Proteomics* **9**, 2558–70 (2010).

[310] Yuan, W. & Krug, R. M. Influenza B virus NS1 protein inhibits conjugation of the interferon (IFN)-induced ubiquitin-like ISG15 protein. *EMBO J.* **20**, 362–71 (2001).

[311] Kwon, J. *et al.* Two closely related ubiquitin C-terminal hydrolase isozymes function as reciprocal modulators of germ cell apoptosis in cryptorchid testis. *Am. J. Pathol.* **165**, 1367–74 (2004).

[312] Setsuie, R., Suzuki, M., Tsuchiya, Y. & Wada, K. Skeletal muscles of Uchl3 knockout mice show polyubiquitinated protein accumulation and stress responses. *Neurochem. Int.* **56**, 911–8 (2010).

[313] Mtango, N. R., Sutovsky, M., Vandevoort, C. A., Latham, K. E. & Sutovsky, P. Essential role of ubiquitin C-terminal hydrolases UCHL1 and UCHL3 in mammalian oocyte maturation. *J. Cell. Physiol.* **227**, 2022–9 (2012).

[314] Karim, R. *et al.* Human papillomavirus (HPV) upregulates the cellular deubiquitinase UCHL1 to suppress the keratinocyte's innate immune response. *PLoS Pathog.* **9**, e1003384 (2013).

[315] Gu, Y.-y. *et al.* The de-ubiquitinase UCHL1 promotes gastric cancer metastasis via the Akt and Erk1/2 pathways. *Tumour Biol.* **36**, 8379–87 (2015).

[316] Mural, R. J. *et al.* A comparison of whole-genome shotgun-derived mouse chromosome 16 and the human genome. *Science* **296**, 1661–71 (2002).

[317] Monaco, G., van Dam, S., Casal Novo Ribeiro, J. L., Larbi, A. & de Magalhães, J. P. A comparison of human and mouse gene co-expression networks reveals conservation and divergence at the tissue, pathway and disease levels. *BMC Evol. Biol.* **15**, 259 (2015).

[318] Sonnhammer, E. L. L. & Östlund, G. InParanoid 8: orthology analysis between 273 proteomes, mostly eukaryotic. *Nucleic Acids Res.* **43**, D234–9 (2015).

[319] Shi, R. *et al.* Analysis of the mouse liver proteome using advanced mass spectrometry. *J. Proteome Res.* **6**, 2963–72 (2007).

[320] Azimifar, S. B., Nagaraj, N., Cox, J. & Mann, M. Cell-type-resolved quantitative proteomics of murine liver. *Cell Metab.* **20**, 1076–1087 (2014).

[321] He, J.-J. *et al.* Proteomic Profiling of Mouse Liver following Acute Toxoplasma gondii Infection. *PLoS One* **11**, e0152022 (2016).

[322] Eden, E., Navon, R., Steinfeld, I., Lipson, D. & Yakhini, Z. GOrilla: a tool for discovery and visualization of enriched GO terms in ranked gene lists. *BMC Bioinformatics* **10**, 48 (2009).

[323] Ashburner, M. *et al.* Gene ontology: tool for the unification of biology. The Gene Ontology Consortium. *Nat. Genet.* **25**, 25–9 (2000).

[324] Gilbert, J., Ou, W., Silver, J. & Benjamin, T. Downregulation of protein disulfide isomerase inhibits infection by the mouse polyomavirus. *J. Virol.* **80**, 10868–70 (2006).

[325] Kocks, C. & Cossart, P. Directional actin assembly by Listeria monocytogenes at the site of polar surface expression of the actA gene product involving the actin-bundling protein plastin (fimbrin). *Infect. Agents Dis.* **2**, 207–9 (1993).

[326] Deady, L. E. *et al.* L-plastin is essential for alveolar macrophage production and control of pulmonary pneumococcal infection. *Infect. Immun.* **82**, 1982–93 (2014).

[327] Carrero, J. a. & Unanue, E. R. *Mechanisms and immunological effects of apoptosis caused by listeria monocytogenes*, vol. 113 (Elsevier Inc., 2012), 1 edn.

[328] Welch, M. D. & Way, M. Arp2/3-mediated actin-based motility: A tail of pathogen abuse. *Cell Host Microbe* **14**, 242–255 (2013).

[329] Nelson, D. R. *et al.* Comparison of cytochrome P450 (CYP) genes from the mouse and human genomes, including nomenclature recommendations for genes, pseudogenes and alternative-splice variants. *Pharmacogenetics* **14**, 1–18 (2004).

[330] Feolo, M., Helmberg, W., Sherry, S. & Maglott, D. R. NCBI genetic resources supporting immunogenetic research. *Rev. Immunogenet.* **2**, 461–7 (2000).

[331] Lewis, D. F. V., Ito, Y. & Lake, B. G. Molecular modelling of CYP2F substrates: comparison of naphthalene metabolism by human, rat and mouse CYP2F subfamily enzymes. *Drug Metabol. Drug Interact.* **24**, 229–57 (2009).

[332] Fabregat, A. *et al.* The Reactome pathway Knowledgebase. *Nucleic Acids Res.* **44**, D481–7 (2015).

[333] Khatri, Y., Gregory, M. C., Grinkova, Y. V., Denisov, I. G. & Sligar, S. G. Active site proton delivery and the lyase activity of human CYP17A1. *Biochem. Biophys. Res. Commun.* **443**, 179–84 (2014).

[334] Zanger, U. M., Turpeinen, M., Klein, K. & Schwab, M. Functional pharmacogenetics/genomics of human cytochromes P450 involved in drug biotransformation. *Anal. Bioanal. Chem.* **392**, 1093–1108 (2008).

[335] Granfors, M. T., Backman, J. T., Laitila, J. & Neuvonen, P. J. Tizanidine is mainly metabolized by cytochrome p450 1A2 in vitro. *Br. J. Clin. Pharmacol.* **57**, 349–53 (2004).

[336] Kamen, L., Henney, H. R. & Runyan, J. D. A practical overview of tizanidine use for spasticity secondary to multiple sclerosis, stroke, and spinal cord injury. *Curr. Med. Res. Opin.* **24**, 425–39 (2008).

[337] Renton, K. W. Regulation of drug metabolism and disposition during inflammation and infection. *Expert Opin. Drug Metab. Toxicol.* **1**, 629–640 (2005).

[338] Kraemer, M. J. *et al.* Altered Theophylline Clearance During an Influenza B Outbreak. *Pediatrics* **69**, 476–480 (1982).

[339] Toft, P., Heslet, L., Hansen, M. & Klitgaard, N. A. Theophylline and ethylenediamine pharmacokinetics following administration of aminophylline to septic patients with multiorgan failure. *Intensive Care Med.* **17**, 465–8 (1991).

[340] Ghannoum, M. *et al.* Extracorporeal treatment for theophylline poisoning: systematic review and recommendations from the EXTRIP workgroup. *Clin. Toxicol. (Phila).* **53**, 215–29 (2015).

[341] Raunio, H. & Rahnasto-Rilla, M. CYP2A6: Genetics, structure, regulation, and function. *Drug Metabol. Drug Interact.* **27**, 73–88 (2012).

[342] Backman, J. T., Filppula, A. M., Niemi, M. & Neuvonen, P. J. Role of Cytochrome P450 2C8 in Drug Metabolism and Interactions. *Pharmacol. Rev.* **68**, 168–241 (2016).

[343] Niwa, T. & Yamazaki, H. Comparison of Cytochrome P450 2C Subfamily Members in Terms of Drug Oxidation Rates and Substrate Inhibition. *Curr. Drug Metab.* **9**, 1145–1159 (2012).

[344] Hashizume, T. Involvement of CYP2J2 and CYP4F12 in the Metabolism of Ebastine in Human Intestinal Microsomes. *J. Pharmacol. Exp. Ther.* **300**, 298–304 (2002).

[345] Parikh, Sweta and Gagne, Peter and Miller, Vaughn and Crespi, Charles and Thummel, Kenneth and Patten, C. CYP2J2 and CYP4F12 are active for the metabolism of non-sedating antihistamines: Terfenadine and astemizole. *Drug Metab. Rev* **35**, 190–190 (2003).

[346] Jin, Y., Zollinger, M., Borell, H., Zimmerlin, A. & Patten, C. J. CYP4F enzymes are responsible for the elimination of fingolimod (FTY720), a novel treatment of relapsing multiple sclerosis. *Drug Metab. Dispos.* **39**, 191–8 (2011).

[347] Jin, R., Koop, D. R., Raucy, J. L. & Lasker, J. M. Role of human CYP4F2 in hepatic catabolism of the proinflammatory agent leukotriene B4. *Arch. Biochem. Biophys.* **359**, 89–98 (1998).

[348] Bardowell, S. A., Stec, D. E. & Parker, R. S. Common variants of cytochrome P450 4F2 exhibit altered vitamin E-{omega}-hydroxylase specific activity. *J. Nutr.* **140**, 1901–6 (2010).

[349] McDonald, M. G., Rieder, M. J., Nakano, M., Hsia, C. K. & Rettie, A. E. CYP4F2 is a vitamin K1 oxidase: An explanation for altered warfarin dose in carriers of the V433M variant. *Mol. Pharmacol.* **75**, 1337–46 (2009).

[350] Azri, S. & Renton, K. W. Factors involved in the depression of hepatic mixed function oxidase during infections with Listeria monocytogenes. *Int. J. Immunopharmacol.* **13**, 197–204 (1991).

[351] Guengerich, F. P. Fifty Years of Progress in Drug Metabolism and Toxicology: What Do We Still Need to Know About Cytochrome P450 Enzymes? In *Fifty Years Cytochrome P450 Res.*, chap. 2, 371–401 (Springer Japan, Tokyo, 2014).

[352] Ma, C. *et al.* On-Chip Construction of Liver Lobule-like Microtissue and Its Application for Adverse Drug Reaction Assay. *Anal. Chem.* **88**, 1719–27 (2016).

[353] Douglas, J. J. & Russell, J. A. The role of genomics to identify biomarkers and signaling molecules during severe sepsis. *Minerva Anestesiol.* **82**, 343–358 (2016).

[354] Grimes, D. A. & Schulz, K. F. Compared to what? Finding controls for case-control studies. *Lancet (London, England)* **365**, 1429–33 (2005).

[355] Fonović, M. & Bogyo, M. Activity-based probes as a tool for functional proteomic analysis of proteases. *Expert Rev. Proteomics* **5**, 721–30 (2008).

[356] Heal, W. P., Dang, T. H. T. & Tate, E. W. Activity-based probes: discovering new biology and new drug targets. *Chem. Soc. Rev.* **40**, 246–57 (2011).

[357] Scudder, S. L. *et al.* Synaptic strength is bidirectionally controlled by opposing activity-dependent regulation of Nedd4-1 and USP8. *J. Neurosci.* **34**, 16637–49 (2014).

[358] Min, M., Mayor, U., Dittmar, G. & Lindon, C. Using in vivo-biotinylated ubiquitin to describe a mitotic exit ubiquitome from human cells. *Mol. Cell. Proteomics* 2411–2425 (2014).

[359] Sahtoe, D. D. & Sixma, T. K. Layers of DUB regulation. *Trends Biochem. Sci.* **40**, 456–67 (2015).

[360] Reyes-Turcu, F. E., Shanks, J. R., Komander, D. & Wilkinson, K. D. Recognition of polyubiquitin isoforms by the multiple ubiquitin binding modules of isopeptidase T. *J. Biol. Chem.* **283**, 19581–92 (2008).

[361] Bremm, A., Freund, S. M. V. & Komander, D. Lys11-linked ubiquitin chains adopt compact conformations and are preferentially hydrolyzed by the deubiquitinase Cezanne. *Nat. Struct. Mol. Biol.* **17**, 939–947 (2010).

[362] Tickler, A. K. & Wade, J. D. Overview of Solid Phase Synthesis of 'Difficult Peptide' Sequences. *Curr. Protoc. Protein Sci.* 18.8.1–18.8.6 (2007).

[363] Innovagen. PepCalc (2015). URL `http://pepcalc.com/`.

[364] Pao, K.-C. *et al.* Probes of ubiquitin E3 ligases enable systematic dissection of parkin activation. *Nat. Chem. Biol.* (2016).

[365] Lin, D. Y.-w., Diao, J., Zhou, D. & Chen, J. Biochemical and structural studies of a HECT-like ubiquitin ligase from Escherichia coli O157:H7. *J. Biol. Chem.* **286**, 441–9 (2011).

[366] Zhang, Y., Higashide, W. M., McCormick, B. A., Chen, J. & Zhou, D. The inflammation-associated Salmonella SopA is a HECT-like E3 ubiquitin ligase. *Mol. Microbiol.* **62**, 786–93 (2006).

[367] Misaghi, S. *et al.* Chlamydia trachomatis-derived deubiquitinating enzymes in mammalian cells during infection. *Mol. Microbiol.* **61**, 142–50 (2006).

[368] Bell, C. C. *et al.* Characterization of primary human hepatocyte spheroids as a model system for drug-induced liver injury, liver function and disease. *Sci. Rep.* **6**, 25187 (2016).

[369] Twine, S. M. *et al.* In vivo proteomic analysis of the intracellular bacterial pathogen, Francisella tularensis, isolated from mouse spleen. *Biochem. Biophys. Res. Commun.* **345**, 1621–1633 (2006).

[370] Schmidt, F. *et al.* Time-resolved quantitative proteome profiling of host-pathogen interactions: the response of Staphylococcus aureus RN1HG to internalisation by human airway epithelial cells. *Proteomics* **10**, 2801–11 (2010).

[371] Efron, B. & Stein, C. The Jackknife Estimate of Variance. *Ann. Stat.* **9**, 586–596 (1981).

[372] Jahan, A. S. *et al.* Usp12 stabilizes the T-cell receptor complex at the cell surface during signaling. *Proc. Natl. Acad. Sci. U. S. A.* **113**, E705–14 (2016).

[373] Wagner, S. A. *et al.* A proteome-wide, quantitative survey of in vivo ubiquitylation sites reveals widespread regulatory roles. *Mol. Cell. Proteomics* **10**, M111.013284 (2011).

[374] Udeshi, N. D., Mertins, P., Svinkina, T. & Carr, S. a. Large-scale identification of ubiquitination sites by mass spectrometry. *Nat. Protoc.* **8**, 1950–60 (2013).

[375] Thomas, S. N., Zhang, H. & Cotter, R. J. Application of quantitative proteomics to the integrated analysis of the ubiquitylated and global proteomes of xenograft tumor tissues. *Clin. Proteomics* **12**, 14 (2015).

[376] Shalit, T., Elinger, D., Savidor, A., Gabashvili, A. & Levin, Y. MS1-based label-free proteomics using a quadrupole orbitrap mass spectrometer. *J. Proteome Res.* **14**, 1979–1986 (2015).

[377] Castillo, M. J., Reynolds, K. J., Gomes, A., Fenselau, C. & Yao, X. Quantitative Protein Analysis Using Enzymatic [18O] Water Labeling. In Coligan, J. E., Dunn, B. M., Speicher, D. W. & Wingfield, P. T. (eds.) *Curr. Protoc. Protein Sci.*, vol. 29, 23.4.1–23.4.9 (John Wiley & Sons, Inc., Hoboken, NJ, USA, 2014). arXiv:NIHMS150003.

[378] Udeshi, N. D. *et al.* Refined Preparation and Use of Anti-diglycine Remnant (K-epsilon-GG) Antibody Enables Routine Quantification of 10,000s of Ubiquitination Sites in Single Proteomics Experiments. *Mol. Cell. Proteomics* **12**, 825–831 (2012).

List of Abbreviations

aa	Amino acid
ABP	Activity-based probe
ABPP	Activity-based protein profiling
AcN	Acetonitrile
ActA	Actin assembly-inducing protein
AIDA	Advanced Image Data Analyzer
APC	Antigen presenting cell
APP	Acute-phase protein
APR	Acute-phase response
Asn	Asparagine
Asp	Aspartate
ATXN3	Ataxin 3
AUCROC	Area under the curve of the receiver operating characteristic
BHI	Brain Heart Infusion
bpm	Beats per minute
BSA	Bovine serum albumin
BTLA	B- and T-lymphocyte attenuator
c-Met	Hepatocyte growth factor receptor
CAA	Chloroacteamide
CBD	Chitin binding domain
CD	Catalytical domain

CFU	Colony forming unit
CIEX	Cation exchange chromatography
CME	Clathrin-mediated endocytosis
conc.	Concentration
CRP	C-reactive protein
CTLA-4	Cytotoxic T-lymphocyte antigen-4
Cy	Cyanine
CYLD	Cylindromatosis (turban tumor syndrome)
CYP / Cyp	Cytochrome P450
Cys	Cysteine
DAPI	4´,6-Diamidino-2-phenylindole dihydrochloride
DC	Dendritic cell
DCM	Dichloromethane
DIC	N,N´-Diisopropylcarbodiimide
DIPEA	N,N-Diisopropylethylamine
DMEM	Dulbecco's modified Eagle's Medium
DMF	Dimethylformamide
DMSO	Dimethyl sulfoxide
DNA	Deoxyribonucleic acid
DTT	Dithiothreitol
DUB	Deubiquitinating enzyme
E.coli	Escherichia coli
EDC	1-Ethyl-3-(3-dimethylaminopropyl)carbodiimide
eGFP	Enhanced green fluorescent protein
EGFR	Epidermal growth factor receptor

Eps15	Epidermal growth factor receptor substrate 15
ESCRT	Endosomal sorting complex required for transport
EtOH	Ethanol
FA	Formic acid
FBS	Fetal bovine serum
FDR	False discovery rate
Fmoc	Fluorenylmethyloxycarbonyl
Gln	Glutamine
Glu	Glutamate
GO	Gene ontology
GSH	Glutathione sepharose
GST	Glutathione S-transferase
HA	Hemagglutinin
HECT	Homologous to E6-AP C-terminus
HEPES	4-(2-hydroxyethyl)-1-piperazineethanesulfonic acid
HGF	Hepatocyte growth factor
His	Histidine
HIS6-Tag	Poly histidin tag
HOBt	Hydroxybenzotriazole
HPA	The Human Protein Atlas
HRP	Horseradish peroxidase
ICU	Intensive care unit
IFN	Interferon
IL	Interleukin
InlA	Internalin A

InlB	Internalin B
IP	Immunoprecipitation
IPTG	Isopropyl-β-D-1-thiogalactopyranoside
ISG15	Interferon-stimulated gene 15
iTRAQ	Isobaric tags for relative and absolute quantification
K	Lysine
KC	Kupffer cell
kDa	Kilo dalton
LB	Lysogeny broth
LC	Liquid chromatography
Lm	Listeria monocytogenes
LPS	Lipopolysaccharide
LRIG1	Leucine-rich repeats and immunoglobulin-like domains protein 1
Lys	Lysine
MΦ	Macrophage
MALDI	Matrix-assisted laser desorption/ionization
MCPIP	Monocyte chemotactic protein–induced protein 1
MDS	Multidimensional scaling
MeOH	Methanol
MES	2-(N-morpholino)ethanesulfonic acid
MesNa	Sodium 2-sulfanylethanesulfonate
miRNA	MicroRNA
MMTS	Methyl methanethiosulfonate
Mo	Inflammatory monocyte
MODS	Multi organ dysfunction syndrome

MoM	Monocyte derived macrophage
MOPS	3-(N-morpholino)propanesulfonic acid
mRNA	Messenger RNA
MSMD	Mendelian susceptibility to mycobacterial disease
Mtt	4-Methyltrityl
MW	Molecular weight
NaOAc	Sodium acetate
NEDD8	Neuronal-precursor-cell expressed developmentally down-regulated 8
Neu	Neutrophil
NF-kB	Nuclear factor kappa B
NK cell	Natural killer cell
NY	Nylon
o/N	Over night
OD	Optical density
p.a.	Pro analysi
p.i.	Post innoculation
PBMCs	Peripheral blood mononuclear cells
PCI	Persistent critical illness
PCT	Procalcitonin
PDI	protein disulfide isomerase
PE	Peripheral endosome
PFA	Paraformaldehyde
PI	Propidium iodide
PI3K	Phosphoinositide 3-kinase
PNE	Perinuclear endosome

POC	Proof-of-concept
ppm	Parts per million
pro-ADM	Proadrenomedullin
PRR	Pattern recognition receptor
PVDF	Polyvinylidene fluoride
R	Arginine
RBR	RING between RING
RF	Regulation factor (log2)
RING	Really interesting new gene
RLR	RIG-I-like receptor
RNA	Ribonucleic acid
RNF135	E3 ubiquitin protein ligase RNF135/Riplet
RP	Reverse phase
RPMI	Roswell Park Memorial Institute Medium
RT	Room temperature
RT-PCR	Reverse transcription polymerase chain reaction
S	Serine
SAA2	Serum amyloid A-2 protein
SCX	Strong cation exchange chromatography
SD	Standard deviation
SDS	Sodium dodecyl sulfate
SDS-PAGE	SDS-poly-acrylamide gel electrophoresis
Ser	Serine
SID	Selective intestine decontamination
SIRS	Systemic inflammatory response syndrome

SNP	Single nucleotide polymorphism
SPE	Solid phase extraction
STAT	Signal transducer and activator of transcription
SUMO	Small ubiquitin-like modifier
T	Threonine
TBK1	TANK-binding kinase 1
tcHGF	Two-chain HGF
tech.	Technical grade
TFA	Trifluoroacetic acid
TipDC	Tumor necrosis factor/inducible nitric oxide synthase producing dendritic cell
TNF	Tumor necrosis factor
TOF	time of flight
TRAF	TNF receptor associated factor
TREM-1	Triggering receptor expressed on myeloid cells-1
Tris/HCl	Tris(hydroxymethyl)aminomethane, pH adjusted with HCl
TTHY	Transthyretin
Ub	Ubiquitin
UBL	Ubiquitin-like modifier
UFM1	Ubiquitin-fold modifier 1
UIPP	Ubiquitin-Isopeptide Probe
v/v	Volume per volume
VA	Vinyl formic acid
VFEA	vinylmonofluoroethylamide
VME	Vinyl methyl ester
VS	Vinyl methyl sulfone

w/v	Weight per volume
WBC	White blood cell
wt	Wild type
Y	Tyrosine

Appendix

Supplementary Data

Supplementary Figures

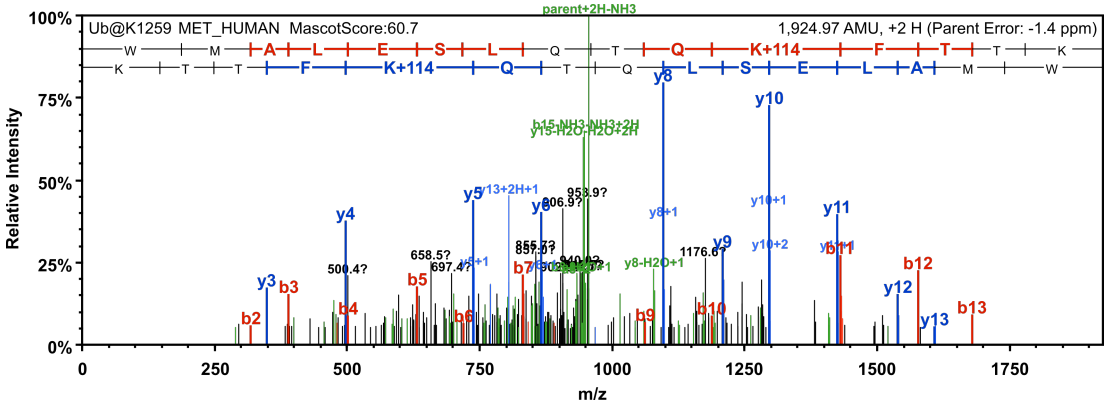

Figure S1. K1259 is ubiquitinated in HeLa S3 cells after 30 min of HGF stimulation. Ub-sites were pulled from HeLa S3 cell lysates by Ub-remnant enrichment. The spectrum presents the tryptic peptide containing the GG-modified K1259 and was manually validated. Blue peaks present y-ions, red peaks b-ions. Green peaks represent different mother-masses. Mascot scores and measurement errors are given.

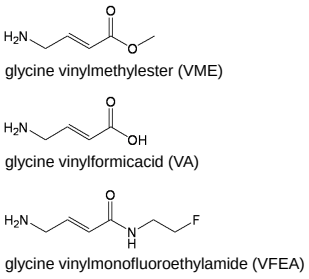

Figure S2. Structures of C-terminal electrophilic warheads used in this study. VA is the precursor-structure used to produce VFEA and the peptide-mimicking UIPP-warheads.

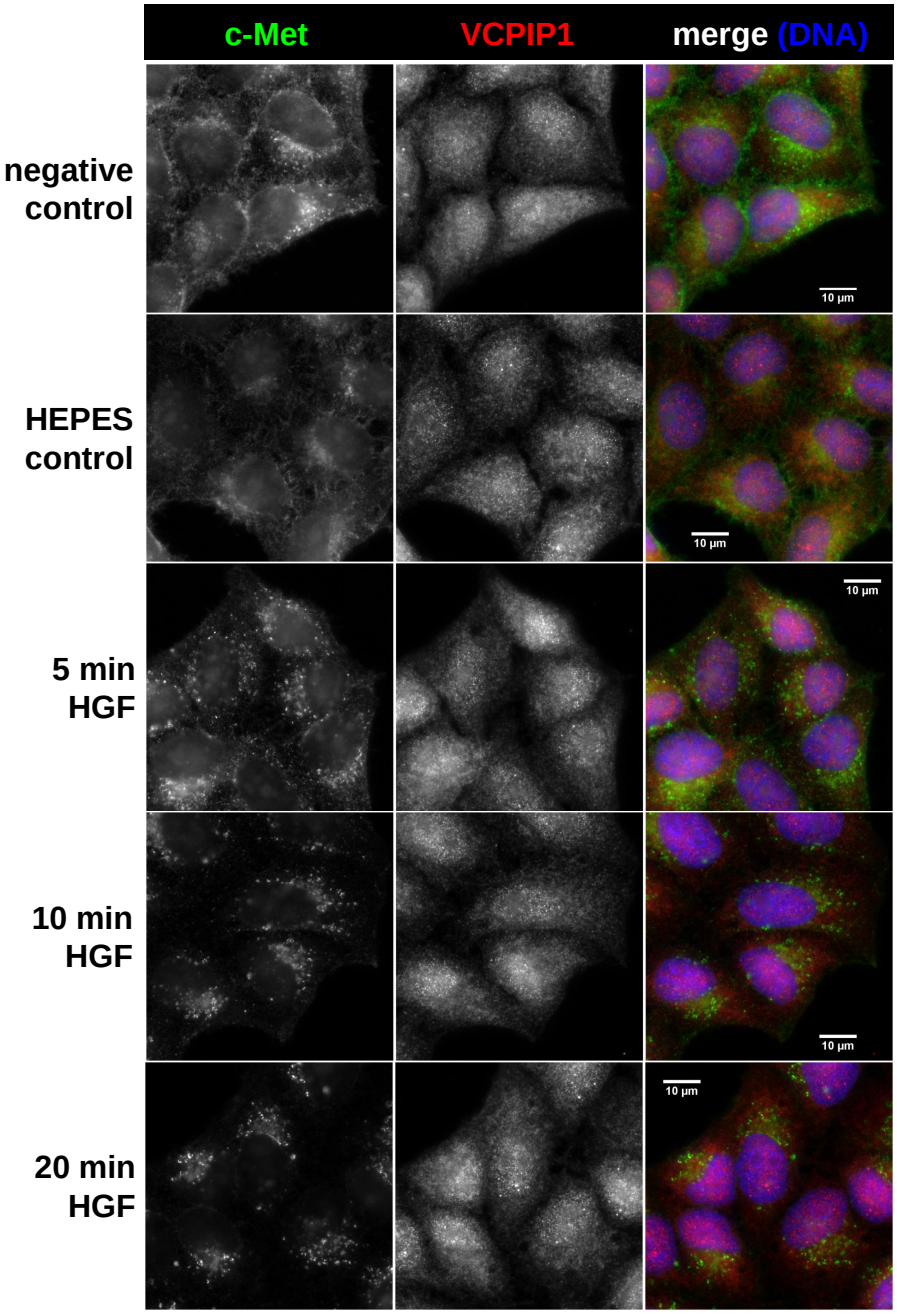

continued on the next page

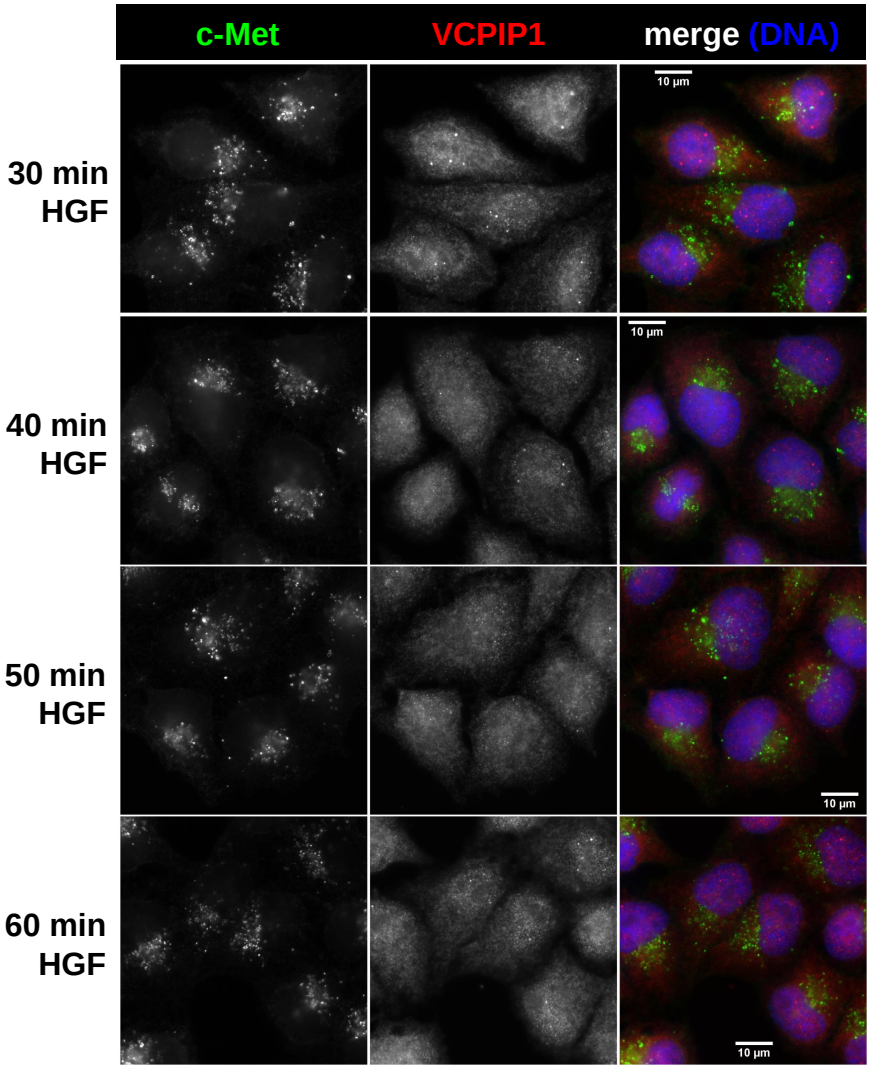

Figure S3. VCPIP1 localization during HGF stimulation in HeLa S3 cells. HeLa cells were stimulated with 10 nM HGF for the indicated time periods and subsequently stained for c-Met (green), VCPIP1 (red) and DNA content (blue). Finally, samples were analyzed via epifluorescence microscopy. The white bar represents 10 µm. The negative control (0 min(neg)) shows cells which were only starved, but not stimulated. The HEPES control is stimulated with the buffer of HGF for 60 min.

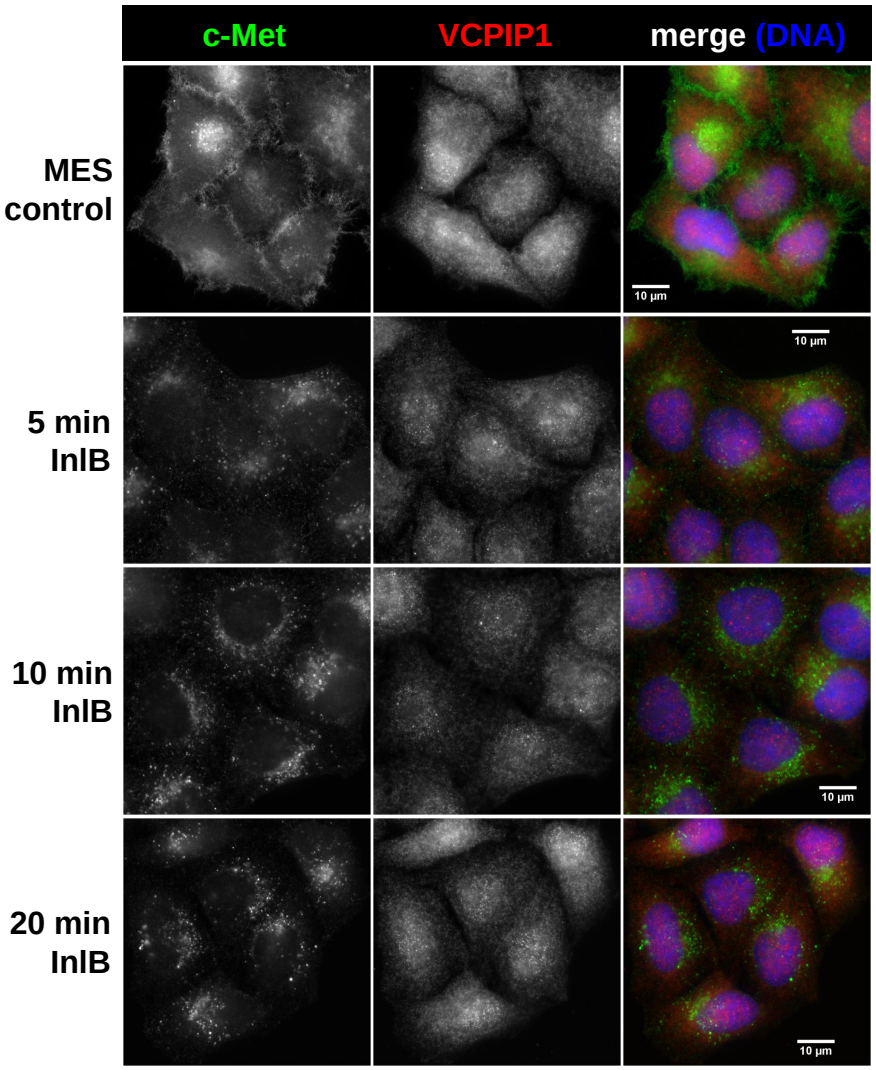

continued on the next page

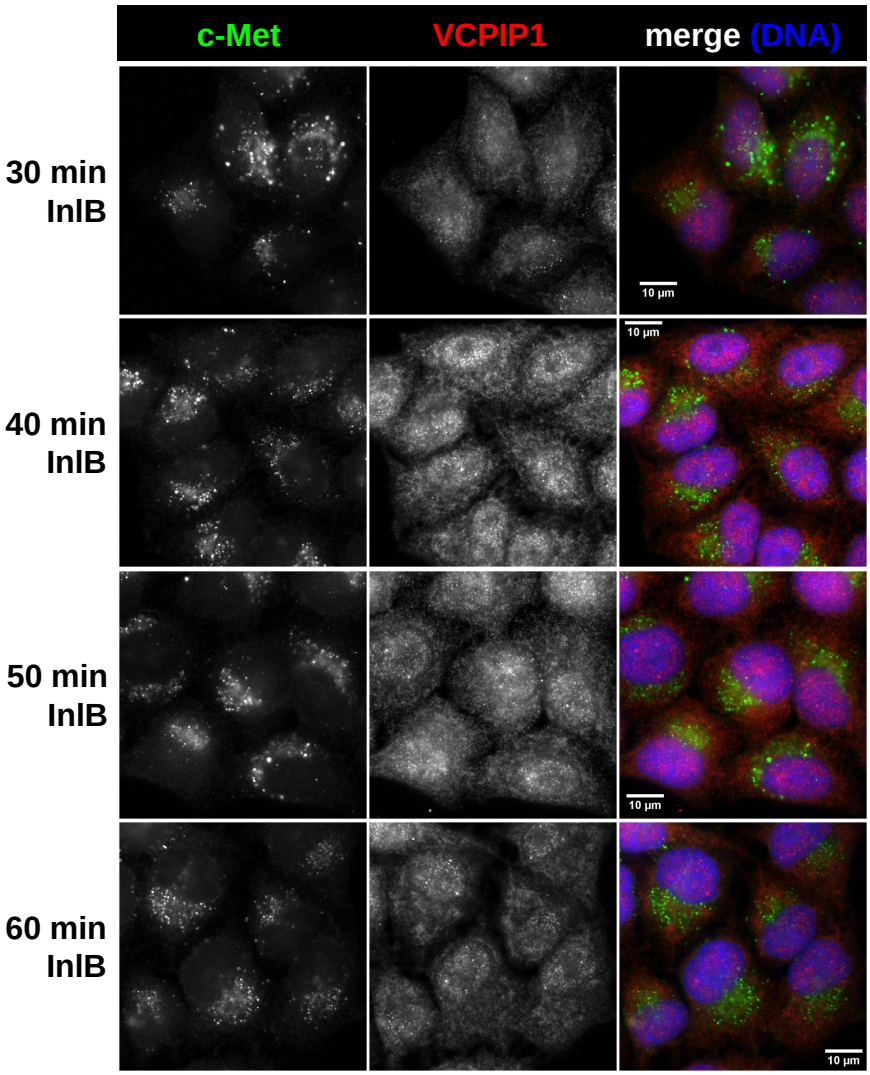

Figure S4. VCPIP1 localization during InlB stimulation in HeLa S3 cells. HeLa cells were stimulated with 10 nM InlB for the indicated time periods and subsequently stained for c-Met (green), VCPIP1 (red) and DNA content (blue). Finally, samples were analyzed via epifluorescence microscopy. The white bar represents 10 µm. The negative control (0 min(neg)) shows cells which were only starved, but not stimulated. The MES control is stimulated with the buffer of InlB for 60 min.

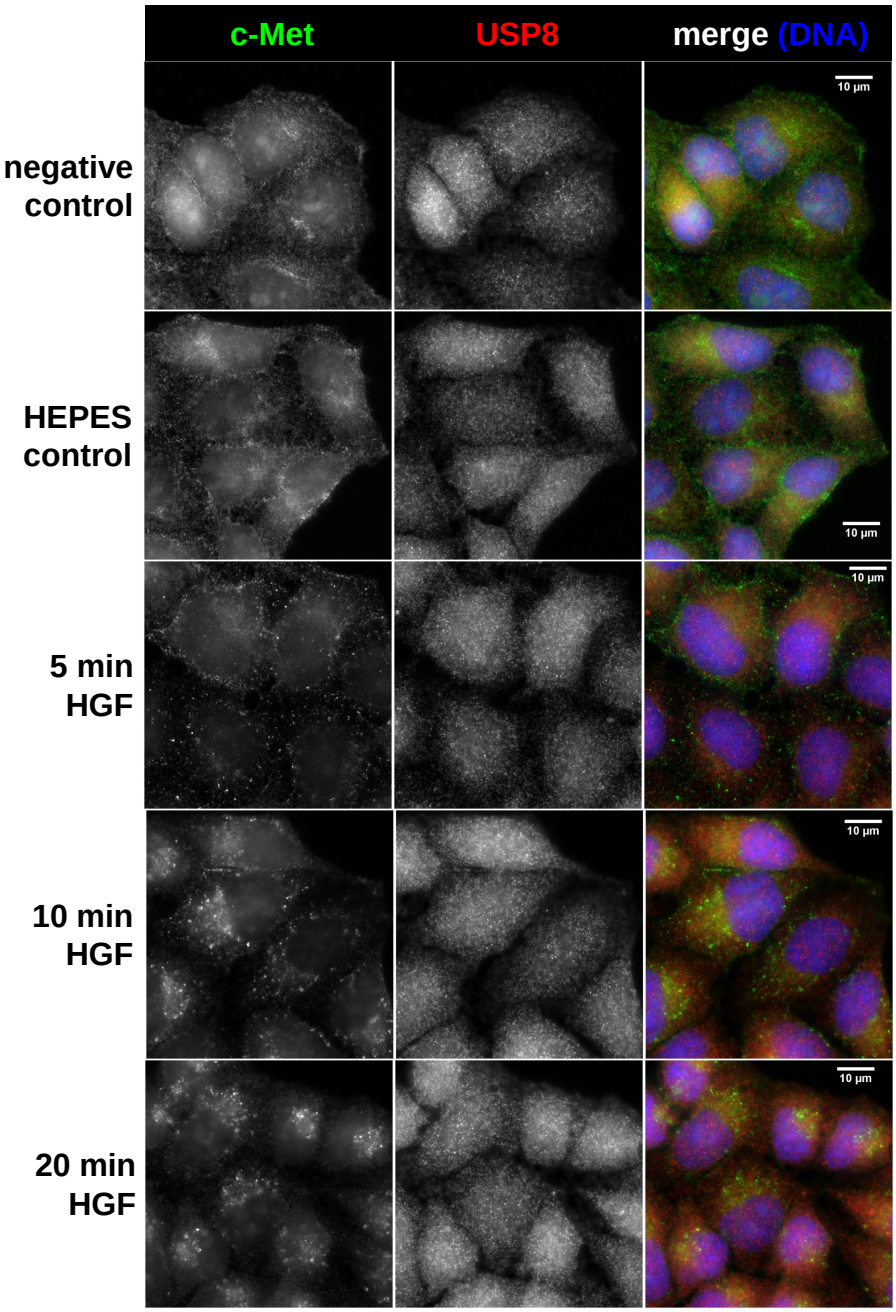

continued on the next page

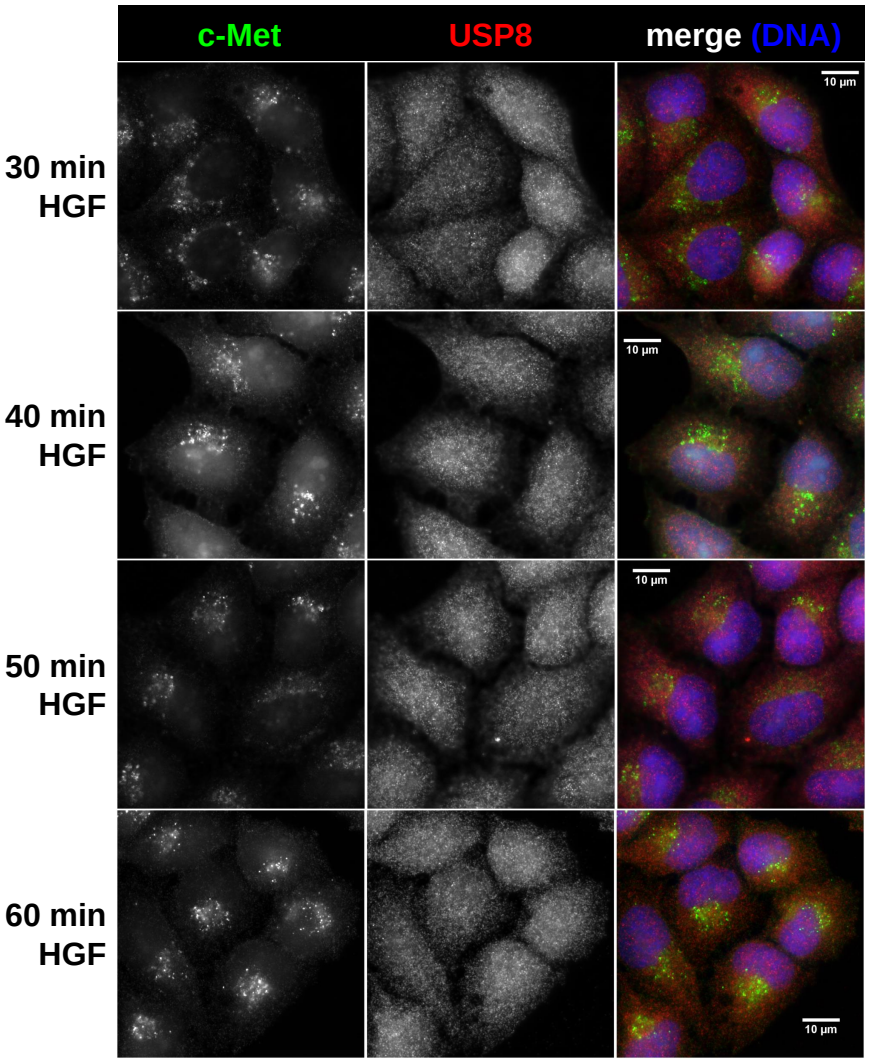

Figure S5. USP8 localization during HGF stimulation in HeLa S3 cells. HeLa cells were stimulated with 10 nM HGF for the indicated time periods and subsequently stained for c-Met (green), USP8 (red) and DNA content (blue). Finally, samples were analyzed via epifluorescence microscopy. The white bar represents 10 µm. The negative control (0 min(neg)) shows cells which were only starved, but not stimulated. The HEPES control is stimulated with the buffer of HGF for 60 min.

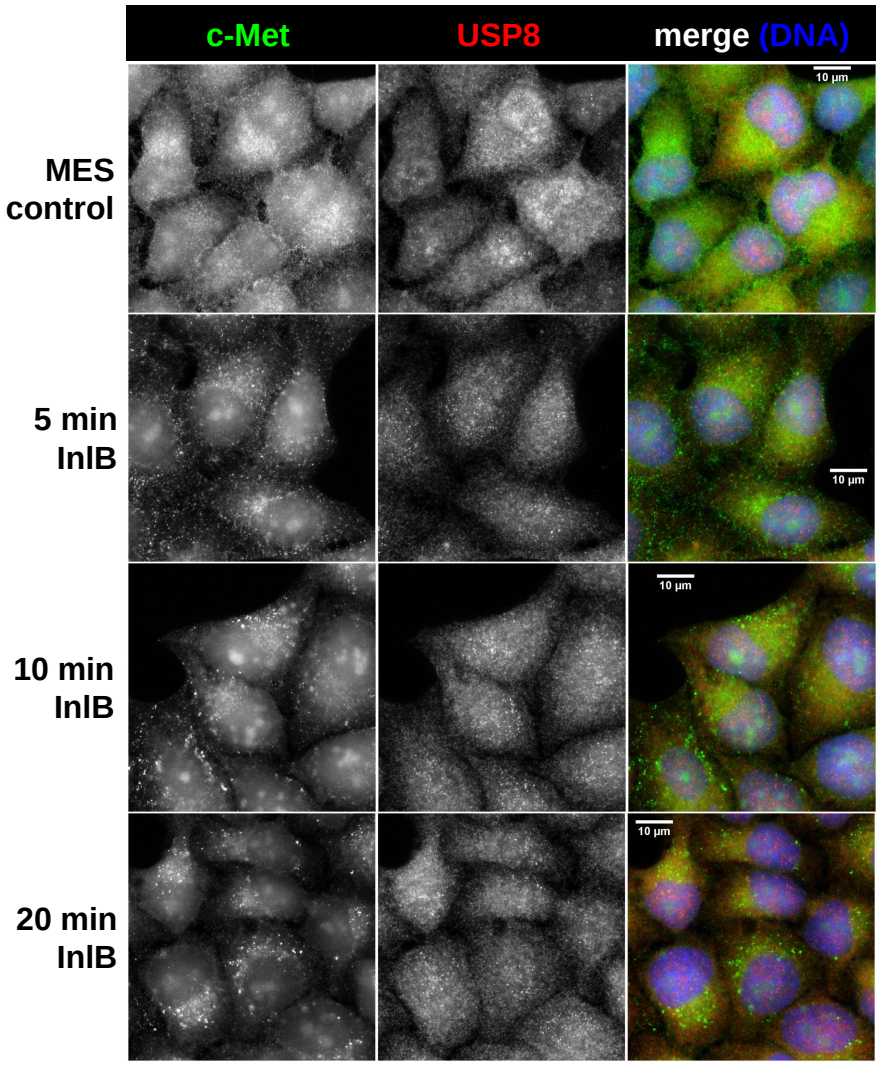

continued on the next page

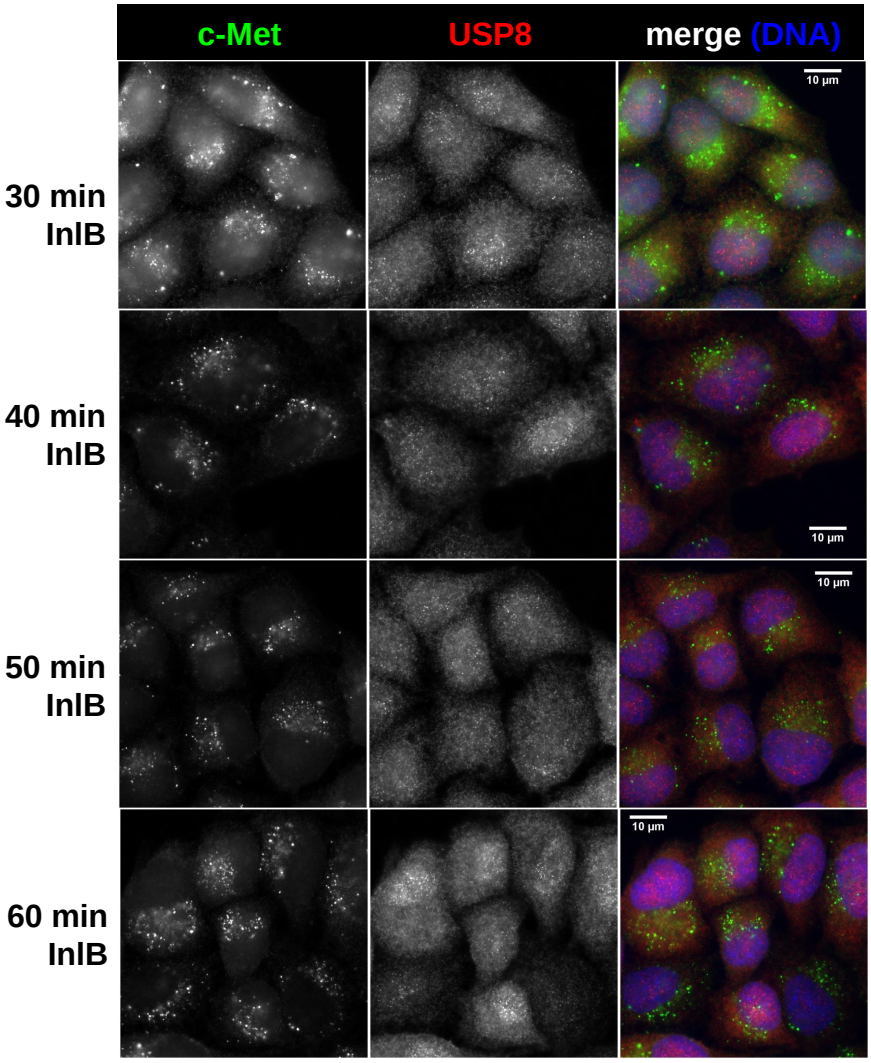

Figure S6. USP8 localization during InlB stimulation in HeLa S3 cells. HeLa cells were stimulated with 10 nM InlB for the indicated time periods and subsequently stained for c-Met (green), USP8 (red) and DNA content (blue). Finally, samples were analyzed via epifluorescence microscopy. The white bar represents 10 µm. The negative control (0 min(neg)) shows cells which were only starved, but not stimulated. The MES control is stimulated with the buffer of InlB for 60 min.

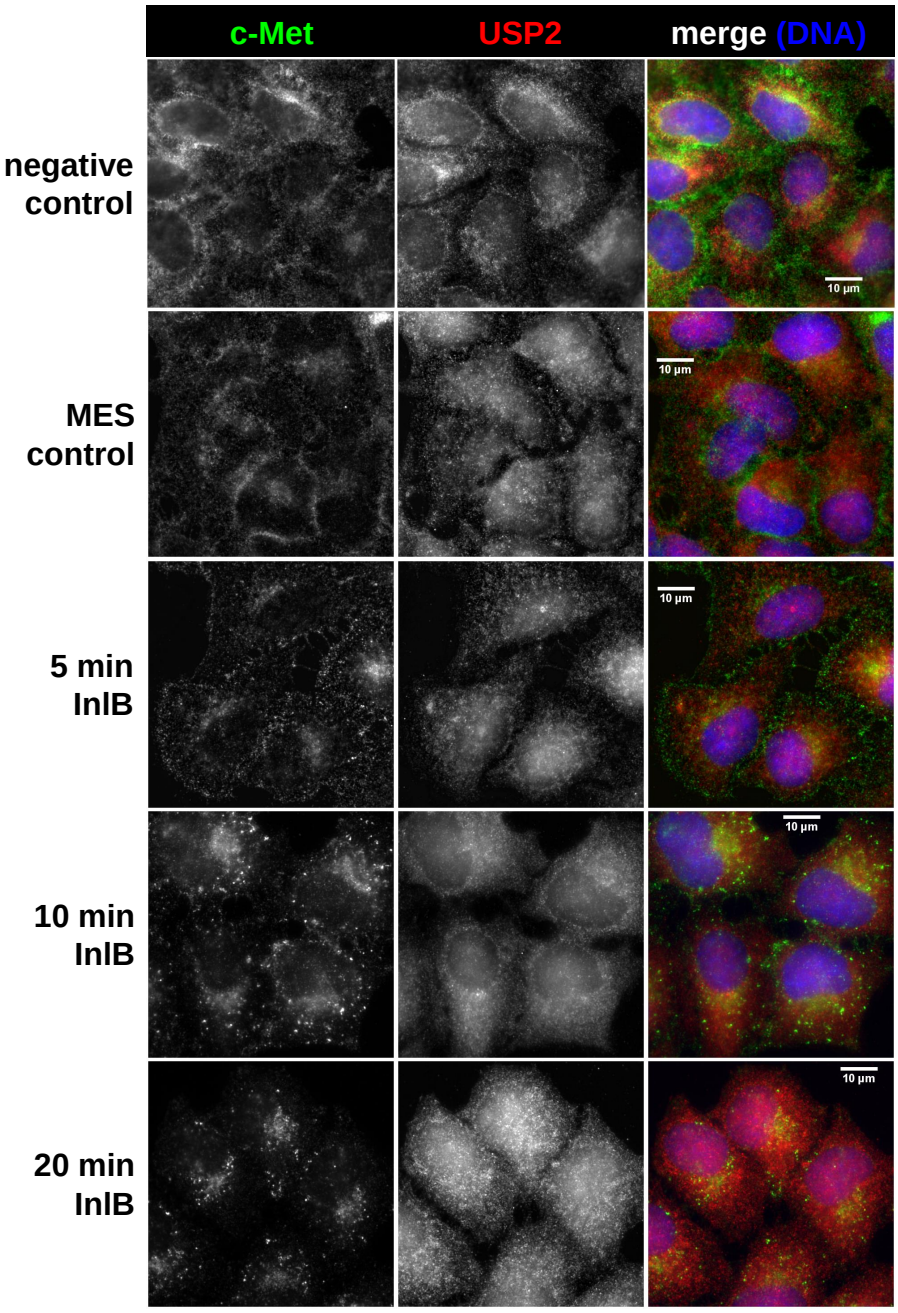

continued on the next page

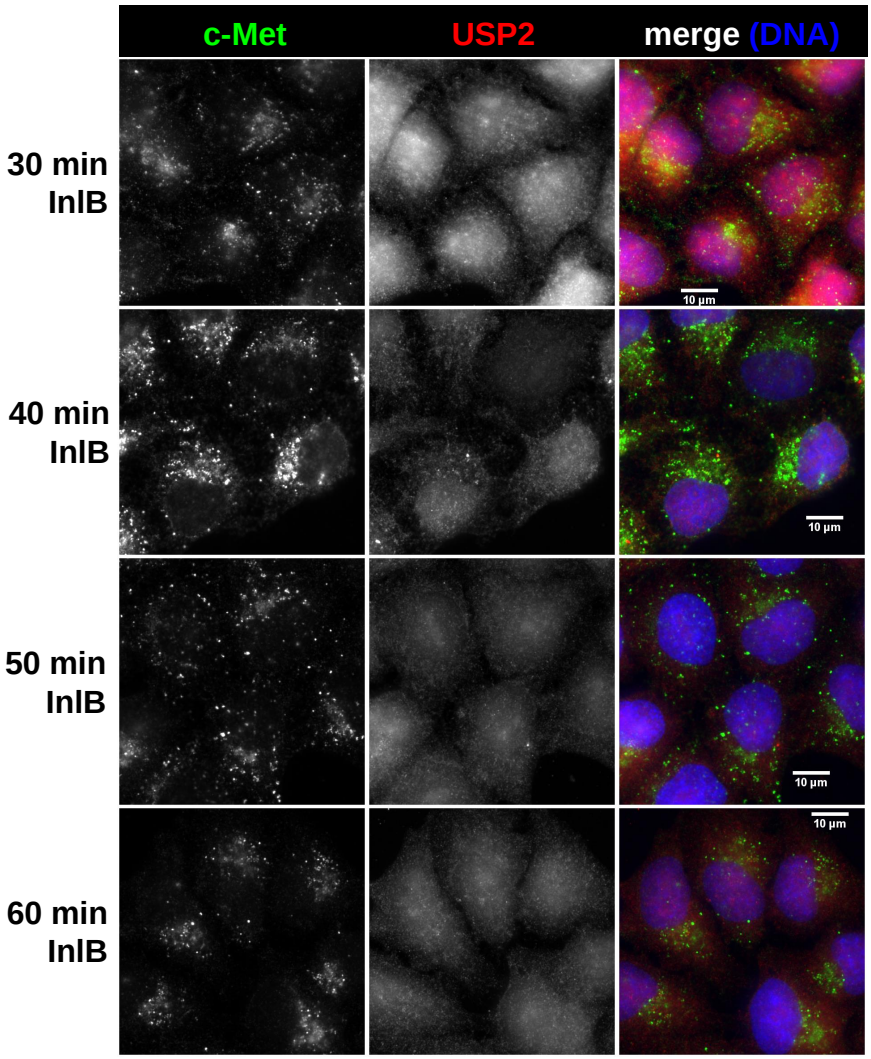

Figure S7. Localization of USP2 at distinct time points of InlB stimulation in HeLa S3 cells. All cells were stimulated with 10 nM InlB for the indicated time periods. Subsequently, stimulation was abolished by fixation of cells. Finally, the cells were stained for c-Met (green), USP2 (red) and DNA content (blue), and USP2 localization was evaluated. The white bar represents 10 µm. The 0 min (neg) sample was only rested but not stimulated. The MES control is stimulated with the buffer in which InlB was present for 60 min.

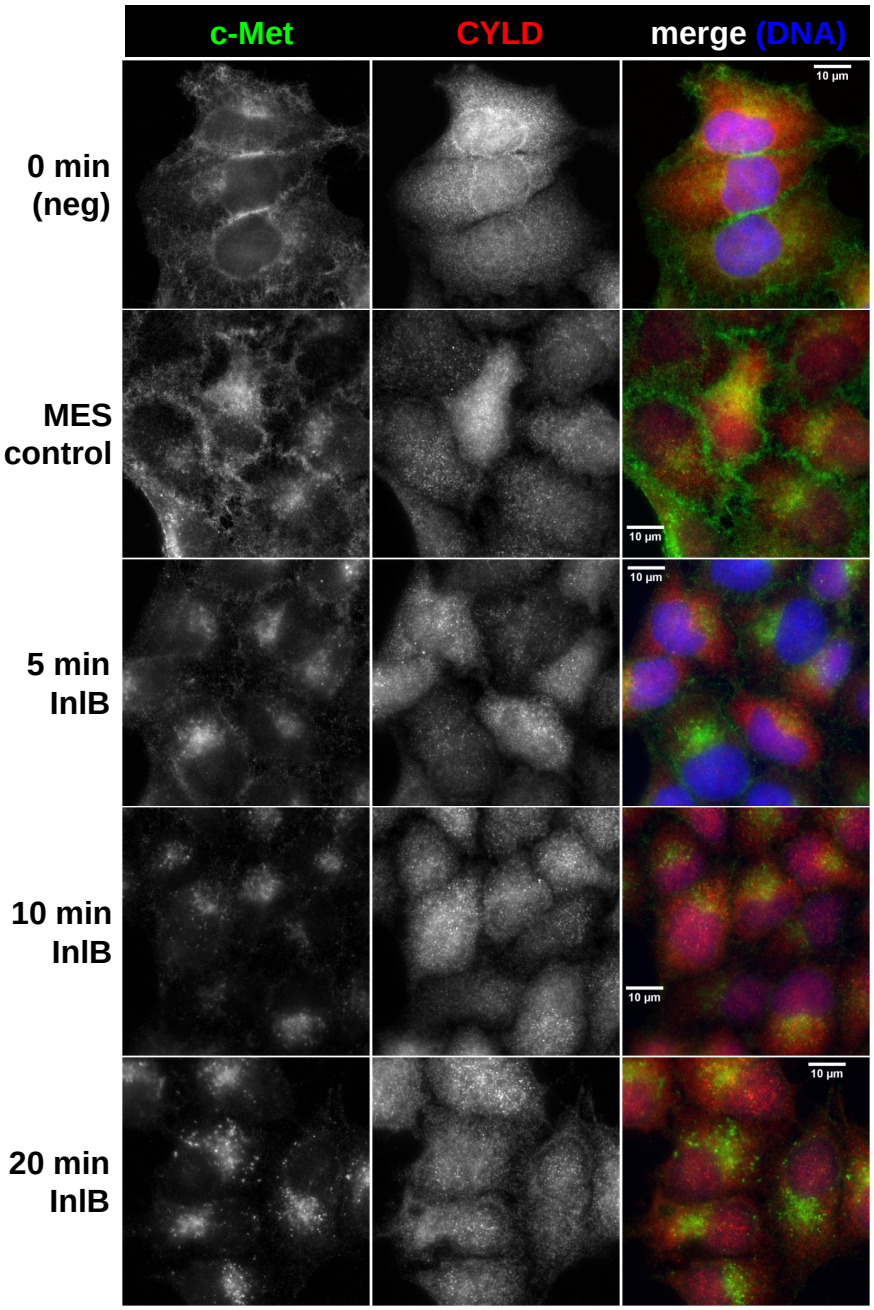

continued on the next page

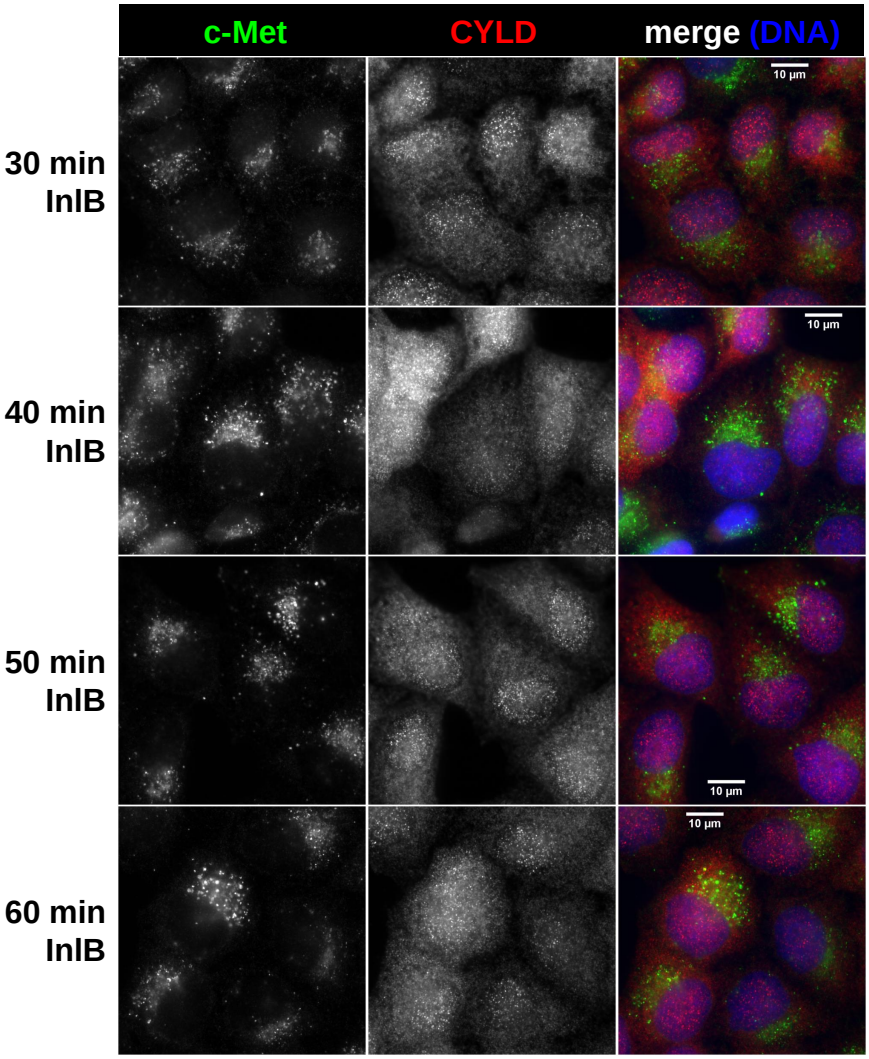

Figure S8. Localization of CYLD at distinct time points of InlB stimulation in HeLa S3 cells. All cells were stimulated with 10 nM InlB for the indicated time periods. Subsequently, stimulation was abolished by fixation of cells. Finally, the cells were stained for c-Met (green), CYLD (red) and DNA content (blue), and CYLD localization was evaluated. The white bar represents 10 µm. The 0 min (neg) sample was only rested but not stimulated. The MES control is stimulated with the buffer in which InlB was present for 60 min.

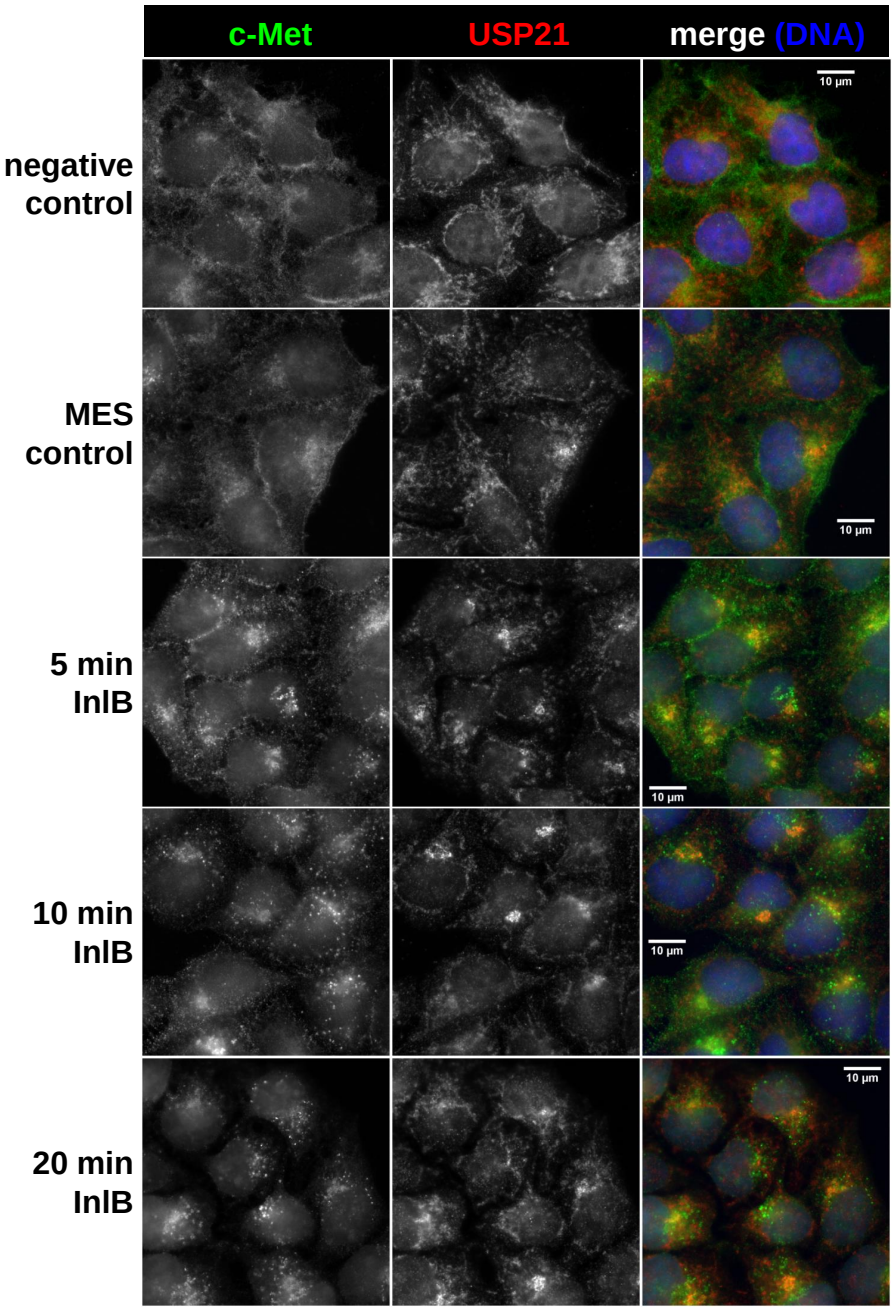

continued on the next page

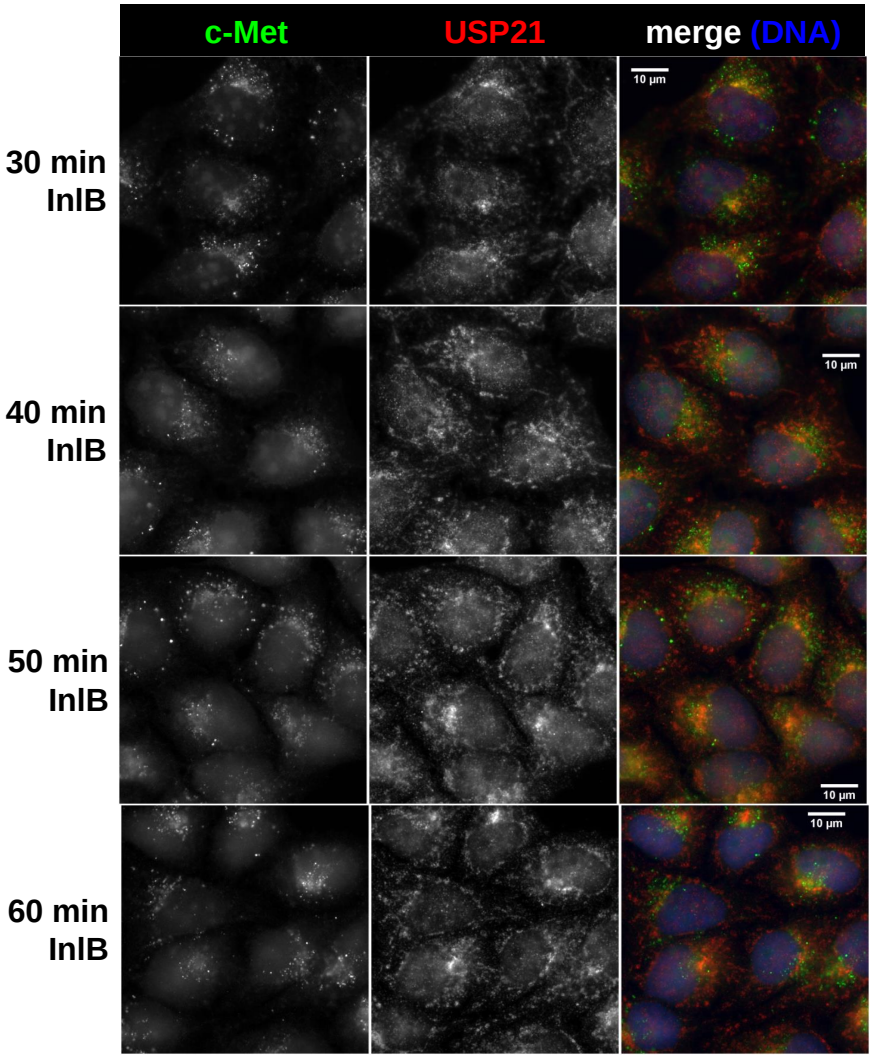

Figure S9. Localization of USP21 at distinct time points of InlB stimulation in HeLa S3 cells. All cells were stimulated with 10 nM InlB for the indicated time periods. Subsequently, stimulation was abolished by fixation of cells. Finally, the cells were stained for c-Met (green), CYLD (red) and DNA content (blue), and USP21 localization was evaluated. The white bar represents 10 µm. The 0 min (neg) sample was only rested but not stimulated. The MES control is stimulated with the buffer in which InlB was present for 60 min.

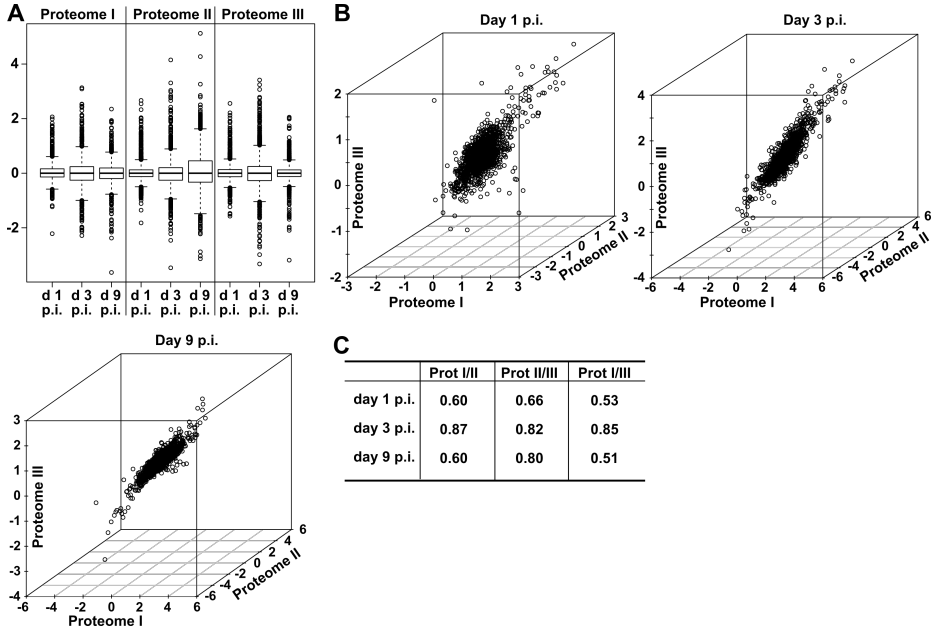

Figure S10. Statistical characterization of proteomic data from Lm infected liver samples. All plots were created using R software package (A) Boxplots of all samples are depicted. The plots indicate the variation in each individual sample by the box, representing 50 % of all data points and containing the median, which was normalized to zero as well as whiskers, which depict the quartiles. (B) Day-wise scatter plots of the replicates show a strong correlation at day 3 p.i. and weaker correlations at day 1 and 9 p.i.. (C) Individual day-wise Pearsson correlation factors for the dataset as calculated by R software.

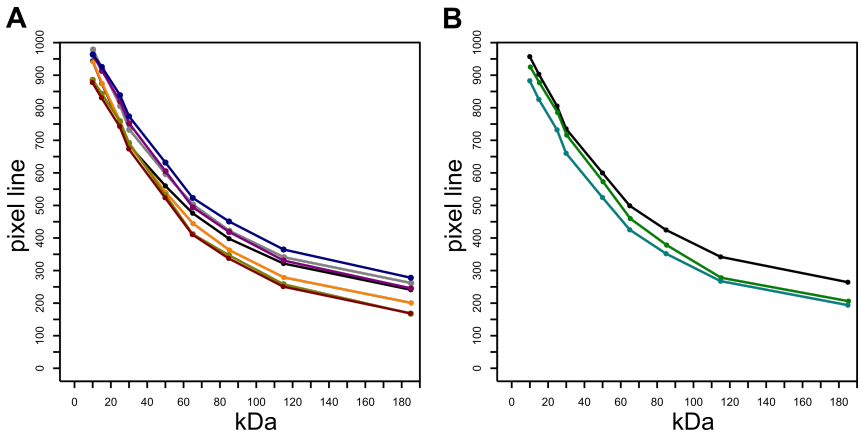

Figure S11. Extrapolation of marker pixel lines of ICU patient samples and healthy control samples utilized in this study for the read out of band molecular weight. (A) Extrapolation of markers from blots of ICU patient samples. (B) Extrapolation of markers from blots of healthy control samples. Lines between the determined marker bands were determined by linear conjunction of neighboring bands.

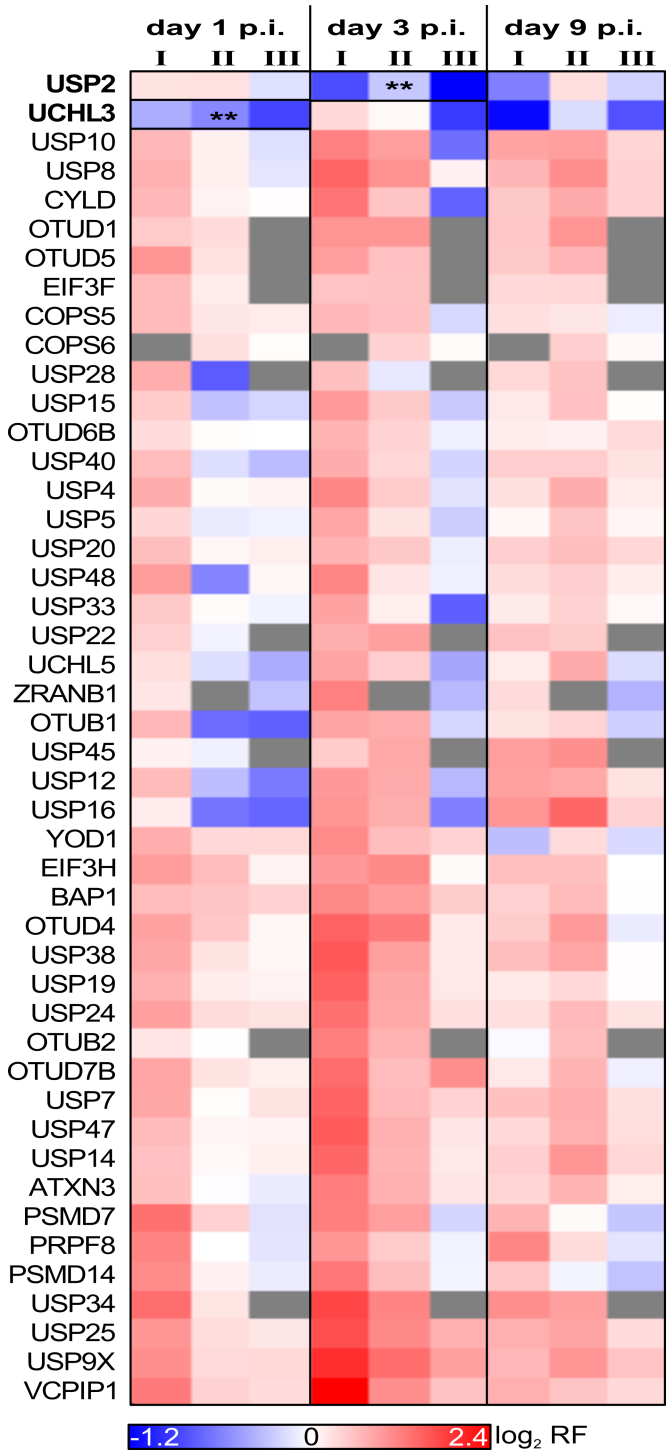

Figure S12. Regulation of active DUBs quantified in hepatic Lm infection illustrating RFs for each replicate. The columns show the regulation factors of each distinct DUB in a day-wise manner listing the three replicates individually. Downregulation is represented in blue, upregulation in red, gray signifies that DUBs were not found and significance in regulation is indicated by two asterisks (p-value < 0.01). Protein names of regulated proteins are displayed in bold. In general, the heat map revealed a high level of noise between the replicates with partly contradictory regulations for single DUBs.

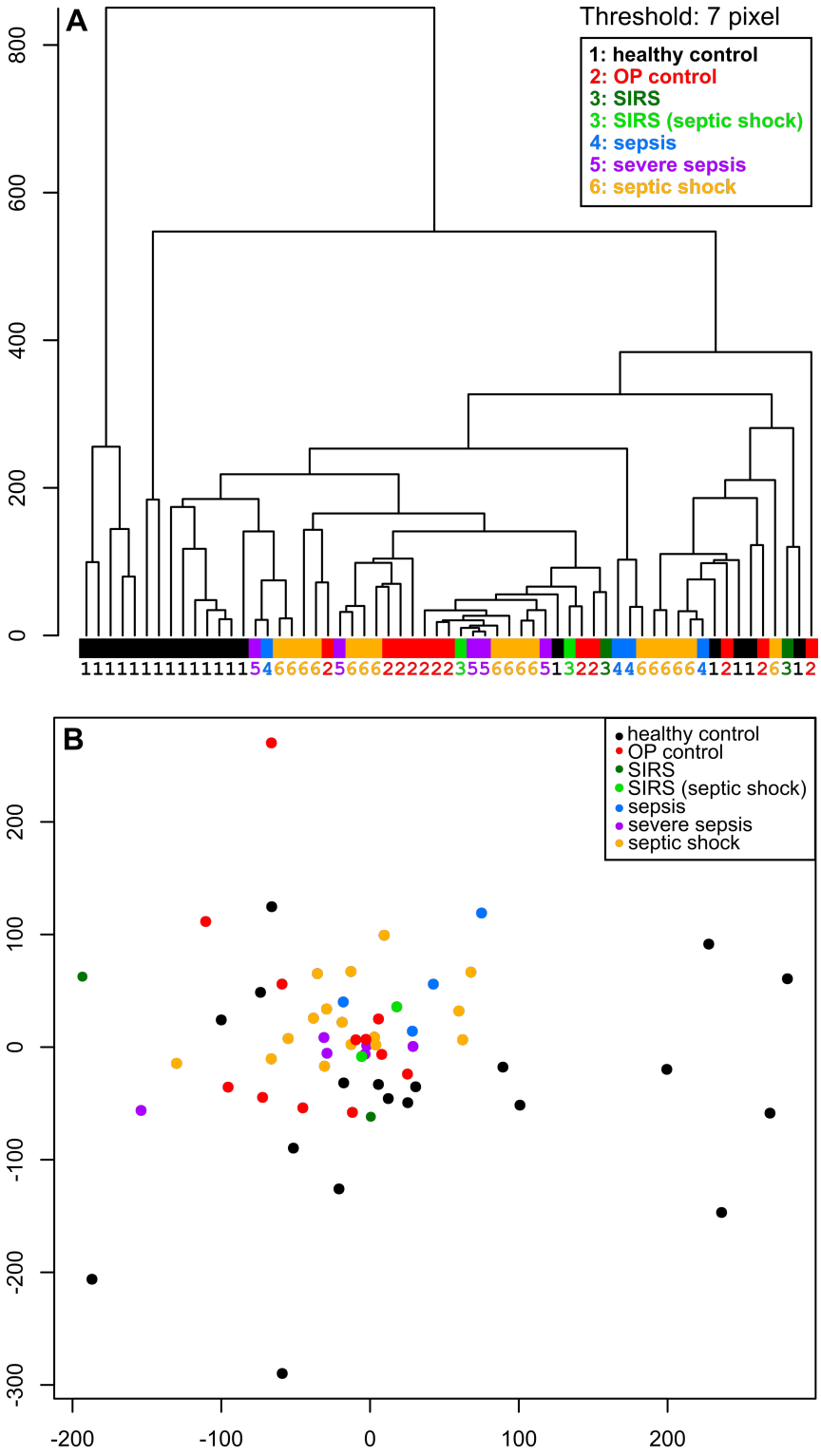

Figure S13. Results of hierarchical clustering and MDS for a threshold of 7 pixel. (A) Hierarchical clustering of all 61 samples. (B) MDS of the all samples. Hierarchical clustering and MDS were carried out for all samples utilizing R software.

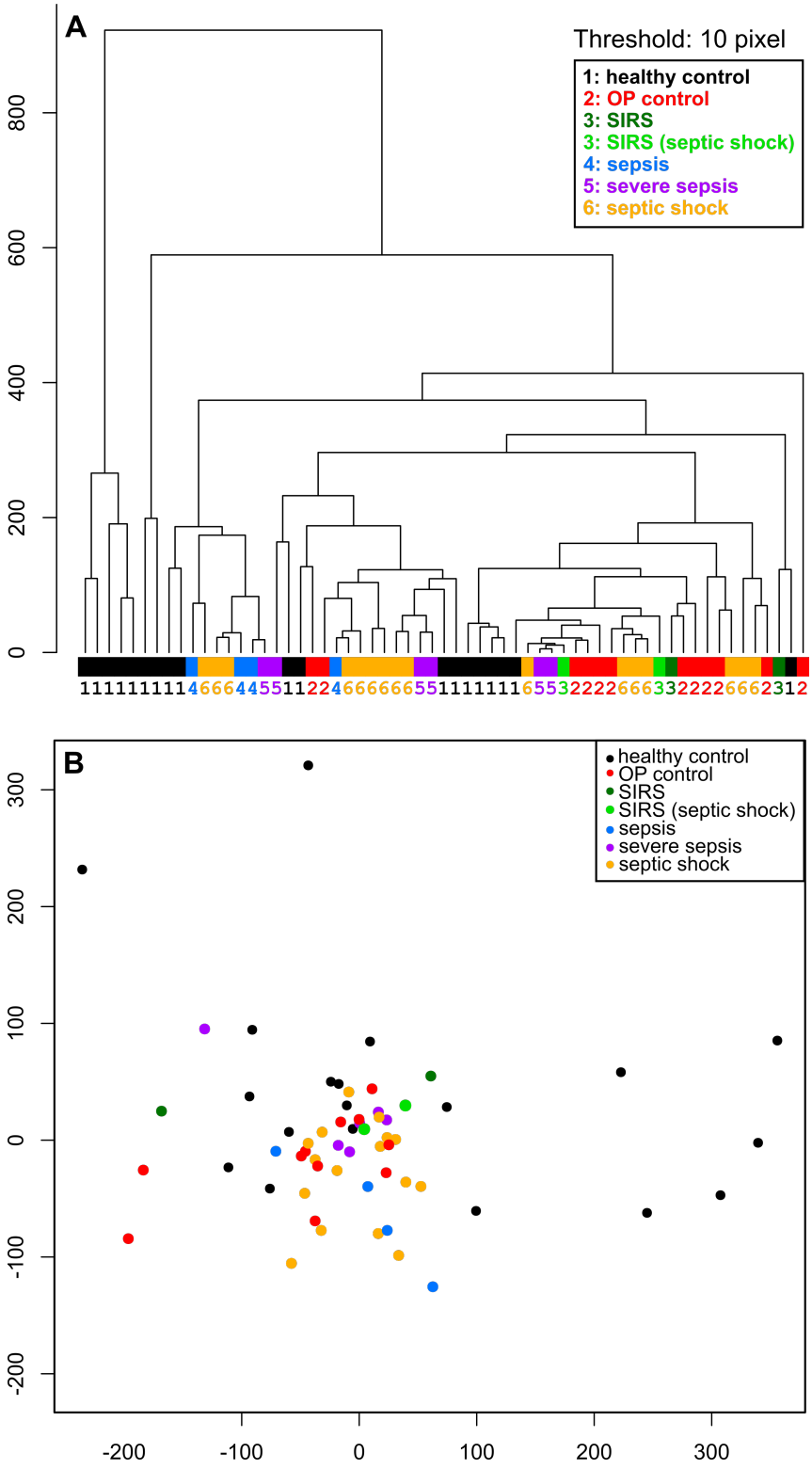

Figure S14. Results of hierarchical clustering and MDS for a threshold of 10 pixel. (A) Hierarchical clustering of all 61 samples. (B) MDS of the all samples. Hierarchical clustering and MDS were carried out for all samples utilizing R software.

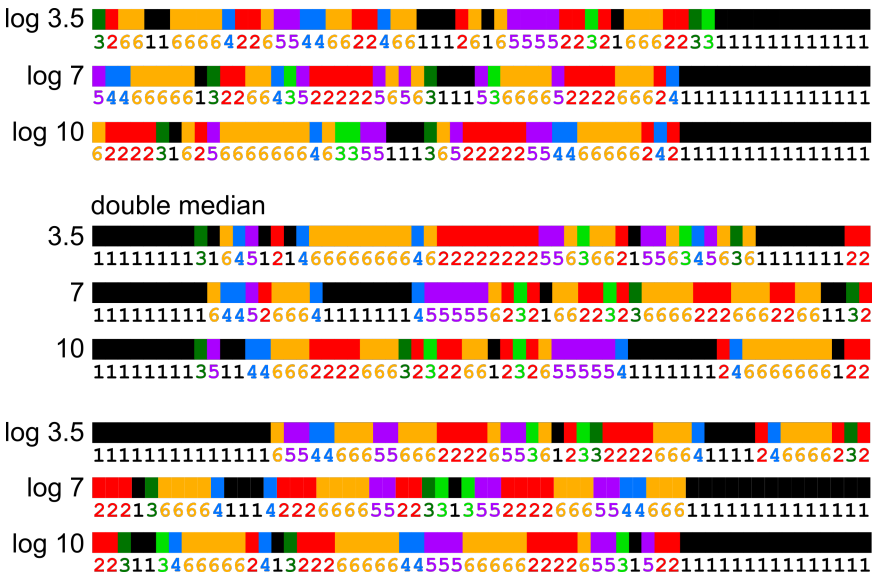

Figure S15. Results of hierarchical clustering of sepsis samples with different pixel thresholds. Hierarchical clustering was carried out for all samples utilizing R software. The thresholds on the left site describe the pixel difference that determines whether to bands were considered the same in different DUB patterns. The addition log indicates a logarithmic scaling of the data. Clusterings with double median were narrowed down to signals which showed intensities above the double median intensity of each individual experiment. The following color-code was used: 1 (black) = healthy controls, 2 (red) = OP controls, 3 (dark green) = SIRS, 3 (light green) = patients with SIRS but succeeding septic shock, 4 (blue) = sepsis, 5 (purple) = severe sepsis, 6 (orange) = septic shock.

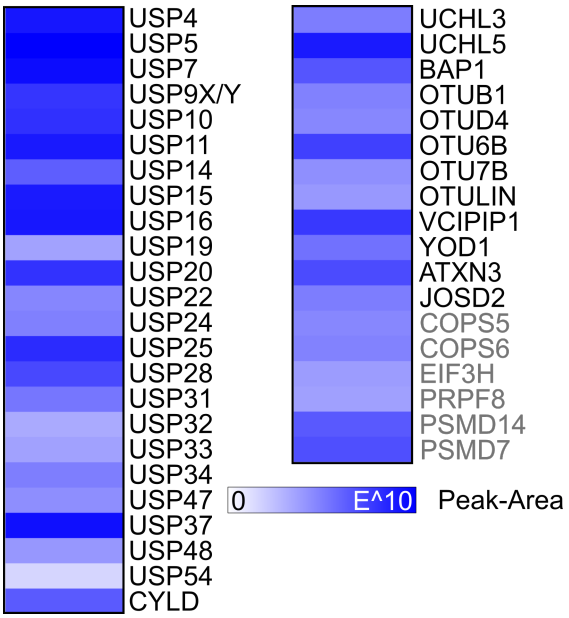

Figure S16. Heat map of DUBs identified via HA-IP in pool of 5 healthy control samples. Gray names indicate DUBs which were identified, but are in theory not reactive towards HAUb-VME. The blue color indicates the peak-area of proteins as determined by PD.

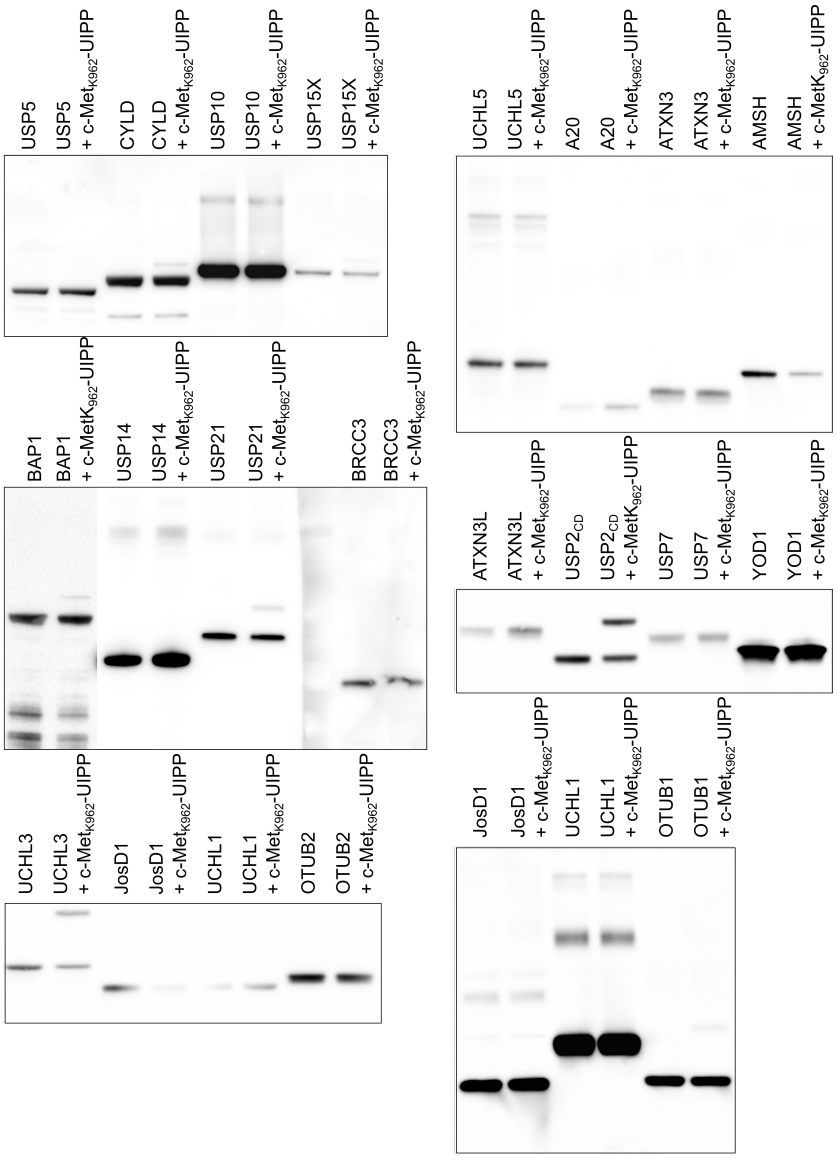

Figure S17. Shift-assays of the c-Met$_{K962}$-UIPP to identify DUBs which potentially remove Ub from the probed site. All recombinant DUBs were incubated with c-Met$_{K962}$-UIPP for 1 h at 37°C and subsequently evaluated by western blotting using an α-HIS$_6$ antibody for detection. A shift in the lane with UIPP as seen for CYLD, USP2, USP21, UCHL3, BAP1, USP15 and OTUB1 indicates binding of the probe to the respective DUB.

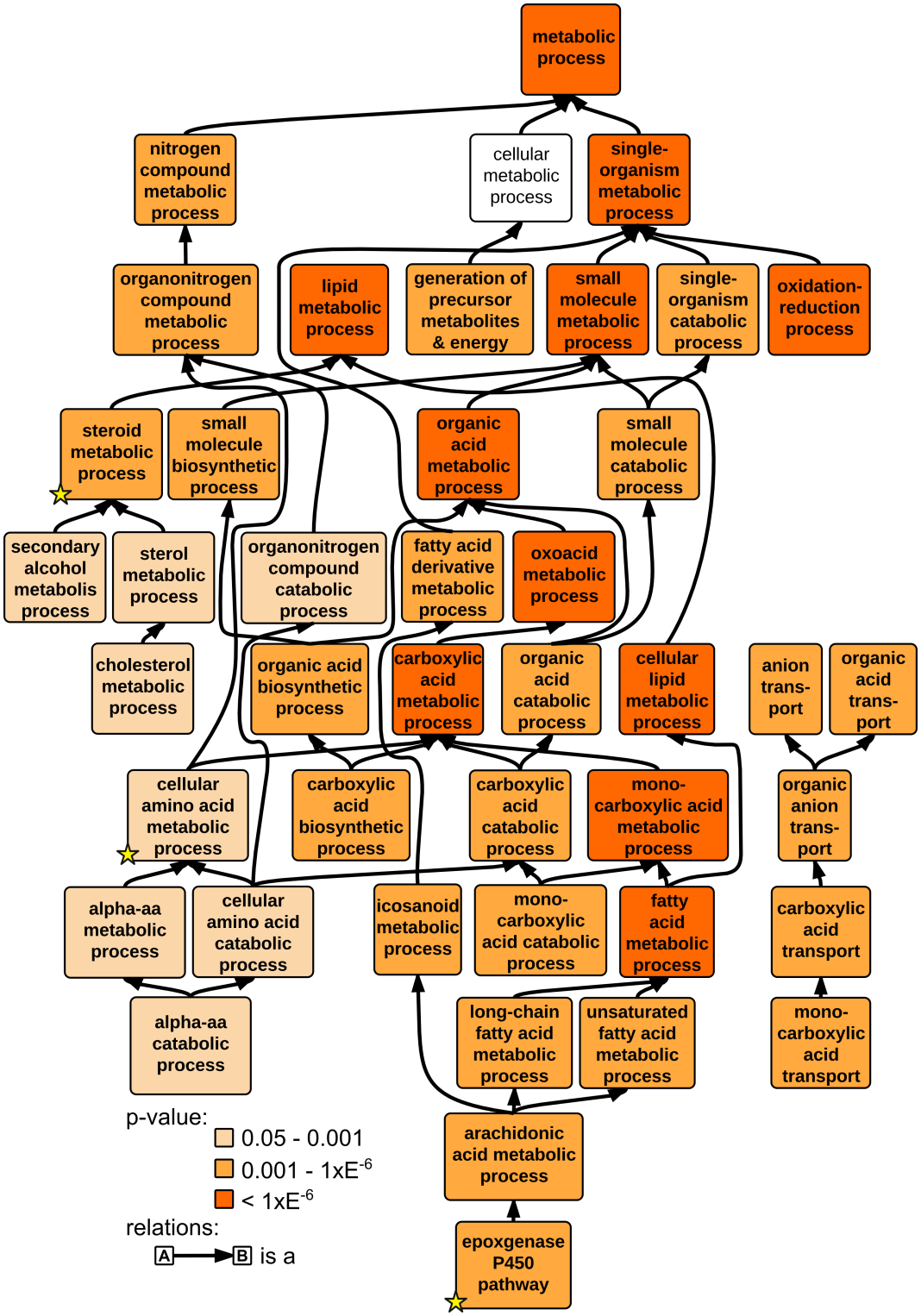

Figure S18. Enriched GO terms regarding biological processes involved in physiological metabolism during Lm infection. Regulated proteins were analyzed for their GO annotation in the category biological processes and enrichment against the whole dataset was calculated utilizing GOrilla tool (GO version 142) [322]. The p-values illustrated are corrected for multiple testing. Processes, which are discussed in more detail are marked with a yellow star.

Supplementary Tables

Table S1. c-Met ubiquitination sites as annotated in PhosphositePlus DB.
[1] Kim, W., Bennett, E.J., Huttlin, E.L., Guo, A., et al., Systematic and quantitative assessment of the ubiquitin-modified proteome. Mol. Cell 2011, 44, 325–40.
[2] Wagner, S.A., Beli, P., Weinert, B.T., Nielsen, M.L., et al., A proteome-wide, quantitative survey of in vivo ubiquitylation sites reveals widespread regulatory roles. Mol. Cell. Proteomics 2011, 10, M111.013284.
[3] Wagner, S. & Beli, P., Weinert, B.T., Scholz, C., et al., Proteomic analyses reveal divergent ubiquitylation site patterns in murine tissues. Mol. Cell. Proteomics 2012, 1578–1585.

Site	Org.	Sequence	Domain	Source
K189	human	AKVLSSVk DRFINFF	Sema	[1]
K223	human	VRRLKETk DGFMFLT	Sema	[1]
K324	human	LQAAYVSk PGAQLAR	Sema	[1]
K765	human	STITGVGk NLNSVSV	IPT/TIG (3.)	[1]
K962	human	LKKRKQIk DLGsELV	/	[1],[2]
K1104	human	LLDNDGKk IHCAVKS	kinase	CST curation set
K1161	human	LVVLPYMk HGDLRNF	kinase	[1]
K1190	human	GFGLQVAk GMKYLAS	kinase	[1]
K1193	human	LQVAKGMk YLASKKF	kinase	CST curation set
K1232	human	LARDMYDk EYYSVHN	kinase	[1]
K1240	human	EYYSVHNk TGAKLPV	kinase	[1]
K1529 K1257	human mouse	LESLQTQk FTTKSDV	kinase	Ub-remnant of HGF-stimulated HeLa S3 cells (Fig S1), [3]
K1318	human	PLYEVMLk CWHPKAE	kinase	CST curation set

Table S2. Parameters used for mass spectrometric measurements. HCD = Higher-energy collisional dissociation, CID = collision induced dissociation. Letters in brackets denote the analysis settings used in d = DUB-enrichment, p = proteome, m = DUB-enrichment in method development.

parameter	value (p/d)	value (s)	value (m)
mass spectrometer	3	3	1, 2
method duration	175 min	175 min	215 min
gradient duration	120 min	120 min	180 min
gradient composition	3.7% - 31.3 % solvent B	3.7% - 31.3 % solvent B	3.7% - 31.3 % solvent B
flow rate (load/run)	6 µL/min, 30 µL/min	6 µL/min, 30 µL/min	6 µL/min, 30 µL/min
MS-mode	data-dependent	data-dependent	data-dependent
method type	Top N	Top N	Top 10
survey cycle	3 s	3 s	/
collision technique	HCD	CID	CID
detector	orbitrap	ion trap	ion trap
scan range	350 - 1500	350 - 1500	400 - 2000
collision energy	38	35	35
charge states	2-4	2-4	2-4
max. collection time	60 ms	30 ms	100 ms
repeat count	1	1	1
exclusion duration	30 s	30 s	50 s

Table S3. Primers used for site-directed mutagenesis of pcDNA 3.1 c-Met-eGFP. All primers were designed to exchange lysine (K) to arginine (R) to produce ubiquitination-deficient mutants. The mutated codon is marked in bold letters in each sequence. Tm = melting temperature.

Name	Primer sequence (5' to 3')	Base exchange	Tm [°C]	GC content [%]
c-Met K962R for	GGCTGAAAAAGAG AAAGCAAATT**AGA** GATCTGGGCAGTG	AAA ⇒AGA	79.5	43.6
rev	CACTGCCCAGATC **TCT**AATTTGC TTTCTCTTTTTCA GCC	TTT ⇒TCT		
c-Met K1103R for	GGACAATGATGGC **AGG**AAAATTCACT GTGCTGTG	AAG⇒AGG	78.0	47.1
rev	CACAGCACAGTGA ATTTT**CCT**GCCAT CATTGTCC	CTT⇒CCT		
c-Met K1104R for	GGACAATGATGGC AAG**AGA**ATTCACT GTGCTGTG	AAA ⇒AGA	78.0	47.1
rev	CACAGCACAGTGA AT**TCT**CTTGCCAT CATTGTCC	TTT ⇒TCT		
c-Met K1103R K1104R for	GGACAATGATGGC **AGGAGA**ATTCACT GTGCTGTG	AAG ⇒AGG AAA ⇒AGA	77.8	48.6
rev	CACAGCACAGTGA AT**TCTCCT**GCC ATCATTGTCCAAC	CTT ⇒CCT TTT ⇒TCT		
c-Met K1259R for	GGAAAGTCTGCAA ACTCAA**AGG**TTTA CCACCAAGTCAG	AAG ⇒AGG	79.4	44.7
rev	CTGACTTGGTGGT AAA**CCT**TTGAGTT TGCAGACTTTCC	CTT⇒CCT		

Accession	Description	GO (biological process)	source	no. of repl.	mean RF d1/d0	mean RF d3/d0	mean RF d9/d0	p-value d1	p-value d3	p-value d9
Q60590	Alpha-1-acid glycoprotein 1 [A1AG1_MOUSE]	acute-phase response	[1,2]	3	**2.077**	**2.658**	0.506	3.16E-10	< 1E-44	1
Q91WP6	Serine protease inhibitor A3N [SPA3N_MOUSE]	acute-phase response	[3], Uniprot-KW (electronical)	3	**1.630**	**3.276**	1.350	2.02E-10	9.15E-13	1
P01027	Complement C3 [CO3_MOUSE]	complement activation	[1,2]	3	**1.514**	**2.257**	0.504	8.75E-11	7.05E-17	1
Q91X72	Hemopexin [HEMO_MOUSE]	positive regulation of response to interferon-gamma	[1]	3	**1.456**	**2.318**	0.534	6.84E-27	< 1E-44	0.469225283
Q8K0E8	Fibrinogen beta chain [FIBB_MOUSE]	cellular response to interleukin-1	[1,2]	3	**1.366**	**2.694**	0.576	3.22E-14	1.09E-31	1
Q63886	UDP-glucuronosyltransferase 1-1 [UD11_MOUSE]	acute-phase response	Uniprot (Ensemble)	3	1.300	**1.715**	0.427	1	4.16E-11	1
Q75N73	Zinc transporter ZIP14 [S39AE_MOUSE]		[4]	3	**1.211**	**2.533**	0.695	1.55E-27	1.54E-36	1
P10810	Monocyte differentiation antigen CD14 [CD14_MOUSE]	innate immune response	[1]	3	**1.153**	**1.803**	0.347	3.24E-08	< 1E-44	1
P04186	Complement factor B [CFAB_MOUSE]	complement activation	[1]	3	1.075	**2.048**	0.572	1	0.000785051	1
P25085	Interleukin-1 receptor antagonist protein [IL1RA_MOUSE]	acute-phase response	[1]	2	1.025	**0.891**	0.112	0.139520283	3.65E-22	1
P06909	Complement factor H [CFAH_MOUSE]	complement activation	[5]	3	0.975	**1.265**	0.138	1	1.22E-12	1
Q00898	Alpha-1-antitrypsin 1-5 [A1AT5_MOUSE]	response to cytokine	[1]	3	0.865	**1.275**	0.174	1	< 1E-44	1
Q921I1	Serotransferrin [TRFE_MOUSE]		[2]	3	**0.795**	**2.189**	0.533	0.006447222	2.90E-14	1
P07361	Alpha-1-acid glycoprotein 2 [A1AG2_MOUSE]	acute-phase response	[1,2]	3	**0.754**	**1.077**	**-0.085**	1.85E-41	< 1E-44	1.72E-06
Q8K182	Complement component C8 alpha chain [CO8A_MOUSE]	complement activation	[6]	3	0.738	2.322	**0.350**	1	< 1E-44	1.51E-07
P05367	Serum amyloid A-2 protein [SAA2_MOUSE]	acute-phase response	[1,2]	3	**0.658**	**1.605**	0.173	< 1E-44	< 1E-44	1
P07309	Transthyretin [TTHY_MOUSE]		[7]	2	0.584	**0.914**	0.231	1	0.001766509	1
P42227	Signal transducer and activator of transcription 3 [STAT3_MOUSE]	acute-phase response	[1]	3	**0.580**	**0.791**	0.127	2.18E-05	2.35E-07	1
P97290	Plasma protease C1 inhibitor[IC1_MOUSE]	complement activation	Uniprot-KW (electronical)	3	0.527	**0.963**	0.038	0.071904088	6.33E-18	1
Q6GQT1	Alpha-2-macroglobulin-P [A2MP_MOUSE]	negative regulation of complement activation	[2]	3	0.489	**0.945**	-0.100	1	< 1E-44	1
Q61646	Haptoglobin [HPT_MOUSE]	acute-phase response	[1,2]	3	**0.485**	**0.903**	0.320	2.31E-39	< 1E-44	1
P12246	Serum amyloid P-component [SAMP_MOUSE]	innate immune response	[1]	3	**0.441**	**0.806**	-0.019	2.92E-21	< 1E-44	1
P08607	C4b-binding protein [C4BPA_MOUSE]	complement activation	[1]	2	0.389	**0.898**	-0.161	1	0.003941319	1
Q9JJ00	Phospholipid scramblase 1 [PLS1_MOUSE]	acute-phase response	[8]	2	**0.365**	**1.568**	0.874	0.000956567	0.000191628	1
Q61838	Alpha-2-macroglobulin [A2M_MOUSE]		[1,2]	3	**0.352**	**-0.831**	-0.891	0.005974896	7.04E-09	1
Q00897	Alpha-1-antitrypsin 1-4 [A1AT4_MOUSE]		[1]	3	0.311	**2.334**	0.160	1	5.90E-08	1
P11276	Fibronectin [FINC_MOUSE]	acute-phase response	[9]	3	0.278	**2.267**	1.033	1	1.12E-05	1
P05366	Serum amyloid A-1 protein [SAA1_MOUSE]	acute-phase response	[1,2]	3	**0.175**	**0.545**	0.282	< 1E-44	< 1E-44	0.021912202
Q8VCM7	Fibrinogen gamma chain [FIBG_MOUSE]	innate immune response	[1,2]	3	**0.092**	**0.861**	0.386	7.59E-10	1.33E-10	1
Q61147	Ceruloplasmin [CERU_MOUSE]		[1,2]	3	**-0.032**	**0.689**	0.617	7.28E-20	7.05E-30	1
P01029	Complement C4-B[CO4B_MOUSE]	complement activation	[1]	3	-0.182	**-0.706**	-0.621	1	0.000353232	1
A6X935	Inter alpha-trypsin inhibitor, heavy chain 4 [ITIH4_MOUSE]	acute-phase response	[1]	3	**-0.955**	**-1.444**	0.598	5.51E-10	2.85E-37	1

Table S4. Proof-of-concept: Acute-phase proteins and complement activating components found in this study.

[1] Gruys, E., Toussaint, M.J.M., Niewold, T.A., Koopmans, S.J., Acute phase reaction and acute phase proteins. J. Zhejiang Univ. Sci. B 2005, 6, 1045–56.

[2] Bode, J.G., Albrecht, U., Häussinger, D., Heinrich, P.C., Schaper, F., Hepatic acute phase proteins - Regulation by IL-6- and IL-1-type cytokines involving STAT3 and its crosstalk with NF-κB-dependent signaling. Eur. J. Cell Biol. 2012, 91, 496–505.

[3] Law, R.H.P., Zhang, Q., McGowan, S., Buckle, A.M., et al., An overview of the serpin superfamily. Genome Biol. 2006, 7, 216.

[4] Liuzzi, J.P., Lichten, L.A., Rivera, S., Blanchard, R.K., et al., Interleukin-6 regulates the zinc transporter Zip14 in liver and contributes to the hypozincemia of the acute-phase response. Proc. Natl. Acad. Sci. U. S. A. 2005, 102, 6843–8.

[5] Ruseva, M.M., Hughes, T.R., Donev, R.M., Sivasankar, B., et al., Crry deficiency in complement sufficient mice: C3 consumption occurs without associated renal injury. Mol. Immunol. 2009, 46, 803–11.

[6] Späth, G.F., Ramadori, G., Rittner, C., Schneider, P.M., Expression of the complement C8 genes during interleukin-6-mediated in vitro induction of the acute-phase response. Exp. Clin. Immunogenet. 1995, 12, 53–60.

[7] Ingenbleek, Y., Young, V., Transthyretin (prealbumin) in health and disease: nutritional implications. Annu. Rev. Nutr. 1994, 14, 495–533.

[8] Lu, B., Sims, P.J., Wiedmer, T., Moser, A.H., et al., Expression of the phospholipid scramblase (PLSCR) gene family during the acute phase response. Biochim. Biophys. Acta 2007, 1771, 1177–85.

[9] Dyck, R.F., Rogers, S.L., Fibronectin is an acute phase reactant in mice. Clin. Invest. Med. 1985, 8, 148–51.

Table S5. Identified but non-regulated members of the cytochrome P450 family.** = found in 2 out of three replicates, * = found in one replicate. Regulation, if observed, was not significant for all listed proteins.

[1] Pan, J., Xiang, Q., Ball, S., Scatina, J., et al., Lipopolysaccharide-mediated modulation of cytochromes P450 in STAT1 null mice. Drug Metab. Dispos. 2003, 31, 392–397.

Gene name	d1/d0 mean RF	d3/d0 mean RF	d9 /d0 mean RF	Regulation in (Lm) infection
Cyp3a13	0.19	0.46	-0.08	
Cyp2a12	-0.04	-0.52	-0.62	
Cyp2d11	-0.07	-0.54	-0.25	
Cyp2d26	-0.19	-0.40	-0.63	
Cyp4f3	0.20	-0.29	-0.38	
Cyp2d10	-0.13	-0.39	-0.39	
Cyp2e1	-0.28	-0.36	-0.41	LPS: stable (mRNA), protein content reduced (STAT1 dependent) [1]
Cyp4v2	-0.09	-0.29	-0.11	
Cyp20a1	0.00	0.13	-0.19	
Cyp4b1	-0.43	0.01	-0.19	
Cyp2j5	-0.14	-0.10	-0.09	
Cyp27a1	0.01	-0.36	-0.19	
Cyp51a1	0.36	-0.29	-0.20	
Cyp7a1**	-1.23	-1.98	-0.83	
Cyp2j6*	0.16	-0.09	-0.21	
Cyp2b19 **	0.04	-1.42	-1.88	
Cyp2c55 **	0.18	0.10	0.30	

Table S6. Non-cytochrome phase I proteins of biotransformation quantified in Lm infected liver. Significant regulation is indicated by symbols (▼= downregulation, ▲= upregulation)

Gene name	Protein name	d1/d0 mean RF	d3/d0 mean RF	d9 /d0 mean RF
Por	NADPH-cytochrome P450 reductase	-0.05	-0.42	-0.40
Fmo2	Dimethylaniline monooxygenase 2	0.03	▼ -0.60	▼ -0.83
Fmo3	Dimethylaniline monooxygenase 3	-0.31	▼ -2.01	▼ -2.03
Fmo1	Dimethylaniline monooxygenase 1	-0.06	-0.61	-0.46
Fmo5	Dimethylaniline monooxygenase 5	-0.06	-0.30	-0.06
Fmo4	Dimethylaniline monooxygenase 4	-0.09	-0.33	-0.34
Adh1	Alcohol dehydrogenase 1	-0.31	▼ -0.90	-0.85
Adh4	Alcohol dehydrogenase 4	-0.32	▼ -0.68	0.38
Adh5	Alcohol dehydrogenase 5	-0.09	-0.14	-0.26
Akr1a1	Alcohol dehydrogenase [NADP(+)]	-0.12	-0.08	-0.24
Maoa	Amine oxidase A	-0.11	▼ -0.58	-0.47
Maob	Amine oxidase B	-0.28	▼ -0.96	-0.75

Table S7. Phase II proteins of biotransformation quantified in Lm infected liver. Significant regulation is indicated by symbols (▼= downregulation, ▲= upregulation). ** = found in 2 out of three replicates, * = found in one replicate.

Gene name	Protein name	d1/d0 mean RF	d3/d0 mean RF	d9 /d0 mean RF
Gsto1	Glutathione S-transferase omega-1	-0.18	▼ -0.61	-0.68
Gstp1	Glutathione S-transferase P 1	0.24	▲ 2.12	▲ 2.03
Gstm6	Glutathione S-transferase Mu 6	-0.14	▼ -0.54	0.20
Gstt1	Glutathione S-transferase theta-1	-0.12	▼ -0.86	▼ -1.14
Gstt2	Glutathione S-transferase theta-2	-0.27	▼ -0.58	-0.77
Gstm3	Glutathione S-transferase Mu 3	-0.14	-0.26	▲ 1.63
Gsta2**	Glutathione S-transferase A2	-0.34	▼ -0.71	-0.19
Gstm1*	Glutathione S-transferase Mu 1	-0.17	-0.27	2.79
Gsta1	Glutathione S-transferase A1	-0.01	0.45	-0.05
Gstm2	Glutathione S-transferase Mu 2	-0.10	-0.45	-0.56
Gsta4	Glutathione S-transferase A4	-0.21	-0.50	-0.53
Gsta3	Glutathione S-transferase A3	-0.09	-0.33	-0.16
Gstm5	Glutathione S-transferase Mu 5	-0.14	-0.03	-0.36
Gstm7	Glutathione S-transferase Mu 7	-0.02	-0.39	0.18
Mgst1	Microsomal glutathione S-transferase 1	-0.35	-0.26	0.18
Gstk1	Glutathione S-transferase kappa 1	0.03	-0.34	-0.60
Ugt2a3	UDP-glucurono-syltransferase 2A3	-0.13	▼ -0.61	-0.91
Ugt1a1	UDP-glucurono-syltransferase 1-1	0.35	▼ -0.83	-0.89
Ugt2b17	UDP-glucuronosyltransferase 2B17	-0.14	-0.06	0.01
Ugt3a1	UDP-glucuronosyltransferase 3A1	-0.21	-0.38	-0.81
Ugt1a9	UDP-glucuronosyltransferase 1-9	0.02	-0.42	-0.38
Ugt1a6	UDP-glucuronosyltransferase 1-6	0.12	0.11	-0.02
Ugt3a2	UDP-glucuronosyltransferase 3A2	0.00	-0.55	-0.61
Cml1	Probable N-acetyltransferase CML1	-0.38	▼ -1.05	-0.27
Acat1	Acetyl-CoA acetyltransferase, mitochondrial	-0.06	▼ -0.46	▼ -0.73
Baat	Bile acid-CoA:amino acid N-acyltransferase	-0.06	▼ -0.53	-0.23
Nat2	Arylamine N-acetyltransferase 2	0.03	0.00	-0.17
Hgsnat*	Heparan-alpha-glucosaminide N-acetyltransferase	0.03	0.06	0.12
Naa50	N-alpha-acetyltransferase 50	0.04	0.20	-0.10
Naa38	N-alpha-acetyltransferase 38, NatC auxiliary subunit	0.02	0.20	0.34
Naa15	N-alpha-acetyltransferase 15, NatA auxiliary subunit	0.07	0.33	-0.04
Acat2	Acetyl-CoA acetyltransferase, cytosolic	-0.06	-0.37	-0.48
Cml2	Probable N-acetyltransferase CML2	0.04	0.27	0.40
Naa16**	N-alpha-acetyltransferase 16, NatA auxiliary subunit	-0.18	-0.01	-0.19
Gnpnat1	Glucosamine 6-phosphate N-acetyltransferase	-0.06	0.02	-0.19
Naa10*	N-alpha-acetyltransferase 10	-0.03	0.12	-0.13

Table S8. Overview of identified DUBS and recorded unique spectra in the HA-IP approach comparing HAUb-VME and HAUb-VFEA. To be considered for this table, DUBs had to be identified by 1 peptide, with a Scaffold 3.0 minimum protein probability of 99 % and a minimum peptide probability of 95 %. Additionally, all identifications with only one unique spectrum, marked in red in the table, were discarded before further evaluation. Furthermore, the molecular weight extracted from Uniprot DB and used for normalization is listed for each DUB.

	contr. I	contr. II	contr. III	VME I	VME II	VME III	VFEA I	VFEA II	VFEA III	MW [kDa]
USP1				35	31	33	31	30	28	87.456
USP3						1	5	3	1	58.868
USP4		1	8	90	69	83	101	77	87	108.343
USP5	1	9	11	72	64	75	80	76	81	95.833
USP7		3	9	135	103	125	133	118	130	128.475
USP8			1	62	43	63	78	72	67	122.611
USP9X		4	3	156	127	138	162	144	148	209.711
USP10				20	16	27	1	1		87.134
USP12				3	2	7	4	4	5	42.914
USP14	1	4	5	76	61	78	82	61	73	56.002
USP15		1	4	86	67	73	87	79	83	112.419
USP16				39	35	45	50	38	42	93.406
USP17L2				5	3	3	4	2	1	60.219
USP19			4	69	52	82	87	80	88	150.549
USP20				18	16	19	21	18	14	36.429
USP22				4	1	6	5	3	4	59.954
USP24	1			63	47	81	53	48	61	294.001
USP25				63	53	76	29	9	20	121.420
USP28				37	37	42	40	27	31	119.318
USP30				2		2				58.221
USP33				41	32	32	41	34	36	102.728
USP34				60	47	60	11	3	9	408.214
USP36				8	7	7	10	6	7	119.913
USP37				38	32	38	18	10	15	110.063
USP38		1		50	51	59	53	55	53	116.102
USP42		3		22	25	25	22	19	24	146.223
USP45				12	9	13	14	17	15	90.361
USP46				13	10	12	13	11	15	42.442
USP47			5	128	115	129	127	122	123	157.455
USP48			1	67	53	68	20	9	18	120.631
CYLD		1		52	39	52	17	7	12	106.586
UCHL1				18	15	15	10	2	6	24.838
UCHL3		4		28	31	20	27	20	25	26.152
UCHL5		1	1	48	39	40	43	32	32	37.617
BAP1			1	33	29	32	34	31	30	80.492
OTUB1				2	2	4				31.27
OTUB2				2		1				27.300
OTUD4	1			1		3			1	123.055
OTUD5				4	2	9				60.306
OTU6B				4	3	6		1		33.758
OTU7A				7	6	7	7	5	5	100.797
ZRANB1				7	4	11	2			80.934
VCIP135				7	5	11				134.503
Ataxin 3				22	15	19	2	1	1	40.533
JOS1				2	1	3				23.152
JOS2				3	2	3				20.776

List of Figures

List of Tables

Acknowledgments

Zuerst möchte ich meinem Doktorvater Prof. Lothar Jänsch danken. Nicht nur für die Betreuung während meiner Doktorarbeit sondern auch für die fachliche und persönliche Unterstützung während der gesamten Zeit vielen Dank. Die hinter mir liegende Zeit hat mich sehr geprägt und zu meiner persönlichen Entwicklung beigetragen.

Ebenso möchte ich Prof. Susanne Engelmann herzlich für die Übernahme des Zweitgutachtens und Prof. Klemens Rottner für die freundliche Zusage den Prüfungsvorsitz zu übernehmen, danken.

Bei meinen Kooperationspartnern möchte ich mich für ihre Unterstützung innerhalb der einzelnen Teilprojekte meiner Arbeit bedanken. Besonders erwähnen möchte ich Dr. Raimo Franke: Danke für spannende Diskussionen und eine tolle Zusammenarbeit, auch wenn die Peptide es nicht immer gut mit uns gemeint haben. Auch danke ich Antje Ritter und Tatjana Arnold für die technische Umsetzung der Synthesen, sowie, für die Proteinproduktion: Dr. Joop van den Heuvel, Daniela Gebauer, Nadine Konisch und Claudia Hanko.

Weiterhin auch einen großen Dank an Prof. Schlüter für die hervorragende Zusammenarbeit sowie an Dr. Uwe Lodes für die Probensammlung und -bereitstellung. Auch bei Dr. Nishanth Gopala und Anette Sohnekind möchte ich mich herzlich für die großartige Kooperation sowie technische Unterstützung bedanken.

Ein lieber Dank geht an die gesamten CPROs, die während der zurückliegenden Jahre dafür gesorgt haben, dass die Arbeitsatmosphäre immer angenehm war und nie das Gefühl aufkam, dass man alleine da steht. Danke an Dr. Manfred Nimtz, Dr. Josef Wissing und Dr. Marco van Ham für die Unterstützung bei technischen Fragen sowie an Kathrin Goltz, Undine Felgenträger und Kirsten Minkhart für die technische Assistenz -Feueralarm!- und die schönen Stunden neben der Arbeit.

Außerdem ein herzliches Danke an Mario Schmidt, Nicole Amsberg, Dr. Björn Bulitta und Dr. Maxi Heyner für Diskussionen und Unterhaltungen, ob fachlich oder privat und die kleinen und großen Hilfen im Labor und außerhalb.

Tausend Dank möchte ich auch Prof. Frank Klawonn sagen: die Engelsgeduld bei der Auswertung der Sepsis-Daten und die Unterstützung bei allen statistischen Fragen sowie ein offenes Ohr haben merklich dazu beigetragen, dass diese Arbeit so weit gediehen ist und ihre jetzige Qualität hat.

Ein ebenso großer Dank gilt Dr. Uwe Kärst, für die immer passende Literatur zum Thema, das unermüdliche Korrekturlesen und für die Aufbauarbeit, besonders während des Schreibens dieser Arbeit. Hier ist das laute „JA“ für dich.

Der letzte und größte Dank an dieser Stelle ist an meine Freunde und meine Familie gerichtet. Ich danke meinen Eltern für ihre unendliche Unterstützung und den unerschütterlichen Glauben an mich; ihr seid meine Wurzeln im Leben.

Außerdem danke ich Simone, Lisette und Rebekka, dafür, dass sie immer da sind auch wenn ich mich manchmal rarmache.

Zuletzt möchte Henning danken: für jede einzelne Sekunde deiner Zeit und die schier unerschöpfliche gute Laune. Du bist wahrlich meine Sonne und hast mich das Fliegen gelehrt. Danke!